N 70 25526
N 70 NGL 21-002-005
NASA CR 109550

THE PREPARATION OF SOME HIGHLY REACTIVE, THREE MEMBERED RING ORGANIC COMPOUNDS AS CRYOCHEMICAL REAGENTS, AND THE LOW TEMPERATURE MASS SPECTROMETRIC STUDY OF THEIR STABILITY AND MOLECULAR ENERGETICS

A THESIS

Presented to

The Faculty of the Graduate Division

by

Richard James Holt

In Partial Fulfillment

of the Requirements for the Degree

Doctor of Philosophy in the School of Chemical Engineering

CASE FILE COPY

Georgia Institute of Technology

September, 1969

THE PREPARATION OF SOME HIGHLY REACTIVE, THREE MEMBERED RING ORGANIC COMPOUNDS AS CRYOCHEMICAL REAGENTS, AND THE LOW TEMPERATURE MASS SPECTROMETRIC STUDY OF THEIR STABILITY AND MOLECULAR ENERGETICS

A THESIS

Presented to

The Faculty of the Graduate Division

by

Richard James Holt

In Partial Fulfillment

of the Requirements for the Degree

Doctor of Philosophy in the School of Chemical Engineering

Georgia Institute of Technology

September, 1969

THE PREPARATION OF SOME HIGHLY REACTIVE, THREE MEMBERED RING ORGANIC COMPOUNDS AS CRYOCHEMICAL REAGENTS, AND THE LOW TEMPERATURE MASS SPECTROMETRIC STUDY OF THEIR STABILITY AND MOLECULAR ENERGETICS

Approved:

_____
Chairman

_____

_____

Date approved by Chairman: _____

ACKNOWLEDGMENTS

I would like to thank Dr. H. A. McGee, Jr., for his suggestions of the cryogenic investigations reported herein and for providing me with equipment and supplies to support the experimental work. The interest shown and responsibilities exercised by Dr. W. T. Ziegler and Dr. E. M. Burgess while serving on my reading committee are appreciated as is the helpfulness and comradeship found amongst my many fellow graduate students in the cryochemistry laboratory. In this respect, the molecular orbital calculations done by Mrs. L. P. Gordon, the preliminary work done by Dr. E. Kirschner on cyclopropanone, and Mr. M. A. Bell's laboratory preparations of cyclopropene and his spade work in the cyclopropenone synthesis are especially acknowledged.

The National Science Foundation traineeship and Universal Oil Products scholarship received by me during my graduate stay are warmly recognized as an essential part of my support as is the National Aeronautics and Space Administration grant NsG-337 NGL 11-002-005 administered through the School of Chemical Engineering.

The encouragement, understanding, and especially the patience of my wife, Pat, were of immeasurable value in forging the completion of this work. The concern of my parents, Mr. and Mrs. R. J. Holt, was also important to me. The typing of Mrs. Lydia Geeslin which follows herein is much appreciated.

TABLE OF CONTENTS

	Page
ACKNOWLEDGMENTS	ii
LIST OF TABLES	viii
LIST OF ILLUSTRATIONS	x
SUMMARY	xii
NOMENCLATURE	xxiv
Chapter	
I. INTRODUCTION AND LITERATURE REVIEW	1
General	1
Primary Effort	2
Secondary Effort	2
Tertiary Efforts	3
Ring Molecules	3
cy-C_3H_4O	3
cy-C_3H_6	6
cy-C_3H_2O	7
cy-C_3H_4	8
II. APPARATUS AND EXPERIMENTAL TECHNIQUES	10
General Cryochemical Techniques	10
Cryochemistry	10
Cryogenic Reactor-Inlet System	11
Synthesis Techniques	12
Storage	12
Transfer	13
Purification	14
Techniques for Varying Sample Temperature	16
Mass Spectrometric Analysis	17
Data	18
Stability of Compound	20
Polymer Study	21
Theoretical Calculations	22

TABLE OF CONTENTS (Continued)

Chapter		Page
	Individual Ring Molecules	22
	cy-C_3H_6	22
	cy-C_3H_4O	22
	cy-C_3H_4	27
	cy-C_3H_2O	28
III.	SYNTHESIS, ANALYSIS, AND STABILITY RESULTS	34
	Cyclopropanone	34
	Reaction and Identification	34
	Temperature Sensitivity and Stability	46
	Stability Discussion	47
	Polymer	49
	Comments on the Low Temperature Reaction	49
	Cyclopropane	50
	Cyclopropene	50
	Cyclopropenone	54
	Verification of Literature Synthesis	54
	Schematic of Separation Experiments	57
	Background Data	57
	Solvent Separations	63
	Non-solvent Syntheses and Separations	64
	Interpretation of Mass Spectra	65
	Summarizing Discussion of Polymers	70
	Summarizing Discussion of Synthesis	73
IV.	DERIVED ENERGETIC RESULTS	80
	Introduction	80
	Definitions, Derivations, and Assumptions	80
	Characteristics Unique to Ring Molecules	87
	Ring Strain	87
	Review of Literature on MS Investigations of Ring Molecules	88
	Relation of Bond Dissociation Energies and Activation Energies for Ring Molecules	89
	Reactivity of Ring Molecules	93
	Procedure	94
	Literature Data and Estimations	95

TABLE OF CONTENTS (Continued)

Chapter		Page
	Calculated Results	101
	Obtaining Consistent Experimental ΔH_f^o Values	101
	Bond Dissociation Energies	105
	Derived Ring Strains and ΔH_{act} Results	105
	Ring Strain	
	Bond and Bond Dissociation Energies	
	Activation Energies for Ring Opening	
	Thermodynamic Heats of Reaction and Reactivity Considerations	112
	Summarizing Comments	116
V.	CONCLUSIONS AND RECOMMENDATIONS	118
APPENDICES		
A.	MASS SPECTRAL DATA	129
	cy-C_3H_6	129
	cy-C_3H_4O	130
	cy-C_3H_4	130
	cy-C_3H_2O	131
B.	IONIZATION AND APPEARANCE POTENTIALS	140
	Literature and Comments on IP Methods	140
	Standard Curves	141
	Linear Methods	141
	Logarithmic Methods	143
	Monoenergetic Electron Methods	143
	Second Derivative Method	143
	Long-Tail Curves	144
	Methods	145
	Discussion	146
	The Effect of Experimental Conditions and Instrumental Settings on IE Curves	147
	Factors Not Affecting IE Curve Shape	147
	Factors Affecting IE Curve Shape	148
	Sample Pressure in Source	151
	Control Pulse Exceeding Ground Potential	154
	Manual Versus Automatic Trap Current Regulation	155

TABLE OF CONTENTS (Continued)

Appendices Page

Calibration from Day to Day 155
Factors Affecting the IE Curve Appearance 156

Procedure and Verification of IP Methods. 156
Semilog Match 158
Linear Match and Initial Break Methods--
Adaptation of X-Y Recorder. 158

Summary 167

Results for Ring Molecules. 167
cy-C_3H_6 167
cy-C_3H_4O. 170
cy-C_3H_4 178

C. EXCESS ENERGIES 185

Introduction. 185

Correlation of Excess Energies. 188
Theory. 188
Method. 189
Discussion. 192

Thermodynamic Calculations. 195

Measurement of $\overline{e}_i$ 202
Instrumental. 202
Flight Times and Ionization 203
Space Resolution. 204
Energy Resolution 204
Excess Energy Ions. 207

Instrumental Adjustments Affecting Peak Shape 208
Intensity Adjustments 208
Focusing Adjustments. 208
Detecting Adjustments 209
Recording Adjustments 214

Experimental Work 214
Procedure 214
Discussion of Procedure 215
Results 219
Discussion of Results 219
cy-C_3H_6

TABLE OF CONTENTS (Concluded)

Appendices Page

$cy\text{-}C_3H_4$

$cy\text{-}C_3H_6O$ and $cy\text{-}C_3H_4O$

Precision, Accuracy, and Limitations 232

D. MOLECULAR ORBITAL CALCULATIONS 233

Introduction 233

Program Procedure 234

Input Data 234

Computation 234

Output 235

Goals and Outline of Calculations 236

Data for Calculations 238

Results 238

Discussion 257

BIBLIOGRAPHY 264

VITA 270

LIST OF TABLES

Table		Page
1.	Mass Spectra of Species Observed in Warming Cyclopropene and Cyclopropanone Raw Products	37
2.	Mass Spectra and AP Identification of Cyclopropane and Cyclopropene	38
3.	Mass Spectra Results of Cyclopropene Experiments	39
4.	Mass Spectra and AP Results of Cyclopropanone Experiments	40
5.	Supplementary Mass Spectra Data for Cyclopropenone Experiments	59
6.	Summary of Mass Spectra from Cyclopropenone Experiments	60
7.	Determining Relative Mass Spectra from Cl Isotopes	67
8.	Possible Product Compounds in Cyclopropenone Experiments	71
9.	Literature Thermochemical Data	96
10.	Bond Dissociation Energies, Bond Energies, and Bond Lengths for Open Chain Molecules	98
11.	Estimated Bond Dissociation Energies and Bond Energies of Ring Molecules (kcal/mole)	100
12.	ΔH_f^o and D^o for Ring Molecules as Calculated from Experimental Data (kcal/mole)	103
13.	Experimental ΔH_a^o and Derived Ring Strain, Ring Energies, and $\Delta H'_{act}$ (kcal/mole)	106
14.	Variation of Argon Linear Match IP with Ion Source Partial Pressure	153
15.	Verification of Techniques for Measuring Ionization and Appearance Potentials (eV)	157
16.	IE Results for Cyclopropane (eV)	168

LIST OF TABLES (Concluded)

Table		Page
17.	Low Temperature Semilog IE Results for the Cyclopropanone System	176
18.	Room Temperature Initial Break IE Results for the Cyclopropanone System	177
19.	Low Temperature and Room Temperature IE Results for Cyclopropene	179
20.	Comparisons of Linear IE Curve Shapes of Cyclopropene Fragment Ions	182
21.	Calculations with Literature Excess Energy Data	193
22.	Peak Widths and Ion Translational Energies for Verification of Experimental Technique	220
23.	Cyclopropane Peak Widths and Ion Translational Energies	221
24.	Cyclopropene Peak Widths	222
25.	Cyclopropene Excess Energies	223
26.	Cyclopropanone and Cyclobutanone Peak Widths and Excess Energies	224
27.	Summary of Excess Energies at AP for all Compounds (kcal/mole)	225
28.	Standard Bond Lengths for MO Calculations	240
29.	X, Y, Z Coordinates Used in MO Calculations	241
30.	Geometry Variations	249
31.	Geometry Variations – MO Results	251
32.	Standard and Known Geometries for ΔH_a and IP	253
33.	Standard and Known Geometries for ΔH_a and IP – MO Results	254
34.	Geometry Variations and MO Results – Fragments Containing H and C	255
35.	MO Results for Oxygen Containing Compounds	256

LIST OF ILLUSTRATIONS

Figure		Page
1.	General Apparatus and Flow Schematic for Handling, Soaking, Distilling, and Calibrating.	15
2.	Rate of Gaseous Evolution from Reaction of Ketene and Diazomethane at -145°	36
3.	Estimation of Normal Boiling Point of Cyclopropanone. . .	45
4.	nmr of Solutions from Cyclopropenone Hydrolysis	56
5.	Schematic of Cyclopropenone Separation Experiments. . . .	58
6.	Possible Reactions and Their Heats.	113
7.	ms of Cyclopropane at 25° and ms of Cyclopropene at -150° and 25°.	132
8.	ms of Product Mass 70 from the Reaction of Diazomethane and Ketene Versus ms of Authentic Cyclobutanone	133
9.	ms of Product Mass 56 from Reaction of Diazomethane and Ketene.	134
10.	ms of Reaction Off Gas and Other Products Resulting from Side Reactions During the Reaction of Diazomethane with Ketene	135
11.	ms of Authentic Acrylic Acid and ms of 30 Percent $HCl-H_2O$ Solution.	136
12.	ms of Dichlorocyclopropene, Tetrachlorocyclopropene, and Product Mass 122.	137
13.	ms of Product Mass 55 and the Heating of Dichlorocyclopropene Polymer.	138
14.	ms of Product Masses 90, 72, and 108 in the Cyclopropenone Hydrolysis	139
15.	Effect of Filament and Trap Currents on Linear IE Curve Shape of Water	149
16.	Verification of Linear Match IP Technique	159

LIST OF ILLUSTRATIONS (Concluded)

Figure		Page
17.	Verification of Semilog Match IP Technique and Evidence of Diffusion Problem at High Sample Source Pressure	160
18.	Verification of Initial Break IP Technique	161
19.	IE Curves for Long-Tail Ions at High Electron Energies	162
20.	IE Curves for Long-Tail Ions at Low Electron Energies	163
21.	Initial Break IE Data for Long-Tail Ions	164
22.	Semilog IE Data for Cyclobutanone at -82° and Product Mass 70 at -75°	171
23.	Semilog IE Data for Product Masses 70 and 56 at Low Temperatures (Mass 70 Shifted Down 0.4 Volts)	172
24.	Initial Break IE Data for Masses 70 and 42 from Cyclobutanone and Product Mass 70 at Room Temperature	173
25.	Initial Break IE Data for Masses 56, 42, and 28 from Product Mass 56 at Room Temperature	174
26.	Examples of IE Interference Problems in Cyclopropanone Experiments	175
27.	Semilog IE Data for Cyclopropene at Low Temperatures	180
28.	Initial Break IE Data for Cyclopropene at Room Temperature	181
29.	Peak Shapes of He Ion at Various Gate Widths	210
30.	Comparison of Peak Widths of CH_2^+ from cy-C_3H_4 and cy-C_3H_6	211
31.	Peak Width Versus Ion Focus Voltage	212
32.	$W_{\frac{1}{2}}$ Versus $\sqrt{M}$	213
33.	$\bar{e}_i$ Versus Electron Energy for Verification of Experimental Technique	226
34.	$\bar{e}_i$ Versus Electron Energy for cy-$C_3H_6 \longrightarrow C_2H_2^+$	227
35.	$\bar{e}_i$ Versus Electron Energy for cy-$C_3H_6 \longrightarrow CH_2^+$	228
36.	Schematic Structure of Molecules Used in MO Calculations	239

SUMMARY

This work is concerned with the development and extension of cryochemical synthesis techniques into the domain of organic chemistry. A class of reactive, 3 carbon membered, ring molecules was chosen for investigation. These species possess abnormal bonding in the form of small valence angles and this leads to poor bonding orbital overlap and weak bonds. This condition is commonly described by the term "ring strain." This abnormal bonding creates a driving force for the molecule to enter into those reactions that would lead to relief of this strain. Thus, at room temperature, the reactivity may be so great that some molecules exhibit only a fleeting existence, and we here describe these species as "cryochemical molecules." The primary effort in this work was to investigate four systems of ring compounds and, from mass spectral and energy measurements at low temperatures, to derive a consistent body of calculated results which would relate such quantities as heats of formation (ΔH_f^o), the bond energies (E), bond dissociation energies (D^o), activation energies (ΔH_{act}), and ring strain. Studies at room temperatures versus those at low temperatures were to be used to discern changes in structure, decomposition, etc. for these reactive molecules. The causes and results of the instability of these molecules would necessarily determine procedures and precautions for their convenient handling. When this work was begun, two of the target molecules, cyclopropanone and cyclopropenone, had never been isolated as pure species and much of the work involved synthesis and separation problems. Cyclopropene, a

reactive olefin; cyclopropane, an energetic model for cyclopropanone; and cyclobutanone, a by-product of the cyclopropanone synthesis, were also investigated.

Although it had long been postulated as a reaction intermediate and although it had shown fleeting, but detectable, existence, cyclopropanone had not been isolated as a pure species. Shortly after this work was begun, two papers appeared almost simultaneously, both describing the low temperature synthesis (-78°) from ketene and diazomethane in solutions of methylene chloride[51] and liquid propane.[52] Reports on the stability and polymerization agreed with the results from our study. We synthesized cyclopropanone by the liquid-liquid, solution free, reaction of diazomethane and ketene at -145°. This is a synthesis with many novel and interesting facets. It is very unusual to find a liquid-liquid reaction which will proceed at such a low temperature without any external form of activation. The reactor, being submerged in a coolant at -145°, quickly conducted away any heat of reaction and prevented the molecule from decomposing (as it does upon formation in the gas phase[46]). The low temperature also served to slow the rate of cyclopropanone polymerization. The use of low temperatures, pure reagents, and a great excess of ketene leads to a yield of better than 50 percent product purity cyclopropanone with the four membered ketone ring, cyclobutanone, as the only side product. Although cyclopropanone can be kept indefinitely at -196°, it appears to begin to slowly polymerize at -90° and reacts so rapidly at room temperature that samples are destroyed within minutes. This reactivity at room temperature causes a severe analysis problem and cyclopropanone can be conveniently studied at only lower temperatures.

In contrast to its formation in the gas phase, no evidence of decomposition was found as it was heated at low pressures from a solid at -196° through any liquid state to a gas at room temperature. The polymer formed was a white, porous looking solid. The ionization potentials, appearance potentials, and excess energies of the principal ions from cyclopropanone and cyclobutanone were experimentally measured and their molecular energetics calculated therefrom. The ionization potentials of cyclopropanone and cyclobutanone were measured to be 9.1 eV and 9.4 eV, respectively. Both these values are supported by molecular orbital calculations reported herein.

Cyclopropene, described in the literature as very reactive and explosive, was investigated both because of this reactivity and as an energetic model for cyclopropenone. It was found to be much easier to handle than one would expect from the literature as it can be synthesized, distilled, and transferred at room temperature with no change in structure and with only an insignificant loss from polymerization (which only became noticeable at room temperature). Unfortunately, the mass spectrum of cyclopropene consists of very intense ion peaks corresponding to the positively charged, intact ring and very weak ions resulting from ring fragmentations. The ionization efficiency curves of the weak ion signals were of such poor quality that reliable experimental appearance potentials could not be obtained for the development of the molecular energetics. The ionization potential of cyclopropene was measured to be 9.6-9.7 eV which was supported by the molecular orbital calculation of 9.6 eV and close enough to a literature value, 9.95 eV, to attribute the difference to experimental error.

Cyclopropene was studied at -145° and room temperature (~ 25°). Although it is known to polymerize at -80° and although the polymerization is believed to be a reaction of the excited double bond diradical,[63] no experimentally detected change in the ionization potential (9.6-9.7 eV) from -145° to 25° leads one to conclude that any formation of a triplet occurs in such small amounts as to be experimentally undetectable. Similarly, cyclopropanone was studied at -90° and 25°. Although it was seen to polymerize quite rapidly at room temperature and although many of its reactions in solution are postulated to proceed through the ring opened dipolar ion (23 kcal/mole more stable than the closed ring[60]), no change in the ionization potential with temperature (9.1 eV) likewise implies no detectable presence of these structures. A difference in structure would, of course, have invalidated physical data taken at room temperature.

According to Breslow,[76] the reaction of tetrachlorocyclopropene with tri-n-butyltin hydride at room temperature produces a volatile mixture of chlorocyclopropenes which, when collected in CCl_4 and hydrolyzed with water, produces cyclopropenone in water solution. Breslow postulates the existence of the free ketone, not the gem diol, even in water solution; however, he states that all attempts to separate and isolate the molecule have led to ". . . at least partial polymerization of the compound." He also reports that the ketone may be extracted from water solution by polar solvents and that it is much less reactive and more stable than its saturated analog, cyclopropanone. His paper strongly suggests that cyclopropenone was synthesized and implies that the failure to isolate cyclopropenone was due only to its tendency to polymerize.

Based on our previous work on cyclopropanone and the reactivity statements of Breslow's[76] paper, we reasoned that cyclopropenone would most certainly be stable enough for cryogenic mass spectrometric analysis once it was separated from its solution. Since it could be extracted, the obvious approach was to find a polar solvent which would allow separation of the ketone at a low enough temperature to prevent polymerization. Although the reported[76] synthesis and nmr analysis for cyclopropenone were reproduced, the isolation of the ketone was not accomplished by any of the following techniques: extraction of the ketone from water solution using different kinds of solvents; performing the hydrolysis step in water soluble solvents; partial hydrolysis of the dichlorocyclopropene sample with less than the stoichiometric amount of water; and drying of the solutions to remove dissolved water. The solutions resulting from the application of these techniques were all analyzed by distilling them at low temperatures into the mass spectrometer. Instead of identifying the ketone, other products were observed which were not reported in the original publication[76] (which fails to report the presence of other products). In addition, this publication[76] identified the mass 72 product as acrylic acid which, from our work does not appear to be a correct analysis. We concluded that further work on cyclopropenone would better define the problem. However, in view of our work, the original synthesis, and the lack of additional publications since the first report of the original synthesis (two years), we also concluded that the approach discussed herein to the synthesis and separation has not been, and likely will not be, very fruitful. Assuming that the original synthesis and analysis were correct, this isolation failure may be a

result of water being needed to stablize the structure and prevent reaction. This need is so great that water and ketone must exist in solvents as a unit and vaporization of the solutions leads to immediate and complete reaction of the ketone. On the other hand, the products of this work and the unsubstantiated original publication,[76] suggest that some other structure(s) was made rather than ketone. A third possible explanation is the existence of a solution equilibrium between the cyclopropenone and its hydrate in which its hydrate possesses a much higher vapor pressure. Dichlorocyclopropene and hydrated cyclopropenone* were found to be cryochemical reagents reacting rapidly at room temperature.

In this work, it was found to be very common for the fragments produced upon electron impact of ring compounds to possess excess translational and vibrational energy, but rare for the measured appearance potential to correspond to a fragment in an excited electronic state. This excess energy may be viewed as residual energy from the fragment formation of multiple bonds. Inclusion of a rearrangement correction term for the energetic difference in the initial and final ring fragmentation products allowed us to assign ring bond energies to particular bonds and enabled D^{o} and an estimation of ring opening activation energies to be calculated which seem to relate well to literature data. By analyzing a series of ring opening problems, it was concluded that a necessary but not sufficient condition for ring opening is that the

---

*Refers to a product of the hydrolysis which appears to be formed by the reaction of cyclopropenone and water.

amount of energy liberated from the formation of the ring be greater than the activation energy for ring opening. It also showed that the most likely ΔH_f^o associated with excited singlet methylene produced from diazomethane is around 90 kcal/mole.

Cyclopropane was investigated as an energetic model from which the molecular energetics of cyclopropanone could be discussed. The literature on cyclopropane discusses strain energies, heats of formation, ionization and appearance potential measurements, structure, mechanisms, and reactions. If mass spectrometric data could be correlated with other existing data for this molecule, the similar interpretation of the new molecule, cyclopropanone, should be possible. The energetics of cyclopropane seemed to be explained by the insertion of an energetic rearrangement term, $R(R_1)_g^{ex}$, in the equations for calculating $D^o(R_1\text{-}R_2)$ and $D^o(R_1^+\text{-}R_2)^*$. This energetic rearrangement term represents the energy difference between a hypothetical initial diradical and the final ground state structure for the fragments which results from breaking two carbon-carbon (C-C) ring bonds. We were able to calculate for cyclopropane the following values (kcal/mole) which compared well with literature data:

$\Delta H_f^o = 13 \pm 3$	(lit. = 12.7)
ring strain** = 36	(lit. = 27 relative to paraffins)
E(C-C) = 75	
D^o (C-C) = 52	(lit. = 49)
ΔH_{act}(ring opening) = 65	(lit. = 65)

---

*R_1 and R_2 represent groups of bonded atoms within the molecule.

**localized to carbon-carbon ring bonds

Heats of formation in the gas phase of cyclopropanone and cyclobutanone were calculated from mass spectrometric data to be 27 ± 8 and 13 ± 5 kcal/mole. Bond energies were used to calculate additional ring strains of 36 and 19 kcal/mole with respect to cyclopropane and cyclobutane, respectively. By a procedure analagous to one used for cyclopropane, the following values were predicted for cyclopropanone:

$$E(C\text{-}C^{\dagger}) = 66; \quad E(C\text{-}C) = 40$$
$$D^{o}(C\text{-}C^{\dagger}) = 45; \; D^{o}(C\text{-}C) = 20$$
$$\Delta H_{act}(C\text{-}C^{\dagger}) = 61; \text{ and } \Delta H_{act}(C\text{-}C) = 35.$$

This latter value supports the theory[60] that cyclopropanone solution reactions proceed with a low activation energy through a ring opened dipolar ion. It should be noted that, without the inclusion of $R(R_1)_g^{ex}$ terms, mass spectrometric results would predict a stronger bond at the distant carbon-carbon bond, d(C-C) = 1.58 Å, than the shorter carbon-carbon bond, $d(C\text{-}C^{\dagger})$ = 1.49 Å. This result particularly points out the necessity of the rearrangement term.

In this work, an experimental procedure was developed to calculate, from mass spectrometric data, the ΔH_f^o for molecules to within about ± 5 kcal/mole. Any lack of precision in the appearance potential and excess energy measurements is partially overcome by using more than one fragment ion to calculate ΔH_f^o. This measurement is only worth the trouble for molecules with structures from which it is not possible to make a good estimate of ΔH_f^o from other methods. It is particularly

---

†carbonyl carbon

adaptable to small rings because the fragments are produced in ground electronic states and correspond to molecules for which ΔH_f^o and ionization potential are usually known and need not be measured. However, it is necessary to check for the occurrence of excess translational and vibrational energies. This technique is the reversal of the normal energetic treatment from which the heat of formation of the fragment ion is calculated from the appearance potential by knowing the ΔH_f^o of the parent molecule.

During the course of this work, secondary efforts were needed to develop techniques for the measurement of excess ion energies and for the measurement of appearance potentials of ions with long-tail ionization efficiency curves. The correlation for measuring excess energies appears to apply well to large classes of compounds but, in this work, its accuracy was limited by poor precision. An X-Y recorder was adapted to measure appearance potentials by the "linear match" and the "initial breaks" methods which reduce the time of recording appearance potential data from greater than 60 to 10 minutes without much loss in precision. This increase in speed of recording the ionization efficiency data also helps to combat uncertainties introduced from slowly changing ion intensity. It allows a rapid check of the entire ionization efficiency curve for abnormalities which may dictate the ionization efficiency method to use.

It was found that the determination of ionization potentials from ionization efficiency curves that have standard shaped curves is obtainable by any number of methods with varying degrees of precision. On the other hand, it was found that the appearance potential of ions

with long-tail curves required methods that will separate the curve into sections pertaining to single processes which must be interpreted individually and that the appearance potential of some long-tail, low abundance ions may be experimentally undeterminable by electron impact methods. Ionization efficiency curves resulting from unknown and calibrating gas ions whose partial pressures in the ion source differ by a factor of 10 or less may be electronically adjusted to obtain a linear match over the range of five to six eV from the point of initial onset without introducing an error of more than 0.2 eV. However, for an intensity ratio of 10, the initial breaks method is difficult to use with electronically adjusted ionization efficiency curves because the signal-to-noise ratio changes and the curves appear different at the point of initial onset. Nevertheless, by looking for good match of the curves over the first two eV of the curve, one can obtain higher precision and still have a method that emphasizes the initial onset region of the ionization efficiency curve.

A tertiary effort is reported that involves the application of molecular orbital theory to these ring systems. This work involved no development of molecular orbital theory but merely the application of certain available computer programs to these ring molecules. We wished to calculate the ionization potential and heats of atomization (ΔH_a) for comparison with experimental data and to use the molecular orbital theory to help predict the structure of these reactive molecules. For a very reactive species, experimental structural determinations may be a long time forthcoming and it was hoped that mass spectrometric data reinforced by molecular orbital theory could provide some valuable insights. Because

of the inability of molecular orbital calculations to predict known molecular structures or even most stable structures from which accurate ΔH_a and ionization potentials could be calculated, theoretical chemists have had to adjust molecular parameters by empirical means such that ΔH_a and ionization potentials could be calculated accurately (on the average) for broad classes of compounds whose actual experimental bond lengths and angles are similar enough to allow a set of "standard" molecular geometries to be used for all molecules in the calculations. Since cryogenic, strained ring compounds owe their existence to abnormal (as opposed to standard) bonding and structure, the goals of synthesizing cryogenic molecules and semi-empirical, standard geometry, molecular orbital calculations appear to be mutually exclusive without some knowledge of how to assign a standard geometry to each particular ring molecule.

Of the four molecular orbital programs used in this work, the Mindo and Klopman programs calculated usable numbers for ΔH_f^o and ionization potentials while, from the results of this thesis, only the Pople program appeared to show any promise of structure prediction. Because of the insensitivity of the ionization potential to geometry changes and the good accuracy of calculated versus experimental ionization potentials, the Klopman and Mindo programs appear to be usable for calculating ionization potential for cryogenic ring molecules. However, the strong geometry dependence (especially the C-C ring bonds) of both Mindo and Klopman programs prevents the use of these two programs for calculating ΔH_f^o until some confidence is gained in assigning standard geometries to abnormal rings. This assignment is further complicated for ring

molecules having unmeasured geometries. Although the triplet calculations appear usable for parent molecules, the application to fragments appears to be also dependent on some better understanding of standard geometries. This confidence in assigning standard geometries may be obtainable by working with many known strained rings, or for a particular ring molecule with a family of substituted derivatives of known structure and properties, good agreement may result from calibrating the programs for this family of molecules as has been done for the cyclopropane and cyclopropene families.[100] Once this confidence is gained, the programs offer a strong potential for mass spectrometric identification and distinction between closed ring and open chain isomers whose ΔH_a and ionization potentials usually differ significantly. For very unstable molecules not amenable to nuclear magnetic resonance or infrared analysis, this seems a very worthy goal.

Although parts of the molecular orbital programs may not yet be sufficiently accurate for absolute use, they still offer the possibility of relative comparison of different structures, triplets, isomers, etc. from which qualitative trends or relative quantitative data can be used for mass spectrometric analysis decisions and calculations. Also included in this area is the prediction of relative stabilities of competing products.

NOMENCLATURE

The following symbols are so defined unless specified otherwise in the text.

Å	= angstroms
amp	= ampere
AP	= $A(R_1^+)$ = appearance potential of species R_1^+, eV
B	= constant in equation
BE	= Bond Energy
BDE	= Bond Dissociation Energy
C	= constant in equation
C_v	= molar heat capacity at constant volume
comp.	= computer MO calculation
d(C-C)	= bond distance between carbon-carbon single bond, angstroms
$D^\circ(R_1\text{-}R_2)$	= Standard Bond Dissociation Energy at 25°C of bond between R_1 and R_2 groups, reactants and products in ideal gas state, kcal/mole
$D^\circ(\triangle)$	= BDE for breaking two ring bonds simultaneously
$D^\circ(\triangle)_g$	= BDE calculated not using $R(R_1)_g^{ex}$ terms
$D^\circ(\triangle)^{ex}$	= BDE calculated using $R(R_1)_g^{ex}$ terms
$DP = D(R_1^+)$	= disappearance potential or initial onset of R_1^+ ion current, eV
e	= charge on fragment ion
est.	= estimated
eV	= electron volts (1 eV = 23.06 kcal/mole)

ex. = excited electronic state

exp. = experiment

$\bar{e}_i$ = observed average translational energy of the fragment ion, eV

$\bar{e}_t$ = excess translational energy of the parent molecular ion activated complex from collision with electron, kcal/mole

$\bar{e}_r$ = excess rotational energy

$\bar{e}_v$ = excess vibrational energy

$\bar{e}_p$ = total translational energy of the parent molecular ion activated complex, kcal/mole

E(C-C) = BE of carbon-carbon single bond, kcal/mole

E = electric field strength

E_s = electric field in ion source

E = internal energy, kcal/mole

ΔE_o^o = change in internal energy at 0°K, reactants and products in ideal gas state

E* = $AP-\Delta H_r^o = \bar{e}_t + \bar{e}_r + \bar{e}_v$ = sum of excess translational, rotational, and vibrational energies from collision with electron, kcal/mole

ΔE^{max} = maximum E* assuming classical heat capacity limit, kcal/mole

$f(V_x)$ = probability distribution for velocity component in X direction

g = ground electronic state

ΔH_f^o = Standard Heat of Formation at 25°C, reactants and products in ideal gas state, kcal/mole

ΔH_a^o = Standard Heat of Atomization from the elements, kcal/mole

ΔH_T = heat of reaction at temperature T(°K)

ΔH°_{r}	= Standard Heat of Reaction at 25°C
ΔH_{act}	= reaction activation energy
ΔH_{c}	= heat of combustion
i	= ion
ir	= infrared analysis
I	= ion intensity
IE	= ionization efficiency
IP	= $I(R_1\text{-}R_2^+)$ = ionization potential of species $R_1\text{-}R_2$, eV
k	= Boltzmann constant
kcal	= kilocalorie
K	= constant in equation
lit.	= literature
m	= mass
m/e	= mass/charge; indicates position of peak in mass spectrum
max	= maximum
ml	= milliliter
mm	= millimeter
ms	= mass spectrometric analysis
μsec.	= microsecond
M(m)	= mass
M_i	= mass of ion
M_n	= mass of neutral
M_p	= mass of parent
MO	= molecular orbital
MW	= molecular weight

N(n)	= neutral fragment
nmr	= nuclear magnetic resonance analysis
N.C.	= no convergence
N_o	= Avogadro's number
n	= number of atoms in molecule
P(p)	= parent molecule
q	= electronic charge
R	= ideal gas constant = 1.987 cal/mole°K
R_1	= fragment species
R_1-R_2	= bonded fragments in parent molecule
RS	= ring strain
$R(R_1)_g^{ex}$	= structural rearrangement energy term from hypothetical excited diradical to the ground electronic state, kcal/mole
S	= 1) distance from ion focus grid 2) total distance traveled in electric field
S_i	= instantaneous position
V	= volts
V	= velocity
V_x	= velocity in X direction
V_{xi}	= initial velocity in X direction
V_t	= terminal velocity of ion leaving electric field
V_{xo}	= terminal velocity of ion leaving electric field at ion focus grid
V^{max}	= maximum ion velocity
t	= time

T	= temperature, °C or °K
T_{rt}	= room temperature
T_p	= temperature of parent molecular ion in activated state
TE	= total energy of molecule
$W_{\frac{1}{2}}$	= ion peak width at half height, sec
W_b	= ion peak width at base, sec
X, Y, Z	= cartesian coordinates
α	= empirical parameter in equation (8)
σ	= ionization reaction cross-section
δ	= nmr proton shift, ppm
ρ	= density

CHAPTER I

INTRODUCTION AND LITERATURE REVIEW

General

This study is concerned with the development and extension of cryochemical techniques into certain aspects of organic chemistry. Cryochemistry is concerned with the synthesis, isolation, and chemical behavior of molecules which do not exist under normal conditions of temperature and pressure because they are either too reactive or too unstable. In this work, cryochemistry is limited to the class of compounds which will exert a mass spectrometrically observable vapor pressure (10^{-4}-10^{-3} torr) at a temperature at which it is stable. This limitation quickly resolves the potential molecules into a class of high vapor pressure molecules of low molecular weight and/or non-polarity and high reactivity and instability. This high reactivity may result from some electronic and/or bonding abnormality and further resolves the class into: 1) those species which are electronically excited and which exist in triplet states (i.e. methylene, etc.) or as free radicals and 2) those ground state singlet species which possess such a strained structure that they are extremely reactive and/or unstable. This thesis is concerned with this latter type of molecule and, in particular, 3-carbon membered, ring compounds.

Primary Effort

The primary effort of this work was to study a series of related, reactive, 3-carbon membered, ring compounds using cryochemical techniques. From mass spectra and energy measurements at very low temperatures, a consistent body of calculated results were to be derived which would contain and relate such quantities as heats of formation, (ΔH_f^o), bond energies, (E), bond dissociation energies (D°) and ring strain (RS). Within this energetic goal, we attempted to consider all different types of mass spectrometric experiments that would yield useful information. For a reactive molecule which is known to react and/or decompose at room temperature, one such experiment would be to obtain energetic data at a low temperature where the molecule is stable and compare that to similar energetic data obtained on the reacting species at room temperature in hopes that a difference in states or structures would be energetically discernible. When this work was begun, two of the target molecules, cyclopropanone and cyclopropenone, had never been isolated and, consequently, much of the work involved synthesis and separation problems and techniques. The reactive olefin cyclopropene, cyclopropane, and cyclobutanone were also studied. The causes and results of instability of these molecules were roughly characterized, and characteristics relative to their convenient handling were also determined.

Secondary Efforts

During the course of this work, many secondary efforts were needed to develop the energetic results. This work includes developing techniques to measure the excess energy of mass spectrometric fragmentation processes,

discussions and development of techniques to measure the ionization and appearance potentials (IP an AP) of ions with long-tail ionization efficiency (IE) curves, and the interpretation of ring fragmentation data. As a result, this work is also an extensive survey of the problems that can be encountered in obtaining mass spectrometric energetic data.

Tertiary Efforts

A tertiary effort is reported that involves the application of molecular orbital (MO) theory to these ring systems. This work involved no development of MO theory but merely the application of certain available computer programs (i.e. those of Pople,[97] Hoffman,[98] Klopman,[11] and Baird[99]) to these ring molecules. We wished to calculate IP and ΔH_f^o for comparison with experimental data and to use MO theory to help predict the structure of these reactive molecules. For a very reactive species, experimental structural determinations may be a long time forthcoming and hence the mass spectrometric data reinforced by MO theory could provide some valuable insights.

Ring Molecules

cy-C_3H_4O

At the outset of this work, cyclopropanone had not been isolated as a molecular species. In 1965-66, literature[40-43] on the preparation of its substituted derivatives began to appear, and, with the successful synthesis of derivatives such as tetramethylcyclopropanone and 2, 2 dimethylcyclopropanone, there came a flurry of activity directed towards the synthesis of the parent itself.

Cyclopropanone had long been postulated as a reaction intermediate and, as early as 1931, Lipp[44] provided evidence suggesting that cyclopropanone was an intermediate in the formation of cyclobutanone from ketene and diazomethane at -70°. Roberts[45] investigated the validity of this proposal by determining the fate of tracer carbon-14 in diazomethane. His calculated and experimental results for the average distribution of carbon-14 at the carbon positions in cyclobutanone were in good agreement:

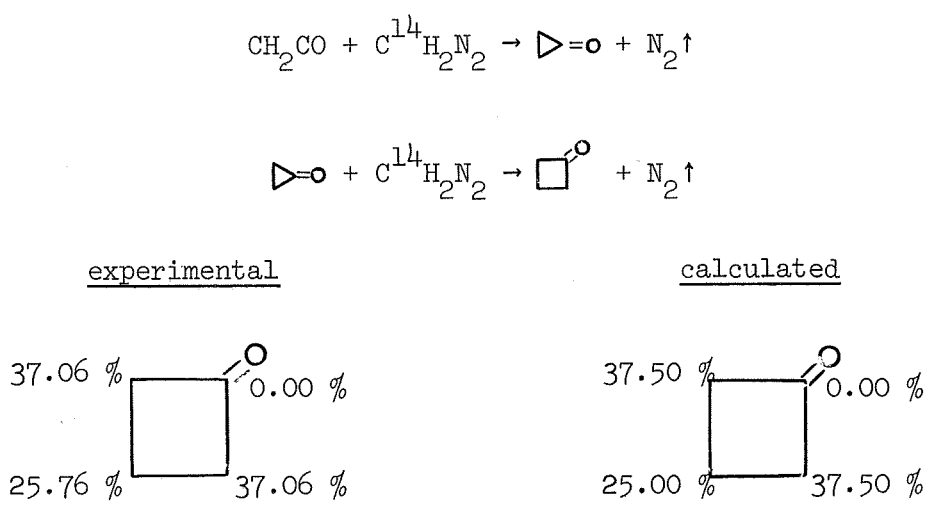

The enhanced reactivity of cyclopropanone with diazomethane versus the relative stability of cyclobutanone under the same conditions was rationalized as a result of the extreme strain in the 3-carbon ring.

Kistiakowsky[46] investigated the reaction of methylene with ketene in the gas phase by flash photolytic decomposition of ketene. He did not observe any transitory formation (as Roberts had seen in the liquid phase), and he postulated that the formation of cyclopropanone must be at least 78 kcal exoergic, which is 13 kcal more than the minimum activation energy

for the decomposition of cyclopropane. Hence, at low gas pressures, decomposition evidently occurred before collisional quenching. Cyclopropanone decomposed into ethylene and carbon monoxide by the breaking of two carbon-carbon bonds. Later, Kistiakowsky,[47] using a time-of-flight (T-O-F) mass spectrometer of 50 msec working cycle and 0.005 mole fraction sensitivity, estimated the life time of cyclopropanone as 360 msec from the flash photolysis of ketene in nitrogen dioxide. This, then, represents the time it takes cyclopropanone to decompose due to the energy released from the reaction of methylene with ketene.

Davidson[48] photolyzed ketene and diazomethane in a liquid nitrogen solution wherein the reaction products were quenched to -196°. Infrared study revealed a band at 1825 cm^{-1} that was attributed to the 3-membered ring by extrapolating the carbonyl liquid stretching frequencies of the 6-, 5-, and 4-membered ketone rings. In an analogous low temperature experiment, he found that methylene reacts with ethylene to form primarily cyclopropane whereas, at room temperature, cyclopropane is cleaved (i.e. a carbon-carbon ring bond is broken) by this heat of reaction to yield propylene. On allowing the postulated cyclopropanone product to warm, it survived long enough to be observed spectrally.

There have been other approaches to the synthesis of cyclopropanone,[49,50] but none seemed as promising as the reaction of ketene with diazomethane. We decided to carry out the reaction at the lowest possible temperature to isolate the molecule as a pure, stable species. This task was realized by a liquid-liquid reaction at -150° and led to further mass spectrometric studies on this new reactive molecule such as determining

its temperature stability and developing its molecular energetics including ΔH_f^o and ring strain estimates. The results of this work are presented herein.

After this work was begun, two papers appeared almost simultaneously, both describing the low temperature syntheses (-78°) of cyclopropanone from the reaction of ketene and diazomethane in solutions of methylene chloride[51] and liquid propane.[52] The use of low temperatures apparently quenched the product to prevent decomposition and the dilute solutions restricted polymerization of the product. The product was characterized in solution by nuclear magnetic resonance (nmr), infrared (ir), and mass spectrometry (ms). Reports on temperature stability and polymer formation were included and agreed with the results from this work. Since the publications of these two papers, a number of papers concerning cyclopropanone have appeared. Although most of them are concerned with the reactions of cyclopropanone,[53-57] there have been some concerned with its structure[58,59]; and there is a recent review paper[60] which summarizes the literature at the time of this writing.

<u>cy-C_3H_6</u>

Cyclopropane was investigated as an energetic base from which the molecular energetics of cyclopropanone could be discussed. The literature on cyclopropane discusses strain energies, heats of formation, IP and AP, structure, mechanisms, and reactions. If mass spectrometric data could be correlated with other existing data for this molecule, the similar interpretation of the new molecule, cyclopropanone, should be obtainable. The detailed discussions of these data from the literature are more

appropriately presented in the text. The investigation of cyclopropane also proved to be a good exercise in the measurement of excess energies, the AP measurement of long-tail ions, and the interpretation of ring strain.

cy-C_3H_2O

In 1965-66, studies of substituted cyclopropenones such as diphenylcyclopropenone[74] and monoalkylcyclopropenone[75] were reported, followed in 1967 by the synthesis of the unsubstituted ketone[76] itself. As reported by Breslow,[76] the reaction of tetrachlorocyclopropene with tri-n-butyltin hydride at room temperature produces a volatile mixture of chlorocyclopropenes which, when collected in CCl_4 and hydrolyzed with water, produce the ketone in water solution. Arguments based on nmr and ir analyses are used to eliminate other possible structures for the product species. For example, it appears not to be the gem-diol, even in water solution. However, all attempts to separate and isolate the molecule have led to "...at least partial polymerization of the compound." Breslow and co-workers also report that the ketone may be extracted from water solution by polar solvents and that it is much less reactive and more stable than its saturated analog, cyclopropanone. This study deduced that cyclopropenone had been synthesized and implied that the isolation problem was due only to the tendency of the product to polymerize. Based on our previous work on cyclopropanone and the reactivity statements of this paper,[76] we reasoned that cyclopropenone would most certainly be stable enough for cryogenic mass spectrometric analysis once it was separated from solution. Since it could be extracted, the obvious approach

was to find a polar solvent which would allow separation of the ketone at a low enough temperature to prevent polymerization. This attack on the problem is discussed more fully and the results are reported in this thesis.

cy-C_3H_4

Cyclopropene, as one of the most reactive of olefins, was investigated for a number of reasons. The reactivity of this molecule is such that it is stable indefinitely at liquid nitrogen temperatures, polymerizes slowly at dry ice-acetone temperatures, polymerizes readily at -36°, and can be kept in carbon tetrachloride solution at -10° but not at room temperature[63]. It has also been reported to polymerize with explosive violence at room temperature[71]. This species was investigated mass spectrometrically at a sufficiently low temperature (-140°) that one could reasonably assume the molecule to be in a stable ground state. The results were then compared to similar ms data obtained at room temperature on the reacting species in an undefined state. A transformation in state or structure caused by warming from -140° to room temperature may be energetically detectable by this mass spectrometric study. Such a finding, of course, would invalidate a large number of experimental data obtained at room temperature. The energetics and strain energy of this molecule would complement the data on other cyclic molecules and provide a base for the study of the energetics of cyclopropenone.

A review of the literature on cyclopropene through 1963 is available[62]. For cyclopropene and cyclopropene derivatives, this review collects and summarizes the available syntheses, chemical reactions, and physical properties and lists 287 references. The heat of formation has been

calculated from combustion data, and the ring strain has been estimated from various reactions. The only previous appearance potentials reported are for the parent m/e 40 and m/e 39. The structure is known and the polymer has been characterized. These data are also incorporated into the appropriate sections of this thesis.

CHAPTER II

APPARATUS AND EXPERIMENTAL TECHNIQUES

General Cryochemical Techniques

Cryochemistry

Cryochemistry depends upon the adaptation of the common bench techniques of chemistry and unit operations of chemical engineering to low temperatures. The chemistry involves synthesis, analysis, and the determination of physical and chemical properties. The chemical engineering consists of designing systems for low temperature use which includes reactors, transfer lines, purifications, and special materials. Although, in this work, the systems were designed for use with a time-of-flight (T-O-F) mass spectrometer, the following remarks clearly apply to other means of identification.

The design of a system is, in most cases, severely restrained by the thermal sensitivity and stability of the species to be studied. Warming can cause a low temperature molecule to lose its original identity by several modes of destruction: 1) unimolecular decomposition; 2) unimolecular isomerization or rearrangement to another structure; 3) bimolecular reactions with itself (polymerization); and 4) bimolecular reaction with other species present. Within these modes of destruction, there emerge several possible handling situations: 1) all of the original molecules present in the sample lose their identity and, therefore, there are no original molecules for analysis; 2) most of the original molecules lose their identity leaving an insufficient number of molecules

for successful analysis; 3) only some molecules lose their identity and there remains a sufficient number of original molecules for analysis but products are formed which will interfere with the analysis; 4) only some molecules lose their identity and there remains a sufficient number of original molecules for analysis and no interfering species are formed; and 5) any one of the first four situations with the added possibility of uncontrollable decompositions or reactions leading to explosion or other dangers. Situations 1, 2, 3, and 5 require treatment that allows no warming, i.e., an apparatus that contains provisions for synthesis, transfer, purification, and analysis at low temperatures. Such a low temperature device has been designed, built, and termed "cryogenic reactor-inlet system" by Malone.[103] This apparatus was used in this work and it will be discussed briefly.

Cryogenic Reactor-Inlet System

The cryogenic reactor-inlet system consists of a 10 inch length, seven-eighths inch diameter tube which is reduced to a 15 inch length, one-fourth inch diameter tube. The resistance wire for electrical heating is wound around six inch sections of both tubes and encased in pots that are cooled by circulating liquid nitrogen. The tubes are connected to a header plate and enclosed in a high vacuum casing which allows the inlet system to be attached to the mass spectrometer. Temperatures can be read by thermocouples which are embedded along the tubes and which are also connected to temperature controllers which regulate the heaters to balance the heat drain by the liquid nitrogen and allow the temperature in each pot to be independently thermostated at any temperature from -196° to room temperature. The system can be mechanically moved

such that an extension piece connected to the end of the smaller tube can be positioned whereby the exit channel through the piece makes grazing contact with the electron beam. The large tube serves as a reactor space in which, for example, reactions involving arcs or discharges can be carried out followed by rapid quench on the walls. By controlling the pots at different temperatures a low temperature, one-step, simple, separative distillation can be effected. The smaller tube then serves as a low temperature inlet system providing a refrigerated pathway for the molecule to the point of analysis.

Synthesis Techniques

In this work the distillation and inlet-analysis provisions of the cryogenic reactor-inlet system were used. The reactor provision was not needed as all the reactive molecules studied belonged to situation 4, in which the only problem is in manipulating the molecule in room temperature apparatus quickly enough so that an ample amount of the sample arrives at its destination unaltered. This type of temperature sensitivity allowed us to work with much greater variety and flexibility of apparatus and techniques than to be limited to only reactions adaptable to the reactor provision of the cryogenic reactor-inlet system. The individual syntheses are discussed in later sections in this chapter devoted to each molecule separately.

Storage

Since most of the molecules investigated were very reactive or unstable, these samples had to be stored at low temperatures to preserve the molecule and prevent explosions. The procedure used was to condense the gaseous molecule as a solid at liquid nitrogen temperatures in a

glass trap. The sample trap was then evacuated of all remaining air, sealed from the atmosphere by stopcocks, and kept in a dewar of liquid nitrogen which was replenished as needed. When the sample was to be used, the trap was again evacuated at liquid nitrogen temperatures (in case air had leaked into the trap) and the sample transferred to other apparatus.

Transfer

The rapid transfer to ensure that some of the original molecules arrived at their destination unaltered was accomplished by the following technique: The existing sample in its low temperature trap was attached by a room temperature line (usually glass) to the destination apparatus (which could be another trap, ms inlet system, etc.). With the destination apparatus at room temperature the transfer system was evacuated to nominally 10^{-2} torr. Next the sample trap stopcock was opened and the entire system was evacuated. This procedure prevented condensable gases in the air from being condensed on the cold samples. This is especially important to these water sensitive samples. Next the destination apparatus was cooled to low temperatures. The pumping was arranged so that the system was evacuated through the low temperature region of the destination apparatus. Removal of the liquid nitrogen dewar from the sample trap caused rapid warming and vaporization of the sample which is attracted to the low temperature region of the destination apparatus by high pressure diffusion, condensation, and pumping.

When this type of transfer is made to the cryogenic inlet system, the mass spectrometer is used to "monitor" the process and, hence, any non-condensables in the sample or decomposition products would be detected. This combination of rapid transfer at low pressures worked well in most

cases to prevent polymerization.

Purification

The raw samples were first analyzed using the cryogenic inlet system. After monitored transfer to the inlet system, thermostated at liquid nitrogen temperatures, the raw sample was slowly warmed for ms analysis. From the ms data one could tell what products were present, at what temperature they exerted a detectable vapor pressure, and whether the sample could be analyzed as such or whether it needed further purification. Purification was required when impurities interfered with the analysis, and these were removed by repeated distillations. Such further distillations were done within the inlet system itself by controlling the two pots at different temperatures or by a technique one might call "flash trap-to-trap distillation with mass spectrometric monitoring."

"Flash trap-to-trap distillation with mass spectrometric monitoring" is performed with two traps as shown in Figure 1. The distance of room temperature line through which the molecules had to travel from one trap to the other was one to two feet while the distance of line to the electron beam of the mass spectrometer ranged from three to eight feet. Using the temperature data from the mass spectrometric analysis, two temperatures were chosen for flash distillations. The temperature of the raw sample trap was rapidly changed from -196° to a temperature just below the boiling point of the desired molecule by replacing the dewar of liquid nitrogen by a dewar of another suitable and precooled low temperature coolant. This allowed the more volatile impurities to vaporize and pass through the second trap at room temperature into the vacuum pump. The progress of the distillation could be followed by intermittently opening

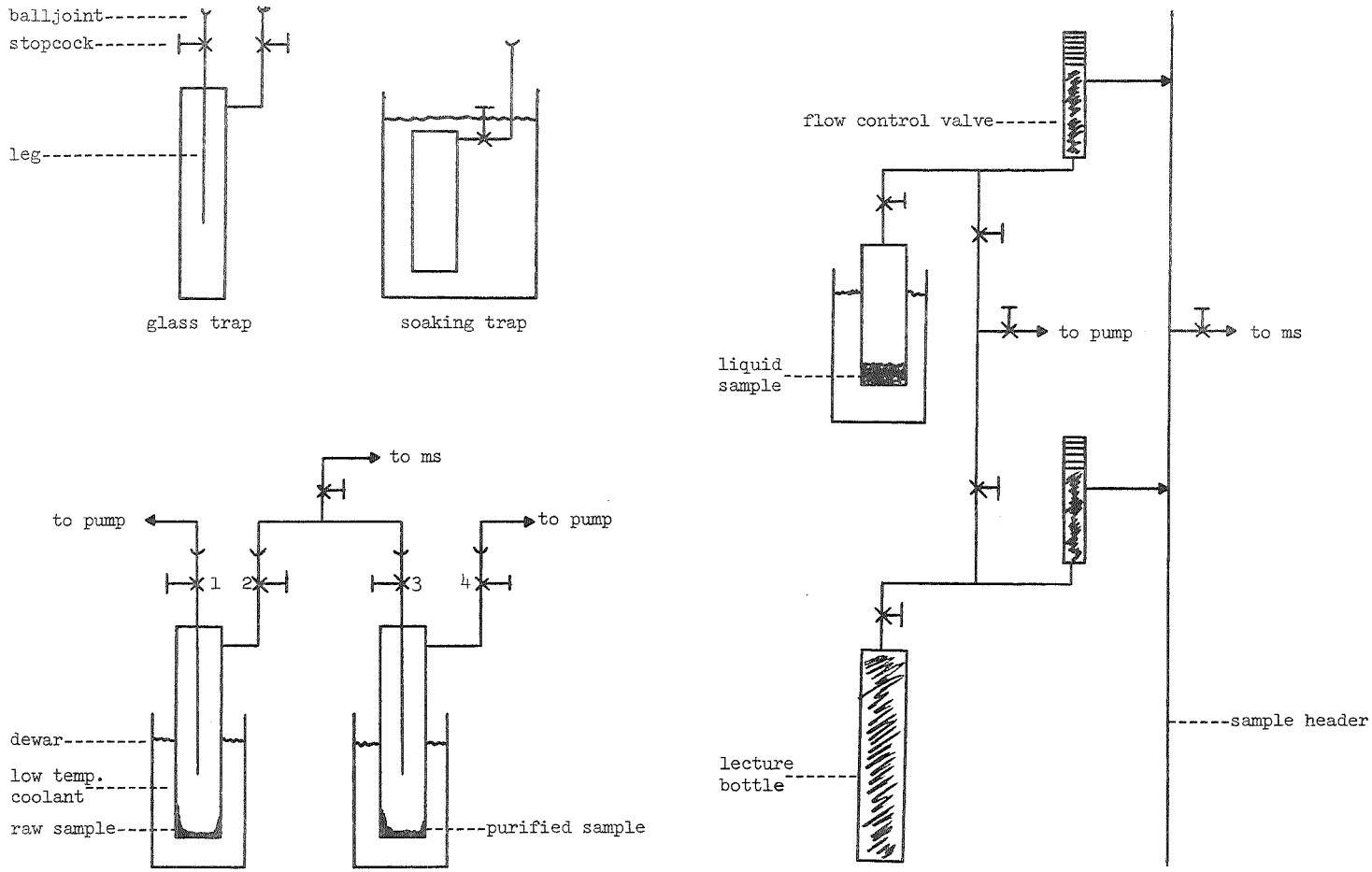

Flash trap-to-trap distillation with ms monitoring

Injection of calibration gases and liquids

Figure 1. General Apparatus and Flow Schematic for Handling, Soaking, Distilling, and Calibrating

the stopcock to the mass spectrometer. The raw sample coolant dewar was then exchanged with another coolant dewar at a temperature which is above the boiling point of the desired molecule and allows the molecule to be flashed off and condensed into the other trap which has been cooled to liquid nitrogen temperatures. The progress of this step could also be checked by the mass spectrometer. When the desired molecule had been collected, the remaining high boiling impurities could be pumped away. This type of distillation not only removed the impurities but, by doing so, also saved much warmup time in the actual analysis experiments.

Techniques for Varying Sample Temperature

The cryogenic inlet system was used to obtain data on molecules at low temperatures. In the following discussions, results from this type of experiment will be termed "low temperature inlet." For some molecules it was desirable to compare data from very low to room temperatures. In several cases, the sample trap connected to the cryogenic inlet was analyzed by warming the trap with a low temperature coolant and instead of condensing the sample in the inlet, the sample was allowed to pass through the inlet system at room temperature and into the mass spectrometer. In this manner the sample, after traveling through the room temperature apparatus and especially the one-sixteenth inch nose piece exit channel, is probably near room temperature. These data are described by "room temperature inlet." Transferring the remainder of the sample into the now cooled inlet system and analyzing provided a means for comparing low temperature and room temperature data. In some analyses, the sample was connected by a room temperature line to the ion source sample inlet line which required the molecules to flow through two feet of

curved one-fourth inch tubing, six inches of one-eighth inch tubing directly into the walls of the ion source reaction chamber, and diffuse out through a one-eighth inch orifice into the electron beam. The molecules must have made many collisions with room temperature walls and were assumed to be at room temperature. These data are referred to as "room temperature line."

Mass Spectrometric Analysis

The T-O-F mass spectrometer, as the principal means of analysis, will be discussed briefly here (see Appendix C for a detailed discussion of excess energy measurement). Molecules in the gas phase are bombarded by a pulsed electron beam to form parent molecular ions and fragment ions. These ions are accelerated down a drift tube whereupon they separate according to their m/e and arrive at an analyzer to produce an electron current reflecting the relative intensities of the various ions formed in the ion source. Ions of different mass arrive at different times and, by recording the output intensity versus time, one obtains a series of peaks each corresponding to a different m/e. This "mass spectrum" can be recorded by directing the output signal into a continuous recorder such as a Visicorder. The energy of the ionizing electron beam is variable between zero and 100 volts. Ionization efficiency (IE) data can be obtained by recording the ion intensity versus electron energy. Previously in this laboratory this recording had been done manually until the adaptation of a Hewlett-Packard model 7001 X-Y recorder to the system.

The X-Y recorder proved to be a very useful addition to the T-O-F mass spectrometric analyzing system. By directing the output ion current and electron energy signals into the X-Y recorder inputs, a continuous,

linear, IE plot of ion current versus electron energy could be recorded in a few minutes. Using the "linear match" or "initial breaks" AP methods (discussed in Appendix B), the AP of a sample ion and calibration ion could be obtained in 10 minutes. The advantages gained by using the X-Y recorder are many and include: 1) the actual time saved in doing an AP was enormous as compared to the previous method of using the Visicorder to collect the data, allowing a great many more measurements per experiment; 2) slowly changing ion output intensities caused by gas flow rates drifting or temperature-vapor pressure changes did not significantly change these rapid IE curves; 3) a quick record of the entire IE curve revealed any unusual problems (such as long-tail ions) and allowed one to choose the best IP technique; 4) quick measurements of IP before experimental difficulties arose would prevent the experiment from being completely useless during the experiments when the sample was "irretrievable"* from the inlet system.

Data

The data obtainable from the cryogenic inlet-mass spectrometer include: 1) mass spectra, 2) IE curves, 3) relative vapor pressure characterizations, and 4) excess energies involved in the electron impact dissociations of molecules. Discussions of instrumental techniques used for obtaining the above data are presented in detail in the appropriate appendix.

Mass spectrometric data require calibrations. The mass peaks of

---

*Once the sample is transferred to the inlet system, it is very difficult to reverse the transfer back to the original container because of the pumping arrangement of the apparatus.

the mass spectrum must be identified as to mass number. The spacing of the mass peaks is directly proportional to the square root of their mass number. Knowing this, a permanent mass scale has been made[103] to fit the Visicorder records. A problem arises because the analog output recording speed changes gradually with time and the mass scale must be periodically adjusted. The marking of low mass numbers is easily obtained by noting the ever present background spectra at m/e 12, 14, 17, 18, 28, and 32. At masses greater than 60, mass marking becomes difficult and above m/e 100 very difficult because the distance between ion peaks becomes very small. This can be overcome by two means: 1) injection of a compound of high molecular weight into the spectrometer, or 2) as in the case of mass spectra of hydrocarbons, at very high ion source partial pressures or high analog sensitivities one can obtain an ion peak for nearly every mass number and simply count them. In obtaining IE data, the energy scale must be calibrated by using a gas for which the IP is accurately known. This was accomplished by: 1) using background molecules; 2) using gases from lecture bottles regulated by a vacuum flow control valve and injected into the ion source sample inlet line; or 3) using vapor (from a liquid whose temperature is thermostated by a coolant) which is also injected into the source sample inlet line. The background and liquid methods were most conveniently used when the intensity of the calibrating gas need not be critically adjusted. The lecture bottle was the best system for adjusting calibrating peak intensities. In obtaining excess energy data it was necessary to calibrate the effect of the analog gate width on peak width for a series of molecules over a range of molecular weights from four to 266. These liquids and lecture bottle gases were injected

into the source in the manner described for IE calibrations as shown in Figure 1.

Absolute vapor pressures were not measured, but the temperatures at which different compounds produced the same ion intensities were compared to give a relative volatility.

Stability of Compound

A logical question to ask about a low temperature compound is by what process is the molecule destroyed and what are the products. The temperature sensitivity of the molecules was studied by exposing the sample to higher temperatures in the following manner. All samples used for these experiments were at least purified of all the impurities which were more volatile than the desired molecule and, if the molecule could survive trap-to-trap distillation, all higher boiling impurities were also removed. The frozen solid, purified sample in a glass soaking trap contained in a dewar of liquid nitrogen was evacuated and then the sample was isolated by closing the stopcocks. The dewar of liquid nitrogen was replaced by another with 2-methylpentane precooled to some desired temperature. The regions of the trap that the sample could reach as a gas were completely submerged in the coolant (see Figure 1). Small samples were used to insure that the trap would not over-pressurize from the vaporized samples. In this manner the trap was "soaked" at a fixed temperature for a definite period of time. The liquid nitrogen dewar was then returned and the sample quenched to -196°. The sample was connected to the mass spectrometer for analysis. Opening the stopcock revealed any gases not condensable at -196°. Slow warming from -196° to the temperature at which the original molecule was observed revealed any volatile

decomposition products of the molecule and also whether the "high" temperature soak had destroyed the molecule. Visual observations helped determine if and how much polymerization had taken place. By doing this at a series of temperatures, the nature and degree of reactivity of the molecule could be studied. Once a temperature was reached which completely destroyed the molecule, higher boiling products such as polymers could be investigated. Thus, starting with a trapped sample of the reactive molecule, the contents of which were known by previous analysis, this temperature soaking experiment would determine: 1) at what temperatures significant destruction of the molecule takes place; 2) if it decomposes, what the decomposition products are; and 3) if it reacts, what the reaction products are.

In the discussion of results of this work, mention is also made of other possible factors that affect the stability of the molecules such as metal versus glass environment and exposure to water, air, etc.

These experiments, in revealing the reactive nature of these molecules, necessarily dictate the handling techniques required for future work.

Polymer Study

In many cases the temperature soakings revealed polymeric residues. Little characterization was done on these polymers but they were heated in their traps to approximately 300° and simultaneously monitored with the mass spectrometer to determine their temperature stability and nature of decomposition. Comments on the solubilities of these residues came as a direct result of trying to clean the traps.

Theoretical Calculations

The application of molecular orbital theory is discussed in detail in Appendix D.

Individual Ring Molecules

cy-C_3H_6

Cyclopropane was purchased from Matheson Corporation, and it had a 99.0 percent minimum purity guarantee. This gas was used as received and all ionization and appearance potential work was done at room temperature. The lecture bottle was connected to the ion source sample tube by tygon tubing and the gas flow rate was controlled by a high vacuum flow control micrometer valve. About 10 different experiments were needed to obtain IE and mass spectral data.

cy-C_3H_4O

Preparation of Reagents. Ketene was prepared by the pyrolysis of acetone on a heated filament by a process that we will discuss here briefly. A coiled, nichrome filament (0.0253 gage; 10 ohms) was suspended from two terminals in the neck of a 500 ml reflux flask. This flask was equipped with a heating mantel, a gaseous nitrogen inlet tube, and a spiral, water cooled, reflux condenser which led to a processing train of two traps, all of which was evacuated by a mechanical vacuum pump attached to the last trap. Acetone was added to the flask and heated until a steady reflux was obtained, and the vapor was thereby pyrolyzed over the filament. The pyrolysis products escaped into the processing train where the first trap condensed unreacted acetone and the second trap was maintained at liquid nitrogen temperatures. Improved ketene yields were produced by

a very dull red (barely visible) filament and shorter filament contact times obtained by continuously flushing the apparatus with gaseous N_2. The apparatus was run about 380 torr pressure and the optimum temperature of the first trap was around -60°. These raw samples were mass spectrometrically analyzed and consisted mainly of ethylene (-180°),* ketene (-145°),* and acetone (-90°)* with traces of methane (-190°),* propane (-150°),* and formaldehyde (-150°).* The raw samples were purified by flash trap-to-trap distillations and the pure ketene was identified by its mass spectrum and IP. In this manner, a six hour pyrolysis yielded five to 10 ml of pure ketene which was stored in liquid nitrogen. Ketene was prepared and reacted in great excess of diazomethane. Excess ketene was continually recovered from the reactions, restored, and reused in subsequent reactions.

Diazomethane was prepared by the reaction of 7.1 gm of bis(N-methyl-N-nitroso) teraphthalamide** with 20 ml of NaOH (20 percent by weight) in 50 ml of carbeitol (2,2′-oxydiethanol) and 200 ml of diglyme (bis(2-methoxyethyl)ether) in a stirred flask which allowed the volatile vapors to escape through a water cooled condenser and then pass into a liquid nitrogen cooled trap. The ethers and NaOH were added to the flask and cooled to zero degrees at which time the solid amide was added and dissolved. Upon heating with a water bath to 30°, the flask contents turn from a clear, yellow-green solution to a yellow solution with white

---

*These temperatures represent the temperature at which the compound exerts a ms detectable vapor pressure.

**This compound is available under the trade name EXR-101 from E. I. duPont de Nemours & Company, Inc.

caking precipitate in about 15 minutes. The original synthesis calls for continued heating to distill the product into the receiving trap, but this resulted in impure yields. Much quicker and more cleancut methods were used. One method was to cool the flask back to zero degrees after the reaction was complete and then to sweep the diazomethane out with gaseous nitrogen. Another method was to use only 100 ml of diglyme which allowed diazomethane to escape readily from the solution at 30°. The former method takes about 90 minutes and the latter about 30 minutes, and both products were much purer than before. The latter method allowed some reaction at zero degrees while dissolving the amide and it was not used due to the possible danger of handling the apparatus with gaseous diazomethane being evolved. The synthesis and handling of diazomethane are easy to follow since its yellow color can be seen in solution and in the vapor phase. Diazomethane is known to explode upon contact with rough surfaces, etc., and precaution was taken. About 20 samples were prepared without any problems, but then a sample exploded during a simple transfer to another trap. This transfer involved distilling diazomethane from one liquid nitrogen trap to another by removing the liquid nitrogen and pumping the evolved product from the rapidly warming trap over into the receiving trap. The explosion was witnessed, and it was evidently caused by the liquid diazomethane super heating; when it finally bumped, it exploded. The explosion was not like a deep thud but more like a sharp crack, and it occurred with much force. The raw samples were analyzed mass spectrometrically and found to consist of mostly diazomethane (-145°) and small amounts of ethylene (-180°), carbon dioxide (-150°), and ether (-50°). These samples were quite easily purified by flash trap-

to-trap distillation. Diazomethane was identified by its mass spectrum and IP. It was noted that analysis via the metal inlet system led to about 50 percent decomposition of the product as indicated by the increase in ethylene and nitrogen. By lining the inlet system with glass, this decomposition was lowered to 10 percent and, thereafter, diazomethane was always handled in glassware. In this manner, a milliliter or so of pure diazomethane was obtained from the indicated amounts of starting materials.

Reaction and Analysis. The reaction of diazomethane and ketene was carried out in a cooled, evacuated trap by arranging, at liquid nitrogen temperatures, a yellow solid ring of diazomethane above a white solid ring of ketene (preferrably an excess of at least fivefold ketene). Upon plunging the trap into a dewar held at -150°, the yellow solid diazomethane became a viscous liquid which slowly ran down into and reacted with the now also liquid ketene producing a white solid and a volatile gas. The reaction was monitored by the mass spectrometer and the volatile gas was identified as nitrogen. The excess ketene was removed by warming to -120°. The raw sample was quickly transferred to the cryogenic inlet system for low temperature analysis which detected two major product masses of m/e 56 and 70, analyzed at -90° and -70°, respectively. These samples could not be purified by flash trap-to-trap distillation as product mass 56 was quickly destroyed by room temperature warming. With this rough knowledge of the reaction products, a series of experiments was designed to reveal the properties of the products. The starting point for each experiment was the product in a sample trap at liquid nitrogen temperature after the removal of excess reactant ketene.

The low temperature mass spectrometric properties of the two

product masses were obtained by transferring the sample to the cryogenic inlet system. The low temperature distillation provision was available for purifying only a few of the initial samples as an irrepairable vacuum leak between the sample tube and the refrigerant space of the high temperature pot occurred and prevented the circulation of liquid nitrogen in this pot. Nevertheless, by simply using low temperature warming, a purity of about 90 percent of m/e 56 (estimated from heights of most abundant peaks) and > 95 percent of m/e 70 at -90° and -70°, respectively, were obtained. Under these conditions, the mass spectra, AP, and excess energies of both products were measured. In addition to these low temperature analyses, we attempted the identical measurements on the products 56 and 70 by injecting the reaction products into the ion source via a "room temperature line." This proved to be a very inefficient process as it appeared that at least 95 percent of m/e 56 was left behind on the walls of the trap as a polymer. However, it was possible to obtain some data and these are reported. With the samples prepared to the starting point discussed above, the temperature stability and polymer formation were studied by the techniques discussed previously in the general section "Stability of Compound."

Although product m/e 56 could be completely destroyed by room temperature warming, product m/e 70 was thermally stable. A pure sample of mass 70 could therefore be obtained by allowing mass 56 to polymerize at room temperature. In this manner, the measurements on product m/e 70 could be obtained on a pure sample. Product mass 70 was identified as cyclobutanone by a comparison of the mass spectra and IP data taken for it at -70° with the equivalent data obtained for an authentic sample of

cyclobutanone* in identical low temperature, cryogenic inlet, experiments. To obtain data which required and involved difficult experimental techniques, some of the data reported here were obtained using the authentic cyclobutanone.

cy-C_3H_4

The method of preparing cyclopropene was essentially that of Closs and Krantz[64] with the modifications of Bell.[72] Since the apparatus and procedure are discussed in detail in these two references, this description of the synthesis will be brief. The apparatus consisted of a three necked, stirred, reaction flask heated by a stirred water bath and fitted with a nitrogen inlet tube, an addition funnel, and an ice water jacketed condenser which was connected by assorted glassware to a processing train of a 2 N sulfuric acid gas wash bubbler followed by a liquid nitrogen cooled product condensing trap all of which was evacuated by pumping through the condensing trap by a Duo Seal mechanical pump. The synthesis of cyclopropene occurs from the ring forming reaction of allyl chloride with sodium amide:

$$CH_2CHCH_2Cl + NaNH_2 \xrightarrow[\text{3) 380 Torr}]{\text{1) mineral oil solvent; 2) 77°C}} \triangle\uparrow$$

Allyl chloride is added very slowly dropwise to a heated, stirred solution of mineral oil and sodium amide. The unstable cyclopropene is evolved as a gas, and it (along with other volatile impurities) is quickly swept along by dry nitrogen gas to the product trap. Cyclopropene begins to

*Obtained commercially from K & K Laboratories, Plainview, New York, #3906.

polymerize at -80°, so the product trap was stored at liquid nitrogen temperatures. Because of the polymerization problem, all transfers of the sample were made as quickly as possible. The above synthesis yielded a condensed product of about 10 percent cyclopropene purity. These raw samples were purified by the "flash trap-to-trap distillation" technique and gave a quite pure product. Six independent preparations of the raw cyclopropene product were made. From each, depending on its amount and purity, several pure samples of cyclopropene could be extracted. Cyclopropene was investigated both at -140° (the temperature when its vapor pressure is about 10^{-2} torr) using the low temperature inlet apparatus and at room temperature. Its temperature stability and polymer formation were studied by the techniques discussed earlier.

cy-C_3H_2O

Reagent Preparations. The earlier reported synthesis of cyclopropenone[76] consists of the reaction of tetrachlorocyclopropene with two equivalents of tri-N-butyltin hydride at room temperature in paraffin oil to produce a volatile mixture of mono, di, and trichlorocyclopropene which, when taken up in CCl_4 and hydrolyzed with cold water, gives an aqueous phase solution of cyclopropenone. Tetracyclopropenone was prepared by the reaction of KOH and pentachlorocyclopropane which, in turn, was prepared from the reaction of trichloroethylene and trichlorosodium acetate. The tin hydride was prepared from the reaction of tri-N-butyltin chloride and lithium aluminum hydride and the entire synthesis scheme is summarized as follows:

$$CHClCCl_2 + Na^+CCl_3CO_3^- \xrightarrow[\text{3) separate and wash; 4) vacuum distill}]{\text{1) } CH_3OCH_2CH_2OCH_3 \text{ solution; 2) } 80^\circ \text{ for 2.5 days}}$$

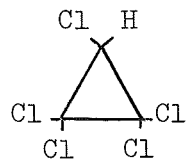

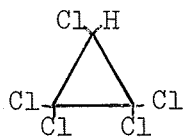

$$+ KOH \xrightarrow[\text{3) HCl; 4) separate and distill}]{\text{1) water solutions; 2) } 100^\circ \text{ for 30 min}}$$

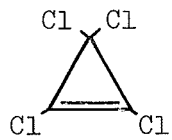

$$(H_3CCH_2CH_2CH_2)_3SnCl \xrightarrow[\text{4) water; 5) separate and dry; 6) distill}]{\text{1) ether solution; 2) } LiAlH_4 \text{; 3) } 25^\circ \text{ for 3 hours}} (H_3CCH_2CH_2CH_2)_3SnH$$

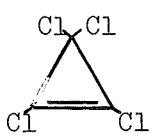

$$\xrightarrow[\text{3) } 25^\circ \text{ for 12 hours; 4) distill}]{\text{1) mineral oil solution; 2) } (H_3CCH_2CH_2CH_2)_3SnH}$$

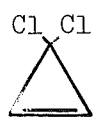

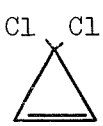

$$\xrightarrow[\text{2) water; 3) separate}]{\text{1) } CCl_4}$$

The procedure for the synthesis of pentachlorocyclopropane was essentially that of West[77] with the modifications of Bell.[73] The distillation product was collected in fractions and identified by mass and infrared spectrometry. The best yield was 11 percent versus the reported 22 percent. This molecule is stable at room temperature and no storage precautions were taken. The tetrachlorocyclopropene procedure was also

a combination of West and Bell with the following modifications. West reports that the reaction takes place in 30 minutes and that cooling is necessary to keep the temperature below 100°. We found that no cooling was necessary as the temperature remained near 25° and resulted in a yield of about 30 percent as compared to the reported 85 percent. By extending the reaction time to three hours with constant shaking, the yield improved to 65 percent. The distilled product originally collected as one product had a purity of 65 percent as compared to a reported 99 percent purity. By collecting the product in fractions, the purest fraction improved to 85 percent tetrachlorocyclopropene and 15 percent pentachlorocyclopropane. The product was identified by mass and infrared spectrometry. This compound is stable at room temperature.

The procedure for the preparation of the tin hydride was essentially that of Kuivila[78] with the modifications of Bell.[73] The yield obtained was 67 percent as compared to the reported 87 percent. Identification was by mass spectrum. Although the hydride is reported[79] to be stable towards water, it reacts with oxygen to form a tin hydroxide precipitate and, consequently, it was stored under argon. When the hydride was used soon after preparation, the yields of dichlorocyclopropene were good. After long standing at room temperature (even under argon), the solution turned cloudy from the white precipitate and resulted in poorer yields of dichlorocyclopropene.

The apparatus[73] for the synthesis of dichlorocyclopropene consisted of a three necked round bottom flask fitted with a dropping funnel, gaseous nitrogen inlet tube, and a neck exiting to a liquid nitrogen trap to which were connected a U-tube manometer and a mechanical vacuum pump.

The optimum procedure[79] was to add 15 grams of the hydride dropwise to a stirred solution of three grams of tetrachlorocyclopropene in 40 ml of paraffin oil which was cooled in an ice water bath. Stirring and reaction was continued overnight and the flask contents were distilled at one torr and room temperature into the receiving trap. The distilled product consisted of a mixture of the mono, di, and trichlorocyclopropenes which was stored at -196° because the products polymerized rapidly at room temperature. This was the starting point for the synthesis of cyclopropenone and various separation experiments.

Synthesis. The first experiment was to reproduce the original synthesis of cyclopropenone by taking up the mixture of chlorocyclopropenes in CCl_4, adding water, and subjecting the CCl_4 and water layers to nmr analysis. When the nmr spectra agreed with that of Breslow,[76] it was concluded that cyclopropenone had been synthesized and the work proceeded to the attempted separation, isolation, and ms analysis.

Separation. The problem was approached with the knowledge that cyclopropenone was only soluble in very polar solvents (such as water) and insoluble in non-polar solvents (such as CCl_4). Its precursor, dichlorocyclopropene, was known to be soluble in non-polar CCl_4 but the extent of its solubility in more polar solvents was not known. The object was to arrive at a final solution which would allow cyclopropenone to be separated from the solvent at a low enough temperature to prevent polymerization. The problem, then, is the choice of a proper solvent and processing scheme.

The prime consideration in the choice of the solvent was the solubility (or non-solubility) of the ketone and water. The solubility of

water and dipole moments of many solvents was obtained from the Handbook of Chemistry and Physics, 45th edition. The solubility of the ketone in these solvents was assumed to increase with increasing dipole moment. There seemed to be only three general "classes" of solvents*: 1) polar and water insoluble; 2) polar and water soluble; and 3) non-polar and water insoluble. Another factor considered for the solvent was the estimated temperature at which the solvent would be observed in the ms experiments. Using these solvents, there are several possible processing schemes available for preparing the final solution which is to be separated by low temperature distillation and mass spectrometrically analyzed. Taking up the dichlorocyclopropene with a non-polar solvent and hydrolyzing with water will yield two phases, one of which is a ketone-water solution. However, using much less than the stoichiometric amount of water should produce one phase, a ketone-solvent-dichlorocyclopropene solution. Further variations include extracting the ketone with polar solvents or drying the solutions to remove water. If the dichlorocyclopropene is taken up in a polar, water insoluble solvent, then the situation is much like the above but with the ketone distributed between the polar solvent and water layers. However, if the dichlorocyclopropene is taken up in a polar, water soluble solvent and hydrolyzed, only one phase can result as the water is soluble. Less than the stoichiometric amount of water can be added to these solvents. From these considerations, there appeared to be only three types of final solutions for low temperature separation: 1) the ketone alone in a solvent (of which water is one

---

*Note that there are no non-polar, water soluble solvents.

possibility); 2) the ketone and dichlorocyclopropene in the same solvent; and 3) the ketone and water in the same solvent.

The factors affecting the choice of solvent and process were then: 1) solubilities; 2) whether or not the solvent would allow the ketone to separate; 3) chemical inertness; and 4) mass spectral interference. The water insoluble, polar solvents seemed to give the most promise and, of those available, methylene and ethylene chlorides were used. Acetonitrile, acetaldehyde, and nitrobenzene* were selected from the water soluble, polar solvents. Carbon tetrachloride and paraffin oil represented the water insoluble, non-polar solvents. It was found that cyclopropenone seemed to be "bound up" with water such that the two were inseparable and always led to polymerization of the ketone. Therefore, later experiments concentrated on using water insoluble solvents and less than the equivalent (designated as drop water) amount of water needed for the reaction. In the course of the experiments, both dichlorocyclopropene and cyclopropenone were found to polymerize quickly, so these experiments consisted of rapid manipulations at room temperature with intermittent liquid nitrogen quenching.

---

*Water is slightly soluble.

CHAPTER III

SYNTHESIS, ANALYSIS, AND STABILITY RESULTS

This chapter is devoted to the presentation and discussion of the most significant chemical results. The raw data for the mass spectra, ionization potentials, and excess energies are presented in Appendices A, B, and C, respectively. Energetics calculated from these results are presented in Chapter IV. It is again more convenient to discuss each molecule separately.

Cyclopropanone

Reaction and Identification

The liquid-liquid reaction of diazomethane with ketene at -145° evolved a gas and produced other products which condensed onto the reactor walls as a white solid. The off gas was passed through the low temperature inlet system at -196° and then directly into the mass spectrometer. The mass spectrum of this non-condensable gas is presented in Figure 10 and shows masses 28 and 14 greatly increased relative to the other masses. It was noted that the ratio of 14 to 28 is about five percent from which we concluded that this gas was nitrogen. However, a rough IP was measured to be around 10.4 eV which is much closer to ethylene (10.6 eV) than to the other possible 28 masses of carbon monoxide (14.0 eV) or nitrogen (15.6 eV). Although the mass spectrum of the off gas usually showed only slight evidence of ethylene, it is quite possible that only a small

amount is sufficient to obscure the higher IP of nitrogen. The rate of gaseous evolution was obtained by measuring the intensities of masses 28 and 14 versus time and is presented in Figure 2. It can be seen that the off gas intensity increases rapidly and linearly until it peaks, at which time it begins to decrease almost as rapidly as it had increased, but it soon slows and approaches an exponential decay rate. The ion source is fed by the off gas and evacuated by a diffusion pump. If the input rate is much larger than the pumpout rate, then the rate of change of ion source intensity (or partial pressure) is equal to the off gas feed rate which is essentially the rate of gaseous evolution from the reaction. If this recorded, increasing, linear rate of change is then an indication of the reaction rate, it would, as such, indicate a concentration independent, zero-order, reaction which we explain as a reaction at the surface of the two meshing liquids. The peak in the curve is then related to the end of the reaction followed by the slower evacuation of the source and reactor space by the diffusion pump whose pumping nature is of exponential form.

The major results of the many samples that were subjected to low temperature analysis with the cryogenic inlet system are summarized in Table 1 and the mass spectra are shown in Figures 8 through 10 (Appendix A). Whenever a large excess of ketene and very pure samples of ketene and diazomethane were used for the reaction, the only products produced were those of m/e 56 and 70 (later identified as cyclopropanone and cyclobutanone), analyzed at -90° and -70°, respectively. In these experiments, it was possible to obtain more than 50 percent purity* of m/e 56 in the total solid

* The purities and product proportions as reported in this thesis were subjective estimations made by the author based on relative ion intensities, the time needed for pumping the sample away, etc.

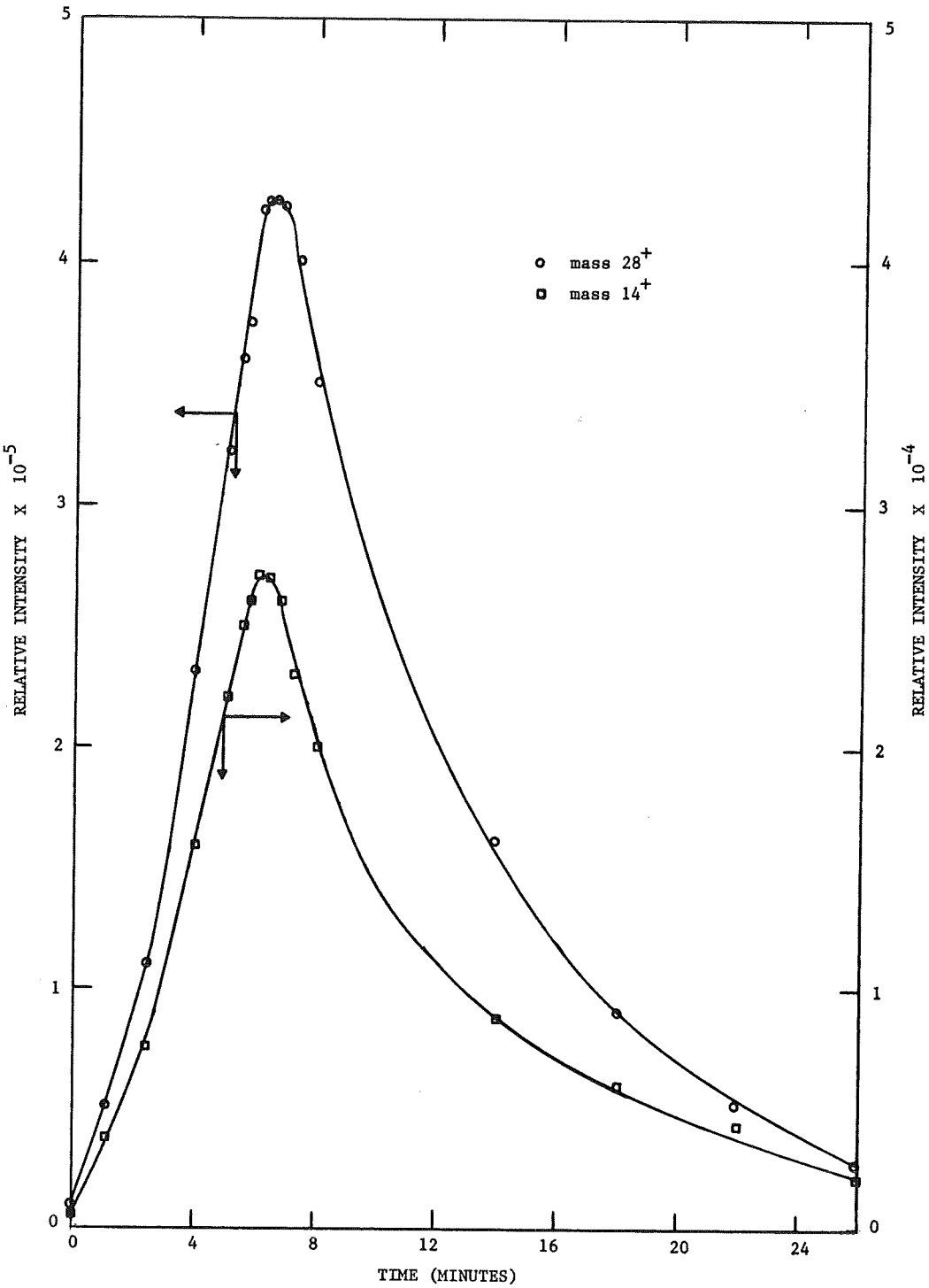

Figure 2. Rate of Gaseous Evolution from Reaction of Ketene and Diazomethane at -145°

Table 1. Mass Spectra of Species Observed in Warming Cyclopropene and Cyclopropanone Raw Products

Compound	MW	Major Peaks- (% of largest m/e)	ms[a] Temp	%[b]	Notes
Cyclopropene synthesis					
carbon dioxide	44	44(100)	-152°	1	c
impurity	42	42(60)41(100)	-145°	1	c
cyclopropene	40	40(60)39(100)	-140°	18	c
CH_2CHCH_2Cl	76	78(10)76(30)42(100)41(5)	-120°	80	c
				100	
Cyclopropanone synthesis					
nitrogen off gas	28	28(100)14(5)			d
excess ketene	42	42(94)41(27)14(100)	-140°		d
cyclopropanone	56	56(15)42(15)28(100)27(40)26(49)	- 90°	50	d
cyclobutanone	70	70(20)42(100)	- 70°	50	d
				100	
diazomethane	42	42(97)28(50)14(100)	-140°		e
ethylene	28	28(100)27(60)26(60)	-170°		e
side product	56	56(100)	-120°		e
side product	56	56,55,....49;42,41,....37	-120°		e
side product	56	56,55,.....,50;39	-130°		e
acetone	58	58(30)43(100)15(30)	- 90°		e
side product	74	74( )57( )	- 80°		e
cyclopentanone	84	84(2)71(1)56(6)43(100)42(50)	- 25°		e

a. temperature at which species first begins to exert a vapor pressure that can be detected by the mass spectrometric apparatus.
b. subjective estimate of product proportions based on peak intensities, pumping speed, etc.
c. percents refer to raw (unpurified) sample.
d. normal reaction; percents refer to raw (unpurified) solid product after ketene removal.
e. impurities and side products.

Table 2. Mass Spectra and AP Identification of Cyclopropane and Cyclopropene

Compound	ms[a] temp	Ion Mass Peaks--% of largest m/e												
		42	41	40	39	38	37	36	28	27	26	15	14	13
cyclopropane	25	100	80	29	65	14	11	3	5	36	16	5	7	3
cyclopropane[38]		100	91	32	70	15				37				
cyclopropane[26]		100	92	30	74	15	11		2	32	13	4	6	
cyclopropene	-140			60	100	36	23	6.8	<5	<2.3	5.7	<0.6	5.7	<2.3
cyclopropene	25			60	100	40	24	6.0	<3.6	<4.8	6.6	<0.9	4.2	<4.7
propyne[73]				100	79	29	20	5						
allene[73]				100	96	40	33	9						
		IP or AP (eV)												
cyclopropane	25	10.3							13.1	13.5	13.1		18.5	
cyclopropane		10.2[27]								13.4[28]	13.1[28]		18.6[b]	
cyclopropene	-140			9.7	10.9									
cyclopropene	25			9.7	10.9					<13.6		<16.0	<15.5	<20.0
cyclopropene[70]				9.95	11.15									
propyne[69]				10.54	12.06									
allene[70]				10.16	12.0									

a. see Table 1
b. average literature value.

Table 3. Mass Spectra Results of Cyclopropene Experiments

Experiment	Ion Mass Peaks--% of largest m/e												
	42	41	40	39	38	37	36	28	27	26	15	14	13
low temp inlet													
T = -150°	1.1	2.8	60	100	36	23	6.8	63.0	2.3	5.7	0.6	5.7	2.3
room temp inlet													
trap temp = -140°	0.6	4.0	58	100	39	23	5.9	3.6	3.3	9.0	0.9	6.6	3.3
trap temp = -130°	3.6	6.0	60	100	39	23	6.0	21.0	5.4	8.3	0.9	4.8	3.0
room temp line													
trap temp = -120°	3.1	6.0	60	100	40	24	6.0	3.6	4.8	6.6	0.9	4.2	4.7
trap temp = - 90°	0.6	3.1	66	100	40	24	4.8	3.6	3.1	6.6	0.6	3.1	1.8

Table 4. Mass Spectra and AP Results of Cyclopropanone Experiments

Compound	Source	ms[a] temp.	Ion Mass Peaks--% of largest m/e														
			70	56	42	41	40	39	38	37	36	29	28	27	26	15	14
cy-C_4H_6O	Lit.[61]	room[d]	30	0	100	9	2	9				7	8	6			
cy-C_4H_6O	exp.[c]	room	25	0	100	11	3	11	4	3	1	1	6	12	7		7
mass 70	exp.[c]	room	24	0	100	11	3	9	3	3	1	2	7	11	6		7
mass 70	exp.[c]	- 70°	20	(3)	100	14		16	5	5	2			12	8		
cy-C_4H_6O	exp.[c]	- 75°	22	0	100	12		14	5	4	2			12	8		
cy-C_3H_4O	Lit.[52]	room[d]	0	18	14								100	38	38		
mass 56	exp.[c]	- 90°	(1)	15	15	5		4	4	4	3		100	35	34		
mass 56	exp.[c]	- 87°	(2)	15	10								100	40	40		
mass 56	exp.[c]	room	(3)	15	5								100	30	25		
mass 56	exp.[c]	heated polymer	0	15	8								100	50	50		
			IP or AP - eV														
cy-C_4H_6O	exp.[c]	- 70°	9.6		10.6								10.6				
mass 70	exp.[c]	- 70°	9.6		10.6								10.8				
cy-C_4H_6O	exp.[c]	room	9.4		11.0								13.3				
mass 70	exp.[c]	room	9.4		11.0								12.7	14.1		15.7	16.7
best value[b] →			9.4		11.0								13.0	14.1		15.7	16.7
mass 56	exp.[c]	- 90°		9.2	9.8 10.2								9.9				
mass 56	exp.[c]	room		9.1	9.9								10.2	12.9	13.5		11.6
best value[b] →				9.1	9.9								10.2	12.9	13.5		11.6

a. see Table 1.
b. author's evaluation of best value to be used for derived energetic calculations.
c. experimental results of this study.
d. assumed temperature.

product. However, when diazomethane was in excess, the reaction product consisted mainly of product mass 70 with little product mass 56 and a new product m/e 84 (which appeared to be cyclopentanone from its mass spectrum). Although the slow diazomethane decomposition in glassware to form ethylene and nitrogen did not prove troublesome, its rapid decomposition in metal systems did. In one experiment, the reactants were transferred into the metal inlet system and condensed one on top of the other. Warm up of the products did not reveal much cyclopropanone or cyclobutanone but a new product m/e 56 at -130° and possibly a new product at m/e 42. It is very conceivable that diazomethane reacted with ethylene (from diazomethane decomposition) to form cyclopropane (m/e 42) and then with cyclopropane to form cyclobutane (m/e 56). Note that these same results could occur from ethylene impurities in either reagent. At times acetone was detected during analysis but it was not concluded whether it had been in the ketene sample, was a reaction product, or had remained as a residue from cleaning the glassware. In a few other experiments there were unidentified m/e 56 parents appearing at very low temperatures (-130° to -120°). Since the mass spectra of these parents consisted of groups of ion masses differing by masses of 1 and 14 within and between groups, respectively, they would appear to be hydrocarbons boiling at a lower temperature than the more polar cyclopropanone. However, it is interesting to inject the possibility of allene oxide which would occur from the attack of methylene on the double bond of oxygen rather than carbon as:

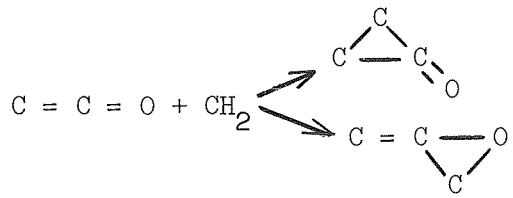

Allene oxide has been postulated as an alternate intermediate structure to cyclopropanone for many reactions and, as yet, it has not been isolated. One would expect its mass spectrum to consist of peaks 56, 42 (allene), 28-26, 16 and 14. Since ketene (m/e 42) is also present at -130°, it was impossible to conclude anything about such a molecule. Also, by using pure reagents and excess ketene, all these other products were eliminated. Furthermore, methylene would have to be known to add to the carbonyl group to support this sort of argument.

Since masses 56 and 70 have the same fragment ions, it was desirable to separate them as much as possible before attempting to collect energy data on the individual fragment ions. But since m/e 56 was destroyed by room temperature trap-to-trap distillation, the separation was performed within the cryogenic inlet system. Although, at these pressures, the molecules appear to boil 20° apart, it was not possible to completely separate the two by simple distillation. The best obtainable separation yielded a product containing about 90 percent of the mass spectrum being from cyclopropanone. This separation problem may result from the two molecules forming a solution but is also because cyclopropanone must be heated past the temperature at which it just appears if one is to obtain enough ion intensity for the energetic measurements. On the other hand, it was possible to remove essentially all the cyclopropanone from the cyclobutanone experiments by either pumping it away or by isolating the trap and letting it warm to polymerize all the cyclopropanone (see comments on stability). Therefore, it was possible to obtain data for product cyclobutanone when only cyclobutanone was present. For this reason, these data

reported for cyclobutanone are not subject to interference problems from cyclopropanone. The interference problems which result from having both ketones (and also air) present during the collection of data on cyclopropanone may or may not be important as each situation must be considered individually. The mass spectra are easily corrected by subtracting out the contributions from cyclobutanone and air. It was found that all the AP of fragments from cyclobutanone were higher than the AP of the same fragments from cyclopropanone and, hence, minor fragment contributions from the butanone did not interfere in the AP measurements on the cyclopropanone fragments. However, these interfering contributions had a much more significant effect on the measured excess energy peak widths (refer to Appendices A, B, and C).

Masses 56 and 70 were analyzed at both low temperatures and room temperature by the techniques discussed previously. The summarized mass spectra and AP data are presented in Table 4 along with the corresponding data for authentic samples of cyclobutanone and any available literature data. From Table 4 many observations can be made. Our results show that the cyclobutanone and product m/e 70 molecules reveal nearly identical mass spectra whether they be measured at -70° or at room temperature and that the I(70) and A(42) for both molecules are nearly identical. Product mass 70 was thus determined to be cyclobutanone formed by the insertion of methylene into the cyclopropanone ring. Since cyclobutanone is a thermally stable compound, data on it were taken at any convenient temperature. The mass spectra of m/e 56 at -90° and room temperature agree well with that reported in the literature. These spectra are exactly what one would predict of this molecule if, as is reported, the species decompose

to carbon monoxide and ethylene upon formation in the gas phase: namely, large peaks at masses 28, 27, 26. The IP of mass 56 is quite low (9.1 eV) as it is, in general, for ring molecules. Note that this IP for cyclopropanone is more than one eV lower than that (10.25 eV)[102] for its open chain isomer, acrolein. This is explained by an increased ground state energy of cyclopropanone relative to acrolein and a decreased molecular ion energy due to the ability of the electronegative ring to accomodate the positive charge. Also, the A(42) = 9.9 eV and A(28) = 10.2 eV are very low, in fact, lower than the $I(C_2H_4)$ = 10.6 eV itself. This is to be expected from a strained ring compound which has very weak ring bonds (needs little energy to break) and which can form new stable bonds upon fragmentation (release energy).

It is sometimes possible to estimate the normal boiling point of a molecule by plotting, for a series of analogous molecules, the molecular weight versus the reciprocal absolute temperature. In Figure 3 this is done for the 7, 6, 5, and 4 C-membered cyclic ketones and 3-C acetone and extrapolated to give the normal boiling point of cyclopropanone as about 60° which is about 40° lower than cyclobutanone. It would seem that this sort of empiricism is based on an assumed constant polarity among the group, but since polarity is not constant, one expects the boiling point of cyclopropanone to be somewhat different than estimated here. Also, shown in Figure 3 are the normal boiling points for a series of ring hydrocarbons. If the same relative volatility is even only approximately true at low temperatures one would expect cyclopropanone to be observed at approximately the same temperature as acetone (-95°) and any

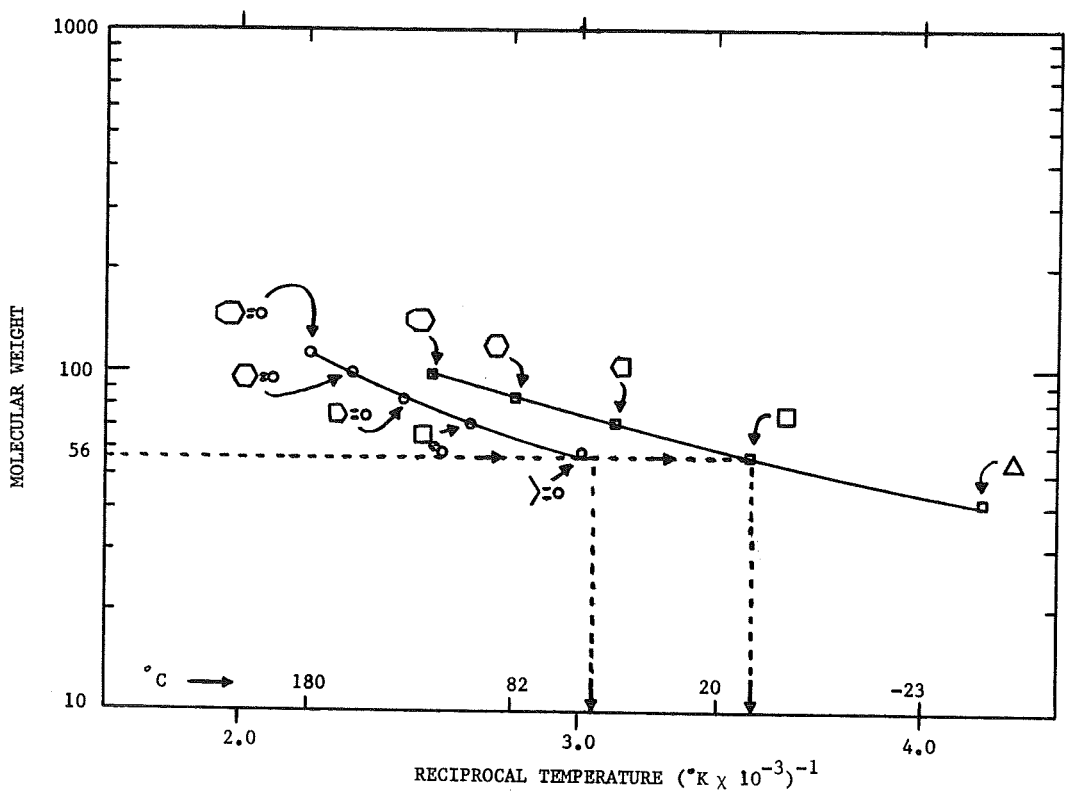

Figure 3. Estimation of Normal Boiling Point of Cyclopropanone

hydrocarbon at m/e 56 should be expected to appear at -40° to -50° lower than that. Considering all the evidence (including the fact that mass 56 will polymerize at temperatures as low as -90°), mass 56 was concluded to be cyclopropanone.

Temperature Sensitivity and Stability

To test the possibility that, with increasing temperature, the cyclopropanone ring might exist as an excited triplet, or open up to form a dipolar ion, or rearrange to some other isomer, the mass spectra and IP were compared at -90° and 25° but no significant differences were found. Molecular orbital[21] calculations have predicted that the open dipolar ion has a ground state triplet which is 23 kcal/mole lower in energy than the closed ring. This difference should be reflected in the IP, and it would be easily observed. However, as the IP of cyclopropanone at -90° and 25° differed at most by no more than five kcal/mole, we can conclude that no such change in structure occurs upon warming.

Although the mass spectra at 25° showed no increase in the ethylene-CO masses relative to the mass spectra at -90°, further experiments were necessary to determine the temperature sensitivity and stability. It was noted that most all of the previous samples had left some polymer around the ringed reaction surface of the trap when they were transferred to the inlet system which could have either been formed during the reaction at a "hot" spot or during the warming to transfer. In any event, the polymerization probably did not take place at -140° but at some higher temperature. Also, in the previously discussed room temperature experiments for obtaining mass spectra, about 95 percent of the original cyclopropanone

was left behind as a polymer and an amount of sample equivalent to that which lasted six hours at -90° lasted only 30 minutes at room temperature. A flow pyrolysis experiment to determine thermal decomposition would be complicated as it would be difficult to tell whether a change in spectra with temperature was the result of decomposition before or after the electron collision. Also, the AP of CH_2CO and C_2H_4 from cyclopropanone are numerically very close to their IP, and one could not distinguish, energetically, the source of these m/e. We decided to study the thermal decomposition of cyclopropanone into the possible ethylene, carbon monoxide, ketene, and methylene products and also its polymer formation by heating isolated samples at constant temperature, quenching, and then analyzing. Cyclopropanone was subjected to a series of these temperature "soakings" from -196° to room temperature. Quenching to -196° and rewarming these samples revealed any ring decomposition products and the status of m/e 56. Visual observations revealed polymer formation. It was found that cyclopropanone could be stored for weeks at -196° with no decomposition or any apparent polymerization. A 30 minute soak at -90° revealed no decomposition but some polymerization. A 60 minute room temperature soak completely destroyed cyclopropanone and revealed polymer formation but no evidence for decomposition. In all of the experiments, the polymer was concentrated about the surface where the white reaction product solid had originally condensed out in a ring.

Stability Discussion

Analysis of the data from the initial cyclopropanone experiments had led us to suspect the molecule was decomposing before electron impact

into ethylene (m/e=28), carbon monoxide (m/e=28), and ketene (m/e=42). The mass spectrum of cyclopropanone contains very intense m/e=28, 27, 26 peaks which are the same peaks as a mixture of carbon monoxide and ethylene would give. The appearance potentials of m/e 42 and 28 in the cyclopropanone spectrum were measured at 9.9 and 10.2 eV, respectively, and were quite close to the ionization potentials of ketene (9.6 eV) and ethylene (10.6 eV). Furthermore, cyclopropanone decomposes upon formation in the gas phase to ethylene and CO. Our subsequent experiments revealed that, even if some of m/e 56 decomposed, a significant amount remains intact and that the amount of decomposition at -90° and room temperature has to be the same as the mass spectra are quite similar. This hardly seems possible not only because of the temperature difference but also because of the different ways the samples are injected into the source. Also, it was shown that cyclopropanone does not decompose (in glassware) from -196° to room temperature. The only other possibilities are the decomposition on the metal walls of the ion source or thermal decomposition on the hot filament in the ion source. Again, the consistency of mass spectra and the introduction of the sample into the electron beam via the cryogenic inlet nosepiece would seem to rule out these possibilities. Note that the AP of any of the cyclopropanone fragment ions cannot be any lower than its IP, 9.1 eV, and that, if the AP of m/e 42 and 28 are higher than reported here, both would lead to less ring strain as discussed in Chapter IV. Although stable indefinitely as a solid, cyclopropanone was found to begin to polymerize at temperatures down to -90°. Since all the polymer product was localized where the frozen solid had been and began at a

temperature where it exerts a detectable vapor pressure, it was concluded that it begins to polymerize when it becomes a mobile liquid. This does not mean that it will not polymerize as a gas but that, in these experiments, it polymerized before much of it could become a gas. Cyclopropanone should always be transferred and handled very quickly within room temperature apparatus. This molecule appeared more reactive than cyclopropene (to be discussed).

Polymer

The polymer was a white, porous-looking, solid which, when heated to 200°, proved to be thermally unstable. The first product observed upon heating was m/e 56 (see Figure 9) which was interpreted as trapped cyclopropanone and not as polymer decomposition. Then heavier, but unidentified, peaks (m/e=58, 57, 56, 74, 73) were observed. The polymer was soluble in benzene, slightly soluble in gasoline, and insoluble in acetone, alcohol, and water.

Comments on the Low Temperature Reaction

The liquid-liquid reaction of diazomethane with ketene has many interesting facets. In the strict sense of the word, diazomethane is one of the few truly cryochemical reagents as it reacts rapidly at -145° without any external source of activation. This phenomenon may be due to the generation of very reactive methylene which attacks electronegative double bonds and strained ring bonds.

The liquid phase reaction was made possible by the close melting points of diazomethane (-145°) and ketene (-151°). Taking advantage of this enabled us to avoid a solution reaction and to obtain pure, isolated

products. It also enabled us to provide a low temperature quench for the initial reaction product, cyclopropanone. This quench removes the heat of reaction and prevents the cyclopropanone ring from decomposing due to the exothermic heat of reaction as cyclopropanone does upon formation in the gas phase. The low temperature also helps to restrict cyclopropanone from further reacting with diazomethane to form cyclobutanone and to prevent it from polymerizing. For one thing, at -145° cyclopropanone is present as a frozen solid which is less mobile and which probably has a higher activation energy for its loss processes. Also the lower temperature kinetically slows any reaction rate.

For good yields of cyclopropanone, one must have pure reagents and an excess of ketene of at least fivefold. Methylene will react with molecules containing double bonds or rings and thus one must allow it to "see" as much ketene and as little of other possible reaction partners as possible.

Cyclopropane

Table 2 summarizes the experimental mass spectra and IP from this work and from the literature for identification of cyclopropane. During the experiments on cyclopropane, there was no evidence of instability, ring opening, or polymerization. The energetics of cyclopropane are discussed in Chapter IV.

Cyclopropene

The raw cyclopropene product (the gas evolved from the reaction and quenched in a liquid nitrogen trap) was warmed slowly from -196° to room temperature and analyzed mass spectrometrically. Table 1 shows the

the compounds present, their major mass peaks, the approximate sample product proportions, and the temperature at which they exert a mass spectrometrically detectable vapor pressure. The product proportion of cyclopropene was at most a poor 20 percent and this necessitated a great deal of "flash trap-to-trap distillation." Repeated distillations completely removed carbon dioxide and allyl chloride but, because their vapor pressures were so similar, it was impossible to completely remove the impurity at mass 42 (identity unknown). The raw samples could have been transferred directly to the low temperature inlet system and warmed slowly to effect the purification and analysis. Doing the purification in the low temperature inlet system proved inconvenient as it greatly prolonged the length of the experiment, and the adsorption properties of allyl chloride on the surfaces of the spectrometer were such that it required three days of pumping to clean it from the background.

Table 3 lists the mass spectra of purified cyclopropene samples both from low temperature and room temperature experiments. Each experiment represents a different sample so the relative amounts of impurities change. These changes (ion intensity variations) can also be due to the temperature-vapor pressure relations for the sample mixture. An analysis of this variation in impurity intensity leads to the following points of interest (mass 28 intensity fluctuations are caused by background nitrogen and will be omitted from discussion). Increasing and decreasing ion intensities at m/e 42 and 41 are accompanied by similar significant changes in masses 27, 15 and 13 and some changes in m/e 26 and 14. This means that, although the amount of impurities 42 and 41 may be reduced to as

low as one to three percent of m/e 39, fragment ions produced from m/e 42 and 41 can have a very significant effect on the same fragment ions produced from cyclopropene because of the very low abundance of these cyclopropene fragment ions. In other words, these ions from cyclopropene that have weak signals also appear to have been produced from the impurities present and the source of these ions cannot be ascribed only to cyclopropene. As will be discussed later in this thesis, these interference problems led to unreliable AP measurements.

Table 2 confirms the identification of cyclopropene. Its mass spectrum with $C_3H_3^+$ as the largest peak distinguishes it from its only isomers, propyne and allene. The I(cy-C_3H_4) from this work is slightly lower than the reported value (9.6-9.7 eV versus 9.95 eV). Any energetic differences (0.3 eV~6 kcal) in I(cy-C_3H_4) in our work and the literature values are too small to be explained in terms of ring isomerization energy or ring strain. The strain energy is about 54 kcal/mole and the energy of isomerization to propyne is 22 kcal/mole. The MO calculations presented in Appendix D predict the IP of the lowest triplet as 1.6 eV lower than the ground state IP. If the abundance of this triplet was as high as 25 percent in a mixture of singlet and triplet, this would lead to about a 0.5 eV lowering of the IP. There was a 0.5 eV scatter in the measured IP but the scatter could not be attributed to a temperature effect. It must be concluded that, if cyclopropene changes structure upon warming, then either: (1) the IP of the new structure is very nearly that of ground state cyclopropene or (2) the new structure is present only in very small quantities. We believe that IP difference with the literature

value is reasonable in view of the amount of scatter in the data and, in general, the poor agreement among workers studying IP by electron impact techniques. Furthermore, neither the appearance potentials nor the mass spectra indicate any change in structure.

Previous work[63] on cyclopropene reports that the molecule is stable indefinitely at liquid nitrogen temperatures, reacts slowly at -80°, and reacts so rapidly at its normal boiling point, -36°, that most of it is lost to the polymer. The polymer has been characterized as

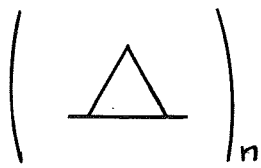

It has also been reported to explode violently at room temperature[71]. From soaking the sample at a series of temperatures from -196° to room temperature, we found no volatile decomposition products but a polymer which was only noticeably formed at about room temperature. In fact, a one-week room temperature exposure destroyed most, but still not quite all, of the molecule. Analysis of this sample showed not only the polymer but some compound of molecular weight 80 which is believed to be the dimer. Workers[71] have found that, in dilute methylene chloride solutions at -25°, a good yield of the dimer is produced. The dimer has been characterized[71] as

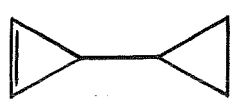

Note that this requires the migration of a H atom. This species was not investigated in this work as the mass spectrometer was too limited for separating and analyzing the above versus another likely isomer below:

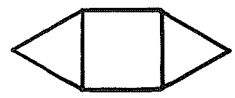

We found no evidence of explosion and it is difficult to see what would cause one. This compound was found much more stable and easier to handle than would be expected from the literature. It is quite possible that sealing the soaked sample from the atmosphere prevents water or oxygen from initiating the chain reaction proposed polymerization mechanism. Also, the low trap pressure may help keep the polymerization rate slow and the polymerization may not be as evident with these small samples. In any case, the molecule can be easily worked with as aforesaid.

Since the polymer was not noticed until temperatures at which the molecule is vaporized, the polymerization may occur in the gas phase.

At room temperature the polymer appeared to be a white, waxy, solid which smears upon contact. The polymer was heated to near 300° and remained stable as mass spectrometric monitoring revealed no decomposition gaseous evolution. The polymer was soluble in benzene, slightly soluble in gasoline, and insoluble in acetone, methanol, and water.

Cyclopropenone

Verification of Literature Synthesis

Our initial attempt to reproduce the Breslow synthesis[76] was roughly done and resulted in poor yields and many impurities. However,

nmr evidence for the 3, 3 dichlorocyclopropene and the ketone were found. Although the CCl_4 solution (before hydrolysis) contained signals for 3, 3 and 1, 3 dichlorocyclopropene at $\delta = 8.0$, $\delta = 7.2$, and 4.5, respectively, the major portion of the nmr spectrum was due to unidentified impurities at about $\delta = 3.3$ and 1.2. After the hydrolysis, the CCl_4 layer revealed no 1, 3 and 3, 3 dichlorocyclopropene signals, but retained all the impurity signals. The D_2O layer from the hydrolysis contained new signals at $\delta = 9.1$ and 5.1. The former signal was identified with the 9.0 reported for the ketone. The entire synthesis was repeated and Figure 4 displays the results of much improved quality. The nmr analyses reveal that the CCl_4 solution before hydrolysis contained the 3, 3 dichlorocyclopropene as the major species present and that the hydrolysis produced a quite pure water layer with a sharp singlet at $\delta = 9.2$*. As in our initial attempt, $\delta = 3.3$ and 3.6 corresponded to some impurity but apparently not the same molecule characterized by $\delta = 9.1$ as the relative strengths of $\delta = 9.1$ to 3.3 changed from sample to sample. These results indicated that the Breslow synthesis had been reproduced. These very same samples used for nmr analysis were also subjected to mass spectrometric analysis and the mass spectra were obtained for the chlorinated cyclopropenes and cyclopropenone product mixture. In all experiments to follow, mass spectrometric analysis alone was used to determine whether dichlorocyclopropene was present before, but not present after, hydrolysis and from this it was assumed that the reaction had proceeded as before to form the species that had given a nmr signal at $\delta = 9.0$-9.2*.

*The position of the signal varies with acidity of the solution[79].

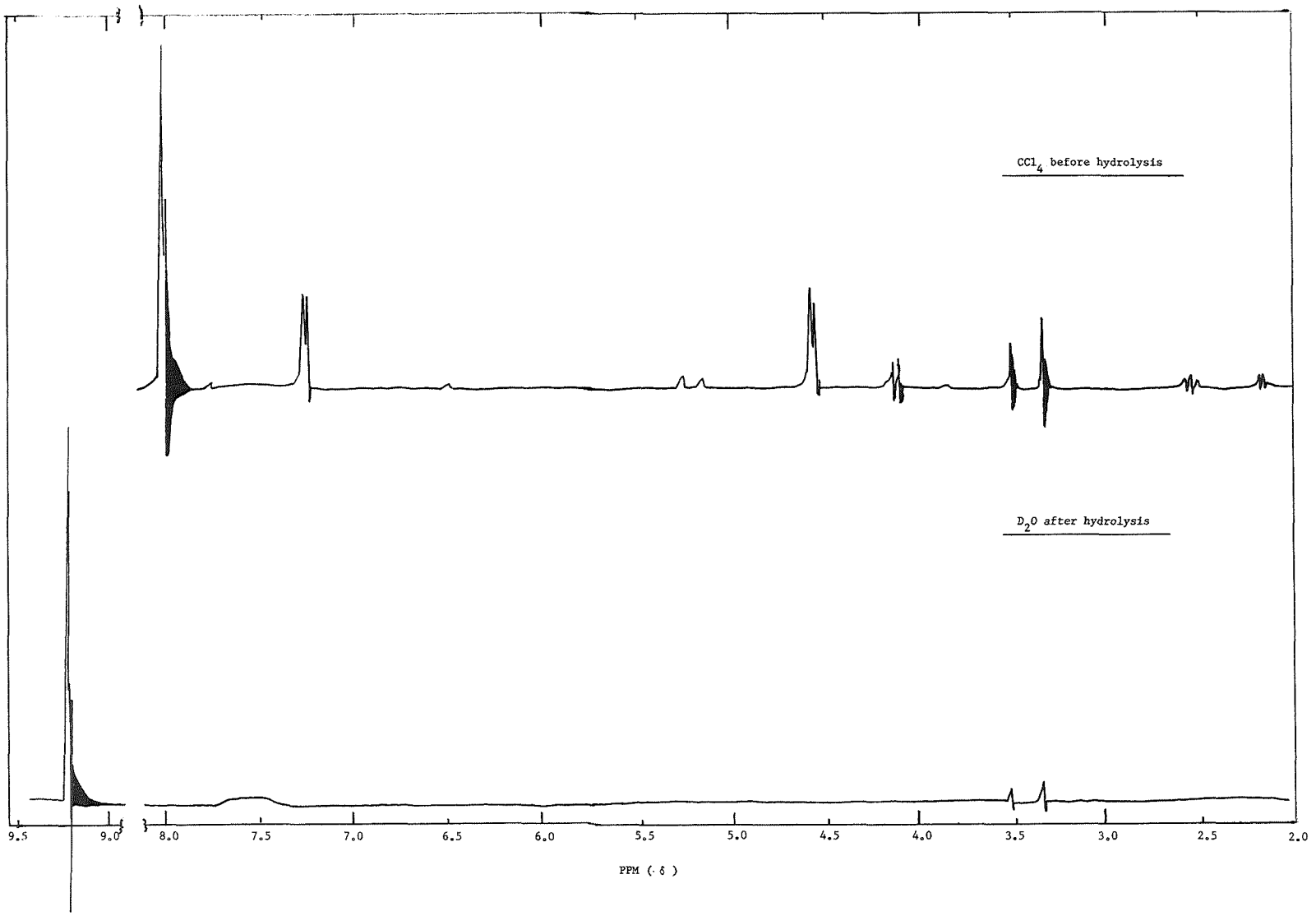

Figure 4. nmr of Solutions from Cyclopropenone Hydrolysis

Starting with three grams of tetrachlorocyclopropene, Breslow[79] reports yields of 39 to 55 percent. With a fresh tin-hydride solution we obtained yields of 39 percent of which about 70 percent was dichlorocyclopropene and the remainder was a mixture of mono, tri, and tetrachlorocyclopropenes. However, using tin solutions which had been stored long enough to turn cloudy drastically reduced the yield to about 15 percent.

Schematic of Separation Experiments

Figure 5 represents a general schematic for the operations involved in the separation experiments. It shows how mass spectral analysis was used during the experiments and, using this figure, one should be able to follow the reported data in Table 6. The primes, double primes, and triple primes refer to samples which were allowed to warm and remain at room temperature, heating the polymer that was formed, and drying the solutions over $MgSO_4$, respectively. In all treatments of the samples the following particular observations were made: 1) was dichlorocyclopropene present before and after the hydrolysis? (i.e., did it react?); 2) what new products resulted from the reaction?; 3) how much water was present? (percent of sample excluding the solvent); 4) what was the solution appearance; and 5) what were the appearance and heating of any polymer that was formed? All of these observations are recorded in Table 6.

Background Data

As will be discussed, cyclopropenone was not successfully isolated. It is more convenient to first present some background and supplementary information which is needed to analyze and discuss the separation problem

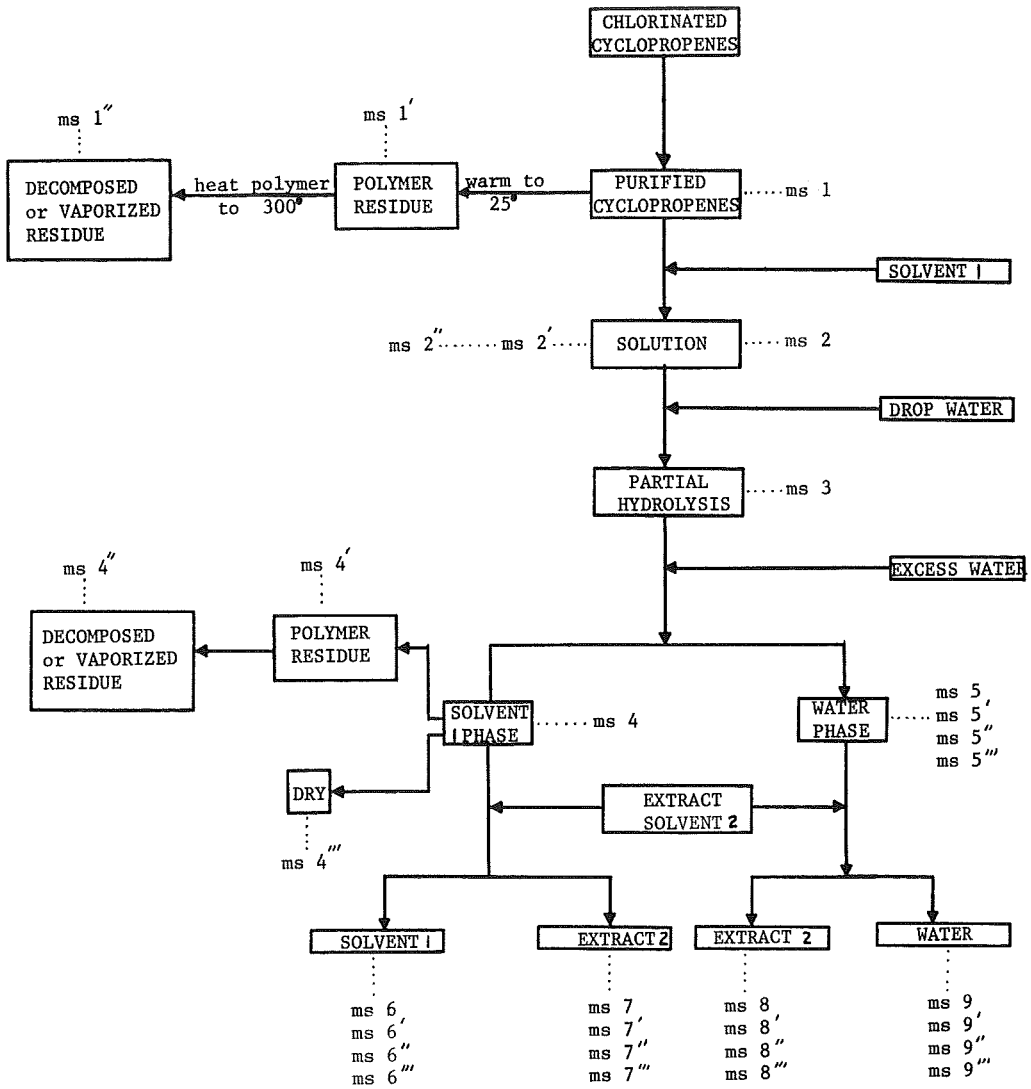

Figure 5. Schematic of Cyclopropenone Separation Experiments

Table 5. Supplementary Mass Spectra Data for Cyclopropenone Experiments

Compound	ms[a] temp	Mass Spectra major and distinguishing peaks (% of largest m/e)
acrylic acid	- 20	72(73)55(58)45(30)44(12)43(12)29(13)27(100)26(54)25(15)
HCl-H_2O solution	- 50	38(30)37(6)36(100)35(20)
H_2O	- 30	18(100)17( )
mono-chlorocyclopropene	- 95	76(8)74(25)39(100)38(35)37(35)
di-	- 70	112(1)110(6)108(8)75(40)73(100)37(40)
tri-	- 50	144,142,109,107,73
tetra-	- 40	180(8)178(15)176(11)145(30)143(95)141(100)108(25)106(40)73(15)71(50)
methylene chloride	-120	86(36)84(58)51(30)49(100)47(18)35(12)
acetaldehyde	-115	44(100)43(70)47(20)29(100)
ethylene chloride	- 90	64(32)63(19)62(100)27(93)26(32)
carbon tetrachloride	- 85	121(30)119(100)117(100)84(30)82(35)49(30)47(60)45(33)37(30)35(60)
acetonitrile	- 70	41(100)40(52)39(19)
nitrobenzene	- 50	
paraffin oil	----	
acrylic acid ethylester		56(12)55(100)45(11)29(29)27(60)26(18)
allyl acrylate		57(19)55(100)41(46)39(35)28(17)27(74)
propargyl alcohol		55(100)39(30)29(23)28(24)27(23)
ethylene (28)[b]	-180	
cyclopropene (40)	-140	
benzene (78)	- 70	
methanol (32)	- 75	
cyclopropenone (54)	?	
cyclopropanone (56)	- 90	
acetone (58)	- 95	
cyclobutanone (70)	- 70	
acrylic acid (72)	- 20	

a. refer to Table 1.
b. molecular weight.

Table 6. Summary of Mass Spectra from Cyclopropenone Experiments

Separation Process		Check for Presence:						
		cy-$C_3H_2Cl_2$		H_2O				
Solvent	Treatment	bef.[a]	aft.[a]	%[b]	polymer[c]	ms[d] temp	Mass Spectra (% of largest m/e)
	distill	1				- 95	monochlorocyclopropene } refer to Table 5
		1				- 70	dichlorocyclopropene
		1				- 50	trichlorocyclopropene
		1					124(25)122(35)89(30)87(100)51(100)
		1					108
	warm	1′	yes	no	30	yes	0 101(10)88(20)59(100)58(40)45(30)43(8)29(35)
	heat	1″					200 101(6)88(12)59(100)58(54)45(33)43(21)29(39)
		1″					200 72(40(55(40)27(100)26(40)25(10)
		1″					200 HCl
	warm (vacuum)	1′	yes	yes	<1	yes	-150 HCl
		1′					- 60 72(4)55(70(27(100)26(30)25(12)
	heat	1″					200 101(6)88(12)59(100)58(45)45(38)43(24)29(45)
		1″					200 72(20)55(70)27(100)26(40)25(15)
		1″					200 HCl
CCl_4		2	yes				
	drop water	3	yes	yes	30	no	- 60 92(30)90(100)64,63(20)62,61(60)29, 27, 26
							- 60 72(75)55(50)27(100)26, 25
							0 72(15)55(65)27(100)26(45)25(10)
	excess water	4	yes	no	50	yes	50
		4′					92(30)90(100)64,63(18)62,61(50)29, 27, 26
		4′					72(30)55(62)27(100)26, 25
		5					- 20 92, 90
		5					- 20 72(55)55(45)27(100)26, 25
		5					- 20 HCl
		5					0 72(14)55(63)27(100)26, 25
$C_2H_4Cl_2$	extract	8			50		- 30 HCl
		8					- 30 72(65)55(65)45(30)27(100)26(30)25(6)
		8					0 72(20)55(70)45(8)27(100)26(80)25(20)
CH_3CN		4					- 10 108(15)74(12)43(95)40(100)
		4					- 10 72(50)55(70)27(100)26(95)25(40)
	excess water	4	yes	no	70	yes	- 40 72(60)55(80)27(100)26(60)25(15)
							- 20 92(30)90(100)64, 62, 29, 27, 26
		4‴			20		- 30 72(32)55(65)27(100)26(50)25
		4″					HCl
		4″					72(20)55(70)27(100)26(45)25(20)
CH_2Cl_2	extract	6‴					72(36)55(50)27(100)26(60)25(20)
C_2H_4O		4‴	yes	no	50	yes	-110 72(25)55(65)27(100)6, 25
CH_2Cl_2, $C_2H_4Cl_2$, $C_6H_5NO_2$							no new results
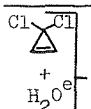 + H_2O[e]		4	yes	no	50	yes	- 80 72(6)55(60)45(20)27(100)26(45)25(25)
		4					- 60 92(30)90(100)64,63(40)62,61(40)29(65)27(100)26(70)
		4					25 55(100)27(20)26(8)25(3)
		4					25 HCl
	heat	4″					HCl and 72, 55, 27, 26, 25
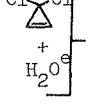 + H_2O[e]		4	yes	no	80	yes	- 30 101(8)88(20)59(100)58(40)45(64)43(32)29
		4					- 30 72(70)55(60)27(100)26(45)25(12)
	heat	4″					200 HCl
		4″					200 101(10)88(20)59(100)58(40)45(70)43(40)29(70)
		4″					200 72(24)55(60)27(100)26, 25

a. check for presence of dichlorocyclopropene (cy-$C_3H_2Cl_2$) before and after water hydrolysis;
b. refer to Table 1; c. check for presence of polymer or residue formed during reaction;
d. refer to Table 1; e. solvent free reaction.

(refer to Table 5). Cyclopropenone was reported[76] to hydrolyze upon standing in water solution at room temperature ($t_{\frac{1}{2}}$ = 1 week) to acrylic acid so the mass spectrum of the acid was obtained from an authentic sample. Likewise, HCl, which is produced as an off gas from reactions of the chlorinated cyclopropenes, was characterized. By simple low temperature distillation of the chlorinated cyclopropenes, a fairly good separation was obtained. The mass spectra of these species are shown in Appendix A. Occasionally the synthesis and purification of chlorinated cyclopropenes produced other products. The mass spectra of two such products, product parent 122 and product parent 108, are shown in Figures 12 and 14. (The identification of all these unknown products will be discussed together after the presentation of the data.)

The temperature stability and polymer formation of the chlorinated cyclopropenes was obtained to help determine what was happening with the ketone. The following observations were made: Tetra and trichlorocyclopropene appeared fairly stable to exposure to air and room temperature; monochlorocyclopropene was stable to temperature and air but reacted in the presence of water; dichlorocyclopropene appeared quite reactive in the presence of water and air with temperature having a less important effect on its stability. When a mixture of chlorinated cyclopropenes was left at room temperature and open to air, the mixture began to turn yellow within minutes and continued to darken to a dark brown polymer. The mass spectra of this yellow liquid, product parent 101, are presented in Figure 13. During the trap-to-trap distillation of chlorinated cyclopropenes which required the product to travel through a room temperature

line, it was noticed that HCl was being produced and some of the arriving product was beginning to turn brown. Some reaction was occurring, and the following set of experiments revealed the necessary conditions for that reaction. A sample of fairly pure dichlorocyclopropene was left overnight open to the air at room temperature. Quenching to -196° and subsequent warmup with mass spectrometric analysis revealed that all the dichlorocyclopropene had reacted and the only volatile product was the product parent 101 (noted earlier) which appeared near room temperature. Heating the brown polymer evolved more product parent 101, a great deal of HCl, and a compound of mass peaks 72, 55, and 27 (referred to as hydrated cyclopropenone). An identical experiment was performed but with the trap evacuated and sealed from the air and the results seemed to catch the reaction midway. Trapped HCl gas was obtained at -150°. Although almost all of the dichlorocyclopropene had survived the experiment, a new product of spectrum m/e 55 and 27 (and possibly 72) was observed near -60°. This time mass 55 was much greater relative to mass 72 than from the first experiment. There was also a brown polymer which when heated evolved product mass 101, HCl, and the hydrated cyclopropenone. In a third experiment, a trap sealed from air and stored at -196° survived with no apparent reaction. From these observations, it was concluded that dichlorocyclopropene reacts with or is catalyzed by either oxygen and/or water in the air liberating HCl gas to form initially a molecule whose predominant mass peaks are 55 and 27 (and possibly 72). Possibly it further reacts to form a yellow liquid which appears to be an ether or alcohol (see Section "Interpretation of Mass Spectra") and

and then to form a brown polymer from which, when heated, product parent 101, HCl, and masses 72, 55, and 27 are evolved.

Solvent Separations

The original synthesis of taking up the mixture of chlorinated cyclopropenes in CCl_4 and adding water to produce an aqueous phase of cyclopropenone was repeated a number of times with fairly consistent results. The addition of a drop of water to the CCl_4 solution of chlorinated cyclopropenes produced only a CCl_4 phase which contained unreacted dichlorocyclopropene and new products, parent mass 90 and masses 72, 55, 27. Water was also present in a significant quantity. Addition of excess water produced another phase and ms analysis of both CCl_4 and water revealed that all the dichlorocyclopropene had reacted and more of the above two products had been produced which were present in both phases but concentrated in the water phase. Upon warming the water phase from -196° the relative heights of 72, 55, 27 change from -20° to 0°. At -20°, HCl is evolved. The m/e 72, 55, 27 molecule was extracted by $C_2H_4Cl_2$ and ms analysis again showed the changing m/e 72, 55, 27 relative peak heights and HCl evolution. In other experiments of this type with CCl_4, the molecule characterized by mass peaks 72, 55, 27 was repeatably made. In a few instances, a molecule whose parent mass appeared to be 108 was present in the aqueous phase (see Figure 14 for mass spectrum). From these results it would seem that a number of molecules can be synthesized from the reaction, but the primary products are the ones characterized by mass peaks 72, 55, and 27 and product mass 90. It was not possible to separate cyclopropenone from water whether by adding much

less than the stoichiometric amount of water or by extraction. It appears that the cause of this is a combination of the facts that water is slightly soluble (by mass spectrometric standards) in all these solvents and that water and this molecule seem to be "bound up" together.

The hydrolysis of dichlorocyclopropene was carried out in a number of other solvents to try to separate cyclopropenone and water. When the chlorinated cyclopropenes were taken up in acetonitrile and water added (soluble in acetonitrile), the dichlorocyclopropene reacted and the two products, product parent 90 and hydrated cyclopropenone, were obtained. Drying the product over $MgSO_4$ did not remove all of the water and analysis revealed 72, 55, and 27 still present with a significant amount of water. However, product parent 90 was removed. A residue was left and when warmed evolved HCl and 72, 55, 27. The CH_3CN solution was extracted with CH_2Cl_2, dried over $MgSO_4$, and upon analysis, it was found to contain m/e 72, 55, 27, and much H_2O. During this extraction it was noted that a yellow color was extracted with the 72, 55, 27 species. In a similar experiment, the chlorinated cyclopropenes were taken up in acetaldehyde, hydrolyzed with one drop of water, analyzed, hydrolyzed with excess water, analyzed, dried, and analyzed. The only significant finding was that ion masses 55 and 27 appeared at a much lower temperature (-110°). Other solvents used for the reaction were methylene chloride, ethylene chloride, and nitrobenzene. No different results were obtained.

Non-solvent Syntheses and Separations

The failure to isolate cyclopropenone led to a few last attempts to obtain even a trace of the ketone by other means. In one experiment,

pure dichlorocyclopropene and water were condensed (under vacuum) one on top of the other at -196°. Plunging the trap to -80° and slowly warming revealed the following results. Almost immediately at -80° a small amount of mass peaks 55 and 27 was noticed and followed by the major product, parent mass 90 at -60°. At 25°, HCl was evolved and a large mass peak 55 was obtained. Heating the polymer further evolved HCl and 72, 55, 27. These data, except for the 25° m/e 55 evolution, are consistent with the previous data. In another experiment, water was added to pure dichlorocyclopropene (open to air) and after the reaction the contents were quenched to -196° and warmed slowly. At -30° product parent 101 (previously obtained from warming a sample of dichlorocyclopropene in the presence of air) appeared along with 72, 55, and 27 formed from the reaction. In still another experiment, water was added directly to the chlorinated cyclopropenes as they were formed in paraffin oil, stirred for a few hours, then flashed off and analyzed. Although some new product masses appeared, none seemed obviously related to the desired ketone and these data were not analyzed any further.

Interpretation of Mass Spectra

The most significant mass spectra of the products of the cyclopropenone experiments are reported in Table 6 (shown in Figures 11-14). Because the mass spectra of many of the products are not available in the literature, the data were first analyzed as to number of chlorine atoms per fragment, and then the most likely structures were suggested.

The natural abundance of chlorine isomers is $Cl^{35}:Cl^{37} = 3:1$ and the probability of any particular Cl atom having mass 35 or 37 is

three-fourths and one-fourth, respectively. Take for example, tetrachlorocyclopropene, which gives a parent ion and fragment ions containing 4, 3, 2, 1, and 0 chlorine atoms. The probability distribution of molecular weights is determined by considering the product of probabilities of each chlorine atom. The relative abundances of peaks in the mass spectra are then the ratio of these probabilities. The calculations for tetrachlorocyclopropene are shown in Table 7. The lowest possible parent molecular weight is 176 considering all four as Cl^{35}. As can be seen, the number of significant peaks corresponding to a particular fragment corresponds to the number of Cl atoms plus one and are in the ratios shown. Note that a single peak indicates no Cl atoms. These calculated relative intensities also apply to the other chlorinated cyclopropenes and any other chlorine products. Table 5 shows that the mass spectra of all the chlorine products and solvents follow these calculated distributions very closely.

The mass spectrum of acrylic acid, HCl, dichlorocyclopropene, and tetrachloropropene are reported in Figures 11 and 12. Two other products from the dichlorocyclopropene synthesis, product parents 122 and 108, are shown in Figure 12. From the relative peak heights of 124:122 and 89:87 it can be seen that product parent 122 contains two chlorine atoms and compound 3 of Table 8 appears to be the most likely molecule. Parent 122 was seen only rarely and with very pure dichlorocyclopropene yields it was not obtained. Furthermore, hydrolysis of purified dichlorocyclopropene did not produce it, so this compound was tentatively ignored.

Table 7. Determining Relative Mass Spectra from Cl Isotopes*

Number Cl Atoms	Ion Mass	Probability		Relative Ratio	
4	176	3/4 x 3/4 x 3/4 x 3/4 = 81/256	= 81/256	81	6
	178	3/4 x 3/4 x 3/4 x 1/4 = 27/256 3/4 x 3/4 x 1/4 x 3/4 = 27/256 3/4 x 1/4 x 3/4 x 3/4 = 27/256 1/4 x 3/4 x 3/4 x 3/4 = 27/256	= 108/256	108	8
	180	3/4 x 3/4 x 1/4 x 1/4 = 9/256 3/4 x 1/4 x 3/4 x 1/4 = 9/256 3/4 x 1/4 x 1/4 x 3/4 = 9/256 1/4 x 3/4 x 1/4 x 3/4 = 9/256 1/4 x 3/4 x 3/4 x 1/4 = 9/256 1/4 x 1/4 x 3/4 x 3/4 = 9/256	= 54/256	54	2
	182	3/4 x 1/4 x 1/4 x 1/4 = 3/256	= 12/256	12	1
	184	1/4 x 1/4 x 1/4 x 1/4 = 1/256	= 1/256	1	**
3	141	3/4 x 3/4 x 3/4 = 27/64	= 27/64	27	3
	143	3/4 x 3/4 x 1/4 = 9/64 3/4 x 1/4 x 3/4 = 9/64 1/4 x 3/4 x 3/4 = 9/64	= 27/64	27	3
	145	3/4 x 1/4 x 1/4 = 3/64	= 9/64	9	1
	147	1/4 x 1/4 x 1/4 = 1/64	= 1/64	1	**
2	106	3/4 x 3/4 = 9/16	= 9/16	9	3
	108	3/4 x 1/4 = 3/16 1/4 x 3/4 = 3/16	= 6/16	6	2
	110	1/4 x 1/4 = 1/16	= 1/16	1	**
1	71	3/4		3	3
	73	1/4		1	1
0	79			only one mass	

*tetrachlorocyclopropene example.

**neglected these low abundance masses.

Product parents 108 and 162 could be the dimer and trimer of cyclopropenone. Parent 108 was also made during water hydrolysis and it was seriously considered as an important product.

Parent 101 produced from warming the chlorinated cyclopropenes has the mass spectrum shown in Figure 13. From the single peaks, we conclude it contains no chlorine atoms and the abundant peaks at masses 59 and 58 imply it is an ether or alcohol. The structure of this species is not obvious and it is noted that it is produced only when pure chlorinated cyclopropenes are allowed to warm and not in the hydrolysis. The most likely explanation is that it is formed from the reaction of dichlorocyclopropene with oxygen and followed possibly by further polymerization reactions.

The other product in the warming of chlorinated cyclopropenes, parent mass 72, was also predominant in the spectra of the hydrolysis experiments. From this it was concluded that this product is formed by the reaction of dichlorocyclopropene with water. Examination of its mass spectra (see Figures 13 and 14 and Table 6) shows single peaks (no chlorine atoms) and the same fragment masses as acrylic acid. However, none of the recorded mass spectra (at least 50 traces) agreed with that of the authentic acrylic acid. Table 5 lists the mass spectra of three compounds: acrylic acid ethyl ester, allyl acrylate, and propargyl alcohol which all produce an abundant fragment mass 55. From an analysis of the mass spectra of many H, C, and O containing compounds, it appears that m/e 55 from the first two compounds may be the ketone structure, CH_2CHCO^+, while 55 from the third is probably the alcoholic structure

$CCCH_2OH^+$. Judging from the large abundance of m/e 27 and the accompanying m/e 26 and 25, this fragment (m/e 27) would appear to be a hydrocarbon. The most reasonable conclusion for this spectrum so closely related to acrylic acid but not acrylic acid is that it must be an acrylic acid isomer. Also, the mass spectra vary a great deal from sample to sample and, furthermore, the mass spectra vary with the temperature of analysis from -80° to room temperature, depending on the solvent characteristics. In the isolated warming of the chlorinated cyclopropenes and the dichlorocyclopropene hydrolysis with a drop of water, the products m/e 72, 55, and 27 appeared at much lower temperatures (-80°) and had a very weak parent ion (m/e 72). As these solutions were warmed, the abundance of m/e 72 increased and the spectra moved toward that of acrylic acid. It must be that either there is a mixture of isomers present or that the initial product is rearranging to another isomeric structure as the temperature is increased. In addition, the very weak parent (4 percent) at -80° could be explained by assuming m/e 55 is really a parent or that m/e 72 is a very unstable molecule. A close examination of all the recorded mass spectral data reveals that, although the abundance of m/e 72 varies, the abundance of other fragments 55, 27, 26, 25 is more consistent. This would be explained by two isomers, with parent ions greatly different in stability but which rearrange to fragment from the same structure and by the same mechanism to give the same fragments. In any event, the initial product appears to be an unstable isomer which rearranges to a more stable isomer to form a solution whose spectra vary with temperature. With this discussion, the most likely structures for

the initial product are structures 7, 11, 17, 18, 19, and 20 in Table 8. This proposed solution of isomers of m/e 72, 55, and 27 will be referred to as "hydrated cyclopropenone".

In the hydrolysis experiments, another product, parent m/e 90, was usually made and its mass spectrum is shown in Figure 14. It apparently contains one chlorine atom and could be any number of structures, possibly structures 5, 21, 22, 23, or 24 in Table 8.

The product parent m/e 108 mass spectrum is shown in Figure 14. It contains no chlorine atoms and could be the dimer of structure 14 or 15 (Table 8). However, neither of these dimers satisfactorily explains the fragment peaks assigned to m/e 108.

Summarizing Discussion of Polymers

The mono, tri, and tetrachlorocyclopropenes were all found to be stable at room temperature and exposed to air. During the hydrolysis of the mixture of chlorinated cyclopropenes, no reaction products of these three were detected, although it must be admitted that this was not examined very closely because dichlorocyclopropene was the most abundant reactant. Furthermore, the most definitive experiments were carried out with purified dichlorocyclopropene. However, dichlorocyclopropene is itself a cryochemical reagent as it begins to polymerize at -20° C to form a thick yellow liquid of low vapor pressure. At room temperature this yellowing takes only a few minutes and proceeds to a brown liquid which, when heated to 200°, becomes a brown-black solid. The reaction of dichlorocyclopropene with both oxygen and water in the air best explains the products formed. In the absence of air the reactions

Table 8. Possible Product Compounds in Cyclopropenone Experiments

No.	Molecule	MW	Expected Mass Spectra	No.	Molecule	MW	Expected Mass Spectra
1		54	54, 28, 26	16	>C=C=C=O	54	
2		88	88[90], 53, 28, 25	17	>C=C=C(OH)OH	72	72, 55, 38
3		122	122[124], 87[89], 52, 28	18	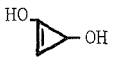	72	72, 55, 38
4		56	56, 42, 38, 27, 26	19	C≡C–C(OH)OH	72	72, 55, 47, 25
5		90	90[92], 55, 28, 27	20	HO–C=C=C–OH	72	72, 55, 38
6	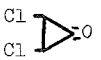	124	124[126], 89[91], 54	21		90	90[92], 74, 55, 25
7		72	72, 55, 38, 26	22		90	90[92], 73[75], 55, 26
8	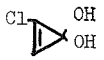	106	106[108], 71	23		90	90[92], 73[75], 55, 26
9	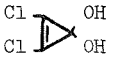	140		24	HO–C=C=C–Cl	90	
10		74		25	O=C=C=C(Cl)Cl	122	
11		55	55, 38, 26				
12	>C=C(I)–C(=O)OH	72	72, 55, 27				
13	–C≡C–C(=O)OH	70	70, 53, 25				
14	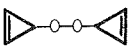	108	108, 54, 38				
15		108	108, 92, 28				

proceed very slowly. By first breaking the vacuum to the cold, isolated, samples of dichlorocyclopropene with an inert gas (such as argon) instead of air and then allowing the solid to warm to room temperature, a clear colorless liquid was obtained which did not turn yellow as quickly. The polymerization was accompanied by the evolution of HCl gas.

Breslow[76] reports that cyclopropenone is stable at -10° and polymerizes at 10°. In our work it was not easy to tell at exactly what temperature the cyclopropenone solutions began to polymerize as the solutions of dichlorocyclopropene always began to turn yellow before the hydrolysis was complete. The residue product was usually a brown oily liquid which became a dark brown solid when heated.

Heating the dichlorocyclopropene polymer evolved HCl, product parent 101, the hydrated cyclopropenone and water. Heating the cyclopropenone polymer liberated HCl, product parent m/e 90, the hydrated cyclopropenone, and water.

Since the polymers in both cases are quite similar in color and composition, the polymerization of dichlorocyclopropene is viewed as an initial reaction with oxygen and/or water from the air followed by the polymerization of these products. It was not possible to evaporate the solvents and leave behind a nice looking polymer for only a viscous brown liquid was obtained. Also, when heated, both polymers evolved HCl which could have been trapped in the liquid solutions and residues or could have resulted from further reaction and elimination of HCl. In the experiment in which dichlorocyclopropene was allowed to warm in a trap sealed from air, HCl was found as a free gas present above the solid

sample, and it was detected at -150°, long before more HCl was evolved from heating the solid residue. In this case, it seemed apparent that the latter HCl was from further reaction. The evolution of HCl from cyclopropenone residue could be due to any number of possibilities. It would be helpful to be able to state that the residue formed is the result of the reaction of only one species and whether or not it contains Cl atoms. As noted in the cyclopropanone experiments, heating of the polymers evolved both trapped molecules and polymer decomposition masses related closely to the original monomer. Therefore, it is really impossible to draw any worthwhile conclusions from heating this brown liquid. The residues and solids involved here were nothing like the cyclopropene and cyclopropanone polymers. This could be the result of having many reacting species (particularly chlorinated ones) and an inherent problem in solution chemistry.*

Summarizing Discussion of Synthesis

Before attempting to draw conclusions from these data, it is convenient to present a summary of the cyclopropanone problem which will be used for comparison in analyzing the cyclopropenone problem. Cyclopropanone exists as a stable, closed ring, structure which exerts a detectable vapor pressure at -90°. On warming from -197° to 25°, it will not decompose but begins at -90° to polymerize and the rate is increased by the presence of water. Although it will polymerize at 25° within minutes, the ring remains closed. When heated, the polymer evolves

* Note that these results exemplify the importance and usefulness of the solution-free synthesis of cyclopropanone.

trapped cyclopropanone and polymer decomposition products. It reacts to relieve the strained sp^2 bonding at the carbonyl carbon and at -95° will undergo reactions:[57]

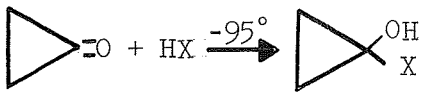

; X = OH, Cl, CH_3OH, CH_3CHO, NH_2R

It must be pointed out that the cyclopropenone experiments were based on the assumption that Breslow's nmr and ir analysis were correct and that, by duplication his synthesis and analysis, cyclopropenone was successfully prepared. Since the ketone was not isolated, these experiments will be used to suggest the most probable reasons for failure although they were not designed for that purpose. Further experiments to more precisely determine the failure are suggested.

The failure to isolate cyclopropenone is explained by either 1) Breslow's reported synthesis and analysis were incorrect and the ketone was not prepared or 2) the ketone was made but cannot be isolated by the techniques applied.

(1) Breslow[79] reports a strong nmr singlet appearing from 9.0 to 9.6 eV depending on the acidity. He reports that there are no other nmr signals present. He eliminates other most likely structures and then assigns the protons to cyclopropenone. We reproduced this sharp singlet and will not quibble with these reported data. However, this does not eliminate the presence of other molecules which contain no H and, since D_2O has no nmr signal, there may be C-O-D structures present. Breslow reports a broad ir absorption at 1850 cm^{-1} and no absorption in the O-H region from which he concludes the presence of C=O and absence

of O-H. We did not attempt the ir analysis and actually should have for this seems to be the key to this analysis. Breslow does not report any other adsorption for cyclopropenone, particularly that of C=C. His statement of no absorption in the O-H region does not say whether he had used D_2O for the hydrolysis and looked for an O-D absorption. Furthermore, he says nothing about the presence of absorptions from other impurities that may be present. He states that cyclopropenone slowly reacts with water to form acrylic acid which, from our work, does not appear to be a correct analysis of the m/e 72, 55, and 27 products. He does not mention any of the other products of the hydrolysis that we obtained (parent masses 108, 122, 101, 90, and 72 at one time or another). He used an unpurified mixture of chlorinated cyclopropenes for the hydrolysis. Another criticism is that there was no ms work reported except on acrylic acid. It therefore appears that cyclopropenone has not been detected spectrally in the gas phase, a serious criticism to its proposed existence. Structures 2 and 15 would, by themselves, possibly explain both the nmr and ir data. Mass 108 was observed in ms but not when using purified dichlorocyclopropene. Mass 88 was never observed by ms analysis.

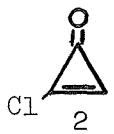

2
(mass 88)

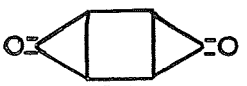

15
(mass 108)

Since Breslow used a mixture of chlorinated products in the hydrolysis, a combination of products is more likely to explain the nmr and ir data. A combination of either structure 3 or 25 with any of 7, 22, or 11 may possibly explain the data.

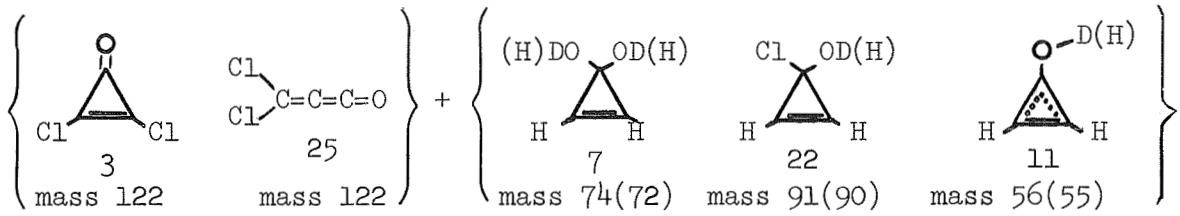

Mass 122 was observed in experiments using mixtures of chlorinated cyclopropenes and quite possibly could have resulted from reaction of water and tetrachlorocyclopropene. In fact, structure 3 reportedly is formed[80] by the reaction of tetrachlorocyclopropene with water in the presence of $AlCl_3$. In this work, masses 90 and 72 were the predominant products of the hydrolysis of purified dichlorocyclopropene and may be explained by the successive replacement of the two chlorine atoms by OH and elimination of HCl.

2) Assuming cyclopropenone was made, it is difficult to explain why never even a trace of it was observed by ms analysis. It is reported[76] to polymerize at 10° and to stable at -10°. Furthermore, Breslow reports that it can be extracted in polar solvents and still retain the same nmr and ir characteristics. The solvents used in this work began to exert ms detectable vapor pressures down to -110°. One would expect to see pure cyclopropenone spectra at a temperature not too different from pure cyclopropanone (-90°). Looking at the detection temperatures of other similar compounds (Table 5), one sees that acrylic acid is the least volatile and it appears at -20°, a full 30° below the temperature at which the ketone supposedly polymerizes. Without knowing the boiling point, it is not easy to predict at what temperature the pure ketone will appear. Assuming very pessimistically that the ketone boils 40° above

its saturated analog cyclopropanone, the pure cyclopropenone would appear during analysis at -50°. This pure ketone in solution with solvents that appear at even lower temperatures, should appear below this assumed -50°. The ketone is known to polymerize in solution at 10°. This polymerization may be retarded greatly by the solvent molecules, particularly with the possibility of hydrogen bonding. Therefore, it would be expected that the pure ketone might begin to polymerize at a lower temperature. However, by reactions with water, acids, and bases, Breslow stresses how much more stable and unreactive the ketone is compared to cyclopropanone. From previous work, we already know that cyclopropanone is readily analyzed at -90° and can be detected for short periods at 25°. There are, therefore, many reasons to expect that cyclopropenone should exert a detectable vapor pressure before it completely polymerizes, and thus it should have been observed in these experiments. Breslow reports that cyclopropenone can be extracted but we found that only the hydrated cyclopropenone (masses 72, 55, 27) was consistently observed as the primary extracted product. However, water always appeared to accompany it in the extraction. If cyclopropenone exists, one plausible explanation is that it is so "bound up" with water that they transfer as a unit during extraction and that, upon vaporization, cyclopropenone reacts both with the water and itself.

Functionally the only difference in the ms analysis and the nmr and ir analyses is that the product was frozen as a solid and then slowly warmed and analyzed at a low temperature. It is possible that there exists an equilibrium between cyclopropenone and its hydrate as:

(10)

If it were the case that the cyclopropenone hydrate exerted a much greater vapor pressure, then, by slowly warming the sample, the hydrate would boil off and the equilibrium (in much excess water) would continue to feed the hydrate vaporization until all the cyclopropenone was gone. This, then, would have to be completed before cyclopropenone exerted an ms detectable vapor pressure. Another possibility is that cyclopropenone exists in acidic water solution as an ion as Breslow reports it to be stable to mineral acids but polymerized by bases.

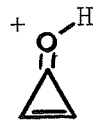

Many experiments can be suggested which would answer these questions and should be done; ir and nmr on the hydrolysis of purified dichlorocyclopropene; ir and nmr on the hydrolysis of the mixture of chlorinated cyclopropenes; nmr, ir, ms analysis on hydrolysis with heavy and normal water; performing the experiments under an inert gas; reacting tetrachlorocyclopropene with water; and continually observing the nmr and ir spectra as a liquid sample of cyclopropenone is slowly vaporized. The two nmr experiments reported in this work were done with heavy water and these samples were subjected to ms analysis by quickly transferring the sample to the low temperature inlet system. Unfortunately, these were the initial experiments tried and the residue which did not quickly transfer was not analyzed. As a result, no products were observed and

no data on products with hydrolyzed heavy water were obtained. This would be extremely important in determining whether OD was added to the 3,3 carbon.

Although these suggested experiments should lead to a definite explanation of the problem, they probably would not lead to a successful isolation of the molecule. Approaches to the synthesis besides the reaction of dichlorocyclopropene and water are beyond the scope of this work.

CHAPTER IV

DERIVED ENERGETIC RESULTS

Introduction

Definitions, Derivations, and Assumptions

The bond dissociation energy, $D(R_1\text{-}R_2)$, of a bond $R_1\text{-}R_2$ is the change in energy at absolute zero in the ideal gas state, ΔE_0^0, for the reaction

$$R_1\text{-}R_2 \rightarrow R_1 + R_2; \quad (T = 0°K)$$

$$\Delta E_0^0 = D(R_1\text{-}R_2)$$

the products being in their ground electronic states. However, ΔH^0 at 298°K is often used in place of ΔE_0^0 for the dissociation energy because the two numbers do not differ greatly and many of the data obtained by measurement of ΔH^0 are not sufficiently precise to warrant the correction especially since, in many cases, the heat capacity data are lacking. Cottrell[12] points out that the heat capacity change of reaction is always positive so that the value of ΔH^0 at 298°K will always be greater than $D(R_1\text{-}R_2)$ as defined above. He further points out that the upper limit to this difference is $\Delta H^0_{298} - \Delta E_0^0 \simeq 2.4$ kcal/mole and that the difference is usually less than one kcal/mole. Benson[4] defines ΔH^0_{298}, the Standard Bond Dissociation Energy, as the enthalpy change in the chemical process in which one mole of a specified bond is broken, reactants and products being in their standard states of hypothetical ideal gas at one atmosphere pressure and 298°K. This quantity will be designated in this work as

$\Delta H^o_{298} = D^o$. Electron impact data are also defined as heats of reaction at absolute zero:

$$R_1\text{-}R_2 + e^- \rightarrow R_1^+ + R_2 + 2e^-; \quad (T = 0°K)$$

$$A(R_1^+) = \Delta H^o_o = \Delta H^o_{f_o}(R_1^+) + \Delta H^o_{f_o}(R_2) - \Delta H^o_{f_o}(R_1\text{-}R_2) \tag{1}$$

$$A(R_1^+) = \quad = \Delta E^o_o(R_1\text{-}R_2) + I(R_1) \tag{2}$$

$$A(R_1^+) = \quad = I(R_1\text{-}R_2) + \Delta E^o_o(R_1^+\text{-}R_2) \tag{3}$$

This definition takes all products as being produced in their ground electronic states. It is also true that the difference in the heats of reaction at 298°K and absolute zero is sufficiently small enough such that the appearance potential may be taken as the heat of reaction at 298°K and Standard Heats of Formation, ΔH^o_f, and Standard Bond Dissociation Energies, D^o, be used in the calculations. This also includes the assumption that all the energy of the bombarding electron is absorbed and no energy appears in the two product electrons. The equations then become:

$$R_1\text{-}R_2 \rightarrow \cdot R_1 + \cdot R_2 \qquad (T = 298°K)$$

$$\Delta H^o_{298} = D^o(R_1\text{-}R_2)$$

$$R_1\text{-}R_2 + e^- \rightarrow R_1^+ + R_2 + 2e^- \qquad (T = 298°K)$$

$$A(R_1^+) = \Delta H_r = \Delta H^o_f(R_1^+) + \Delta H^o_f(R_2) - \Delta H^o_f(R_1\text{-}R_2)$$

$$A(R_1^+) = \quad = D^o(R_1\text{-}R_2) + I(R_1)$$

$$A(R_1^+) = \quad = I(R_1\text{-}R_2) + D^o(R_1^+\text{-}R_2)$$

At this point we have the products being formed in their normal vibrational distribution at 298°K and in their ground electronic states. However, there are many examples of processes in which the products possess "excess" (greater than T = 298°K) translational and vibrational energy. Products may also be produced in excited electronic states. The occurrence of excess energy is, in general, related to the production of fragments that result from the breaking and formation of multiple bonds. This work is particularly concerned with measurement and correlation of these excess energies. In the gas phase at low pressures, molecules possess small interactional forces and one can assign properties to individual molecules. At room temperature, rotational and translational energies are generally at their classical limit while vibrational energy is quantized. These quantum oscillators may or may not be active at room temperature. For most molecules, thermal agitation is far insufficient to produce an excited electronic state. Appendix C of this thesis is devoted to the measurement of excess translational energies of product ions from electron impact experiments. Fragment ions produced with excess translational energies possess an increased peak width which can be interpreted as being equivalent to an increased temperature of the gas. The neutral fragment is assumed to have a complementary excess translational energy which is calculated from a momentum balance. The sum of these excess translational energies is identified with the excited molecular ion before fragmentation, and this ion is also assumed to possess excess vibrational energy which is related to the excess translational energy by the classical total degrees of vibrational freedom and an empirical constant. In this manner the total excess translational,

vibrational, and rotational energies for a particular appearance potential may be calculated and is designated as E^*. The problem of excited electronic states is much more difficult. If experimental electronic spectra are known, then the energies of the excited states are available. If not, they must be estimated. In this work, several MO computer programs (see Appendix D) were used to calculate these data. Thermochemical data, where available, were also used to approximate these data. With these excess energies the equations are

$$R_1\text{-}R_2 \rightarrow \cdot R_1 + \cdot R_2 \qquad (T = 298°K)$$

$$\Delta H^o_{298} = D^o(R_1\text{-}R_2)$$

$$R_1\text{-}R_2 + e^- \rightarrow R_1^+ + R_2 + 2e^- \qquad (T = T_p)$$

$$A(R_1^+) = \Delta H^o_r + E^* = \Delta H^o_f(R_1^+) + \Delta H^o_f(R_2) - \Delta H^o_f(R_1\text{-}R_2) + E^*$$

$$A(R_1^+) = \qquad = D^o(R_1\text{-}R_2) + I(R_1) + E^*$$

$$A(R_1^+) = \qquad = I(R_1\text{-}R_2) + D^o(R_1^+\text{-}R_2) + E^*$$

where the electronic state of each species must be specified.

In this introductory discussion, we have defined the bond dissociation energy (D^o) as a heat of reaction which is to be experimentally measured. It is useful in predicting overall heats of reaction in terms of bonds broken and bonds formed (see equation 7). However, it is much more useful in predicting the relative rates of competing chemical reactions.[4] Another term used in this work is "bond energy" (E) which is not an experimental number but an abstract quantity which is used to

estimate heats of atomization, ΔH_a. By looking at large amounts of experimental data, workers have found that experimental ΔH_a can be accurately estimated by assigning a bond energy to each chemical bond in the molecule. ΔH_a is then taken as the sum of the individually assigned bond energies:

$$\Delta H_a = \left[\sum_{\text{bonds}}^{\text{all}} E \right] \equiv \Delta H_a(E)$$

In general, a bond energy is assigned depending on the pair of bonded atoms and the hybridization. However, the most striking fact of bond dissociation energies, D^o, and the biggest problem with bond energies, E, is that for bonds between the same two atoms they both depend greatly on atomic environment. This means that experimentally measured D^o can only strictly be used to calculate heats of reactions involving those molecules for which D^o were measured, and that D^o becomes an approximation when applied to other molecules. For estimating E, workers have obtained the best results by correlating E with bond lengths and bond orders. Cottrell[12] has explained the difference in D^o (104 kcal) and E (99) of Ch_3-H in methane by reasoning that 99 kcal is needed to break the bond plus a "rearrangement" energy of five kcal to convert CH_3 into its planar structure. Thus the removal of 1, 2, 3, and 4 hydrogens takes about 104, 105, 106, and 81 kcal, respectively, and the sum, 396 kcal corresponds to the ΔH_a. Note that the bond energy is 396/4=99 kcal. In this example the bond energy and bond dissociation energies are not too dissimilar. However, D^o for the removal of one then another H from ethane takes 98 and 39 kcal, respectively. The problem is that after the removal of the

second H, the species forms a π bond and produces ethylene. The sum of 103 and 41, divided by 2 no longer equals the E (99 kcal), but the ΔH_r to produce ethylene and 2H atoms from ethane. Similarly, Pauling[18] explains the difference in the first and second dissociation energies (121 and 101 kcal) of H-O-H by arguing that it also takes 121 kcal to initially remove the second H atom but 17 kcal is regained when oxygen pairs up its valence electrons. This is exactly the case of ring compounds in which the fragments form new bonds. A part of this work attempted to calculate a rearrangement energy, designated as $R(\ \ )_g^{ex}$, to determine a more meaningful interpretation of D^o for ring molecules. This rearrangement energy was taken as the energy difference between a hypothetical initial diradical and the observed final ground state.

Therefore, the problem has now become that of dissociating rings to form fragments which most probably possess excess translational and vibrational energy, possibly excess electronic energy, and interpreting bond dissociation energies with the aid of the proposed rearrangement terms. With this introductory discussion, equations 1, 2, and 3 for the fragmentation of 3-carbon membered rings are

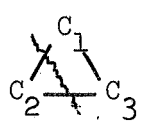

$\longrightarrow$ $:C_2 + C_1{=}C_3$; $\quad (T = 298°K)$

$\Delta H^o_{298} = D^o(\triangle)_g$

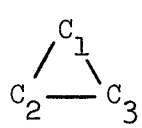

$+ e^- \longrightarrow$ 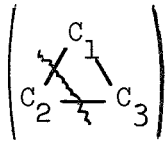 $\longrightarrow C_2^+ + C_1{=}C_3 + 2e^-$; $\quad (T = T_p)$

$$A(C_2^+) = \Delta H_r^o + E^* = \Delta H_f^o(C_2^+) + \Delta H_f^o(C_1{=}C_3) - \Delta H_f^o(\Delta) + E^*$$

$$A(C_2^+) = \qquad = D^o(\Delta)_g + I(C_2) + E^*$$

$$A(C_2^+) = \qquad = I(\Delta) + D({}_+\Delta)_g + E^*$$

and including the rearrangement term

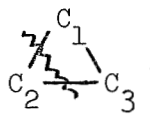

$\longrightarrow \cdot\dot{C}_2 + \cdot C_1{-}C_3\cdot$; $\quad (T = 298°K)$

$$\Delta H_{298}^o = D^o(\Delta)^{ex}$$

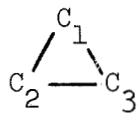

$+ e^- \longrightarrow$

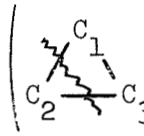

$^- \longrightarrow C_2^+ + C_1{=}C_3 + 2e^-$; $\quad (T{=}T_p)$

$$A(C_2^+) = \Delta H_r^o + E^* = \Delta H_f^o(C_2^+) + \Delta H_f^o(C_1{=}C_3) - \Delta H_f^o(\Delta) + E^* \qquad (4)$$

$$A(C_2^+) = \qquad = D^o(\Delta)^{ex} + R(\cdot\dot{C}_2)_g^{ex} + R(\cdot C_1{-}C_3\cdot)_g^{ex} + I(C_2) + E^* \qquad (5)$$

$$A(C_2^+) = \qquad = I(\Delta) + D({}_+\Delta)^{ex} + R(\cdot\dot{C}_2^+)_g^{ex} + R(\cdot C_1{-}C_3\cdot)_g^{ex} + E^* \qquad (6)$$

where $D^o(\Delta)_g = D^o(\Delta)_g^{ex} + R(\cdot\dot{C}_2)_g^{ex} + R(\cdot C_1{-}C_3\cdot)_g^{ex}$

and $D^o(\quad)_g$ = the dissociation into ground electronic states

$D^o(\quad)^{ex}$ = the dissociation into hypothetical initial diradical

Characteristics Unique to Ring Molecules

In as much as many standard definitions and calculations are not applicable to ring molecules, these points of concern will be discussed here. Since the energetic properties of ring molecules seemingly have not yet been explained or organized into a consistent body, part of this chapter is devoted to exploratory calculations in which strain energies, bond dissociation energies, heats of reaction and activation energies are interrelated.

Ring Strain

Ring strain is a relative term used to describe the energetic result of having bonding angles between the centers of carbon atoms which differ greatly from the normal angles of sp^3~109° and sp^2~120°. For 3-membered carbon ring compounds, this may be viewed superficially as "straining" the bond angle from 109° to 60°. The properties associated with ring strain can best be rationalized by noting that these molecular orbitals are not directed along the line joining the two centers of the atoms which results in poorer orbital overlap and an associated weaker bond. In any discussion of ring strain, it must always be recognized that ring strain involves experimental data on and is thus relative to some other chemical compound(s). For example, cyclopropane ring strain derived from heats of combustion are relative to paraffins. This sort of number applies to the entire molecule and corrections must be made for the C-H bond energies to be able to assign the ring strain only to the C-C ring bonds. Heats of hydrogenation of unsaturated ring compounds are compared to those of unsaturated open chains and hence are relative to those chains. In this work, the reported ring strains are to be inter-

preted to apply solely to the ring bonds. This was done in order to try to correlate the bond dissociation energies and bond energies with available literature values. Ring strain in this thesis is taken as the difference in the experimentally derived ΔH_a and the ΔH_a calculated from empirical bond energies which are estimated from the experimental interatomic distances in each molecule:

$$\text{ring strain} \equiv \Delta H_a(\text{exp}) - \Delta H_a(E)$$

where $\Delta H_a(E)$ has been previously defined.

Review of Literature on MS Investigations of Ring Molecules

The literature contains very little work on the ms energetics of any type of ring molecule. In an early investigation of cyclopropane, Field[27] determined the appearance potential process by assuming the products that came nearest to calculating the measured experimental AP. In this manner he concluded that the parent molecular ion (and also the molecular ion minus one, two, etc. hydrogens) was not a ring but an open structure. He also estimates that the endothermicity of the ring opening is at least 50 kcal/mole. Later, Franklin[1] determined that some of the fragment ions had such large amounts of excess energy that Field had actually assumed the wrong process. Field's data certainly were not precise enough to conclude that the ring had opened up upon electron impact. Besides, there are workers who argue that open compounds actually close to give a ring structure. The energetics of cyclopropane for which these experimental data existed were reinvestigated in this work to provide a model for cyclopropanone. From studies on the reaction of cyclopropane, Ogg[36,27] calculates the activation energy needed to open the cyclopropane

ring as about 50 kcal/mole by the following equations:

$$\text{cy-}C_3H_6 + I_2 \longrightarrow C_3H_6I_2 \qquad \Delta H_r = -17.2 \text{ kcal/mole}$$

$$2I \longrightarrow I_2 \qquad \Delta H_r = -35.9 \text{ kcal/mole}$$

$$C_3H_6I_2 \longrightarrow \cdot CH_2CH_2CH_2\cdot + 2I \qquad \Delta H_r = +102 \text{ kcal/mole (estimated)}$$

$$\text{cy-}C_3H_6 \longrightarrow \cdot CH_2CH_2CH_2\cdot \qquad = +49 \text{ kcal/mole}$$

This calculation is definitely a heat of reaction and seems that it would better be interpreted as $D^o(C\text{-}C) = 49$. The kinetics of the thermal isomerization of cyclopropane to propylene have been studied[37,38] and the activation energy of the isomerization, 65 kcal/mole, has been identified with the energy needed to open the ring. This number seems to be a more reasonable activation energy for the opening of the ring. This apparent discrepancy between the bond dissociation energy and the energy needed to open the ring brings up a very basic point of concern which we discuss below.

Relation of Bond Dissociation Energies and Activation Energies for Ring Molecules

For the normal dissociation of a bond, the heat of reaction is defined to be the bond dissociation energy and, since the activation energy for the reverse recombination reaction of the radicals is usually negligible , is also approximately equal to the activation energy for dissociation as:

$$R_1\text{-}R_2 \longrightarrow \cdot R_1 + \cdot R_2$$

$$\Delta H_r^o \equiv D^o \simeq \Delta H_{act} \text{ (dissociation)}$$

For the dissociation of a ring molecule into a diradical, the activation energy for the reverse recombination reaction of the diradical is no longer negligible and, in the case of cyclopropane, appears to be about 16 kcal/mole as:

$$\Delta \longrightarrow \cdot C\text{-}C\text{-}C\cdot$$

$$\Delta H_r^o \equiv D^o = 49$$

$$\Delta H_r = \Delta H_{act}\ (\text{dissociation}) - \Delta H_{act}\ (\text{recombination})$$

$$49 = 65\text{-}16$$

Furthermore, the dissociation of a ring molecule into two separate fragments or molecules is a completely different problem which may or may not be related to the dissociation into the diradical. It seems unreasonable to expect the bond dissociation energy as defined by a heat of reaction into molecules to have much meaning because it is no longer a dissociation into radicals. This bond dissociation energy, designated here as $D^o(\triangle)_g$, would better be described as a bond decomposition energy and is the type of dissociation energy we would calculate from ms data. An attempt to relate our ms calculations to other literature dissociation data required us to propose a calculated energetic rearrangement term, $R(R_1)_g^{ex}$, which would allow us to calculate a bond dissociation energy into hypothetical diradicals as:

$$D^o(\triangle)_g \equiv D^o(\triangle)^{ex} + R(\cdot R_1)_g^{ex} + R(\cdot R_2)_g^{ex}$$

This calculation for cyclopropane is:

$$\Delta \longrightarrow C{=}C + CH_2$$

$$D^o(\triangle)_g \equiv \Delta H_r = 56 \text{ kcal/mole}$$

$$\tfrac{1}{2} D^o(\triangle)_g = 28 \text{ kcal/mole} \neq D^o(\text{C-C}) = 49 \quad \text{(lit.)}$$

$$D^o(\triangle)_g = D^o(\triangle)^{ex} + R(C_2H_4)_g^{ex} + R(CH_2)_g^{ex}$$

$$56 = D^o(\triangle)^{ex} + (-47) + (0)$$

$$D^o(\triangle)^{ex} \simeq 103$$

$$\tfrac{1}{2} D^o(\triangle)^{ex} = 52 \simeq D^o(\text{C-C}) = 49 \quad \text{(lit.)}$$

Note that there is no guarantee that the activation energy for dissociation will be the same as or will be related to the activation energy for decomposition.

$\triangle \longrightarrow \cdot\text{C-C-C}\cdot$ $\qquad \Delta H_{act}$ (dissociation) = 65

$\triangle \longrightarrow \text{C} = \text{C} + CH_2$ $\qquad \Delta H_{act}$ (decomposition) = ?

The relation between energetic quantities is shown in the schematic on the following page. Also shown is cyclopropanone whose results are presented later in this chapter. Note that the $\Delta H_r \equiv D^o(\overset{O}{\triangle})_g = -41$ kcal/mole of cyclopropanone is a negative quantity. It would be quite interesting to predict an activation energy for ring opening at the d(C-C) = 1.58 Å bond in cyclopropanone in order to support or dispel the theory that cyclopropanone solution reactions proceed with a low activation energy through the ring opened dipolar ion. As we will discuss, this theory is either supported or dispelled depending on whether or not we applied the rearrangement energy term, $R(\quad)_g^{ex}$, to our calculations. In addition, a study of the activation energy required for ring decomposition was made to allow us to determine an energetic explanation of why cyclopropanone decomposes upon formation in the gas phase.

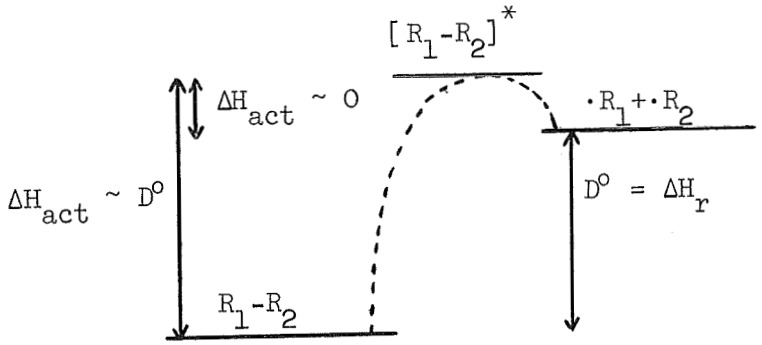

(normal)

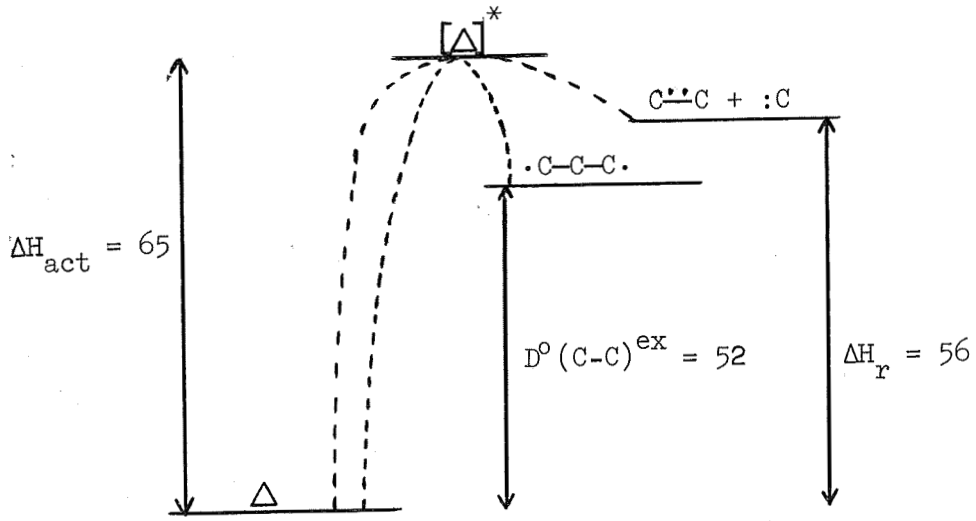

(cy-C_3H_6)

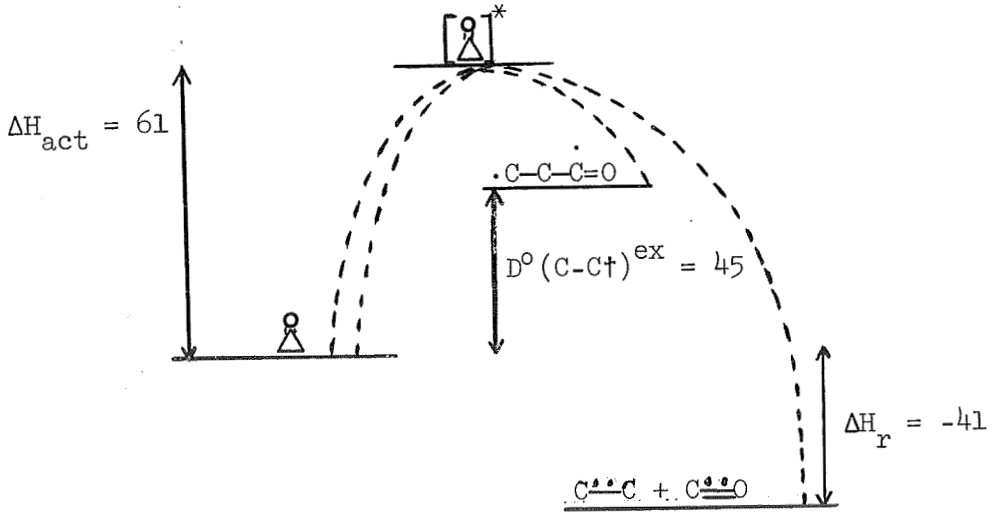

(cy-C_3H_4O)

Reactivity of Ring Molecules

Our problem was to first relate ms dissociation energies to literature experimental quantities and then to relate bond dissociation energies to reaction energetics. This relation was attempted by making a number of exploratory calculations using D, E, and ring strain values and comparing the calculated results to experimental quantities in hopes that an empirical relation or intuitive notion would be revealed.

Since the reactivity of these ring molecules cannot be discussed by equating activation energies with bond dissociation energies, we proposed to also approach the problem from a thermodynamic point of view. Although the driving force for a spontaneous reaction is a negative free energy of reaction, it is a fact that, for most reactions,[4] a negative heat of reaction is also an effective gage for spontaneous reactivity. In this respect, we calculated some heats of reactions by using the experimentally derived ΔH_f^o for cy-C_3H_4O and cy-C_4H_6O in this thesis as follows:

$$\Delta H_r^o = \left(\sum_{\text{prod.}} \Delta H_f^o\right) - \left(\sum_{\text{react.}} \Delta H_f^o\right) \simeq \left(\sum_{\text{broken}}^{\text{bonds}} D^o\right) - \left(\sum_{\text{formed}}^{\text{bonds}} D^o\right) \quad (7)$$

$$\simeq \left(\sum_{\text{broken}}^{\text{bonds}} E\right) - \left(\sum_{\text{formed}}^{\text{bonds}} E\right)$$

By comparing these heats of reaction for alternative and competing reactions, we hoped to obtain some obvious clues for relating reactivity. The results of both the exploratory ΔH_{act} calculations and ΔH_r comparisons in relation to ring reactivity are reported in this chapter.

Procedure

The following is an outline of the procedure used in this work. It allows for an analysis of the sources of error in the calculated results. The sources of such errors are: 1) experimental AP; 2) excess translational and vibrational energy; 3) excited electronic states; 4) assumption of neutral fragments; and 5) literature ΔH_f^o values.

Procedure: Developing Energetics

I. Experiment

- A. Measurements
  1. I(molecular ion)
  2. A(fragment ion)
  3. Peak width of fragment ions
- B. Calculate excess energy, E^*, of fragmentation reaction from peak width

II. Preliminary Work

- A. Assumptions
  1. Stoichiometry of fragmentation (i.e. neutral fragments)
  2. Electronic states of fragments
- B. Data. ΔH_f^o and IP of fragments from literature

III. Derived Energetics

- A. ΔH_f^o(parent molecule)
  1. ms--check assumptions and data by calculating ΔH_f^o from AP of more than one ion by equation 4.
  2. Literature comparison--ΔH_f^o from ΔH_c experiments.
  3. Estimation from E values.

B. D^o

1. Calculation $D^o(\quad)_g$ by equation 2
2. Estimation of $R(R)_g^{ex}$ and calculation $D^o(\quad)^{ex}$ by equation 5.
   a. electronic spectra
   b. thermochemical data (literature)
   c. MO calculations

C. Ring Strain (RS)

1. $RS(E) = \Delta H_f^o(exp.) - \Delta H_f^o(E)$
2. $RS(D^o) = \Delta H_f^o(exp.) - \Delta H_f^o(D^o)$

D. Ring Opening

1. Isomerization--calculation of ΔH_{act}
2. Decomposition--calculation of ΔH_r using ΔH_f^o of parent

Literature Data and Estimations

The ΔH_f^o, IP, and D^o data used in this work are presented in Table 9. Where available, values from different sources are given to show agreement or disagreement. In the last column, the D^o is calculated from the ΔH_f^o to show consistency and general precision. In general, agreement is good; however, there are some points of concern: 1) the ΔH_f^o of diazomethane is available only from an ms measurement of the AP (CH_2^+). This work[21] did not include any measurement of excess energies nor did it check the ΔH_f^o result from the AP of other fragment ions; 2) many values for the ΔH_f^o of CH_2 were found in the literature: 57[2], 57[3], 66[15], 85[13], 88[4], and 95[14] kcal/mole. The first three numbers are calculated from ms data while the fourth and fifth are based on electronic spectra. The

Table 9. Literature Thermochemical Data

Species	Mass	ΔH_f^o	IP	D^o(C–C)	D^o(R-H) = ΔH_f^o(R) + ΔH_f^o(H) - ΔH_f^o(R-H)
C_2H_6	30	-20[3],-20[9]	11.65[2]	88[4],88[7]	98[4],98[5]
$C_2H_6^+$					25[2]
C_2H_5	29	26[5]			39[4],39[6]
$C_2H_5^+$					83[2]
C_2H_4	28	12.5[1],12[3]	10.4[2],10.6[1]	163[4],167[5],122[6]	103[4],104[5]
$C_2H_4^+$		256[3]			78[2]
C_2H_3	27	65[1],63[1]	8.9[1]		43[4],41[6]
$C_2H_3^+$		269[1],278[3]			87[2]
C_2H_2	26	54[1],54[3]	11.4[2],11.4[1]	230[4],230[5]	114[6],125[4],112[7]
$C_2H_2^+$		314[1],317[3]			
C_2H	25	113[3]	12.8		136[6],125[4]
C_2H^+		409[3]			
CH_4	16	-18[1],-18[3]	12.8[2],12.8[1]		105[4]
CH_4^+		278[3]			31[2]
CH_3	15	32[3],33[1]	9.8[1],9.8[2]		106[4],105[5]
CH_3^+		258[3],259[1]			121[2]
CH_2	14	57[2],57[3],88[4],90[5]	10.3[4],11.9[2],12.0[1]		123[6],106[4]
CH_2^+		332[3],333[1],324[4]			79[2]
CH	13	141[1],143[3]	11.1[2],11.0[1]		80[6],81[4]
CH^+		395[3],399[1]			
C	12		11.2		
C^+		85[2]			
CO	28	-26[3],-26[9]	14.0		
CO^+		296[3]			
C_2H_2O	42	-15[3]	9.4-9.6		
$C_2H_2O^+$		203[3]			
H	1	52.1[4]			
C_{gas}	12	170.9[4]			
O	16	59.6[4]			
H_2O(gas)	18	-57.8[9]			
H_2O(liquid)	18	-68.3[9]			
CH_2N_2	42	46[21]			
cy-C_3H_4	40	66.6[65]			
C_3H_6	42	4.9[4]			
cy-C_3H_6	42	12.7[4]			
(1,1 dimethyl)	70	2.6[8]			
C_4H_{10}	58	-3.8[3]			
cy-C_4H_8	56	6.3[4]			
(methyl)	70	-0.8[8]			
C_3H_4O	56	-23[3]	10.1[3],10.25[102]		

last is from an analysis of existing literature data specifically to determine the best available ΔH_f^o. In spite of this poor agreement on ΔH_f^o (CH_2), there is general agreement on the value of ΔH_f^o of the CH_2^+ ion (~ 332 kcal/mole). From the electronic spectra of methylene, it is known that the ground state is a triplet but that the lowest lying singlet is very close to the triplet. Hoffmann's[16] MO calculations support this idea that there is a low lying singlet close to the ground state triplet (within considerably less than one eV) and also predict another singlet about 0.9 eV higher. In his explanation of available data on CH_2, Prophet[14] points out that an excited state of 0.9 eV is needed to explain some data. Hamill[17] has experimentally found excited states of the molecular ion at 0.7 eV, 1.2 eV, and 2.1 eV. The basic point of dispute seems to stem from the IP's measured by ms and spectroscopic methods of 11.9 and 10.3 eV. Workers agree on the $\Delta H_f^o(CH_2^+)$ instead of $\Delta H_f(CH_2)$, and this IP difference produces the difference in ΔH_f^o of CH_2. Spectroscopic methods are generally more reliable and consequently the more respected workers quote a value of about 90 kcal/mole. However, it would seem that, since the ΔH_f^o of the ground state would be the lowest value, it would seem more reasonable to use the lowest ΔH_f^o as the ground state. Choosing $\Delta H_f^o = 90$ leaves no rational explanation of $\Delta H_f^o = 57$. Furthermore, ms work always seems to correlate better with the lower value and this is the value used in this work for the CH_2 neutral fragment. The AP and excess energy experiments of CH_2^+ and N_2^+ from CH_2N_2 which would involve the $\Delta H_f^o(CH_2^+)$, $\Delta H_f^o(CH_2)$, and $\Delta H_f^o(CH_2N_2)$ would be an excellent check on these numbers. Table 10 relates the bond dissociation energies and bond energies to bond lengths in an attempt to arrive at a consistent body of

Table 10. Bond Dissociation Energies, Bond Energies, and Bond Lengths for Open Chain Molecules

Type Molecule	Type Hybrid Bond	Bond Length Å	D^o kcal/mole lit.	D^o kcal/mole *	E kcal/mole lit.	E kcal/mole *
general	C_{sp^3}-C_{sp^3}	1.54	83-88	86	83[8]	83
	C_{sp^3}-C_{sp^2}	1.52			85[8]	
	C_{sp^3}-C_{sp}	1.46			91[8]	
	C_{sp^2}-C_{sp^2}	1.48	96	96		
	C_{sp^2}-C_{sp}	1.42			96[8]	
	C_{sp} – C_{sp}	1.38			103[8]	
	C_{sp^3}-H	1.102	91-98	98		94
	C_{sp^2}-H	1.086		104		99
	C_{sp} – H	1.057	110-125	110		103
	C=C	1.34	122-167		143[8],147	145
	C≡C	1.20	230	230	187[8]	187
aldehyde	C=O	1.22	166-176	175	171[18]	170
ketone	C=O	1.23	179	180	174[18]	175
acids	C=O	1.24				
CO_2	C=O	1.16	128	128	192	192
CO	C≡O	1.129	256	256	256	256
paraffin average	C-C	1.537		86		83
	C-H	1.094[10]		96		96.5
CH_4 (methane)	C-H	1.09				99
C_2H_6 (ethane)	C-C	1.54				83
	C-H	1.102				94
C_2H_4 (ethylene)	C=C	1.35				143
	C-H	1.086				99
C_2H_2 (acetylene)	C≡C	1.20				187
	C-H	1.057				103
CH_3COCH_3 (acetone)	C-C	1.52				85
	C-H	1.089				98
	C=O	1.24				175(180)[a]
CH_2CO (ketene)	C-H	1.075				100.5
	C=C	1.31				150
	C=O	1.17				180(160)[a]
C_3H_4O (acrolein)	C=C					145
	C_{sp^2}-C_{sp^2}					88
	C_{sp^2}-H					99
	C=O					175(174)[a]

*Values chosen for use in this work.

a. Value needed for accurate ΔH_a.

data to use in the energetic calculations. The E values were taken largely from Mortimer[8] and Pauling.[18] In the bottom of the table are listed the geometries and E values for the molecules for which this set of E values correctly predicts ΔH_a: methane, ethane, ethylene, acetylene, acetone, ketene, and acrolein. Table 11 lists D^o and E correlated with known structures of the ring molecules investigated.

In this work it was not attempted to determine the mechanisms of molecular ion fragmentations. Firstly, there are always too many possibilities and, secondly, we were not in a position to accurately calculate the energies of all the structures involved. The basic choice is whether the two ring bonds break simultaneously or consecutively. Because of the extensive rearrangements and breakage and formation of multiple bonds in the fragments, it would appear that at least some of the ring fragmentations are by consecutive C-C bond breaking. However, in this work, a simultaneous process was assumed from which the energies of the hypothetical initial diradical states of the fragments could be estimated.

In the estimation of $R(R_1)_g^{ex}$, one has to account for energy differences due to changes in geometry and the formation of new bonds. In thermochemical estimations, bond energies and electronic spectra were used as follows: $R(CH_2)_g^{ex}$ was taken to be essentially zero because the electronic spectra predict very little energy difference in the singlet and triplet. $R(C_2H_4)_g^{ex}$ in cyclopropane is the energy difference in the structure of d(C-C) = 1.51, d(C-H) = 1.089, H-C-H angle of 115.1° and two unpaired electrons to the ethylene structure of d(C=C) = 1.34, d(C-H) = 1.083 and H-C-H angle of 117.1°. This initial structure is essentially

Table 11. Estimated Bond Dissociation Energies and Bond Energies of Ring Molecules (kcal/mole)

Molecule	Type Hybrid Bond	Bond Distance Å	Normal[a] D^o	Normal[a] E
paraffins	C–C	1.537	86	83
	C–H	1.094	96	96.5
cyclopropane	C–C	1.51	91	87
	C–H	1.089	103	98
cyclopropene	C–C	1.515	90	86
	C=C	1.30	145	145
	$C^{\dagger}$–H	1.070	107	101
	C–H	1.087	104	99
cyclopropanone	C–C	1.58	80	78
	$C^{\dagger}$–C	1.49	92	88
	C–H	1.085	104	99
	C=O	1.18	180	175
cyclobutanone	$C^{\dagger}$–C	1.53	87	84
	C–C	1.55	85	82
	C–H	1.089	103	98
	C–H	1.10	99	95
	C=O	1.215	179	175
cyclobutane	C–C	1.55	85	82
	C–H	1.092	100	97

a. number estimated from the bond distance using Table 10.
† carbonyl or sp^2 carbon.

that of having removed two H atoms from ethane which can be estimated as follows: assuming no changes in geometry, one would estimate the energy to remove 2H atoms from ethane as twice the bond energy (E = 94 kcal). The rearrangement energy of this structure to ethylene would then be the heat of reaction of ethane to ethylene and two hydrogen minus twice the bond energy [136 - 2(94) = -52 kcal/mole]. From D^o(C-C) data in Table 10, one might estimate about +5 kcal/mole for extending the d(C-C) from 1.51 to 1.54 Å and obtain about 47 kcal/mole for $R(C_2H_4)_g^{ex}$ in the cyclopropane fragmentation. Similarly, the $R(C_2H_4)_g^{ex}$ in cyclopropanone was estimated at -58 kcal/mole. The $R(CO)_g^{ex}$ from cyclopropanone is the energy difference in the structure of d(C=O) = 1.18 and two unpaired electrons to the structure d(C≡O) = 1.12 of carbon monoxide. The first structure is essentially that of removing one oxygen atom from CO_2 with no structure changes. This may be easily shown as:

$$\begin{array}{ccccc} O{=}C{=}O & \xrightarrow{+192} & :C{=}O + O & \xrightarrow{-66} & C{\equiv}O + O \\ & \searrow & 126 & \nearrow & \end{array}$$

where E(C=O) = 192 and D^o(C=O) = 126 in CO_2. Therefore, $R(C{=}O)_g^{ex} \sim -66$ kcal/mole. By this approach, the $R(CH_2CO)_g^{ex}$ was also estimated from its known structure and bond dissociation and bond energies.

Calculated Results

Obtaining Consistent Experimental ΔH_f^o Values

Before any energetic quantities could be derived from experimental measurements, it was first necessary to check for and obtain some consis-

tency in the experimental data. This was accomplished by calculating the ΔH_f^o of a parent molecule from experimental AP and E^* measurements on more than one fragment ion from the parent. Table 12 presents these results in this order: the parent molecule; m/e of ion fragment; the experimental AP and E^* measurements from Appendices B and C, respectively; an array of possible stoichiometries for each observed m/e; and a calculation of the heat of formation of the parent molecule by equation 4. Note that a good check on the ΔH_f^o of cyclopropane is obtained by three ground state fragmentation processes and that a fourth is off about 10 kcal. This latter value is not unreasonable in view of the fact that the experimental number, $E^* = 103$, for this process is not very accurate. What is more important is the observation that assuming the observed products to be excited triplets produces ΔH_f's much too high. Only in the case of $E^* = 103$ kcal in which the experimental data were ambiguous (see Appendix C) was there any hint of the existence of excited triplets. Therefore, the assumption of ground state singlets for these mass spectrometric energetic calculations seems to be a good one. For cyclopropanone and, in particular, for cyclobutanone, there is frequently more than one choice for the product ion and always many choices involving the further fragmentation of the product neutrals. However, most of the further neutral fragmentations relate to ΔH_f^o's much too high and can be eliminated. It is unfortunate, but the judgment of which ΔH_f^o is most accurate depends mostly upon the precision of the experimental E^* and AP and not the choosing of processes. However, as witnessed by the reoccurrence of $\Delta H_f^o = 13$ kcal/mole for cyclobutanone, these errors and subjectiveness are partially overcome by the number of independent ion AP's used. As discussed in

Table 12. ΔH_f^o and D^o for Ring Molecules as Calculated from Experimental Data (kcal/mole)

ms Exp. Ion m/e	AP	E*	Dissociation Stoichiometry	Parent[a] ΔH_f^o	Bond Dissociation Energy $D^o(\triangle)_g$	$D^o(\triangle)$	$D^o(\triangle^+)_g$	$D^o(\triangle^+)^{ex}$	$R(R_1)_g^{ex}$ R_1	Estimate Thmo.[b]	MO[b]
27	311	19	cy-C_3H_6 → $(C_2H_3^+)_g$ + $(CH_3)_g$	10*							
			→ $(C_2H_3^+)^{ex}$ + $(CH_3)^{ex}$	> 70							
26	302	16	→ $(C_2H_2^+)_g$ + $(CH_4)_g$	13*							
			→ $(C_2H_2^+)^{ex}$ + $(CH_4)^e$	> 73							
14	427	103	→ $(CH_2^+)_g$ + $(C_2H_4)_g$	21*	51	98	86	133	CH_2^+	0	
		18	→ $(CH_2^+)^{ex}$ + $(C_2H_4)^{ex}$	11-21					C_2H_4	-47	-67
28	302	---	→ $(C_2H_4^+)_g$ + $(CH_2)_g$	> 11*	62	109	64	111	CH_2	0	
			→ $(C_2H_4^+)^{ex}$ + $(CH_2)^{ex}$	> 64					$C_2H_4^+$	-47	
28	235	0	cy-C_3H_4O → CO^+ + C_2H_4	73							
			→ CO^+ + C_2H_3 + H	177							
			→ CO^+ + C_2H_2 + 2H	235							
			→ CO^+ + C_2H_2 + H_2	131							
			→ CO^+ + $2CH_2$	172							
		>17	→ $C_2H_4^+$ + CO	> 19*	-30	91	0	121	C_2H_4	-58	-83
			→ $C_2H_4^+$ + C + O						CO	-66	
42	227	0	→ CH_2CO^+ + CH_2	27*	9	65	18	73	CH_2CO	-55	
			→ CH_2CO^+ + CH + H	163							
27	298	---	→ $C_2H_3^+$ + H + CO	>- 2							
26	312	---	→ $C_2H_2^+$ + H_2 + CO	>-24							
			→ $C_2H_2^+$ + 2H + CO	> 80							
42	254	26	cy-C_4H_6O → CH_2CO^+ + C_2H_4	13*	10	123	23	136	C_2H_4	-55	
			→ $C_3H_6^+$ + CO	-25					CH_2CO	-58	
			→ CH_2CO^+ + CH_2 + CH_2	79							
28	300	18	→ $C_2H_4^+$ + CH_2CO	-41							
			→ CO^+ + C_3H_6	19*							
			→ CO^+ + C_2H_4 + CH_2	83							
			→ $C_2H_4^+$ + CO + CH_2	5*					CO	-66	
									CH_2	0	

Table 12. ΔH_f^o and D^o for Ring Molecules as Calculated from Experimental Data (kcal/mole)

ms Exp. Ion m/e	AP	E*	Dissociation Stoichiometry	Parent[a] ΔH_f^o	Bond Dissociation Energy $D^o(\triangle)_g$	$D^o(\triangle)$	$D^o(\triangle^+)_g$	$D^o(\triangle^+)^{ex}$	$R(R_1)_g^{ex}$ R_1	Estimate Thmo.[b]	MO[b]
27	326	33	cy-$C_4H_6O \rightarrow C_2H_3^+ + H + CH_2CO$	13*							
			$\rightarrow C_2H_3^+ + H + CH_2 + CO$	59							
15	362	---	$\rightarrow CH_3^+ + CH + CH_2CO$	22*							
			$\rightarrow CH_3^+ + C_2H_3 + CO$	-64							
			$\rightarrow CH_3^+ + CH + CH_2 + CO$	68							
14	385	24	$\rightarrow CH_2^+ + C_3H_4O$	-51							
			$\rightarrow CH_2^+ + CH_2CO + CH_2$	14*	85	143	142	200			
			$\rightarrow CH_2^+ + C_2H_4 + CO$	-42							
27	314	12	cy-$C_3H_4 \rightarrow C_2H_3^+ + CH$	88							
15	369	0	$\rightarrow CH_3^+ + C_2H$	2							
14	358	0	$\rightarrow CH_2^+ + C_2H_2$	28							
13	462	12	$\rightarrow CH^+ + C_2H_3$	2							
			$\rightarrow CH^+ + C_2H_2 + H$	51							
			Summary								
			cy-C_3H_6	13 ± 3	56	104	75	121			
			cy-C_3H_4O	27 ± 8	-30,9	91,65	0,18	121,73			
			cy-C_4H_6O	13 ± 5	10,85	123,143	23,142	136,200			
2	3	4	columns[c] 5	6	7	8	9	10	11	12	13
			equations[d]	4	2	5	3	6			

*most probable process based on consistency in ΔH_f^o calculations.

a. Heat of formation of parent molecule calculated from ms data.
b. Thermodynamic and molecular orbital estimates of energetic rearrangement term.
c. Enumeration of columns of Table for reference in the text.
d. Equation in text used to calculate these data.

Appendix B, little confidence was placed in the AP's of the fragments from cyclopropene and, as expected, the ΔH_f^o calculations are poor.

Bond Dissociation Energies

In Table 12, the bond dissociation energies of the two C-C ring bonds calculated with and without $R(\ )_g^{ex}$, $D^o(\triangle)^{ex}$ and $D^o(\triangle)_g$, from equations 5 and 2, respectively, are presented. The values for $R(\ )_g^{ex}$ are also shown in the last columns of Table 12. The thermochemically estimated $R(\ )_g^{ex}$ values were used in the calculations. In all cases of Table 12, the dissociation energy of the molecular ion is greater than that of the molecule. This indicates that a non-bonding or anti-bonding electron was removed which resulted in a strengthening of the ion C-C ring bonds. The importance of including the $R(\ )_g^{ex}$ term is pointed out in the cyclopropanone dissociation into the ground and excited states. Interpreting $D^o(\triangle)_g$ as the sum of D^o for two C-C ring bonds, the data for the dissociation into CH_2CO^+ ($D(\triangle)_g$ = 9 kcal) compared to that for $C{=}C^+$ ($D(\triangle)_g$ = -30 kcal) indicate that the (C-C) bond is stronger than the (C-C†) bond. However, inclusion of $R(\ )_g^{ex}$ terms and calculating $D^o(\triangle)^{ex}$ indicate that (C-C†) bond ($D(\triangle)^{ex}$ = 91 kcal) is stronger than (C-C) bond ($D(\triangle)_g$ = 65 kcal), which is much more reasonable in view of the fact that the former bond length is 1.49 Å as compared to the latter's 1.58 Å. Also, $R(\ )^{ex}$ converts these small and negative D^o values into larger, positive, more reasonable numbers.

Derived Ring Strain, Ring Energies, and ΔH_{act} Results

Table 13 presents a comparison of ring strains and ΔH_{act} calculated

---

† carbonyl carbon

Table 13. Experimental ΔH^o_a and Derived Ring Strain, Ring Energies, and ΔH_{act} (kcal/mole)

	$-\Delta H^o_a$				Ring Strain					Sum	Ring Energies			ΔH_{act}-Ring Opening		
		as calc. from:				as calc. from:				Bent			lit.			
Molecule	lit.	ms	D^o	E	lit.	E	E^*	D^o	$D^o(\triangle)^{ex}$	Angles	E(C–C)	$D^o(C–C)^{ex}$	$D^o(C–C)$	est	lit.	products
cy-C_3H_6	813[4]	813 ± 3	891	849	27[113]	36	26	78	78	147°	75	52	49[36,27]	65	65[37,38]	C=C–C
cy-C_3H_4O	---	853 ± 8	860	825	---	72		107	93	158°	66	45		61		C=C + CO
	---				---				107		40	20		35		C=C=O + CH_2
cy-C_4H_6O	---	1042 ± 5	1105	1087	---	45		63	49	87°				61	52[105]	C=C=O + C=C
cy-C_4H_8	1098[4]		1140	1124	26[113]	26	26	42		76°	75			74		
cy-C_3H_4	656[65]		747	717	54[65]	61		91		170°						
column 1	2	3	4	5	6	7	8	9	10	11	12	13	14	15	16	17

*Relative to paraffinic hydrocarbons.

in this work with available literature quantities. As discussed previously, we hoped to relate ms dissociation energies to the literature values and then to discern a relationship between these dissociation and activation energies. The literature values for ΔH_a^o, ring strain, $D^o(C\text{-}C)$, and ring dissociation and decomposition activation energies are shown in columns 2, 6, 14, and 16, respectively. ΔH_a^o calculated from our experimental ms ΔH_f^o in Table 12 are listed in column 3. The remaining data of Table 13 were calculated using the following equations:

Column	Equation
4	$\Delta H_a = \sum_{\text{bonds}}^{\text{all}} D^o \equiv \Delta H_a(D^o)$
5	$\Delta H_a = \sum_{\text{bonds}}^{\text{all}} E \equiv \Delta H_a(E)$
7	$\Delta H_a(\text{ms}) - \Delta H_a(E) \equiv RS(E)$
9	$\Delta H_a(\text{ms}) - \Delta H_a(D^o) \equiv RS(D^o)$
10	$2D^o(C\text{-}C) - D^o(\triangle)^{ex} \equiv RS(\triangle)^{ex}$
11	$\sum^{\text{ring}} (\text{normal bond angles}) - \sum^{\text{ring}} (\text{strained ring angles})$
12	$\left[\sum^{\text{ring}} \text{normal } E(C\text{-}C)\right] - RS(E) = 3 \text{ strained } E(C\text{-}C)$
or	$\left[\sum^{\text{ring}} \text{normal } E(C\text{-}C)\right] - RS(E) = 2a + b$; $a = \text{strained } E(C\text{-}C^{\dagger})$
	$\left[D(\triangle^{O})^{ex} - D(\triangle^{O})^{ex}\right] = (2a) - (a+b)$; $b = \text{strained } E(C\text{-}C)$

† carbonyl carbon

Column	Equation
13	$D(\triangle)^{ex} = 2D^{o}(C\text{-}C)^{ex}$
or	$D(\overset{O}{\triangle})^{ex} = 2a$; $a = D^{o}(C\text{-}C^{\dagger})^{ex}$
	$D(\overset{O}{\triangle})^{ex} = a+b$; $b = D^{o}(C\text{-}C)^{ex}$
15	Same as 12; use D^{o} for E

Ring Strain. The ΔH_a^o and ring strains listed in columns 5 and 7, respectively, are calculated from bond energies (E) in the usual manner as has been discussed previously. These ring strains are localized to the three carbon-carbon ring bonds. The RS(E) for cyclopropane can be made to coincide with the literature ring strain (which is experimentally determined relative to the paraffinic series) by subtracting about 1.5 kcal from each E(C-H) bond energy, a correction for the C-H bond lengths of 1.089 and 1.094 Å from cyclopropane to the paraffinic series. Due to the change from sp^3 to sp^2 hybridizations at the carbonyl carbon in going from cyclopropane to cyclopropanone and from cyclobutane and cyclobutanone, one would expect these first two molecules to show additional strain. Indeed, cyclopropanone and cyclobutanone were calculated to have additional ring strains of 36 and 19 kcal/mole, respectively. However, these values appear somewhat larger than expected. The heats of formation of cyclopropanone and cyclobutanone calculated herein, from which the ring strains are calculated, would appear to be totally independent of each other aside from the fact that the same techniques of measuring AP and E^*

---

† carbonyl carbon

were used. There are many arguments supporting the ΔH_f^o calculated for cyclobutanone. The cyclobutanone experiments were obtained on pure samples under such experimental conditions that the sample could be manipulated to give more precise E^* and AP data. Table 12 shows the consistent results for calculating the ΔH_f^o from five separate processes. In particular, as m/e 42 was the major fragment, the AP and E^* measurements were judged to be quite reliable. Furthermore, high resolution mass spectrometry[61] has shown that m/e 42 is predominantly CH_2CO^+ (not $C_3H_6^+$) and, thus, the stoichiometric process appears to be the correct one. If one accepts 19 kcal/mole as the increased strain in the four-membered ring, then the increased strain of 36 kcal/mole for the three membered ring seems more reasonable. The cyclopropanone experiments were carried out with difficulties and the results are not as unambiguous as those of cyclobutanone. Table 12 includes the available processes for the ring fragmentations. To obtain a lower ring strain, one would have to have a lower heat of formation and, judging from the processes available, this possibility seems very unlikely. Since the set of bond energies (Table 11) calculates reasonable ring strains for cyclopropane and cyclopropene, the only number subject to discussion is E(C=O) = 175 kcal/mole which likewise seems to be quite reasonable as a higher value of E(C=O) would lead to an even larger ring strain. Assuming that: the bond energies are a good consistent set; that the liquid-liquid synthesis at -145° is the actual reaction of diazomethane with ketene; and that the heat of formation of diazomethane is correct, any lowering of the ring strain of cyclopropanone by more than 7 kcal/mole would result in an equivalent error in its heat of formation and make the diazomethane and ketene reaction an

endothermic reaction at 25° in the gas phase.

The ΔH_a^o and ring strain numbers listed in columns 4 and 9 were calculated analogously to the E calculations but using D^o values which one would estimate for any non-ring, normal bonds and which are listed in Table 11. If one assumes that all the ring strain is relieved when the molecule is decomposed, then we might expect to calculate this ring strain by taking the difference in D^o for two normal carbon-carbon bonds (see estimation in Table 11) and the $D^o(\triangle)^{ex}$ calculated for the two ring bonds from experimental data. This calculation is reported in column 10. Comparison of columns 9 and 10 from the two different ring strain calculations, both using D^o values, shows good agreement for cyclopropane and cyclopropanone but poorer agreement for cyclobutanone. The value of these calculations remains open to question as they were simply made to determine if there were some means to calculate or predict the effect of ring strain on experimental numbers.

A numerical value for the total sum of strained ring angles was calculated in column 11. As far as we could ascertain, there was no obvious quantitative relation between these values and the ring strains.

Bond and Bond Dissociation Energies. In column 12, Table 13, we calculated empirical bond energies, E, by distributing the ring strain among the three carbon-carbon ring bonds. For cyclopropane, this distribution is easily and equally done but for the unequal C-C bonds of cyclopropanone we assumed that the energetic difference in breaking two (C-C) bonds and that of one C-C bond and one ($C-C^{\dagger}$) bond would be the difference

---

†carbonyl carbon

in one (C-C) bond and one ($C-C^{\dagger}$) and took this difference as being the equivalent to the D^{o}( )^{ex} difference where D^{o}( )^{ex} has been discussed previously. This was the calculation procedure we used whenever we wanted to distribute an energetic amount among the cyclopropanone ring bonds. In column 13, the dissociation energy for a cyclopropane (C-C) ring bond was taken as one half the ms value of D^{o}( )^{ex} = 104 kcal/mole and this result, 52 kcal/mole, compares favorably with what we earlier had defined as the dissociation energy of one C-C ring bond from the data of Ogg. The D^{o} quantities in column 13 for cyclopropanone were calculated in an analogous calculation with distribution among the unequal ring bonds.

Activation Energies for Ring Opening. In column 15, we repeated the calculation of column 12 substituting the normal D^{o} values of Table 11 once again for the E values. It was found that the ring strain calculated from D^{o} numbers and distributed among the (C-C) ring bonds resulted in a strained D^{o} that is numerically equal to the activation energy for cyclopropane isomerization. Values for cyclopropanone were obtained analogously. This body of data is explained as follows: In the normal dissociation of one bond, the D^{o} is the heat of reaction, but it is also the activation energy of reaction since the reverse activation energy for the recombination of radicals is always very small and usually assumed to be zero. However, the reverse activation energy for the recombination of molecules to form rings is now quite large and the activation energy for the bond dissociation of a ring can assume any value which may or may not be related to D^{o}. By using D^{o} values which can be associated with activation energies in single bonds, in the calculation of the strained bonds, we obtained an overall gross result which yielded the activation energy

of breaking a ring bond. Cyclopropane, although it has a bond energy of 75 kcal, actually has a lower energy of activation to open the ring of 65 kcal. The D^o = 52 kcal/mole is an average of two bond dissociation energies and cannot be related to activation energies. Using the same reasoning and calculation, we would expect cyclopropanone to have an activation energy for ring opening at its bonds of 35 and 61 kcal compared to its bond energies of 40 and 66 kcal. Experimentally, strain energies manifest themselves in low activation energies and thus it was desirable to estimate these activation energies for cyclopropanone. Note that the proposed ΔH_{act} of 35 kcal/mole would support the postulation[21] that many cyclopropanone reactions may proceed with a low activation energy through the ring opened, dipolar ion.

Thermodynamic Heats of Reaction and Reactivity Considerations

Figure 6 displays a number of reactions for which the heats were calculated using the ΔH_f^o measured in this work and are displayed over each arrow. (Note that these ΔH_r^o are for the reactants and products in the ideal gas state at 25°.) The numbers in parentheses are for the high value of $\Delta H_f(CH_2)$ = 90 kcal/mole. The numbers in brackets are experimental activation energies. The heat of polymerization of cyclopropane was taken from Mortimer[8] while those for cyclopropanone and cyclopropene were taken as the difference in energy of bonds broken minus bonds formed (see equation 7) plus the relief of angle strain. The following comments apply to these calculated heats of reaction. Frey[23] has reacted methylene from diazomethane with cyclobutane to produce methylcyclobutane which will decompose to propylene and ethylene. However, if the gas pressure is increased to remove the excess energy that the product contains from the

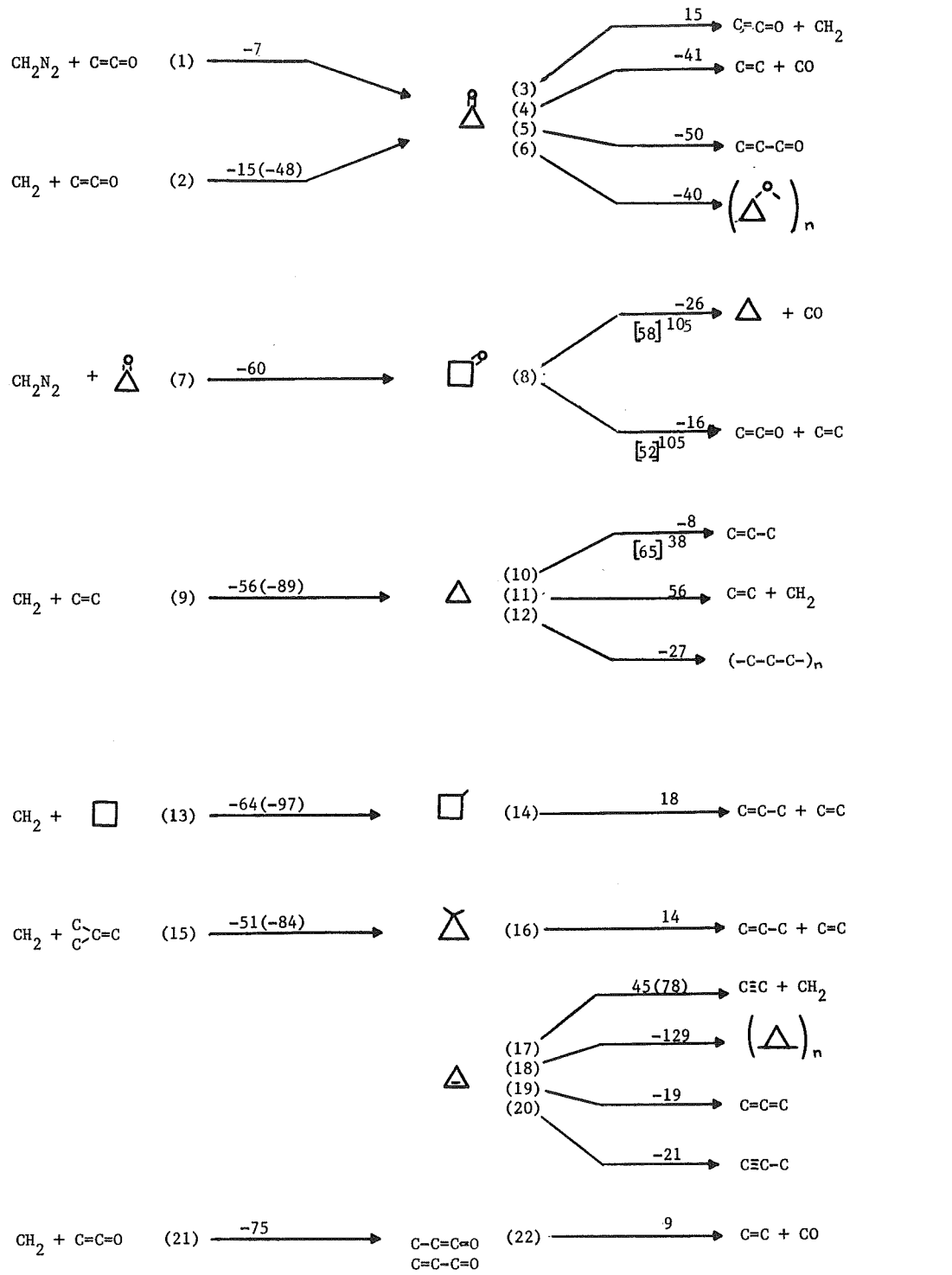

Figure 6. Possible Reactions and Their Heats

heat of reaction, then the methylcyclobutane will not decompose. Also, by reacting CH_2 from ketene he produced methylcyclobutane with no apparent decomposition. CH_2 is produced from diazomethane in the excited singlet while from ketene it is also formed in the ground triplet.[13] However, the energy difference between this singlet and triplet has always been predicted as very small. If the activation energy for ring opening of 74 kcal/mole estimated in this work for cyclobutane can be assumed to be that for methylcyclobutane, then it may be postulated that the singlet from diazomethane and the triplet from ketene be associated with the heats of formation 90 and 57 kcal/mole because the calculated heats of reaction -97 and -64 kcal/mole, respectively, bracket the activation energy. In a similar experiment, Frey[24] studied the reaction of CH_2 from diazomethane with ethylene to form cyclopropane which opened to propylene unless quenched. Since the activation energy for cyclopropane ring opening has been measured as 65 kcal/mole, we would need to associate ΔH_f^o = 90 kcal/mole for CH_2 to obtain a ΔH_r^o (-89 kcal/mole) which is greater than 65 kcal/mole. In another reaction of interest, Frey[25] reacted methylene from diazomethane with isobutene to form 1,1 dimethylcyclopropane which did not open up. Using the $\Delta H_f^o(CH_2)$ = 90, we calculated ΔH_r^o = -84 kcal/mole which would seem to be enough to open the cyclopropane ring. This example implies that the hypothesis that the heat of reaction for the formation of the ring must liberate an amount of energy greater than the activation energy for ring opening is a necessary, but not a sufficient, requirement. In this example, the product apparently had enough degrees of vibrational freedom to absorb the excess energy and prevent it from being concentrated at a single ring bond. From the gas phase

reaction of ketene produced methylene with ketene, Kistiakowsky[46] observed ethylene and CO which he proposed were the decomposition products of the first formed cyclopropanone ring. Note that to evolve an amount of heat greater than the 35 kcal/mole minimum activation energy estimated in this work, the high value $\Delta H_f^o(CH_2)$ = 90 kcal/mole must be used to obtain a heat of reaction of -48 kcal/mole. Either our estimated activation energy of 35 kcal/mole or the earlier statement that $\Delta H_f^o(CH_2)$ = 57 kcal/mole be associated with the triplet CH_2 from ketene, or the assumption that CH_2 from ketene is the triplet is in error. Triplet CH_2 is known to insert randomly and, since Kistiakowsky did not observe cyclopropanone, it is feasible that CH_2 inserted in ketene to form an open chain compound (see reaction 21) which decomposed to ethylene and CO. This explanation would not affect any of our other hypotheses. If the CH_2 that reacted with ketene was produced from ketene as the singlet, then all the calculated quantities appear logical. Demore[48] repeated the reaction of CH_2 from diazomethane with ethylene at 20°K and obtained the quenched cyclopropane product. He also reacted CH_2 from diazomethane with ketene at 20°K and observed what was thought to be cyclopropanone. These examples again point out the value of low temperatures for both a quenching of excited species and a slowing of reactions.

Figure 6 also shows an array of possible reactions (see reactions 1, 3, 4, 5, 6, 7, 8, and 9) in the synthesis of cyclopropanone from ketene and diazomethane. Note that, as calculated, the synthesis of cyclopropanone is only slightly exothermic and much less so than the other reactions; hence, the need of low temperatures and excess ketene. Reactions 17-20 display the ΔH_r^o for the possible reactions of cyclopropene. Note

that the decomposition of the ring is an endothermic reaction and that the polymerization is the most exothermic reaction followed by the less exothermic isomerization to methylacetylene. It is interesting that cyclopropene ring decomposition has not been experimentally observed and that cyclopropene, when heated from low temperatures, begins to polymerize at a temperature (-80°) much lower than it will isomerize to methylacetylene (325°). This reactivity indicates that the activation energy for polymerization is lower than that for isomerization and also that the activation energy for decomposition is very large. The activation energies characterizing cyclopropene reactivity increase with increasing endothermicity. Thus the heats of reactions of cyclopropene are so grossly different that its reactivity follows and may be predicted from this exothermic trend.

Summarizing Comments

We have obtained consistent heats of formation for the ring molecules investigated and straightforwardly calculated ring strains and bond energies (E) which we believe to be reliable. Introduction of the rearrangement energy term allowed ms data to be related to the literature values as $D^{o}(C\text{-}C) = 52$ for cyclopropane agreed well with the literature value of 49 kcal/mole. The rearrangement term also allowed a more reasonable distribution of energy among the ring bonds of cyclopropanone. We believe these results using the rearrangement term are significant and indicate that values derived from ms measurements on ring molecules must involve these terms. For ring molecules, it appears that bond dissociation energies are not only not equal to activation energies for ring opening but there also appears to be no simple relation between the two.

Exploratory calculations with normal D^o values led to interesting but inconclusive results. Assigning ΔH_f^o = 90 kcal/mole to the singlet methylene leads to a series of consistent results for ring opening reactions and induces us to conclude that a necessary, but not sufficient, condition for ring opening is that the heat of reaction from the formation of the ring be greater than the activation energy for ring opening or decomposition. Although in some cases the reactivity of cyclic molecules correlated with calculated exothermicity, we can draw no valid conclusions relating the two because of the lack of kinetic data. The results assembled in this thesis on ring molecules form an interesting body that awaits a rational explanation unique to ring molecules.

CHAPTER V

CONCLUSIONS AND RECOMMENDATIONS

1. Cyclopropene was successfully synthesized at room temperature. It is stable indefinitely at -196° and can be distilled and transferred at room temperature under high vacuum with no structural changes and with only an insignificant loss from polymerization. This molecule was found to be much easier to handle than expected from previous data on its reactivity and explosiveness. Only at room temperature was polymerization noticeable. It possesses a very unusual mass spectrum as the parent molecular ion as well as all ions which possess the unopened ring are all very intense while peaks that result from fragmentation of the ring structure are relatively very weak. This low abundance along with very shallow AP curves precludes the possibility of obtaining reliable experimental AP's for the development of the molecular energetics. The IP of cyclopropene was measured at 9.6-9.7 eV which was supported by an MO calculation of 9.6 eV, but it was slightly less than an earlier value of 9.95 eV. Due to the lack of precision in ms work, the difference was not believed large enough to be attributed to anything other than experimental error.

2. Cyclopropanone was synthesized and isolated as a pure species from the liquid-liquid reaction of diazomethane and ketene at -145°. This is a novel reaction in that it is truly one of the few cryochemical reactions which will proceed at low temperature without external activa-

tion. Improved yields and fewer by-products were obtained with purer reagents and with ketene in excess of fivefold. Although it begins to polymerize at about -90° and polymerizes very rapidly at room temperature, it can be stored indefinitely at -196°. Although cyclopropanone is reported to decompose upon its formation in the gas phase reaction of methylene and ketene, it was found that, after quenching to low temperatures, heating the molecule up to temperatures as high as 25°C did not produce any evidence of decomposition or structure changes, but rather it increased the rate of polymerization. The enhanced reactivity at the carbonyl carbon is the result of the relief of angle strains obtained as the bonding changes from sp^2 to sp^3 bonding. The mass spectra, IP's, and excess fragmentation energies of cyclopropanone and cyclobutanone were obtained from which their molecular energetics were then deduced. The IP of cyclopropanone (9.1 eV) was more than a volt lower than its open isomer, acrolein, and it was supported by MO calculations which also supported the experimental value for cyclobutanone (9.4 eV).

3. Cyclopropene was studied at -145° and room temperature. Although it is known to polymerize at -80° and although the polymerization is believed to be a reaction of the excited double bond diradical,[63] no experimentally detected change in the IP (9.6-9.7 eV) from -145° to +25° was observed. This leads one to conclude that any formation of a triplet occurs in such small amounts as to be experimentally undetectable. Similarly, cyclopropanone was studied at -90° and +25°. Although this species polymerizes quite rapidly at room temperature and although many of its reactions in solution are explained to proceed through the open ring dipolar ion (23 kcal/mole more stable than the closed ring),

no change in the IP (9.1 eV) also implies no detectable presence of these structures.

4. Several points may be made regarding the cyclopropenone synthesis and isolation.

a) Although the reported synthesis and nmr analysis for cyclopropenone were reproduced, the isolation of the ketone was not accomplished by any of the following techniques: extraction of the ketone from water solution using different kinds of solvents; performing the hydrolysis step in water soluble solvents; partial hydrolysis of the dichlorocyclopropene sample with less than the stoichiometric amount of water; and drying of the solutions to remove dissolved water. The solutions resulting from the application of these techniques were all analyzed by distilling them at low temperatures into the mass spectrometer. Instead of identifying the ketone, other products were observed which were not reported in the original publication[76] (which fails to report the presence of other products). In addition, this publication[76] identified the m/e 72 product as acrylic acid which, from our work, does not appear to be a correct analysis. It was concluded that further work will better define the problem and that, in view of this work, the original synthesis, and the lack of additional publications since this first reported synthesis (two years), the approach discussed herein to the synthesis and separation has not been and likely will not be very fruitful.

b) Assuming that the original synthesis and characterization are correct, this isolation failure may be a result of hydrogen bonded water being needed to stablize the structure and prevent reaction. This need is so great that water and ketone must move amongst solvents as a

unit, and vaporization of the solution leads to immediate and complete reaction of the ketone. On the other hand, the products of this work and the unsubstantiated original publication suggest that some other structure(s) was made rather than the ketone. A third possible explanation is the existence of a solution equilibrium between the cyclopropenone and its hydrate in which its hydrate possesses a much higher vapor pressure.

c) Dichlorocyclopropene and "hydrated cyclopropenone" were found to be cryochemical reagents polymerizing rapidly at room temperature.

5. The energetics of cyclopropane seemed to be explained by the insertion of an energetic rearrangement term, $R(R_1)_g^{ex}$, in the equations for calculating $D^o(R_1\text{-}R_2)$ and $D^o(R_1^+\text{-}R_2)$. We were able to calculate for cyclopropane the following values which compared well with literature data:

$\Delta H_f^o = 13 \pm 3$	(lit. = 12.7)
ring strain* = 36	(lit. = 27 relative to paraffins)
E(C-C) = 75	
D^o(C-C) = 52	(lit. = 49)
ΔH_{act}(ring opening) $\simeq$ 65	(lit. = 65)

From the ms calculated heats of formation of cyclopropanone and cyclobutanone of 27 ± 8 and 13 ± 5 kcal/mole, respectively, bond energies were used to calculate additional ring strains of 36 and 19 kcal/mole with respect to cyclopropane and cyclobutane. By a procedure analogous

---

*localized to carbon-carbon ring bonds

to the one used for cyclopropane, the following values were predicted for cyclopropanone:

$$E(C\text{-}C^{\dagger}) = 66;\ E(C\text{-}C) = 40;$$

$$D^{o}(C\text{-}C^{\dagger}) = 45;\ D^{o}(C\text{-}C) = 20;$$

$$\Delta H_{act}(C\text{-}C^{\dagger}) = 61;\ \text{and}\ \Delta H_{act}(C\text{-}C) = 35.$$

This latter value supports the theory that cyclopropanone solution reactions proceed with a low activation energy through a ring opened dipolar ion. Note that, without the inclusion of $R(\ )_g^{ex}$ terms, ms results would predict a stronger bond at the distant carbon-carbon bond d(C-C) = 1.58 Å than the $d(C\text{-}C^{\dagger})$ = 1.49 Å bond. This result particularly points out the necessity of the rearrangement term.

6. This reported ms experimental procedure can evidently be used to calculate ΔH_f^o to within about ± 5 kcal/mole. Any lack of precision in either AP or E^* measurements is partially overcome by using more than one fragment ion to calculate ΔH_f^o. This measurement is only worth the trouble for molecules with structures from which it is not possible to make a good estimate from other methods. It is particularly adaptable to small rings because the fragments are produced in ground electronic states and correspond to molecules for which ΔH_f^o and IP are usually known and need not be measured. However, it is necessary to check for the occurrence of excess translational and vibrational energies. This technique is the reversal of the normal energetic treatment from which the heat of formation of the fragment ion is calculated from the AP by knowing the ΔH_f^o of the parent molecule.

---

†carbonyl carbon

7. The following conclusions about the ms energetics of ring compounds may be made: although it is very common for the fragments produced upon electron impact of ring compounds to possess excess translational and vibrational energy, it is rare that the measured appearance potential corresponds to a fragment in an excited electronic state. The excess energy may be viewed as residual energy from the fragmentation and formation of multiple bonds. Inclusion of a rearrangement correction term for the energetic difference in the initial and final ring fragmentation products allows one to assign ring bond energies to particular bonds and enables both D^{o} and an estimation of ring opening activation energies to be calculated. These seem to relate well to literature data. By analyzing a series of ring opening problems, it appears that a necessary, but not sufficient, condition for ring opening is that the amount of energy liberated from the formation of the ring be greater than the activation energy for ring opening. This analysis also revealed that the most likely ΔH_f^o associated with excited singlet methylene from diazomethane is around 90 kcal/mole.

8. The following improvements were realized with the adaptation of an X-Y recorder for AP measurements.

a) The X-Y recorder using the "linear match" or "initial break" methods can reduce the time previously required for manual recording of IE data from greater than an hour to about 10 minutes without much loss in precision.

b) The rapidity with which the IE data can be recorded combats slow changes in ion intensities.

c) The X-Y recorder allows a quick check of the entire IE

curve to detect any abnormalities which may dictate the IE method to be used.

9. The following conclusions were made concerning the technique used in this work for the measurement of excess energies.

a) The correlation appears to apply well to a large class of compounds.

b) The accuracy is limited by poor precision in making the experimental measurements.

c) The poor precision of the experimental data prevented a definite conclusion about the theoretical soundness of relating experimental excess fragmentation energies to calculated thermodynamic states.

10. The following conclusions were made concerning the general measurement AP's and the particular problem of long-tail ions.

a) The determination of IP from IE curves that have standard shapes is obtainable by any number of methods with varying degrees of precision. On the other hand, the AP of ions with long tails requires methods that will separate the curve into sections pertaining to a single process. The AP of some long-tail, low abundance ions may be experimentally undeterminable using instrumentation of the sort employed here.

b) IE curves resulting from ions whose partial pressures in the ion source differ by a factor of 10 or less may be electronically adjusted to a linear match over the range of five to six eV from the point of initial onset without introducing an error of more than 0.2 eV. Although electronic adjustment produces curves that will overlap, the initial breaks method is difficult to apply because the signal/noise changes and the IE curves appear different at the point of initial onset.

However, by looking for good overlap of the curves over the first two volts of the curve, one can obtain higher precision and still have a method that emphasizes the initial onset region of the IE curve.

11. The following conclusions were made concerning the application of MO calculations to strained ring molecules.

a) From the results of this work with the four MO programs (Mindo, Pople, Klopman, and Hoffman), only Pople appeared to show any promise of structure prediction.

b) Because of the inability of molecular orbital calculations to predict known molecular structures or even most stable structures from which accurate ΔH_a and ionization potentials could be calculated, theoretical chemists have had to adjust molecular parameters by empirical means such that ΔH_a and ionization potentials could be calculated accurately (on the average) for broad classes of compounds whose actual experimental bond lengths and angles are similar enough to allow a set of "standard" molecular geometries to be used for all molecules in the calculations. Since cryogenic strained ring compounds owe their existence to abnormal (as opposed to standard) bonding and structure, the goals of synthesizing cryogenic molecules and semi-empirical MO calculations seem to be mutually exclusive without some knowledge of how to assign a standard geometry to a ring.

c) Because of the insensitivity of the IP to geometry changes and the good accuracy of calculated versus experimental IP (assuming the Mindo systematic oxygen IP error is correctable), the Klopman and Mindo programs appear to be usable for calculating IP's of cryogenic ring molecules. However, the strong geometry dependence (especially the C-C

ring bonds) of both Mindo and Klopman prevent the use of these two programs for calculating ΔH_f^o until some confidence is gained in assigning standard geometries to abnormal rings. This assignment is further complicated for ring molecules of unmeasured actual geometries. Although the triplet calculations appear usable for parent molecules, the application to fragments appears to be also dependent on some better understanding of standard geometries.

d) Confidence in assigning standard geometries to ring molecules may be obtained by working with many known strained rings. Or, for a particular ring molecule with derivatives of known structure and properties, good agreement may result from calibrating the programs for this family of molecules as has been done for cyclopropane and cyclopropene families.[100]

e) Once this confidence is gained, the programs offer a strong potential for ms identification and distinction between ring and open isomers wherein ΔH_a and IP usually differ significantly. For very unstable molecules not amenable to nmr or ir analysis, this seems a very worthy goal.

f) Although parts of the programs may not yet be sufficiently accurate for absolute use, they still offer the possibility of relative comparison of different structures, triplets, isomers, etc. from which qualitative trends or relative quantitative data can be used for ms decisions and calculations. Also included in this area is the prediction of relative stabilities of competing products.

The following work should be done.

The ideas and techniques developed in this work concerning the

synthesis of small rings and the determination of excess energies, heats of formation, etc. should be extended to other cryogenic, strained ring molecules with special emphasis on:

a) Low temperature reactions of diazomethane with other reagents.

b) Further work on the synthesis and isolation of cyclopropenone.

c) Addition of atomic species to cyclopropene and cyclopropenone.

The techniques of measuring excess energies and obtaining heats of formation, etc. should be employed to rectify inconsistent data or to obtain inestimable data such as:

a) The debatable molecular energetics of cyclic B_2H_6.

b) The heat of formation of abnormally structured molecules.

The measurement of excess energies and appearance potentials of CH_2^+ and N_2^+ from diazomethane should be made to determine the best values for the heats of formation of CH_2 and CH_2N_2.

A study of the effect of low and high temperatures on the mass spectra and appearance potentials of molecules with a large number of vibrational degrees of freedom and/or known electronic states.

More precise experimental techniques should be developed such as:

a) RPD and/or second derivative AP methods,

b) improvement in electronic circuitry involved in obtaining experimental excess energy data.

The theoretical soundness of relating experimental excess energies to calculated thermodynamic states should be reinvestigated if the precision of mass spectrometrically obtained excess energies and appearance potentials improves to the level required for such an investigation.

Molecular orbital generalizations should be developed for ring compounds because of the potential in product identification and deriving molecular energetics.

APPENDIX A

MASS SPECTRAL DATA

This appendix contains figures presenting the raw mass spectral data for the molecules studied for which it was possible to effect a fair separation of the molecule and its impurities. Unless stated otherwise, all mass spectra were obtained at 70 eV. Both positive and negative ion spectra were checked for cyclopropanone, cyclopropane, and cyclopropene. Negative ion spectra cannot be recorded with existing laboratory instrumentation and CCl_4 was injected into the spectrometer for a rough calibration. Negative ions were observed for Cl^- at masses 35 and 37 and even the OH^- at mass 17 from background water was visible. Under these same experimental conditions, no negative ions were detected for the ring systems.

cy-C_3H_6

Figure 7 pictures the mass spectrum of cyclopropane. Table 2 (Chapter III) compares this spectrum to literature spectra which agree as well as expected. There are some interesting points to be made about the spectrum. The high abundance of the ions pertaining to the ring (m/e 42, 41, ..., 36) indicates that the positively charged ring is a stable structure. This is reasonable in view of the fact that cyclopropane ring is known to have an electronegative character. Field[27] used energetic arguments to claim that the ring opened up with electron bom-

bardment. This idea is questioned in the energetic section of this work. It is not surprising that mass 39 is abundantly present. This cyclic ion is the simplest possible aromatic system and, as we shall see, is the most abundant ion in cyclopropene. It is interesting to note the lack of abundance of the two most obvious fragment ions:

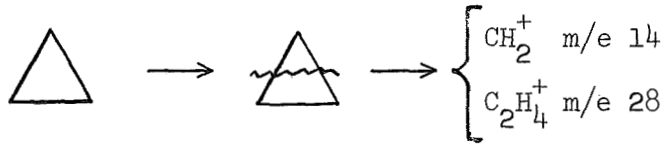

The greater abundance of fragment $C_2H_3^+$ (36 percent) and $C_2H_2^+$ (16 percent) w.r.t. $C_2H_4^+$ (five percent) indicates that the fragmentation probably involves a two-step procedure with an intermediate rearrangement process. These more abundant fragments also produced more normally shaped IE curves (see Appendix B).

cy-C_3H_4O

The mass spectrum of the reaction off gas is presented in Figure 10. Comparison of product mass 70 spectrum and cyclobutanone spectrum in Figure 8 supports the conclusion that they are the same molecule. Figure 9 characterizes cyclopropanone under various conditions. Note that, as expected, its mass spectrum shows very weak ring bonds, possibly giving both CO^+ and $C_2H_4^+$. Also note the similarity of this spectrum to cyclobutanone.

cy-C_3H_4

Figure 7 compares the nearly identical mass spectra of cyclopro-

pene at low temperature (-140°) and room temperature. This mass spectrum is very unusual. The ion peaks corresponding to the intact (m/e 40, 39, ... , 36) ring are very intense. The fact that the ring should so readily accept a positive charge is explained by the theory of aromatic compounds. A ring will be aromatic if it possesses 4N + 2 electrons (N = 0, 1, 2, ...). Planar cyclopropenyl cation

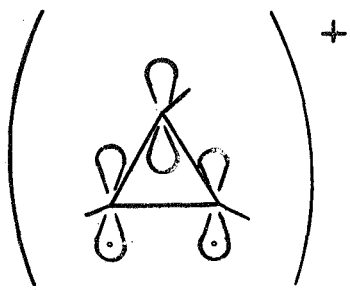

with only two electrons in the p orbitals would be aromatic and, hence, contain considerable electron delocalization stablization. The intensities of ions resulting from the fragmentation of the cyclopropene ring are all less than 10 percent of the most abundant peak. In addition, part of these small mass signals may be produced from the fragmentation of an impurity present in the sample (m/e 42, 41, ...).

cy-C_3H_2O

The mass spectra of the cyclopropenone experiments are presented in this appendix but are more conveniently analyzed in Chapter III.

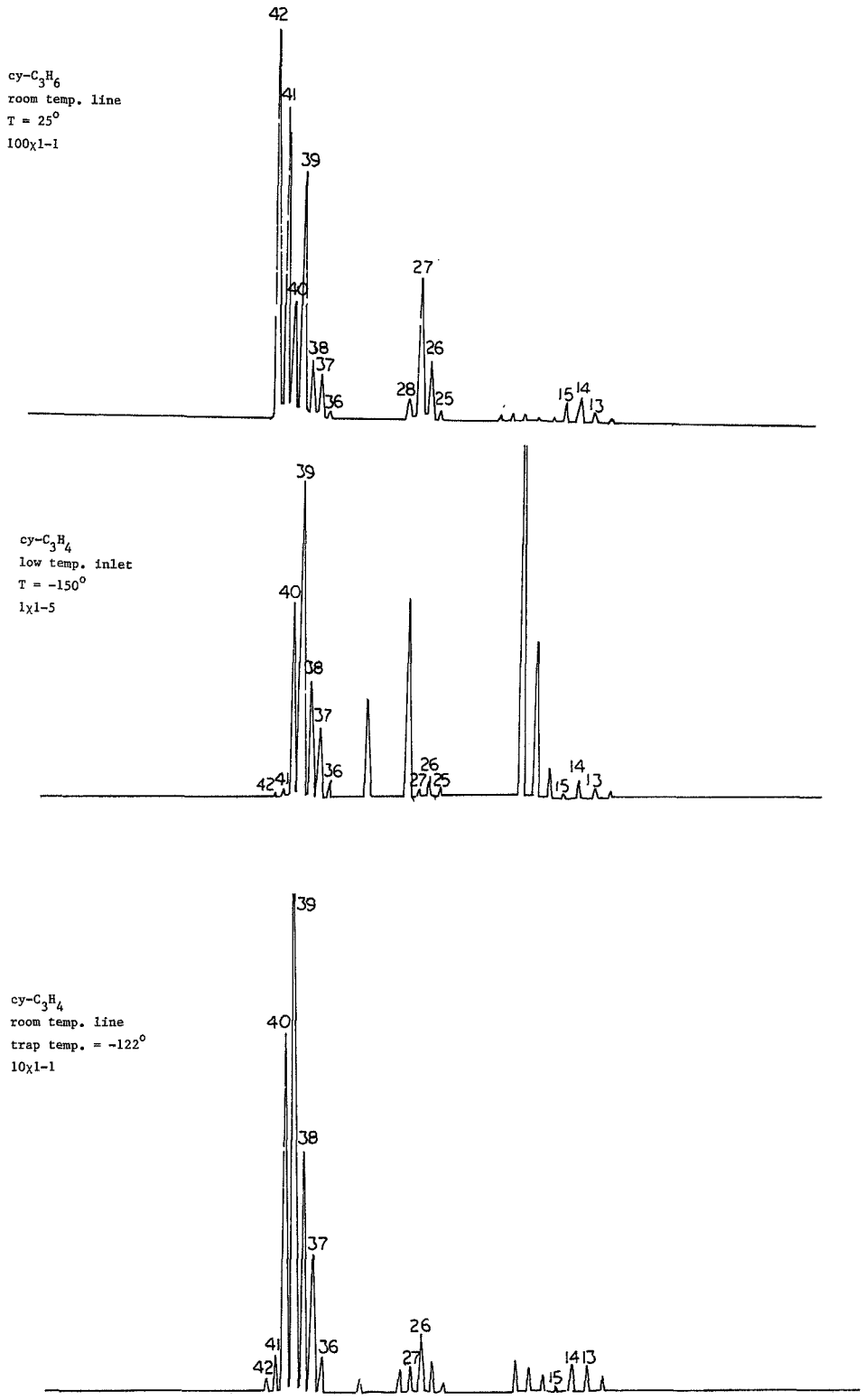

Figure 7. ms of Cyclopropane at 25° and ms of Cyclopropene at -150° and 25°

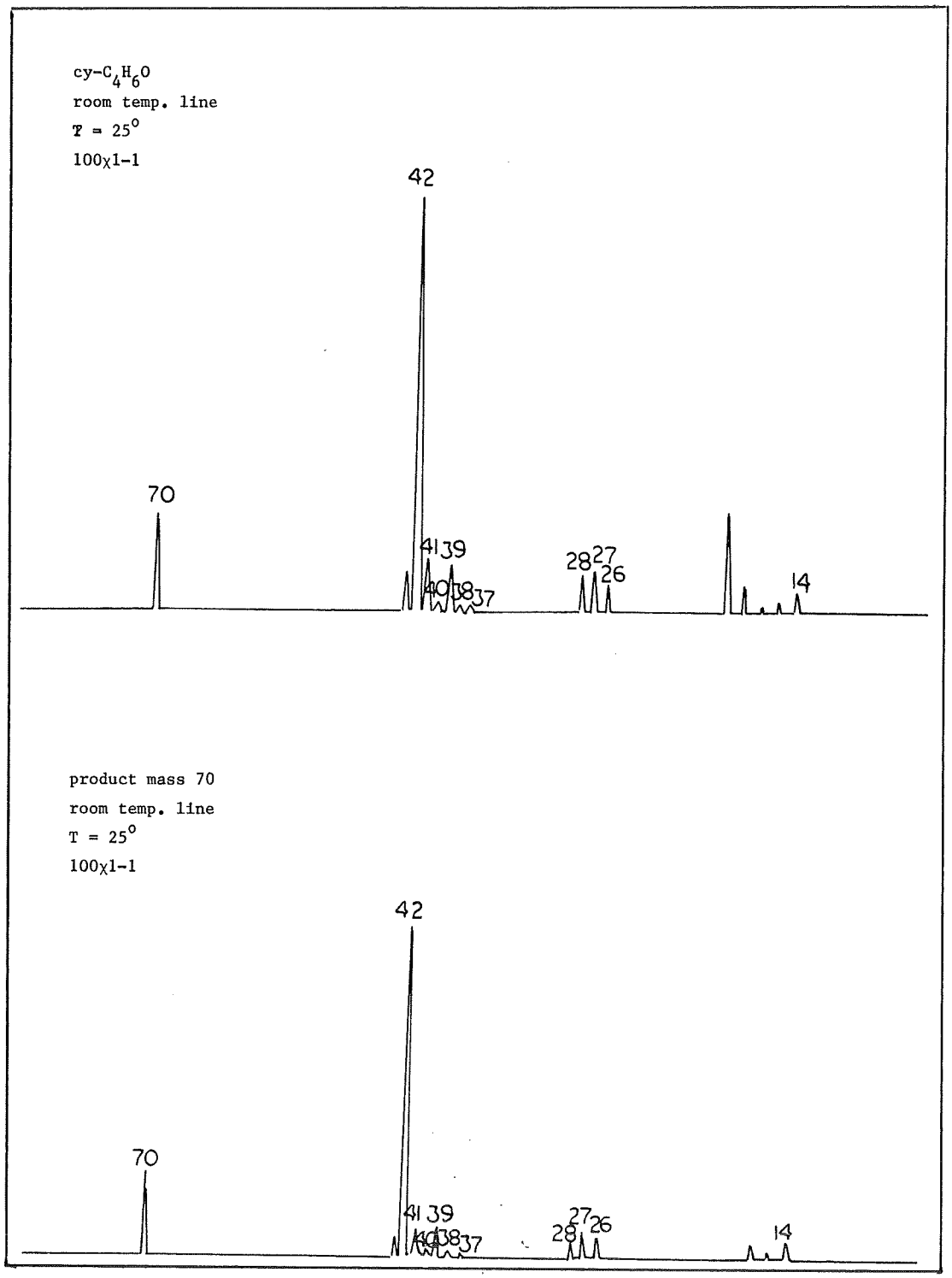

Figure 8. ms of Product Mass 70 from the Reaction of Diazomethane and Ketene Versus ms of Authentic Cyclobutanone

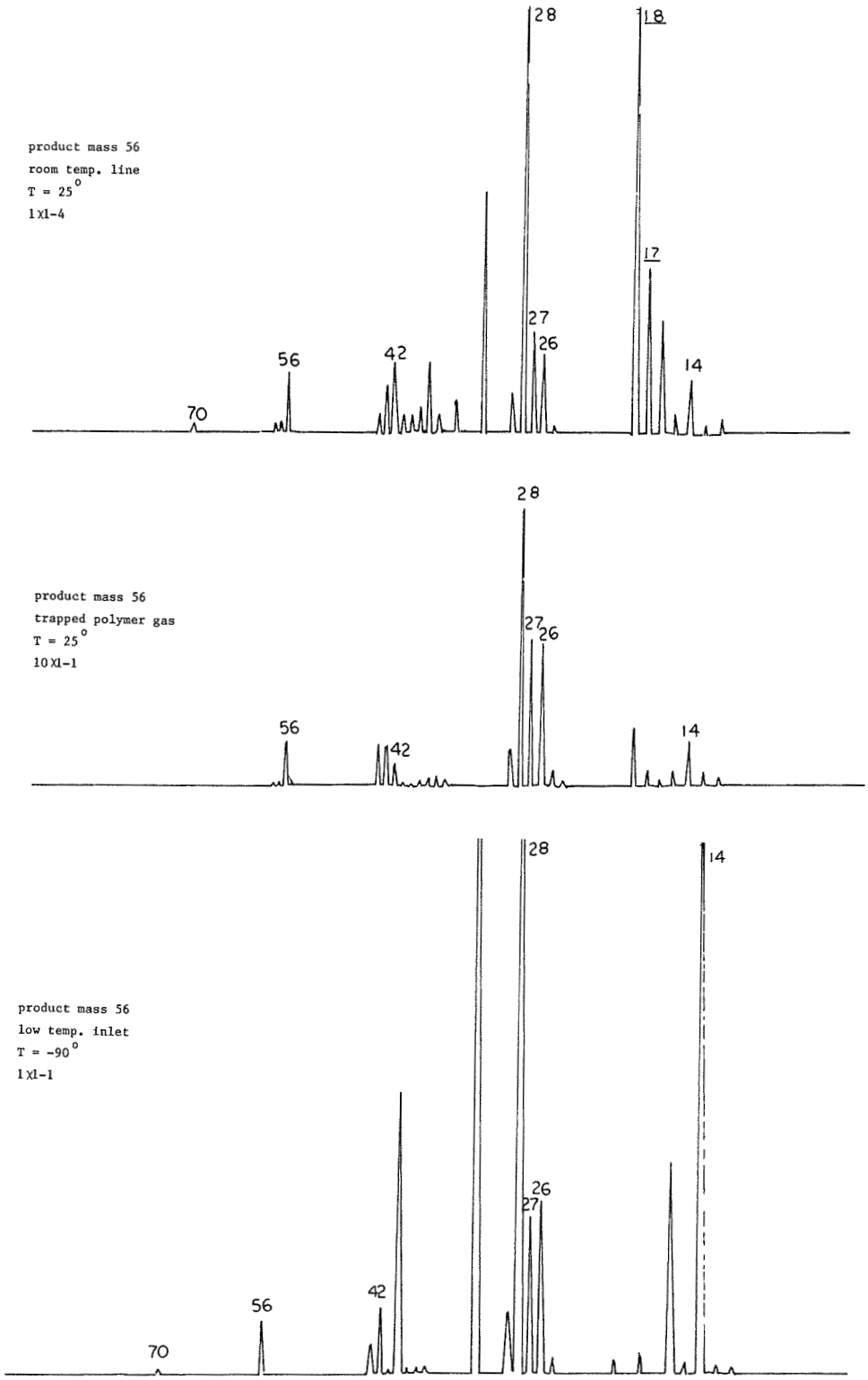

Figure 9. ms of Product Mass 56 from Reaction of Diazomethane and Ketene

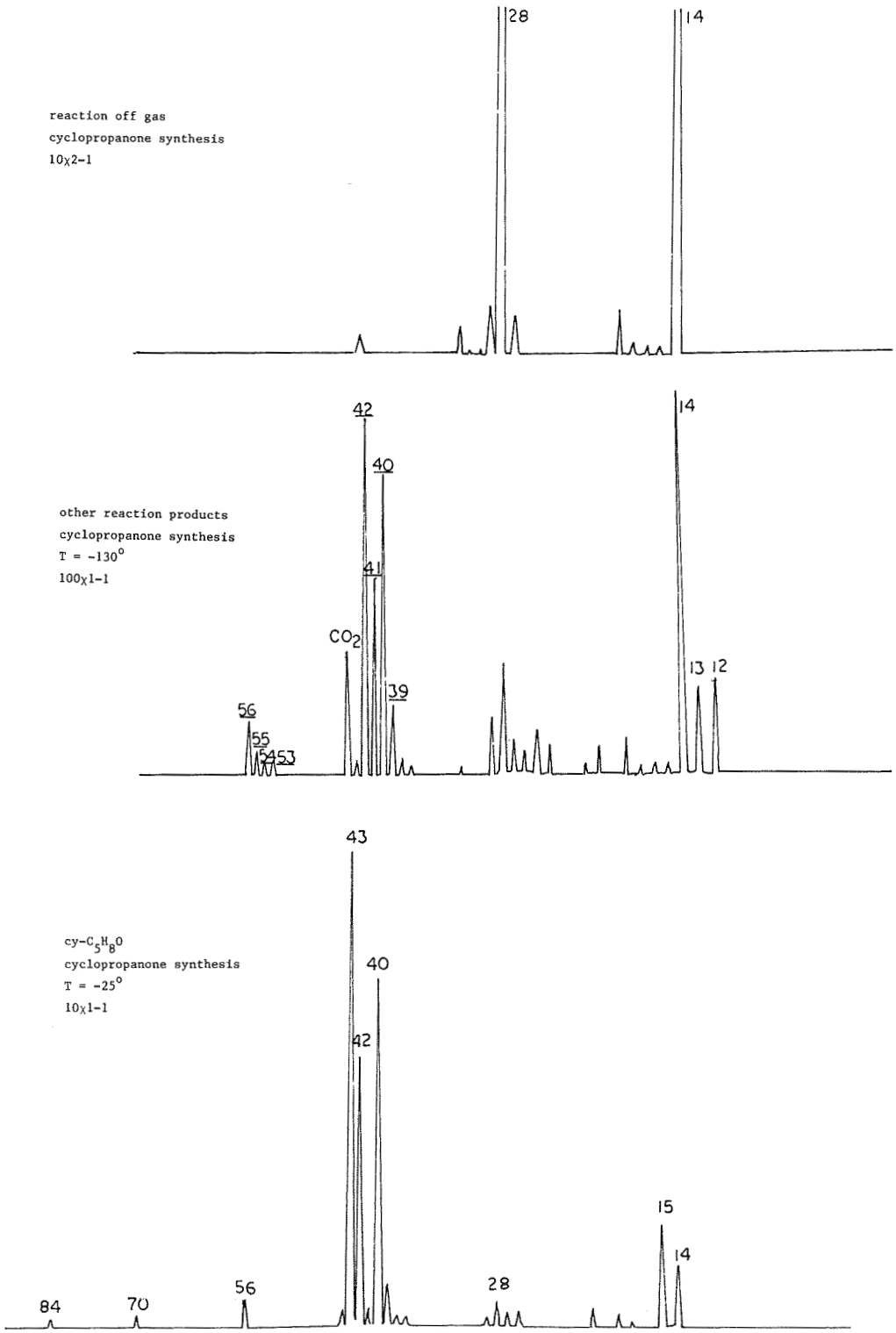

Figure 10. ms of Reaction Off Gas and Other Products Resulting from Side Reactions During the Reaction of Diazomethane with Ketene

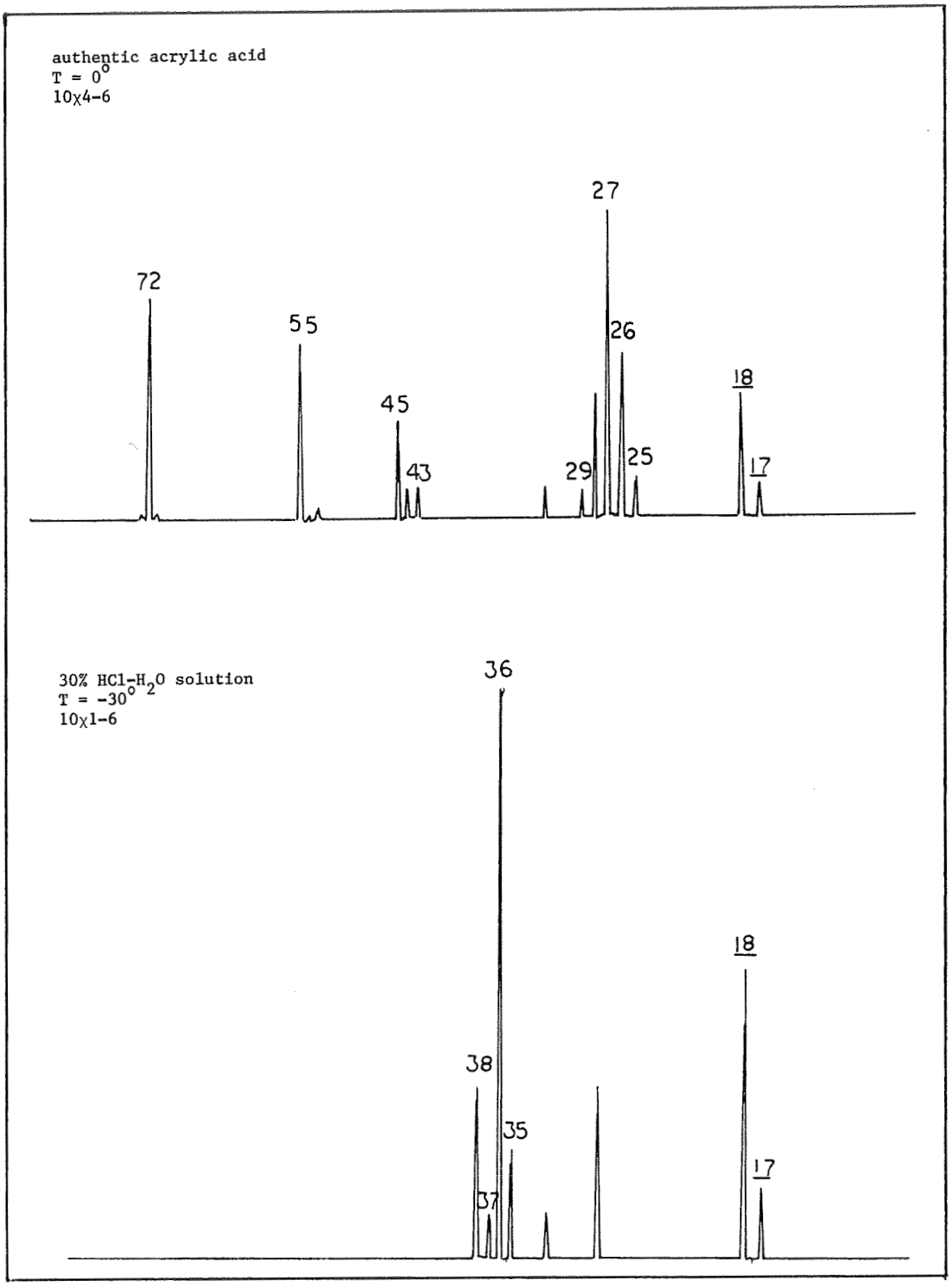

Figure 11. ms of Authentic Acrylic Acid and ms of 30 Percent $HCl-H_2O$ Solution

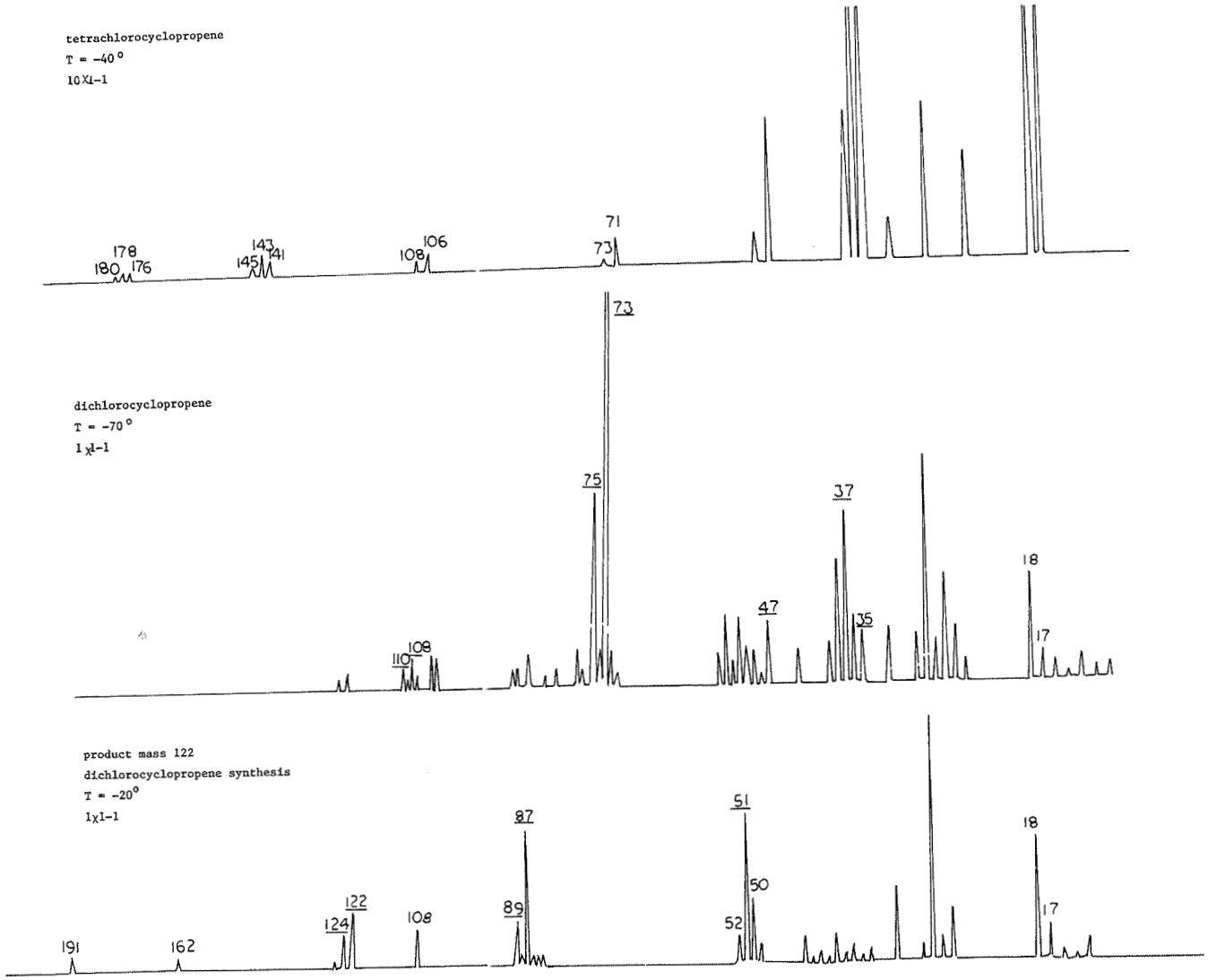

Figure 12. ms of Dichlorocyclopropene, Tetrachloricyclopropene, and Product Mass 122

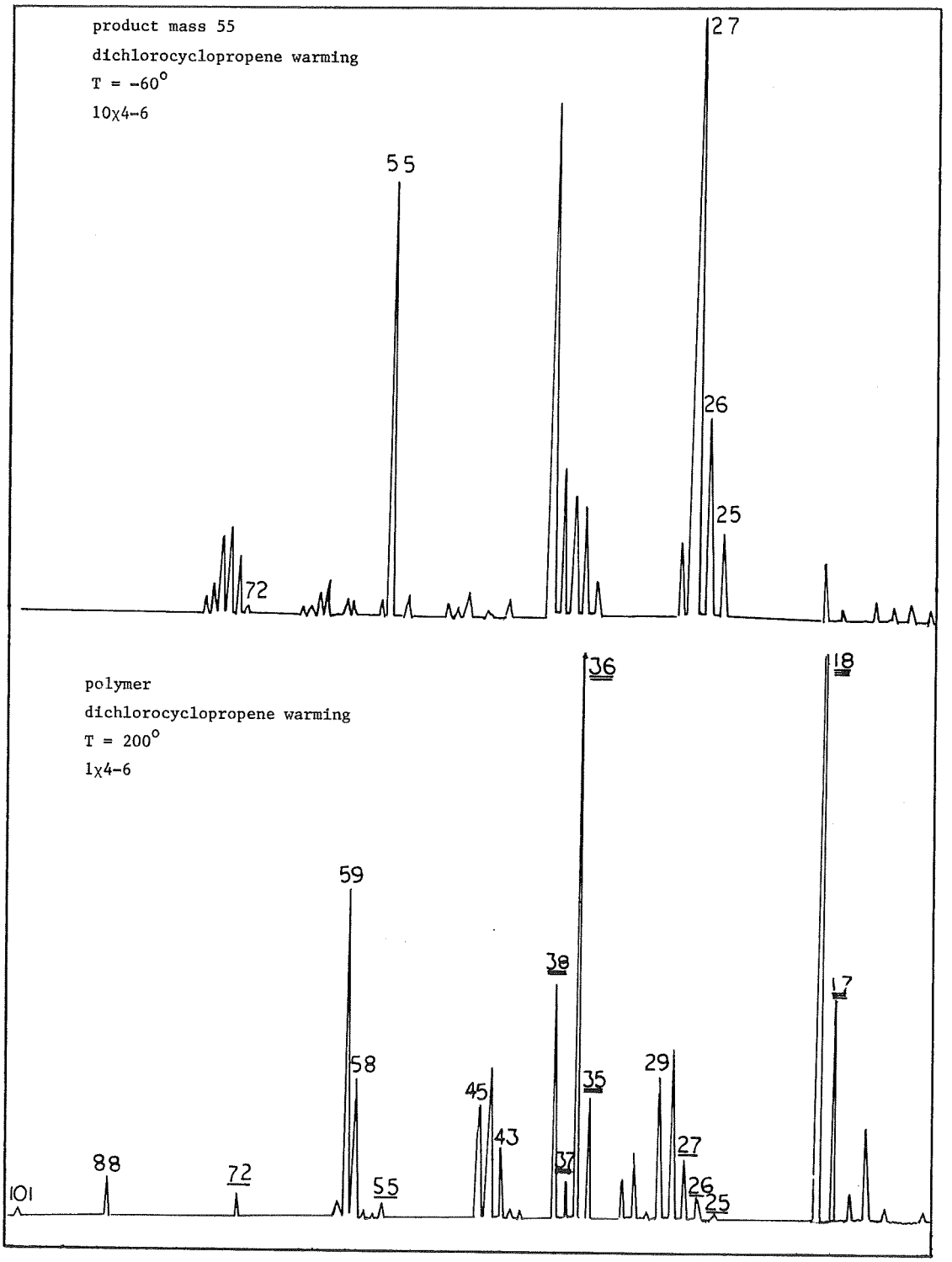

Figure 13. ms of Product Mass 55 and the Heating of Dichlorocyclopropene Polymer

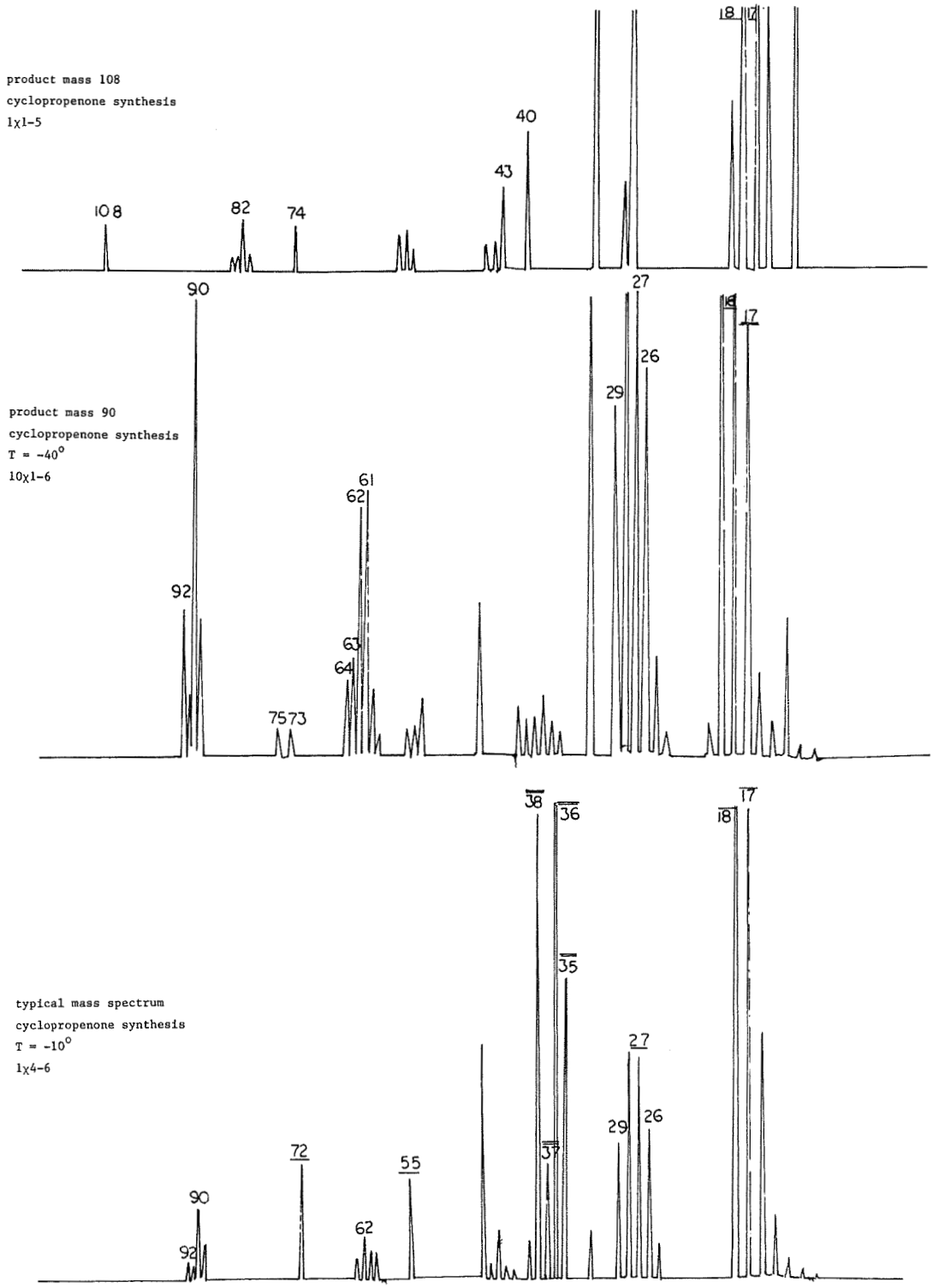

Figure 14. ms of Product Masses 90, 72, and 108 in the Cyclopropenone Hydrolysis

APPENDIX B

IONIZATION AND APPEARANCE POTENTIALS

The purpose of this appendix is to discuss and verify the IP methods used in this work and to present and summarize the IP and AP data for the ring systems. Included are discussions of special problems and the adaptation of the X-Y recorder to the IP measurements.

Literature and Comments on IP Methods

A great deal of work has been done on extracting IP from IE data. However, almost all of the work concerned curves with the characteristic shape of those of the inert gases. This shape of curve will be referred to as "standard curves." The usual assumption that ionization probability increases linearly with electron energy has been verified by a number of workers[81-83] for standard gases. These types of detailed studies made with monoenergetic electrons and on gases such as He (whose nearest excited state is about 19 eV from the ground state) yield unambiguous, reliable results. However, for most mass spectrometers (Bendix T-O-F included), the ionization is produced by a beam of electrons containing a distribution of energies. Electrons emitted by a filament at a certain temperature possess a thermal distribution of energies which adds to any energy given to the electron by acceleration. This results in premature ionization of a compound by high energy electrons even when the electron energy from acceleration is still well below the IP of the compound. The magnitude of the effect depends upon the filament temperature

and the nature of the filament itself. Since the high energy section of the thermal distribution is exponential, the IE curves begin with an exponential curved region of about two volts, followed by an intermediate curved region of one to two volts which passes into an apparently linear region of a few volts. The curve continues to increase upward until at about 40 volts it begins to flatten out. The behavior of the IE curve is exhibited in Figures 19 and 20 and the initial exponential segment is apparent in the semilog plot of Figure 17. Due to this initial exponential region, the decision as to which point should be taken as the appearance potential has been a point of some dispute. Also because of this initial exponential region and for the many instrumental factors that affect the electron energy, it is necessary to calibrate the energy scale using a gas with an accurately known IP, usually a rare gas or a simple polyatomic molecule. The problem then becomes how to compare and relate the IE curve of the unknown gas with that of the calibrating gas. Once the IP relative to the standard is measured, then the absolute IP is obtained. It is necessary to briefly discuss the methods available for obtaining IP so that the reasons for choosing one over the other can be better understood.

Standard Curves

Linear Methods

These methods are applied to IE data displayed on linear X-Y plots such as Figure 16. The most obvious thing to do is to ignore the curved region and extrapolate the linear portion of the curve to the energy axis. This method, "linear extrapolation,"[84] normalizes the sample and

calibrating gas by either making the ion currents equal at 70 eV or by making the linear portions parallel. Because of instrumental noise, etc., it is not always obvious exactly where the linear portion lies and, hence, the subjective extrapolation usually produces results reliable to 0.1-0.2 eV.

The method of "vanishing current"[85] or "initial breaks" assumes that the IE curve approaches the energy axis with a non-zero slope and the point of initial onset has significance as the AP. A serious criticism is that the ion current is found to approach the axis asymptotically and the AP, where the ion current emerges from the background noise level, depends on the sensitivity and the signal/noise ratio. This method also requires normalization of the curves by either of the two previously mentioned methods or by plotting the data on such scales as necessary to make the linear portions parallel. Because of the subjective nature of determining the ion current onset, this method is also reliable to 0.1-0.2 eV.

A less subjective modification of this method is the "extrapolated difference" method,[86,87] which is empirical in that a plot of the difference in the energy ordinates, ΔV, for the calibrating and sample ion versus the ion intensity is extrapolated to zero ion intensity for the IP voltage difference. In this method, the straight line portions are adjusted to be parallel.

We used a technique which combined some of the above ideas and was easily adaptable to the X-Y recorder. The method involved overlapping the IE curves for the sample and calibrating gas from the initial onset to about one to two volts into the linear region. Henceforth, this

will be referred to as the "linear match" method and the expected precision was also 0.1-0.2 eV.

Logarithmic Methods

All the variations of this technique stem from Honig's[88] assumption that the initial exponential increase can be derived from assuming a thermal distribution of electron energies. Honig derived the slope of the semilog IE curve at the IP. This "critical slope"[88] method does not require a normalization procedure. Lossing, et al.[89] found that semilog plots of IE curves yielded parallel straight lines and he arbitrarily took as the IP the energy when the ion current was one percent of its value at 50 eV.

The semilogarithmic matching method[90] involves overlapping the semilog plots of the calibrating and sample ions by shifting both the intensity and energy axes. All of these logarithmic methods yield results of about ± 0.1 eV precision.

Monoenergetic Electron Methods

Although monoenergetic electron impact work is rare, Fox, et al.[91] have developed the "RPD" method which allows one to obtain electrons of 0.1 eV wide slice from the thermal distribution of the electron beam. Using this technique, workers have found that the ionization probability indeed does vary linearly with electron energy and that segmented straight lines are obtained for ions resulting from many processes.

Second Derivative Method

Morrison[92,93] has provided a theoretical analysis which shows that, if the ionization probability for the excitation of a molecule to a single electronic state of the ion is a polynomial of degree one, then

the plot of the second derivative of the ion intensity versus electron energy will yield a sharp peak at the ionization potential whose shape is the reverse of the thermal distribution of energy of the filament electrons. Assuming that the experimental ionization efficiency curve is the result of the arithmetic additions of individual ionization probabilities for each state of the ion, the second derivative curve should reveal a peak for each process.

For sample ions with IE curves of the same shape as the calibrating ion, we conclude that IP from all the above methods could be used to estimate the true IP. However, the precision from one method to another varies depending upon the degree of subjectiveness inherent in each method as well as upon the theoretical basis. We decided to use either the "linear Match" or the "initial break" along with the "semilog match." If a number of measurements was made to remove some of the subjective nature, then an accuracy of 0.1 eV was to be expected.

Long-Tail Curves

Long-tail ions are those that possess an IE curved region much longer than a standard ion. This is very often the case of low intensity fragment ions. The problem of measuring the AP becomes the problem of comparing two curves that are not shaped alike. At this point, some theoretical hypotheses are necessary. If one accepts the addition of separate processes with each linear (in its electron energy) dependency, then one would expect an overall IE curve for monoenergetic electrons to be a series of segmented straight lines. This is the hypothesis in most favor today and is substantiated by many RPD, second derivative, and photoionization experiments. For two such processes whose IP are

separated by only a few volts, one would expect an electron beam of thermal energy spread to smear the two segmented straight lines into a long, but fairly steep, curved tail. On the other hand, if there were many processes taking place with the low energy processes being also of low probability and IP's only slightly separated by small eV, then one could visualize a monoenergetic IE curve of many closely spaced segmented straight lines. The closer the spacing, the more this IE curve would appear curved rather than as segmented straight lines. There are some monoenergetic data that do appear to be a curved probability process. In any event, the spread in the electron beam energies would most certainly yield a long, shallow tail.

Methods

With long-tail ions, then, any linear region is a gross result being produced by more than one process. Extrapolation of this straight line would give a number with no real meaning. This is the main reason that the "linear extrapolation" method fell into general disuse. The "initial breaks" method has the significant advantage that ionization potentials tend to approach the true values. Its limitation is that one still has to calibrate versus a standard ion and to do so a normalization procedure is necessary. Previous normalization procedures will not work. The semilogarithmic methods obviously will not work is there is more than one process contributing to the initial part of the curve.

RPD and second derivative methods can separate IE curves into contributions from the various processes that occur, and both are directly applicable to long-tail ions.

Discussion

Most of the long-tail ions encountered in this work were also of low abundance. The occurrence of shallow, long-tail ions that are also of low abundance produces recorded ion intensities that fluctuate near the AP. To obtain RPD data one must subtract two ion intensities to obtain the much smaller ion intensity from small slice of electron beam. From experience on the T-O-F mass spectrometer, these subtracted results will include much scatter. If one plotted the data, it would be impossible to tell whether it is a curve or segmented straight lines, both of which are possible. A curve drawn through the data would then have to be extrapolated, and hence one has returned to the original difficulty. The situation is further aggravated by closely spaced IP's.

It would seem that the second derivative method with scattered data, when differentiated, would produce more scatter. Besides that, the peak produced by this method indicates that the IP is as wide as the thermal distribution on the electrons. Since the curved portion of the IE curves for the T-O-F is about four eV, we would expect the half width to be at least one eV. Two IP's separated by less than one eV with scattered data would probably produce a large unresolved peak.

For these low abundance, long-tail ions, it appears that the processes must be at least two eV apart to be successfully separated by any experimental method. If this were the case, by taking only the first two volts of the IE curve and assuming only one process was taking place, it was reasoned that, by multiplication* of the sample ion intensities,

---

*See section in this appendix on "Sample Pressure in the Source" for an estimate of the error introduced by multiplication of ion intensities.

the sample and calibrating gas could be made to overlap. The overlap could be either linear or semilog and the multiplication by instrumental electronic means or correction to the raw data. Thus, it was proposed to normalize the curves at two volts above the AP. If this procedure failed, then it was reasoned that the processes lay too closely spaced or that the ion intensities were too low to be detected.

The Effect of Experimental Conditions and Instrumental Settings on IE Curves

The two most important instrumental effects of the T-O-F mass spectrometer, the distribution of thermal energies on the electron beam and the calibration of the energy scale, were discussed in the previous section. The observed peak intensity (I) is a function of the density of the electron beam (ρ_e), the density of the sample (ρ_s), the gross ionization cross section σ (eV) (which is a function of electron energy), and a combined electronic factor of the instrument (K) as:

$$I = K \rho_e \rho_s \sigma (eV)$$

This section is devoted to discussing some of the instrumental myths pertaining to IP measurements.

Factors Not Affecting IE Curve Shape

It has been generally advised that, once an electronic setting has been changed, the energy scale must be recalibrated. This was concluded because most of the electronic adjustments are continuously variable which, once changed, cannot be exactly reset. This is entirely true, but there are many factors that are linear and which can be

counterbalanced by other linear adjustments. Tests were tried in which electronic settings were changed and then the X-Y recorder gain was used to try to reproduce a previously recorded IE curve. Factors found to be linear were analog sensitivity (must be zeroed), multiplier voltage, multiplier gain, and control pulse height.

Factors Affecting the IE Curve Shape

Increasing the filament current increases the filament temperature which: increases the maximum thermal energy; increases the average thermal energy; and increases the exponential decay rate. These effects, in turn, decrease the initial onset of ionization (i.e. ion current appears at a lower electron energy), decrease the uncalibrated IP, and increase the IE exponential growth. These effects are displayed in Figure 15 for both high and low trap currents. The filament currents of 3.9 and 2.9 amps were the maximum and minimum usable currents. As can be seen, the change in filament current moves the onset more than one eV downscale. Increasing the filament current increased the ion current, but for Figure 15, the ion current was electronically adjusted to make the linear portions parallel so that the shapes could be compared. Although a higher filament temperature reduces the effect of the energy distribution of the electron beam on the IE curve, it also reduces the lifetime of the filament and increases the prospect of surface ionization and subsequent diffusion into the ionization chamber which would interfere with the IP measurement (see Figure 17). For these reasons, we chose to run at near minimum filament current. It was found that the filament current could not be changed and reset to the same current and obtain the same calibration curves. It is recommended

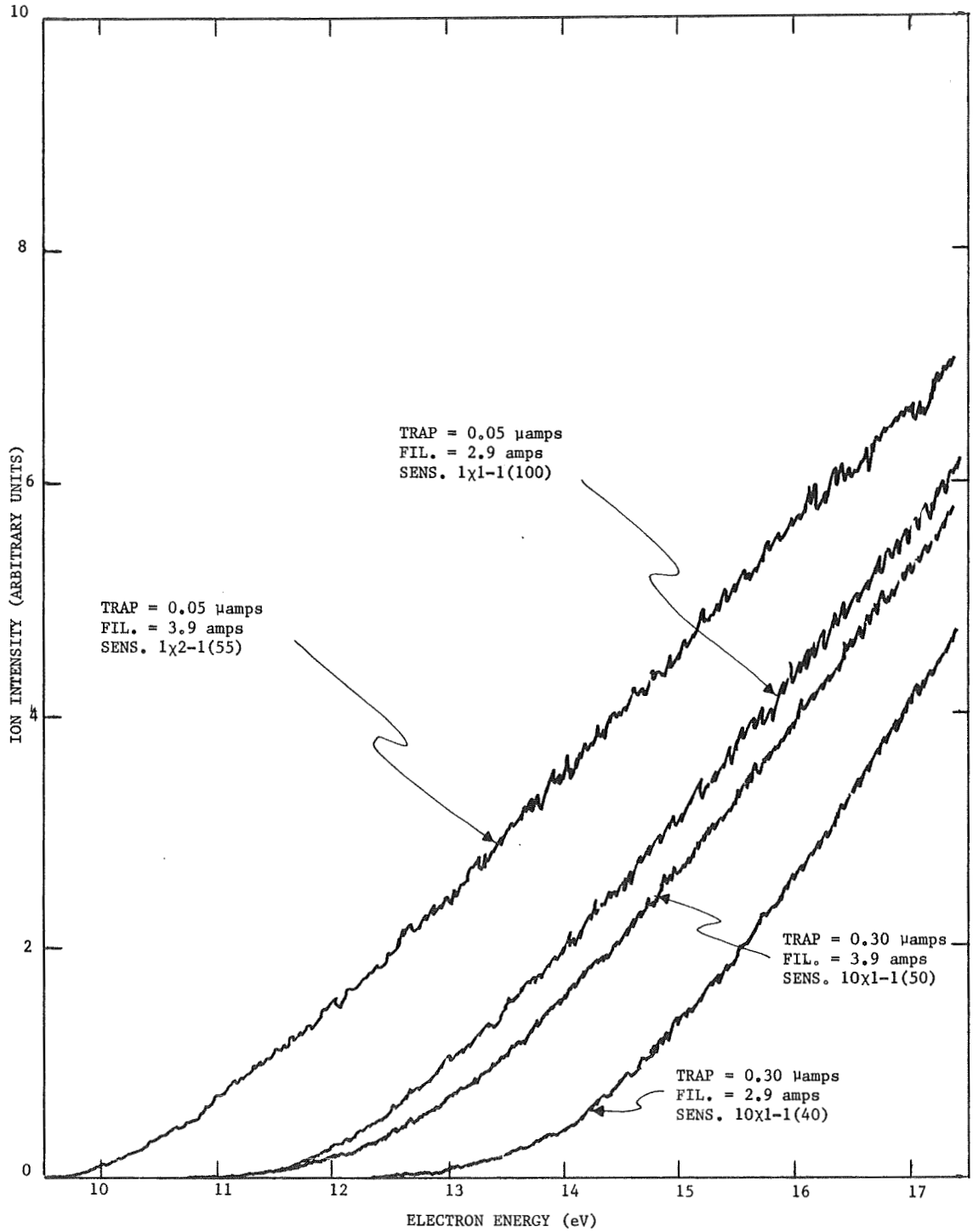

Figure 15. Effect of Filament and Trap Currents on Linear IE Curve Shape of Water

that a filament never be changed during a calibration experiment.

Figure 15 also shows the effect of changing the trap current (i.e. electrons/time). Increasing the trap current from 0.05 to 0.30 microamps greatly increased the ion current (10 times) which was then reduced by electronic adjustment so that the linear portions were parallel and the curves could be compared in Figure 15. Before the curves were adjusted, the increase in trap current had decreased the point of initial onset; after adjustment, the onset increased. This indicates that, to increase the trap current, the portion of the electrons of average energies is increased relative to the portion of high energy. When the intensity of the curve is reduced, then the sensitivity eliminates the high energy electrons which were producing recordable ions before. Thus, the onset moves up (i.e. increasing electron energy) and the exponential rate decreases. This strongly implies that the actual distribution of electrons reaching the ionization region is not what it is at the filament and is determined by the control grid bias which varies to keep the trap current constant. The electron gun consists of: a filament kept at a negative potential; a series of grids with rectangular openings for collimating the electrons; a first grid (called the control grid) to which an adjustable rectangular pulse with adjustable bias is applied; the ionization region; magnets to collimate the electrons; and a trap anode to collect and measure the electron current. The electrons are accelerated by the potential between the negative filament bias and ground and, consequently, the electron energy is numerically equal to this negative bias. Another negative bias, that applied to the control grid, is adjustable from -10 to -50 volts more

negative than the filament bias which prevents electrons from traveling into the grid opening. The periodic pulse on the control grid then causes it to become positive w.r.t. the filament and allows the electrons to pass through the opening. Since the trap current can be increased by increasing the control grid bias, it must be that not all electrons travel through the chamber and a large portion must be left behind. By increasing the control grid bias, the pulse is more positive w.r.t. the filament bias and this stronger initial pull must propel more electrons out. Since the electron beam is always rich in high energy electrons, the semilog IP methods still hold (see Figure 17). We decided to use a trap current of 0.125 microamps for semilog plots. We found that IE curves run at 0.130 and 0.120 microamps did not differ significantly, and thus this much variation in controlling the trap current during an experiment can be tolerated. It is noted experimentally that a decrease in the electron energy causes the trap current to decrease. This may be caused by a poorer focusing of the electron beam. It is important to note that the control grid bias is increased to obtain more trap current during the collecting of IE data. Therefore, it would not be surprising to find that compared IE curves for sample and calibrating ions obtained over widely separated electron energy ranges possess different initial curve shapes.

Sample Pressure in Source

Many of the IP methods involve normalization of the sample and calibrating ions at 70 eV, at the linear region, or at the exponential region. This normalization (adjusting the ion intensity to be the same) is done to insure that both the sample and the calibration gas are being

ionized under the same conditions in the ion source and, hence, will have the same shaped IE curves. Tests were carried out to determine if and how much effect the sample pressure would have on the IE curve shape. The results are shown in Table 14 for agron using a trap current of 0.125 microamps and a filament current of 3.6 amps. For a base case argon intensity, several IE curves were obtained over different electron energy ranges (while the curves of 12-15 eV did not include any linear portions, the curves of 12-18 eV went well into the linear region). Next the argon intensity was increased by increasing the flow rate of argon into the ion source. By using the analog sensitivity and recorder gain, the argon intensity was lowered until the IE curve shape would overlap the initial IE curves taken at the base case intensity. In other words, argon at one source pressure was calibrated against itself and at another source pressure by electronically adjusting the ion intensities. Table 14 shows consistent results except for case 11. Since all of case 11 results are inconsistent by the same amount, we attribute this to a misreading of the energy scale and neglect these data. It can be seen that, on the average, comparing peaks up to 10 times difference in source sample partial pressure produces an error of less than 0.15 eV and that, for any particular case, the error is less than 0.25 eV. For the linear match IP, these results indicate that trying to adjust peak intensities exactly is a waste of time. Just getting intensities within a factor of two and using the instrumental gain to finely adjust the match seems a more appropriate procedure. Using this chart, one could calibrate a series of fragment ions at one intensity of calibrating gas. Precisely adjusting the intensity of a gas to a set value by changing

Table 14. Variation of Argon Linear Match IP with Ion Source Partial Pressure

Case	Ion Intensity at 70 eV	Ion Intensity relative	Ion Intensity rat.[c]	IP Error[d] (eV) 12-19[f]	12-18	12-17	12-16	12-15	avg.
1[a]	.1χ1-1(25)[b]	250	1						
2	.1χ2-1(35)	700	3	-0.07	-0.10	-0.09	-0.06		-0.08
3	.1χ4-1(40)	1600	7	-0.20	-0.03	-0.08	-0.06		-0.08
4	1χ1-1(40)	4000	15	-0.25	-0.17	-0.16	-0.20		-0.20
avg.				-0.17	-0.10	-0.12	-0.12		-0.12
5[a]	1χ1-1(40)	4000	1						
6	1χ2-1(40)	8000	2	+0.03	+0.04	-0.07	-0.07	-0.03	-0.02
7	1χ4-1(40)	16000	4	-0.24	-0.18	-0.09	-0.14	+0.11	-0.10
8	1χ4-1(100)	40000	10	-0.19	-0.05	-0.20	-0.14	-0.12	-0.15
avg.				-0.13	-0.06	-0.12	-0.11	-0.01	-0.09
9[a]	1χ4-1(100)	40000	1						
10	10χ1-1(90)	90000	2	-0.03	-0.08	-0.14	-0.09	+0.10	-0.05
11	10χ2-1(40)	180000	4	-0.30	-0.30	-0.25	-0.30	-0.22	-0.25
12	10χ4-1(100)	400000	10	-0.08	0.0	-0.13	-0.20	-0.18	-0.10
avg.				-0.06	-0.04	-0.14	-0.15	-0.04	-0.07
13	10χ4-1(100)	400000	1000	-0.27	-0.31	-0.41	-0.35		-0.34
	Summary		2-3						-0.05
			4-7						-0.09
			10						-0.15
grand avg.[e]				-0.12	-0.07	-0.13	-0.12	-0.03	-0.09

a. base cases
b. designation to be interpreted as follows: .1χ1, analog sensitivity setting; -1, multiplier voltage setting; and (25), 25% of full scale analog ion current output reading.
c. ratio ≃ (case/base case)
d. IP error = IP(case) - IP(base case)
e. does not include case 13, only ratios 1 to 15.
f. range(eV) of IP Measurement

(and waiting for the flow to stabilize) its flow rate can be a tedious and time consuming job. To correct the AP whose intensity was adjusted down to match the other, one would have to add the amount in the table; to correct an AP adjusted up to match, subtract the amount.

The effect of changing sample source pressure on the initial breaks IP was also investigated. For a given recorder sensitivity, an increase in sample source pressure will decrease the point of initial onset. An intensity increase of 10 times lowers the onset about one eV. If one tries to electronically adjust the lower intensity curve to match the higher, an IE curve is obtained which matches well but which contains a different element of signal to noise and herein lies the problem. Since the curves now appear different, the subjective determination of the point of initial onset led to an error in the above case of about + 0.3 eV. However, since the actual adjusted curves matched fairly well, we proposed to use the idea of the linear match at the initial electron energy IE range of two eV, and we thereby obtained better results (0.1-0.2 eV). This procedure is referred to in the tables as normalization at the disappear potential (DP).

Control Pulse Exceeding Ground Potential

Throughout the history of the measurement of IP, there has been the fear that the control pulse would go above ground. The electrons would be accelerated through a potential from the negative bias on the filament to the positive value of the control pulse and the electron energy would be greater than indicated by the filament bias. It was found that, for a clean and properly focused source and well adjusted collimating magnets, there was usually enough trap current such that

the control grid bias was never raised high enough to cause the pulse to go above ground during an IP experiment. In fact, it could only be made to happen with very poor magnet adjustment. The resulting effect is to continue to give ion current at electron energies up to five eV below the IP and as such, the effect is immediately obvious. Since the manual control bias varies from -10 to -40 volts relative to the filament, adjusting the control pulse height to 15 volts would make it impossible for the pulse to go above ground until the electron energy dropped below five eV. This would allow measurements of IP's as low as eight eV with no fear of the control pulse going above ground.

Manual Versus Automatic Trap Current Regulation

It has long been an accepted practice to never use the automatic current regulator in IE curves because the automatic regulation will continue to produce trap current at electron energies where the manual trap regulation will not. Both manual and automatic regulation involve changing the control grid bias but automatic regulation must allow a larger range of control biases. We found that, as long as the manual regulation was working sufficiently to produce IE curves, the IE curves produced by the automatic regulation were identical. Therefore, the only requirement for the use of the automatic regulation was checking the manual beforehand to see whether it could perform the task. Almost all of the IE curves in this work were obtained in automatic regulation.

Calibration from Day to Day

In this work it was found that the calibration of the machine did not change significantly from day to day as long as the same filament and trap currents were used. As discussed previously, the filament

current cannot be reset exactly, but it was found that, by turning the filament off using one of the safety interlocks, i.e., by switching the pressure gage from 10^{-4} to 10^{-2} and without adjusting the filament current knob, the filament, when calibrated again, would be almost exactly what it had been. This is a handy fact to know in case the filament must be turned off.

Factors Affecting the IE Curve Appearance

The appearance (as opposed to the shape) of an IE curve is determined by the fluctuations in the recorded ion current. These fluctuations can usually be traced to low sample pressures or instrumental noise. At sample pressures which require less than 1 X 1 analog sensitivity, fluctuations began to be a problem. The noisiest instrumental effect (especially when the multiplier glass is dirty) is the multiplier voltage. Using the lowest multiplier voltage setting (1) and high recorder gain settings produced the optimum signal/noise ratio. These fluctuations can be damped by using higher analog time constants but only at the expense of signal response time.

Procedure and Verification of IP Methods

In all IP and AP measurements in this work, the sample and calibrating gases were simultaneously present or injected into the ion source. Initially, the IP of the calibrating gas was measured, followed by measuring the IP of the sample gas, and then followed in turn by an IP recheck of the calibrating gas. As time progressed, experience proved that sometimes the check IP was not needed and, occasionally, one calibration curve was used to calibrate a number of ions.

Table 15. Verification of Techniques for Measuring Ionization and Appearance Potentials (eV)

Ionization Process	Lit.	Linear Match IP	Linear Match (exp.-lit.)	Initial Break IP	Initial Break (exp.-lit.)	Semilog Match IP	Semilog Match (exp.-lit.)
$H_2O \rightarrow H_2O^+$	12.59						
$A \rightarrow A^+$	15.76	15.69	-0.07	15.75	-0.01	15.79	+0.03
						15.69	-0.07
$He \rightarrow He^+$	24.46	24.24	-0.22	24.1	-0.36		
$C_2H_6 \rightarrow C_2H_6^+$	11.6	11.69	+0.09	11.60	0.0		
$C_3H_8 \rightarrow C_3H_8^+$	11.2	11.07	-0.13	11.09	-0.11		
$CH_2Cl_2 \rightarrow CH_2Cl_2$	11.4	11.6	+0.20	11.30	-0.10		
$\rightarrow CH_2^+$	16.9			16.9	0.0		
$C_2H_2 \rightarrow CH^+$	21.9			22.1	+0.2		
$\rightarrow C_2H_2^+$	11.4			11.7	+0.3		
				11.3	-0.1		
				11.3	-0.1		
$CH_3NO_2 \rightarrow CH_3^+$	11.1			11.25	+0.15		
	11.35			11.25	-0.10		

Semilog Match

Although not necessary, most of the semilog data in this work were normalized exactly. The procedure consisted of adjusting the sample and calibrating gas intensities to be equal over the first few volts of the IE curve. Then the ion intensities were recorded on the Visicorder at electron energy intervals of 0.2 eV from the initial onset upwardly for about three to four volts. Repeating the procedure back down to the initial onset gave a check on the data to (1) eliminate random errors and (2) observe whether the sample pressure was changing. This procedure takes about one hour, and it was quite common for the sample pressure to have drifted requiring that the calibration be repeated. Fluctuations in the flow rate of the calibrating gas and fluctuations in the sample vapor pressure due to temperature changes led to the development of faster methods of measuring IP using the X-Y recorder. Figure 17 verifies the semilog match technique by calibrating water versus argon and includes a curve to display the effect of ions formed at the filament surface diffusing into the ionization region. This diffusion, although disconcerting, does not prevent the IE curves from being accurately determined and can be removed by lower sample pressures. Table 15 shows verification results using the semilog match, linear match, and initial breaks methods along with the accepted literature values.

Linear Match and Initial Break Methods--Adaptation of the X-Y Recorder

The procedure consisted of first measuring the IE curve over a large electron energy range (see Figure 19) to see what type of curve the particular ion possessed. From this, it was decided which IP method to use. For example, Figure 19 shows that cy-$C_3H_6^+$ and H_2O^+ have the

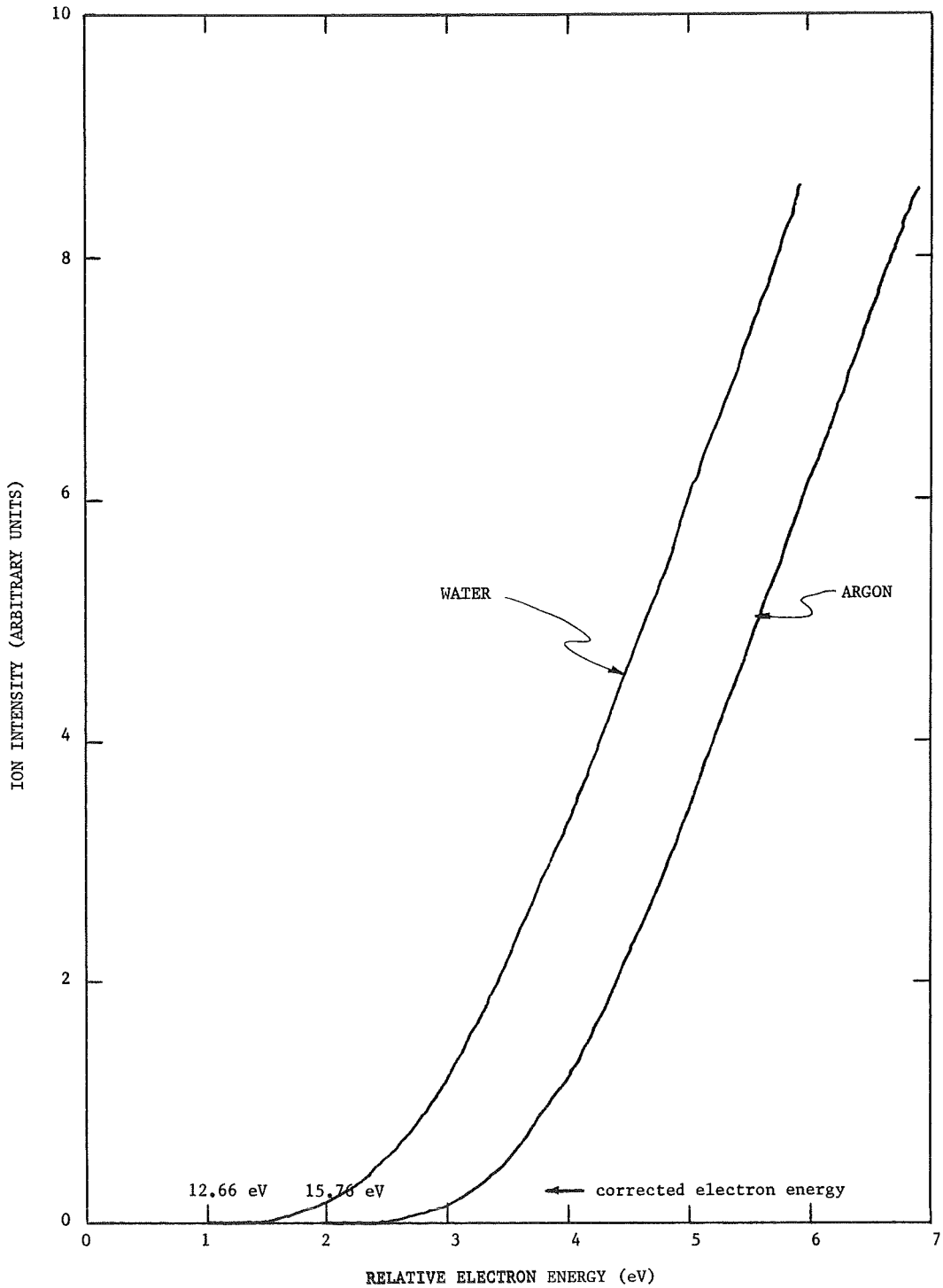

Figure 16. Verification of Linear Match IP Technique

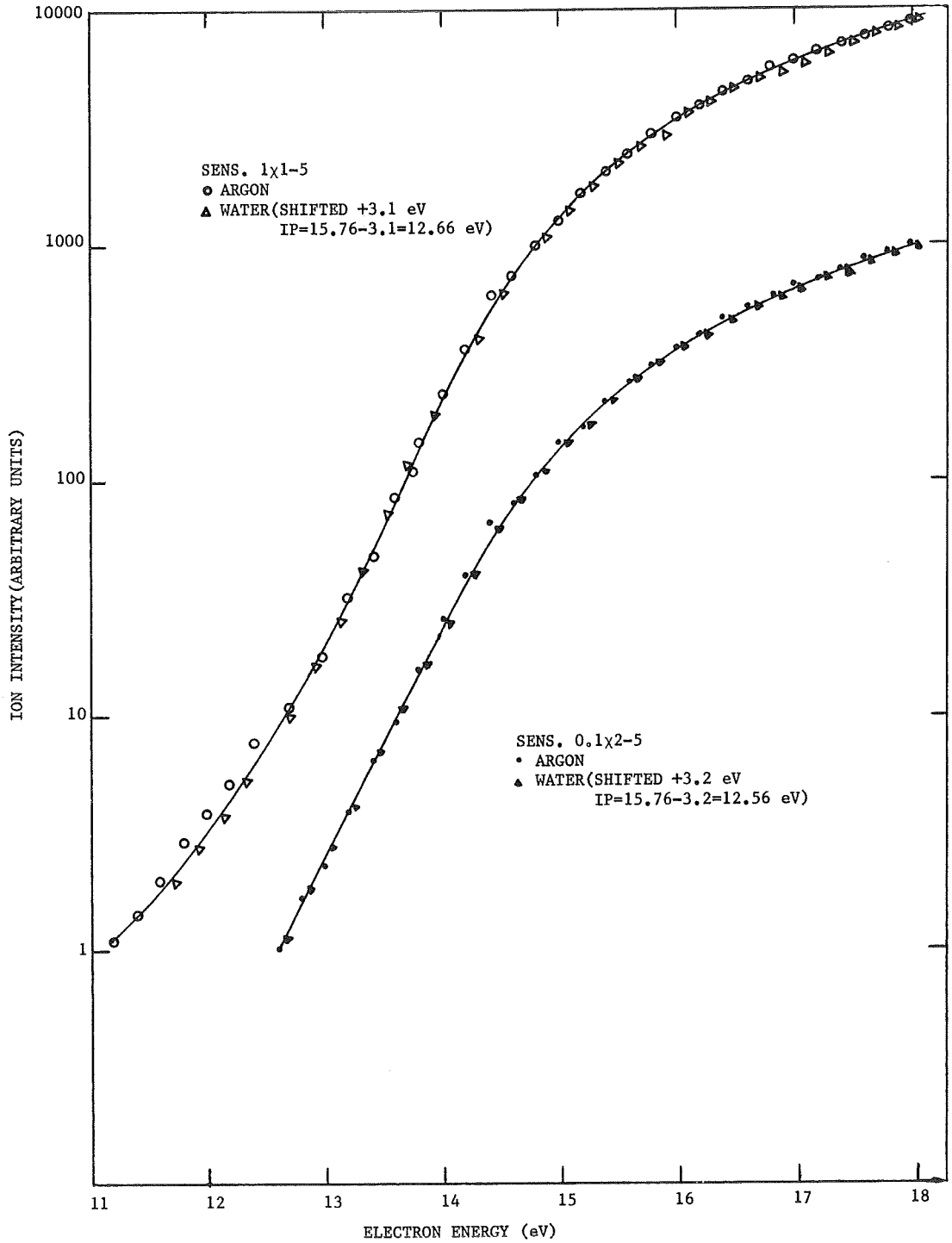

Figure 17. Verification of Semilog Match IP Technique and Evidence of Diffusion Problem at High Sample Source Pressure

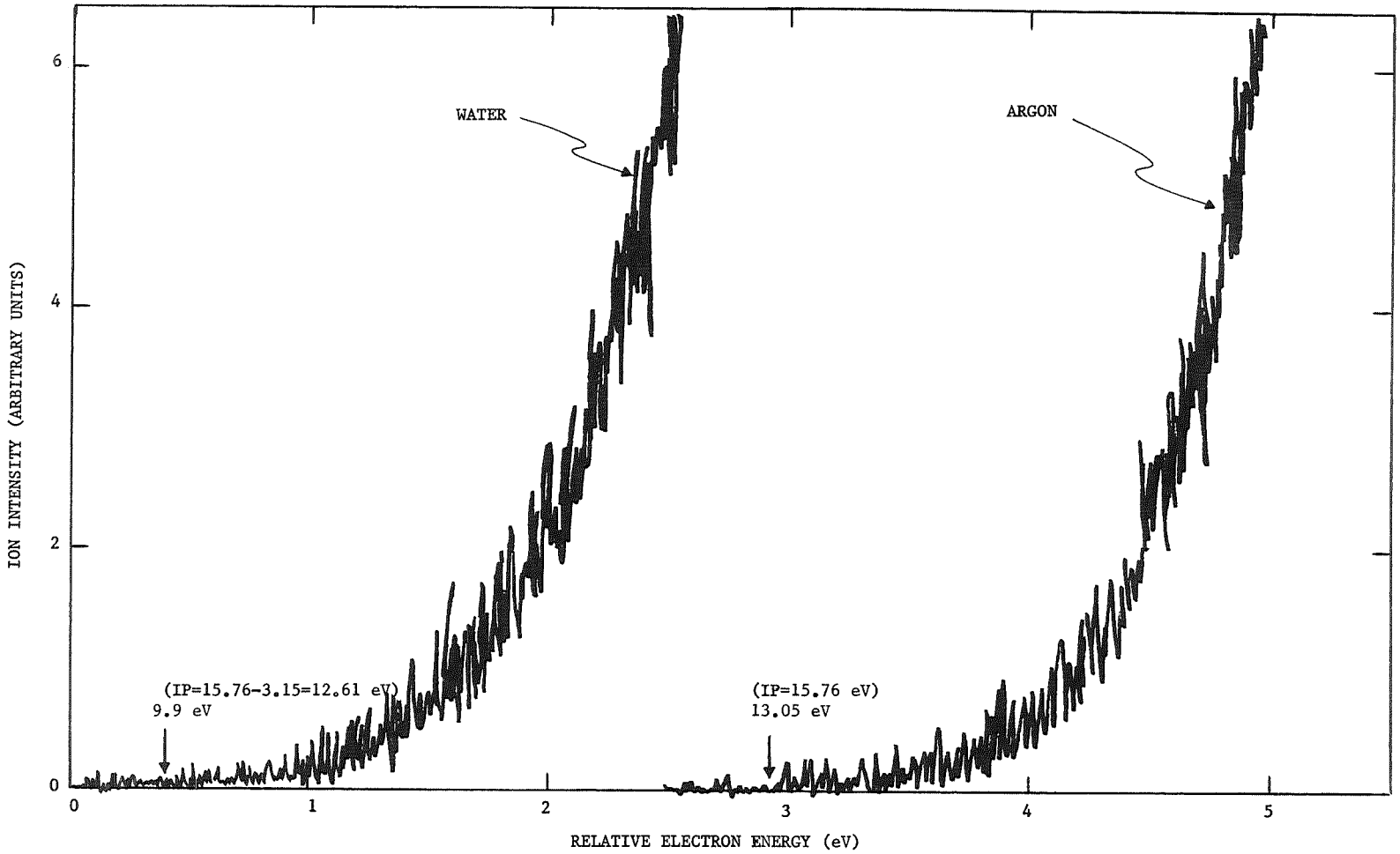

Figure 18. Verification of Initial Break IP Technique

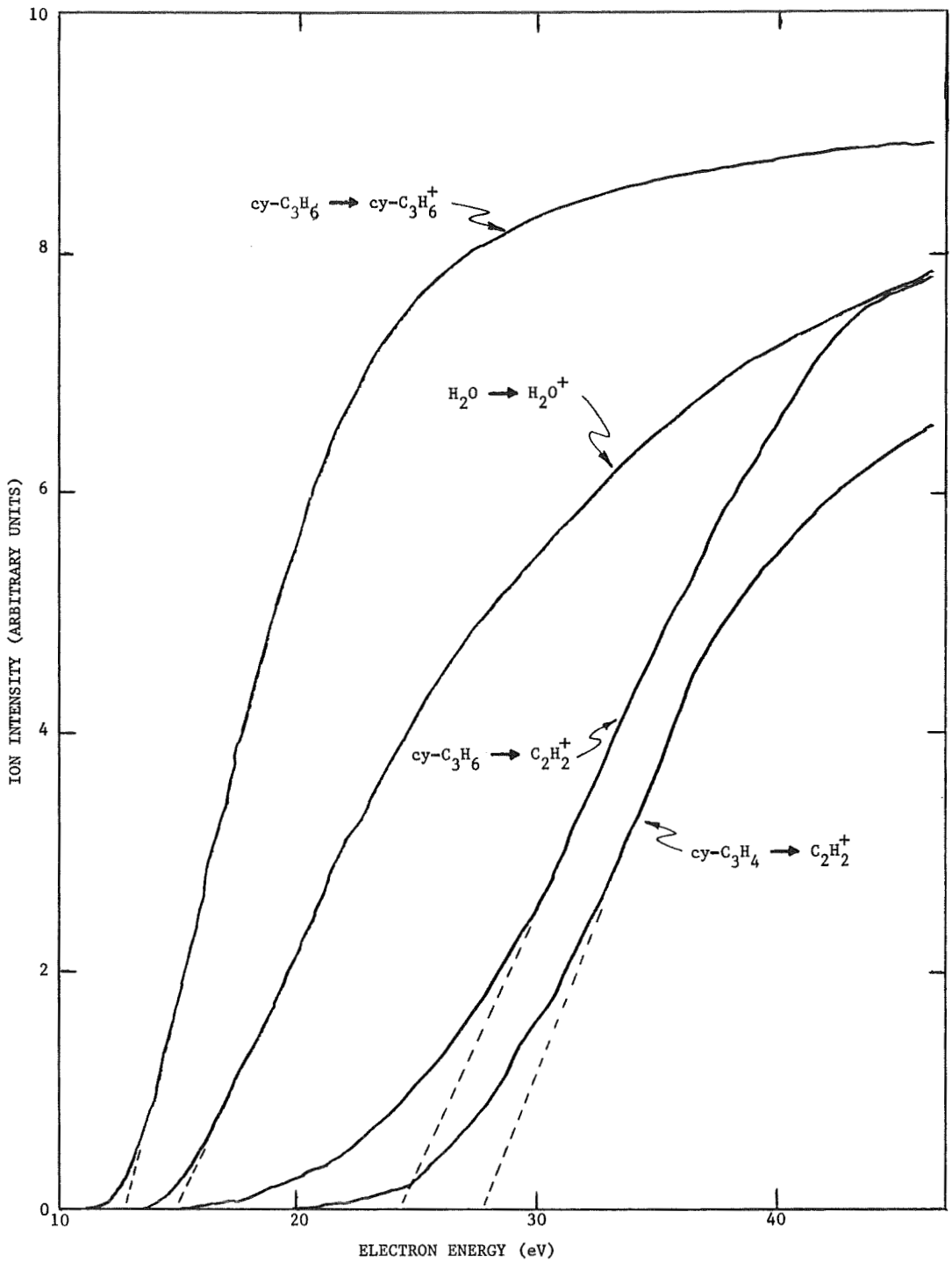

Figure 19. IE Curves for Long-Tail Ions at High Electron Energies

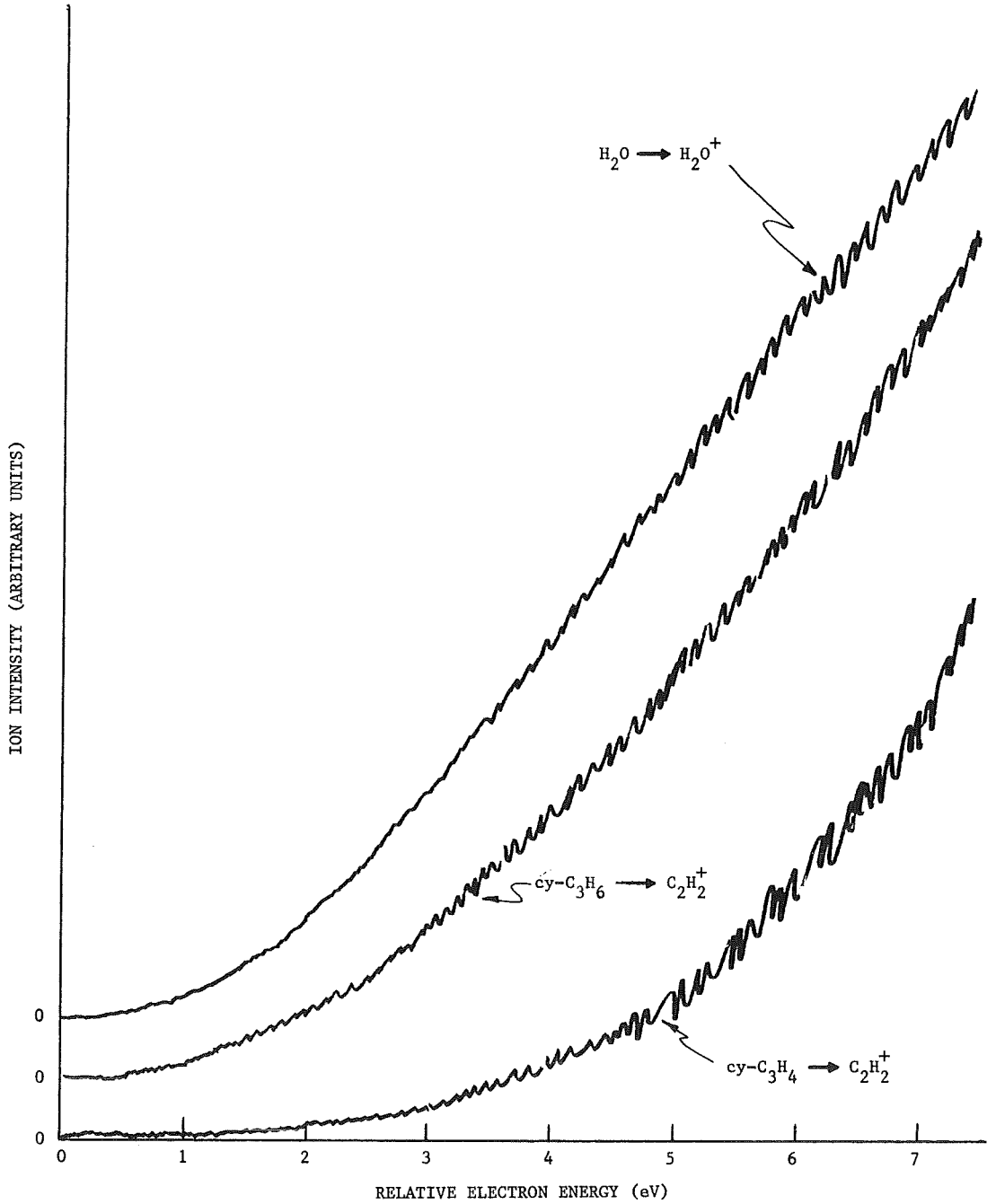

Figure 20. IE Curves for Long-Tail Ions at Low Electron Energies

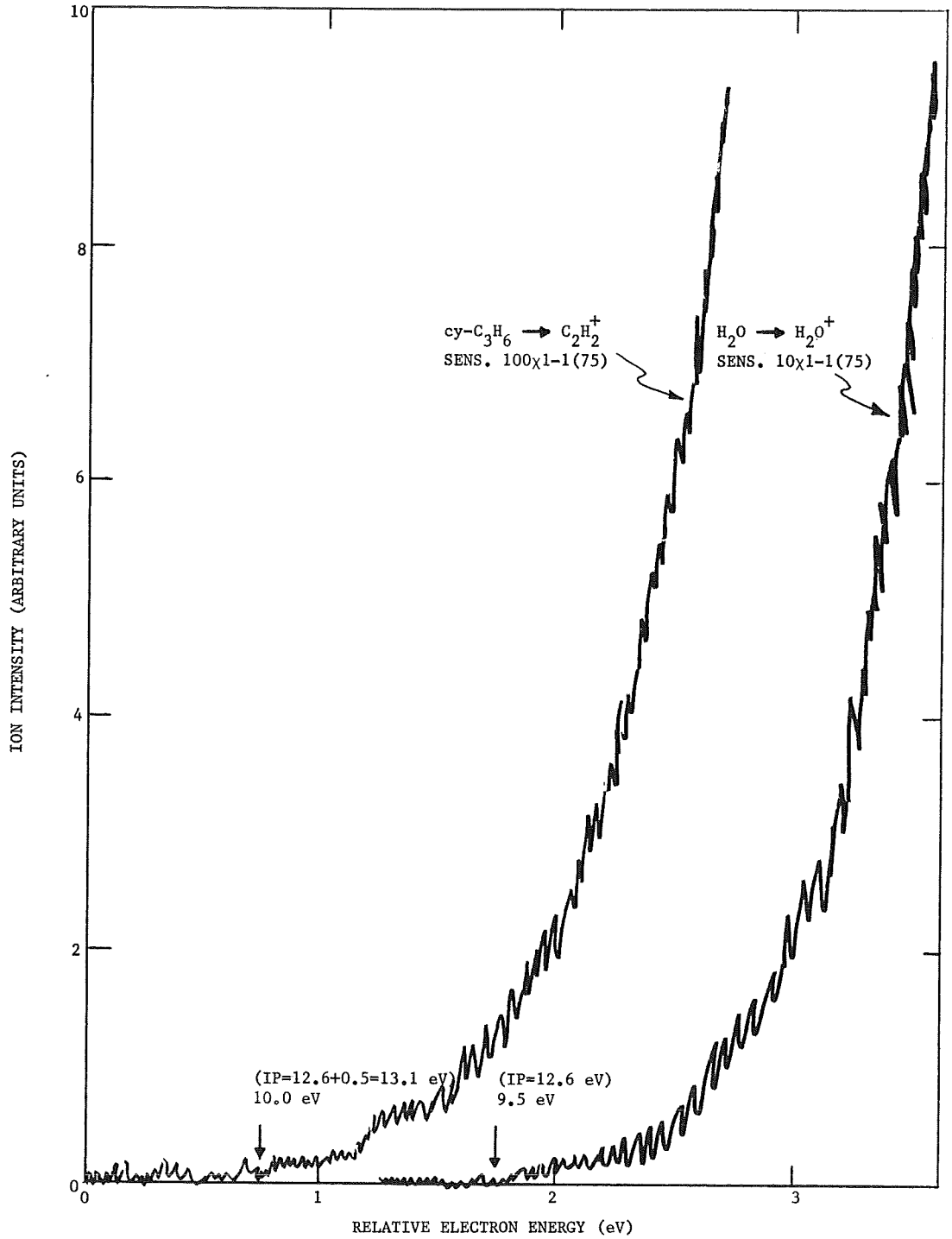

Figure 21. Initial Break IE Data for Long-Tail Ions

"standard" type curves and any method of IP measurement can be used. The $C_2H_2^+$ ions from cy-C_3H_6 and cy-C_3H_4 have tails of 10 eV or so, and an IE method which separates the processes must be used.

The procedure for obtaining a linear match IP was to record on the X-Y plotter the unknown ion IE curve from the point of initial onset until a few volts into the linear region such as shown in Figure 16. The calibrating gas IE curve was then adjusted either by varying the sample flow rate or electronically to give exactly the same IE curve shape. By placing a second sheet of X-Y recording paper over the one containing the sample IE curve, the calibration IE curve could be drawn over the sample curve. The difference in IP was then the shift in electron energy (EE) necessary to match the curves. A smoothly drawn IE curve was best obtained with time constants greater than 0.1 but a fast enough response to changes in EE required time constants less than 0.1. Thus an optimum time constant of 0.1 was used that allowed fairly smooth (no fluctuations) IE curves to be drawn with a fast enough response to changes in EE so that the matching curve could be drawn quickly (five minutes) by increasing and decreasing the EE. Since detecting the point of initial onset of the ion current in the "initial breaks" method depends on the appearance of the IE curve, most all IE measurements of ions that had standard shapes were normalized by approximately adjusting the sample source pressures. The point of initial onset is most easily detected when: the IE curve approaches the energy axis with a steep slope; the X-Y recorder has no zero drift; and there is a minimum of noise. These conditions were best met using: ion intensities at 70 eV of 1 X 1 to 10 X 1; 1 X 1 analog sensitivity for the IP measurement;

0.1 time constant; maximum multiplier gain; minimum multiplier voltage (1); recorder electron energy sensitivity of 0.5 volt/inch; recorder ion intensity sensitivity of 0.05 volt/inch and 0.125 microamps trap current. An example of this type curve is shown in Figure 18.

The method of initial breaks was used to measure the AP of long-tail fragment ions. The initial portion of the IE curves of H_2O^+ and $C_2H_2^+$ previously discussed in Figure 19 are shown in Figure 20. The long tails begin to show a distinction as $C_2H_2^+$ from cy-C_3H_6 approaches the energy axis with much more curvature than does $C_2H_2^+$ from cy-C_3H_4. After normalizing H_2O^+ and $C_2H_2^+$ from cy-C_3H_6 at 70 eV, IP's were measured by initial breaks and yielded AP of $C_2H_2^+$ around 13.6 eV. Although $C_2H_2^+$ approached the energy axis with curvature, it still did not have the slope of the H_2O^+ curve.

As discussed previously, three ways to adjust the curves so that they will match are: (1) increase the $C_2H_2^+$ ion intensity by increasing multiplier voltage or recorder gain; (2) decrease H_2O^+ intensity by recorder gain; or (3) increase $C_2H_2^+$ sample pressure or decrease H_2O^+ pressure. The first two change the appearance of the curve while the third is most easily obtained by measuring the calibrating gas at a number of source intensities and finding the best fit to the $C_2H_2^+$ ion. Figure 21 shows the comparison of the initial breaks with H_2O^+ at 10 times the source sample pressure as $C_2H_2^+$. It was possible to make the IE curves approach the energy axis similarly by electronically increasing the ion intensity of $C_2H_2^+$ 10 times. This gave an AP for $C_2H_2^+$ of 13.1 eV which is the same as the number obtained by RPD measurements. Of course, our method is more subjective but it is interesting to note that this method

could produce an AP that did agree with RPD measured AP and also that this AP could be interpreted and explained in the energetics of cy-C_3H_6. Furthermore, $C_2H_2^+$ from $C_3H_4^+$ could not be made to match the H_2O^+ curve by any manner of electronic and/or pressure adjustment, and, most interestingly, this AP as measured could not be interpreted in the energetics of cy-C_3H_4.

Summary

The results of the verification of the "linear match," "initial breaks," and "semilog match" are shown in Table 15. The most subjective of the methods, "initial breaks," was obtained for quite a few compounds. From tabulated results it was concluded that the lack of precision in the "initial break" and "linear match" methods could be overcome by more measurements on the same number or that good agreement by two different methods would confirm the precision. It was also concluded that the best way to check the precision of the "initial break" method on long-tail ions was to measure the AP at different ion intensities as a precise result does not vary with intensity. With these IP methods developed and the intensity corrections of Table 14, one should be able to make short work of any unknown AP.

Results for Ring Molecules

cy-C_3H_6

The IP and AP's from this work are listed in Table 16 and are compared with available literature values. There are many points of interest. The IP of the parent mass 42 agrees with some literature values but there seems to be an abnormal spread in the data for a parent

Table 16. Results for Cyclopropane (eV)

Ion Mass	Ion Intensity at 70 eV	Experimental AP: Init. Break 70 eV[b]	Experimental AP: Init. Break DP[b]	Experimental AP: Lin. Match	Literature AP: Lin. Ext.[26]	Literature AP: Init. Break[26]	Literature AP: Init. Break[27]	Literature AP: RPD[28]	Literature AP: S'log[29]
42	1 2-1(85)	10.5							
	10 1-1(75)[a]			10.55	10.2	10.2	10.2[c]		10.53
	100 1-1(60)	10.2[c]							
28	1 1-1(90)	13.3							
	1 2-1(80)	13.8	13.1[c]						
	10 2-1(75)	13.1[c]							
27	1 1-1(40)	13.9							
	1 1-1(75)	13.6							
	1 2-1(85)	13.9	13.5[c]						
	10 1-1(70)	13.4							
	100 1-1(50)	13.7			15.4	13.6	13.4	13.4[c]	
26	1 1-1(70)	14.0							
	1 2-1(75)	14.8	13.1[c]						
	1 2-1(86)	14.8							
	10 1-1(70)	13.8							
	100 1-1(50)	13.7	13.1[c]		17.3	14.6	13.6	13.1[c]	
15	1 1-1(55)	17.1	16.2						
	1 2-1(80)	17.7	16.3						
	10 2-1(80)	15.7	14.0						
14	1 1-1(80)	18.8							
	1 2-1(80)	18.4[c]			21.8	18.8	18.5[c]	19.3	
	10 2-1(75)	18.7							

a. Refer to Table 14
b. Normalized ion and calibrating gases to be of equal intensities at 70 eV or at the disappearance potential(DP)
c. Best value-refer to Table. 4

ion compared to the reliability of other electron impact data on parent ions. The AP of mass 28 is complicated by the presence of background N_2 (IP = 15.5 eV). Since the AP of mass 28 is lower than N_2, the measurement of the AP is basically the same as handling long-tail ions. The procedure is to electronically adjust the initial portion of the curves to approach the energy axis similarly. The experimental data bear out this interpretation as at higher sample pressures the contribution to mass 28 from background N_2 becomes negligible, the IE curves overlap, and the AP are the same as electronically adjusting at lower sample pressures. Masses 27 and 26 both exhibit long-tail IE curves and note that, in general, as the sample pressure is increased, the AP decreases. This is the direct result of trying to compare two curves which approach the energy axis differently. When the curves were electronically adjusted to match, the AP compared very well with RPD data. For all AP of ions which may not approach the axis with the same curvature, the most obvious verification of precision is to measure the AP at various ion intensities. Also note that other workers[26] tried to use the linear extrapolation method for AP and the results were errors as large as four eV! The AP of mass 15 was unobtainable because the long tail was too shallow for the electronic adjustment to match the calibrating gas. The AP of mass 14 is thought to be a reliable number because of the little change with intensity and agreement with the liaterature. The investigation of cy-C_3H_6 provided a good exercise in measuring AP's of long-tail ions. The IP of mass 26 has previously been shown in Figure 21.

cy-C_3H_4O

Obtaining the AP's of the fragments of products m/e 56 and 70 at -90° and -70° was done with great difficulty due to interference problems of every nature. Although ethylene and ketene were apparently completely removed from the cyclopropanone spectrum by low temperature separation, cyclobutanone was not. Although there was no interference problem in obtaining the AP of m/e 28, whose abundance is very large from product m/e 56 and very small from product m/e 70, there was some problem in A(42); small from m/e 56 and large from m/e 70. As it turns out, AP(42) from 56 is about 1.0 eV lower than from m/e 70, so a method that emphasizes the initial portion of the curve should be used. In later experiments, the initial breaks method was used. The intensity of product m/e 56 spectrum could not be raised by warming (due to the increased presence of product m/e 70) and, as such, the amount of background N_2 was sufficient to interfere with the AP(28). This problem was also overcome by the method of initial breaks. Similarly, ions from m/e 56 interfered with AP's of product m/e 70. Although there was no problem for AP(42) whose abundance is large from 70 and small from 56, there was a problem in AP(28) which was small from 70 and very large from 56. In fact, the value measured at -70° of 10.8 eV is closer to A(28) = 10.2 eV from 56 than A(28) = 13.0 eV from 70. Besides these problems, mass 56 caused a shift in the electron energy scale of one to two eV during the course of an experiment and, furthermore, gave a small peak at mass 40 which interfered with the argon calibrating gas*

*This shift in eV scale and the occurrence of a m/e at 40 may have been the same problem.

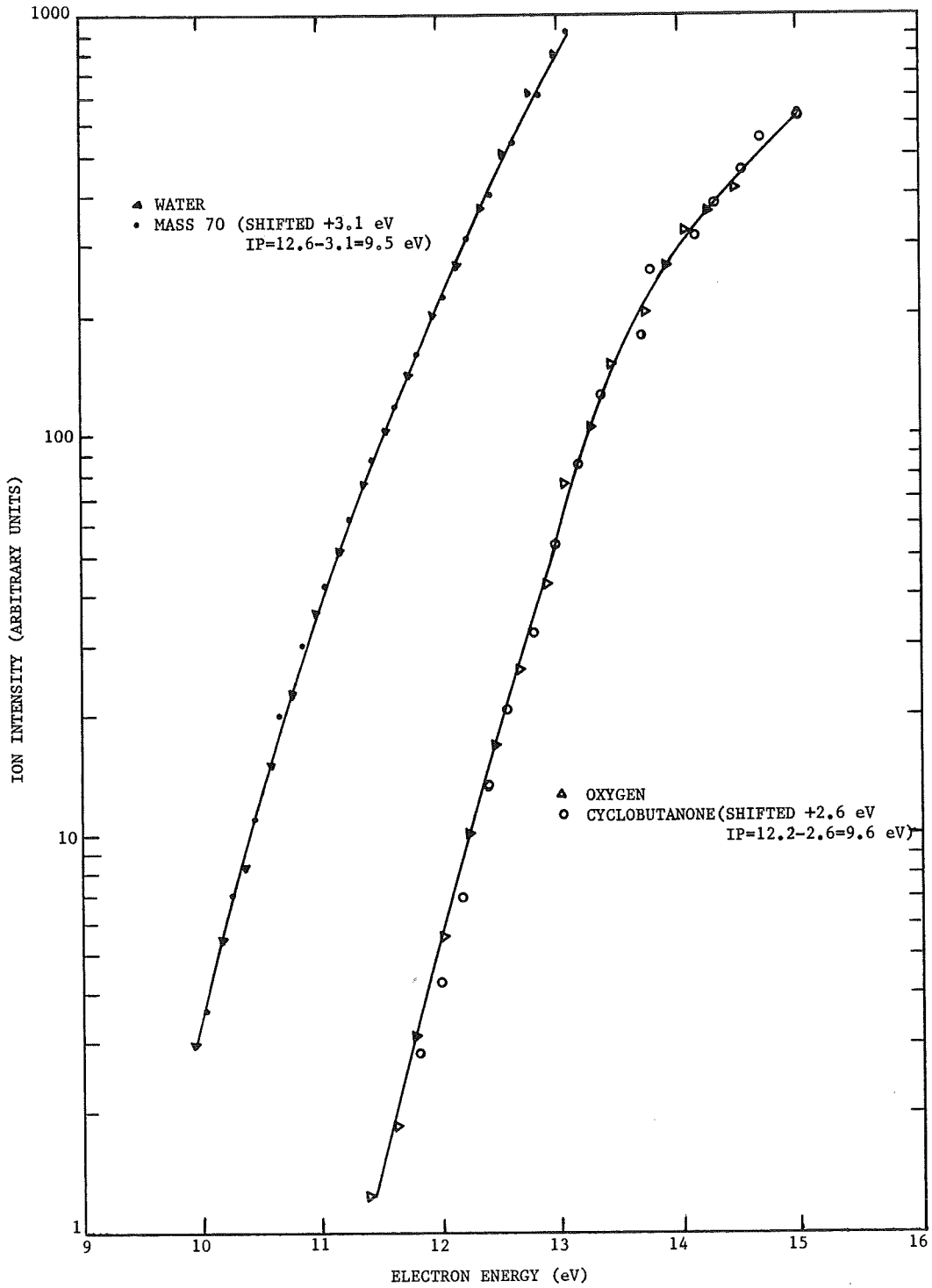

Figure 22. Semilog IE Data for Cyclobutanone at -82° and Product Mass 70 at -75°

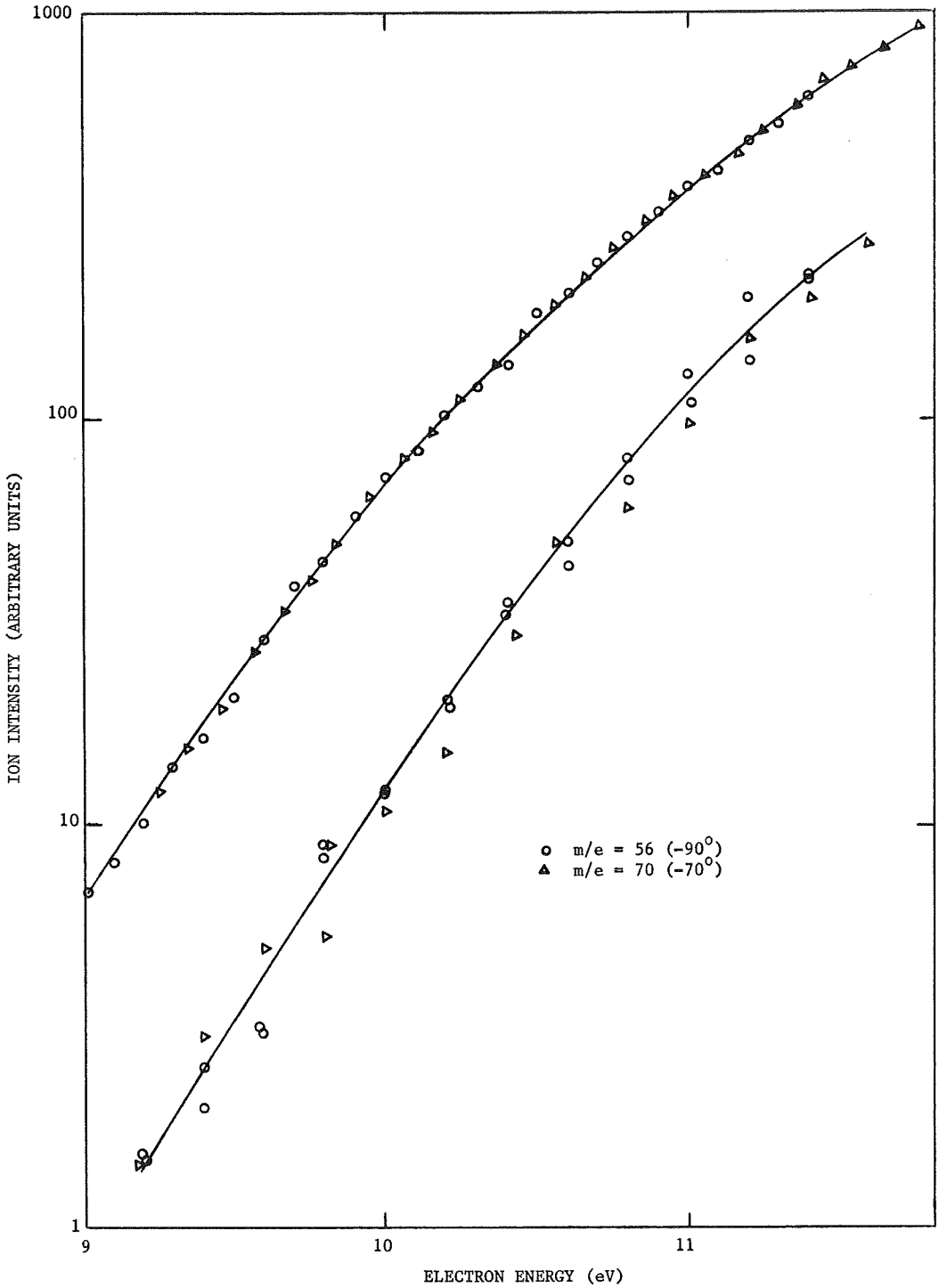

Figure 23. Semilog IE Data for Product Masses 70 and 56 at Low Temperatures (Mass 70 Shifted Down 0.4 Volts)

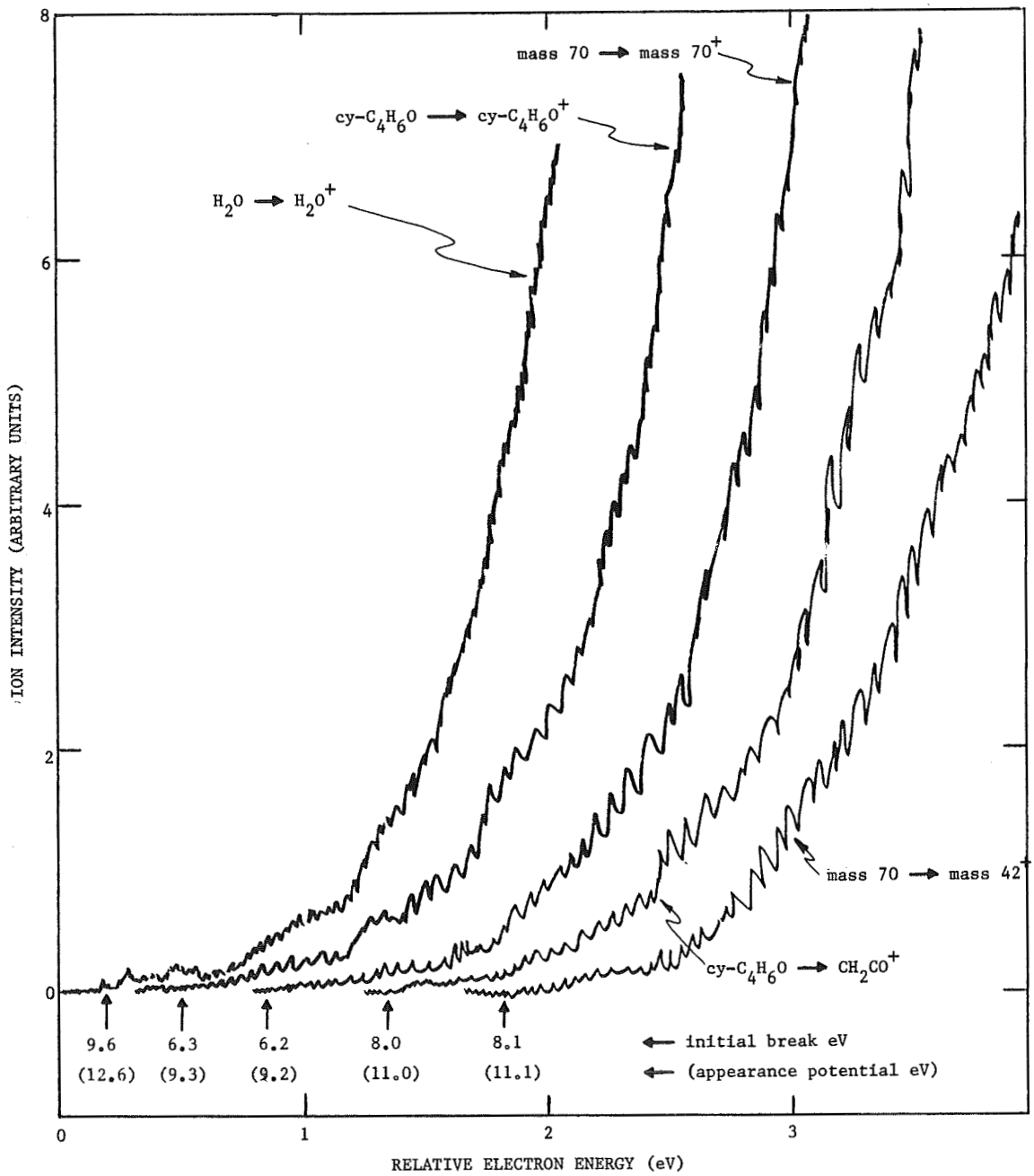

Figure 24. Initial Break IE Data for Masses 70 and 42 from Cyclobutanone and Product Mass 70 at Room Temperature

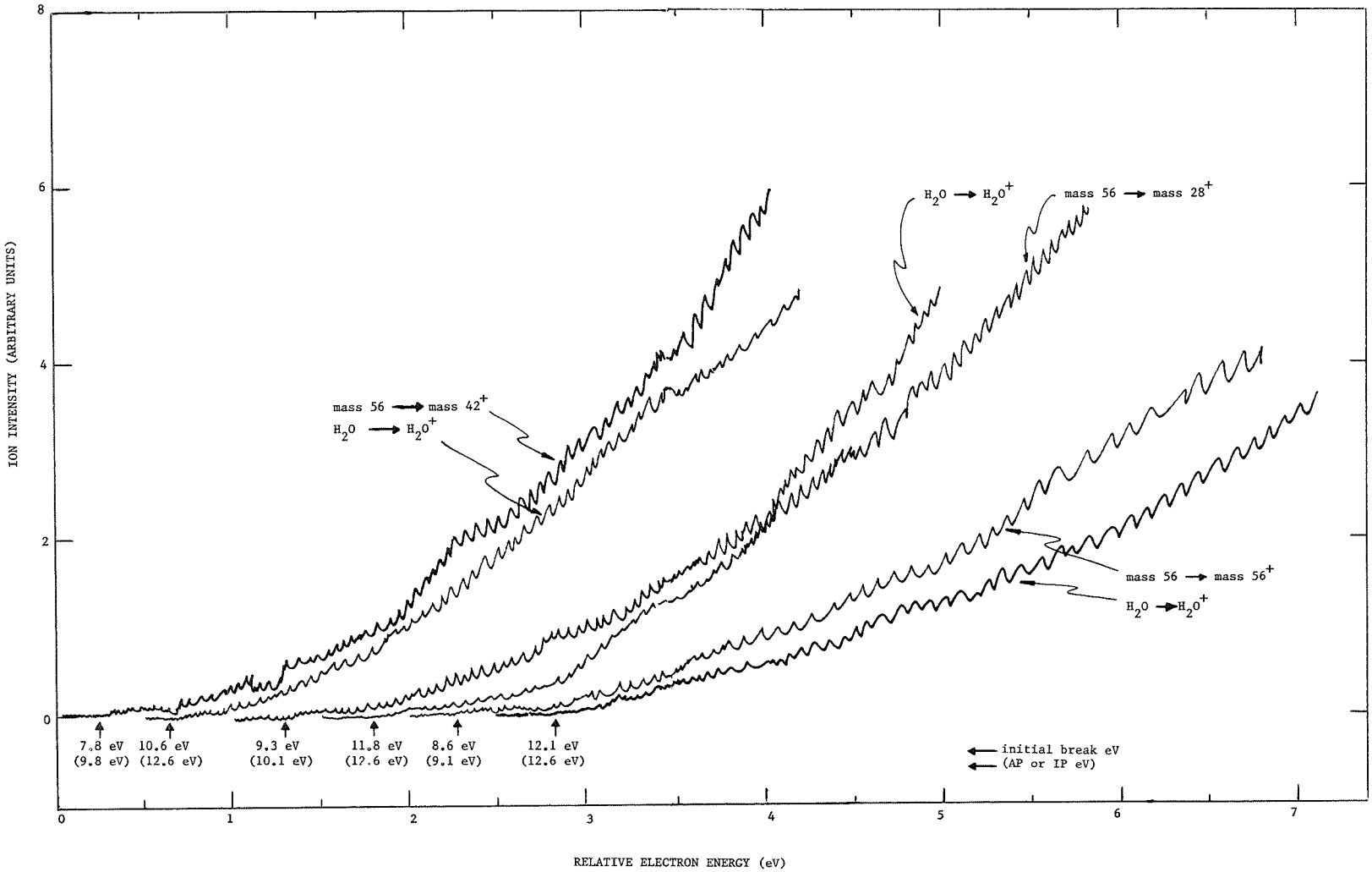

Figure 25. Initial Break IE Data for Masses 56, 42, and 28 from Product Mass 56 at Room Temperature

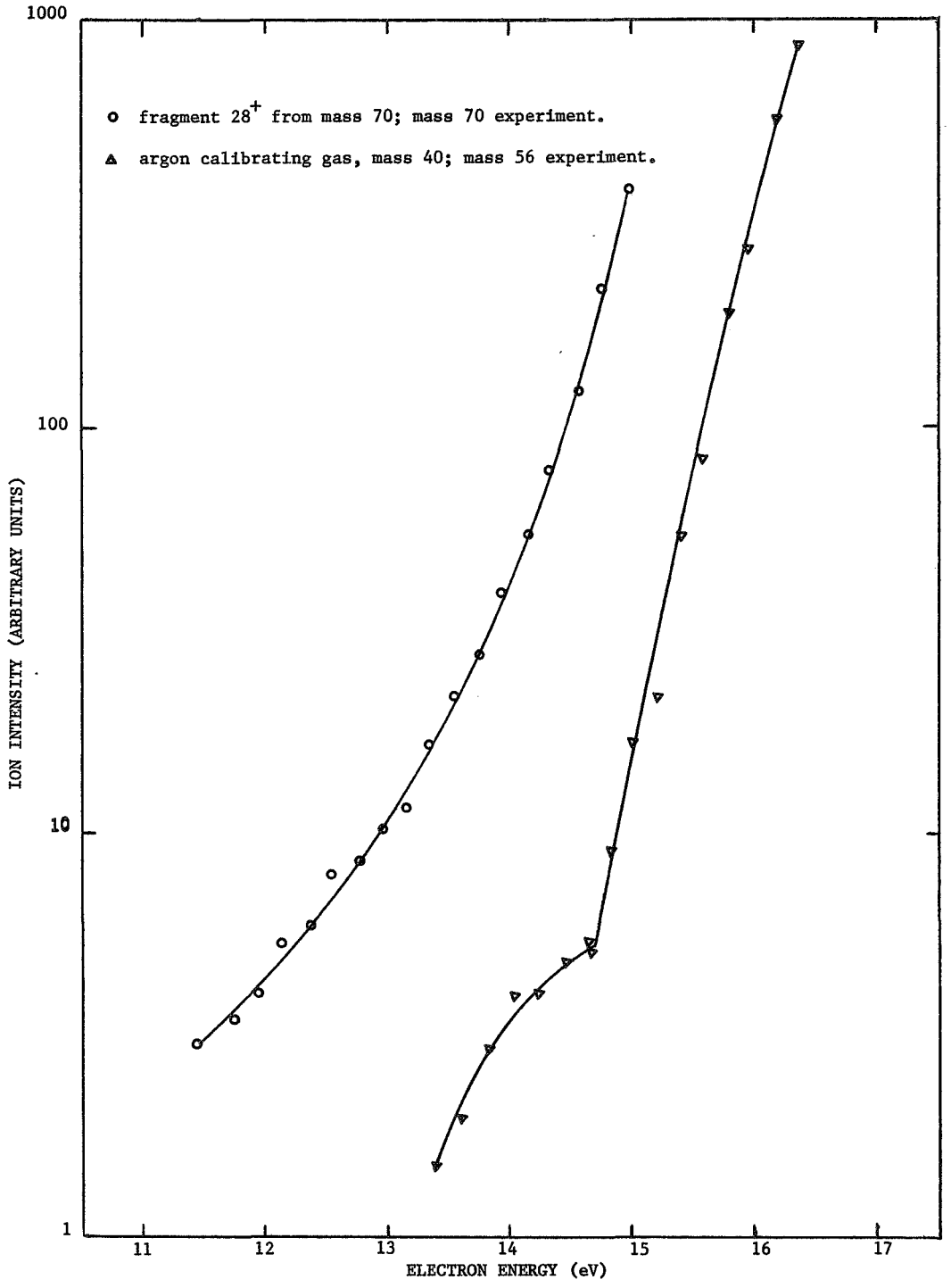

Figure 26. Examples of IE Interference Problems in Cyclopropanone Experiments

Table 17. Low Temperature Semilog IE Results for the Cyclopropanone System

Parent	Ion Mass	ms Temp.[c]	IP or AP eV	IE Curve Quality[a]	Best Value eV
Product Mass 56	56	-90	8.9	good	
			0.4<I(70)[b]	good	
		-94	9.3	good	
			0.4<I(70)[b]	good	
		-75	9.5	fair	
			0.6<I(70)[b]	fair	
		-87	0.3<I(70)[b]	fair	
		-93	9.3-9.6	fair	
			0.3<I(70)[b]	fair	9.2
	42	-93	10.7	fair	
		-87	9.8-10.2	fair	9.8-10.2
	28		9.9	poor	9.9
Product Mass 70	70	-60	9.6	good	
		-75	9.8	good	
		-75	9.3	fair	
			9.6	good	9.6
	42	-75	10.6	fair	10.6
		-75	11.0	poor	
	28	-75	10.8	fair	10.8
		-75	10.0	very poor	
cy-C_4H_6O	70	-55	9.5	fair	
			9.7	good	
			9.3-9.8	fair	
		-82	9.6	good	9.6
	42	-55	11.5	poor	
			10.6	fair	
		-70	10.6	poor	
		-82	10.6	fair	10.6
	28		10.6	poor	10.6
Reaction Off Gas	28	-145	10.1	fair	
			10.8	fair	

a. Subjective comment based on curve appearance and match with calibrating gas curve.

b. A small fragment peak at m/e 40 from cy-C_3H_4O made calibration versus argon(m/e 40) unreliable and cy-C_3H_4O (m/e 56) was also calibrated versus cy-C_4H_6O(m/e 70)

c. Refer to Table 1

Table 18. Room Temperature Initial Break IE Results for the Cyclopropanone System

Parent	Ion Mass	Ion Intensity[b]	IP or AP eV	IE Curve Quality[a]	Best Value eV
Product Mass 56	56	0.1X4-1(85)	9.1	fair	
		0.1X2-1(65)	9.2	good	
		0.1X2-1(75)	9.0	poor	9.1
	42	0.1X2-1(50)	9.9	fair	
		1X1-1(30)	9.8	good	
		1X2-6(65)	10.1	good	9.9
	28	1X1-1(40)	10.1	poor	
		1X1-1(50)	11.6	poor	
		10X2-1(100)	10.4	poor	10.2
	27	0.1X2-1(50)	13.8	fair	
		1X1-1(10)	12.9	good	12.9
	26	0.1X2-1(50)	13.8	fair	
		1X1-1(70)	13.2	poor	13.5
	14	0.1X2-1(60)	11.6	poor	
		1X1-1(10)	14.9	very poor	11.6
Product Mass 70	70	1X4-1(60)	9.2	good	
		10X1-1(70)	9.4	good	9.4
	42	1X1-1(70)	11.3	fair	
		10X1-1(70)	11.0	fair	
		10X4-1(50)	11.1	good	11.0
	28	1X4-1(60)	14.3	poor	
		10X1-1(70)	12.7	fair	12.7
	27	10X1-1(50)	14.1	fair	14.1
	15	1X4-1(50)	15.7	very poor	15.7
	14	1X4-1(80)	16.7	very poor	16.7
cy-C_4H_6O	70	1X2-1(80)	9.4	very good	
		10X1-1(70)	9.3	very good	9.4
	42	10X1-1(70)	11.2	fair	
		10X1-1(70)	11.0	good	11.0
	28	1X4-1(80)	13.3	very poor	13.3

a. Refer to Table 17
b. Refer to Table 14

(see Figure 26). Since hydrocarbon molecules do not produce m/e 18 upon fragmentation, the calibration problem was solved in later experiments by using water as the calibration gas. More consistent results were obtained by calibrating the AP of masses 56, 42, and 28 versus 56 and 70, 42, and 28 versus 70. Since the relation of I(56) to I(70) was a fairly consistent determination, mass 70 was calibrated versus the standard, which thus determined all the other APs. These low temperature, semilog results are shown in Figures 22 and 23 and are collected in Table 17.

The room temperature measurements using the initial breaks technique and water as a standard are shown in Figures 24 and 25 and are collected in Table 18.

cy-C_3H_4

The IP and AP results for cyclopropene are given in Table 19. The IP of the parent was measured a number of times at various temperatures and the results ranged from 9.4 to 10.0 eV. Excluding the data from the linear match method (the most inaccurate of the methods), the range was from 9.4 to 9.8 eV. Figure 27 compares a semilog match IP at -150° with a higher temperature (-140°), higher intensity IP both taken with the low temperature inlet system. The curves for both IP appear fairly smooth but the IP at the lower intensity is 0.3 eV higher than the high intensity IP. In cases like these, the high intensity IP with less scattered data and a steeper, more easily aligned, semilog IE curve was chosen to be the more accurate number. Consideration of all the data obtained and IP methods used has led to 9.6-9.7 eV as the best value for the IP(cy-C_3H_4). This best value is about 0.3 eV lower than the

Table 19. Low and Room Temperature IE Results for Cyclopropene

		Room Temp. Line				Room Temp Inlet System		Low Temp Inlet System			
Ion Mass	Ion Intensity at 70 eV	Trap Temp	Init. Break 70 eV[c]	Init. Break DP[c]	Lin. Match AP	Trap Temp	S'log AP	ms Temp	S'log AP	Best[b] Value AP	Lit. Value AP
40	.1×4-1(30)					-152	9.8				
	1×1-1(10)[a]							-150	9.8		
	1×1-1(10)					-145	9.4				
	1×2-1(50)	-153	9.8		10.0						
	1×2-1(10)					-143	9.6				
	10×1-1(45)	-130	9.7		10.0			-140	9.5		
best values			9.7		10.0		9.6		9.7	9.6-7	9.95
39	.1×2-1(30)					-152					
	1×2-1(50)	-153	1.2[d]		1.2[d]						
	10×1-1(10)							-140	1.2[d]		
	1×1-1(10)							-150	1.3[d]		
	10×1-1(10)	-130	1.2[d]		1.2[d]						
	1×4-1(10)					-130	1.2[d]				
	10×2-1(10)					-152	1.1[d]				
best values			1.2		1.2		1.2		1.2	10.9	11.15
28	1×1-1(45)	-142	15.2	14.8	14.4						
	1×1-1(50)	-130	14.1	13.7							
	1×2-1(100)	25	12.7							none	
27	.1×2-1(75)	-153	14.6								
	1×1-1(55)	-142	14.6	14.2							
	1×2-1(50)	-130	13.6	13.5							
	1×2-1(100)	25	14.2							<13.6	
26	.01×4-1(25)							-125	17.6		
	.1×2-1(100)	-153	17.1	16.6							
	1×1-1(10)	-137						-137	11.7		
	1×1-1(50)	-125	17.4	14.6							
	1×2-1(100)	25	16.2								
	10×2-1(60)	-130	16.4							none	
15	1×1-1(10)	-142	17.8	16.3							
	1×1-1(40)	-130	16.7	16.0						<16.0	
14	.1×2-1(90)	-153	18.2	17.2							
	1×1-1(40)	-141	17.3	16.5							
	1×1-1(100)	-130	16.0	15.3							
	1×2-1(100)	25	16.6	16.0							
	1×1-1(10)							-137	15.9	<15.5	
13	.1×2-1(70)	-153	21.4	21.2							
	1×1-1(48)	-142	21.3	20.2							
	1×2-1(100)	-130	20.5	19.4							
	1×2-1(100)	25	20.7							<20.0	

a. Refer to Table 14
b. Refer to Table 4
c. Refer to Table 16
d. AP is relative to IP of m/e 40 (i.e. A(39)=1.2 eV greater than I(40), etc.)

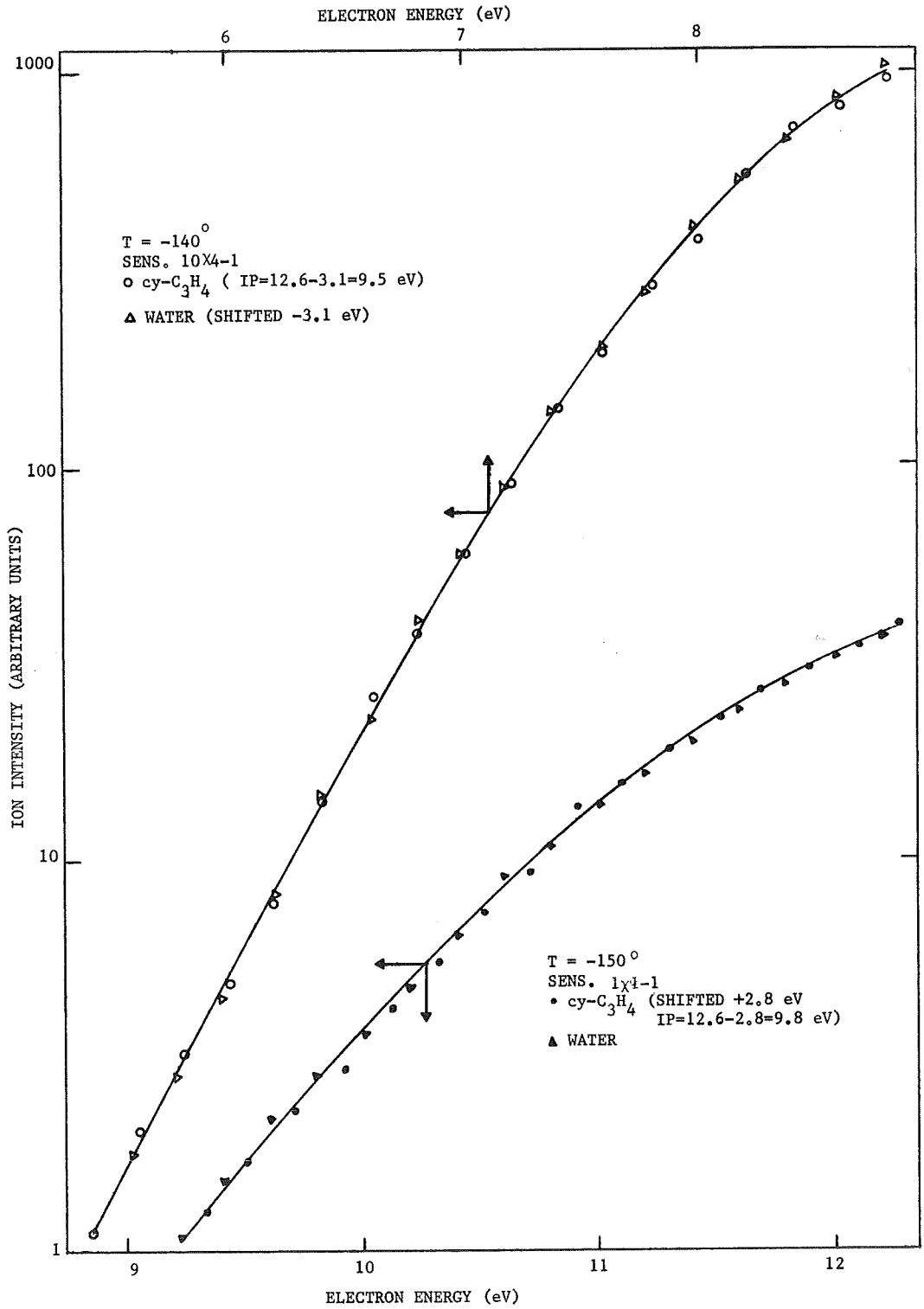

Figure 27. Semilog IE Data for Cyclopropene at Low Temperatures

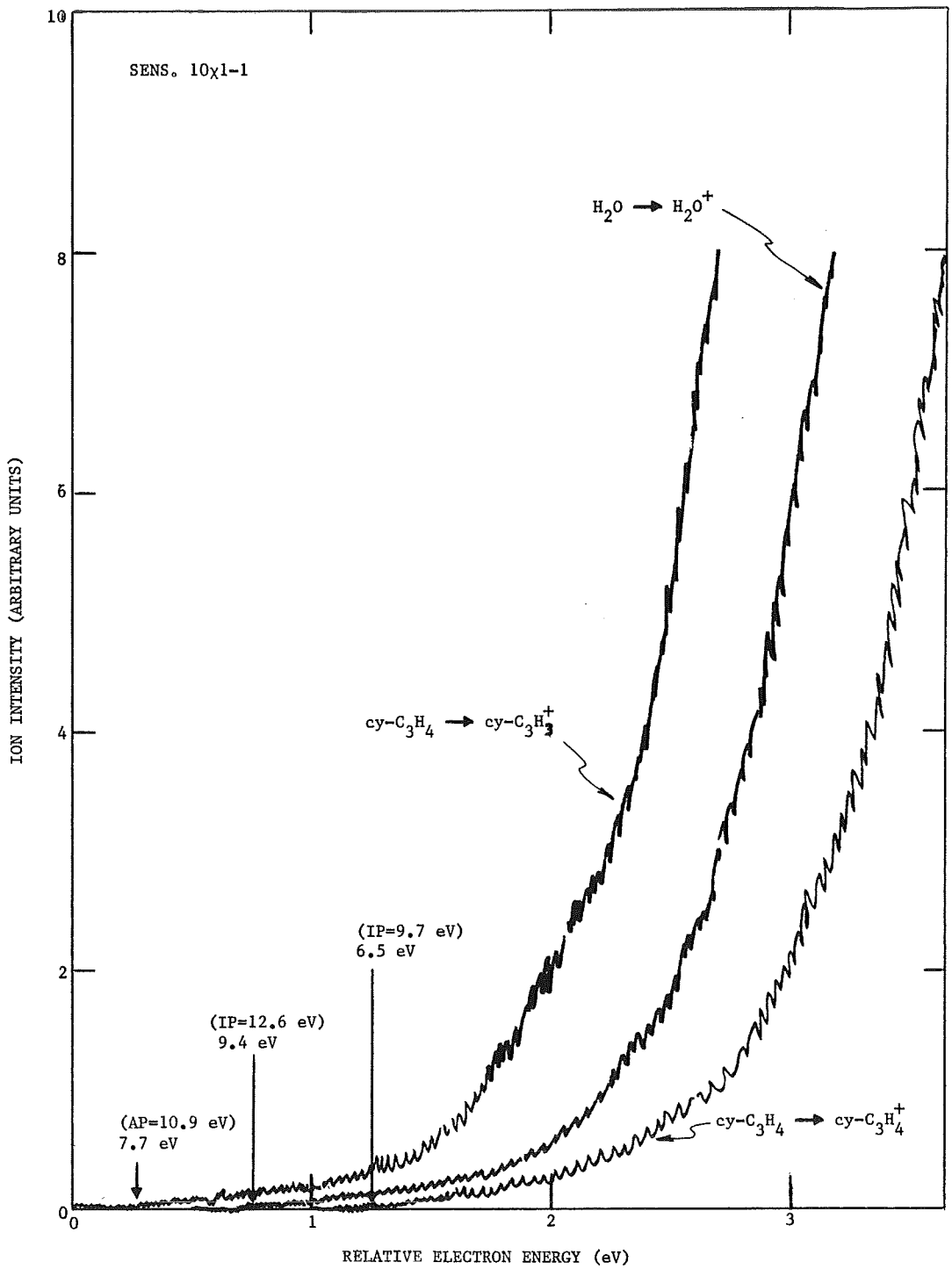

Figure 28. Initial Break IE Data for Cyclopropene at Room Temperature

Table 20. Comparisons of Linear IE Curve Shapes[a] of Cyclopropene Fragment Ions

Ion Mass		Ion IE Curve		
		tail length ΔeV	linear length ΔeV	slope at energy axis ΔeV/ΔI
18	(water)	4.0	4.5	1.1
40	(molecular ion)	4.0	2.0	1.1
39		3.2	2.8	1.1
14		10.0	10.0	1.6
28	(partly N_2)	3.7	10.0	3.0
27		6.0	5.0	2.5
15		7.0	9.0	
26		8.0	7.0	2.5
13		7.0	8.0	2.5
12		8.0	9.0	

a. normalized at 70 eV

literature value of 9.95 eV[3] which was obtained by a semilog method. This difference is reasonable in view of the amount of scatter in the IP measured and, in general, the poor agreement among workers on IP. Mass 39 ($C_3H_3^+$) was usually calibrated against mass 40 and the agreement among the series of measurements was excellent. $A(C_3H_3^+)$ was invariably measured to be 1.2 eV higher than $I(C_3H_4^+)$. Figure 28 shows the initial break behavior for masses 39 and 40 at room temperature. Ion mass 28 was of such low abundance that the interference effect of N_2 could not be satisfactorily removed and thus no value for $A(C_2H_4^+)$ is reported. The remaining ions (masses 27, 26, 15, 14, and 13) were all produced in low abundances (< 6.0 percent) and all exhibit shallow, long-tail, IE curves. Figure 20 shows a typical curve of the group, m/e 26, compared to water. Table 20 contains some semi-quantitative data which describe the shapes of the IE curves of these long-tail ions. The lengths of the curved tail and linear regions are listed as Δ eV. Also listed is the average slope of the IE curve as it approaches the energy axis over the first volt. This gives some idea as to the nature of the curve shapes. Not only did the fragment ions have shallow curves but they also had some interfering ion contributions from impurities as discussed in Chapter III. The background intensities and approximate AP of the ion masses were checked before the cyclopropene experiment. The background ions were present in very small amounts and the AP were somewhat above what was measured during the experiment. Thus it was concluded that m/e 27, 26, 15, 14, and 13 were not from any background but from the sample that was introduced. The AP of m/e 42 and 41 were at least three eV greater than m/e 40 and two eV greater than m/e 39, so there is no possibility

of fragments from 42 interfering from the energy measurement on m/e 40 and 39. Although the semilog match IE curves for the low abundance fragment ion $C_2H_2^+$ did not exhibit extremely poor curve shapes and although these curves matched fairly well with the standard curves, no consistency was obtained from sample to sample. These results indicated the folly of trying to measure the AP of a low intensity ion especially when it may be formed from more than one source. As a result, no value is given for $A(C_2H_2^+)$ from cy-C_3H_4. To a lesser degree, the same considerations hold for the remaining low abundance ions and only a value for the upper limit of the AP is given.

APPENDIX C

EXCESS ENERGIES

As discussed previously, the development of the molecular energetics of a system involving fragment ions and neutrals which possess excess electronic or excess translational, $\bar{e}_t$, rotational, $\bar{e}_r$, and vibrational, $\bar{e}_v$, energy is meaningless without a quantitative measurement of the electronic energy and the sum $|E^* = \bar{e}_t + \bar{e}_r + \bar{e}_v|$. In view of the amounts of excess energy in the ions of cyclopropane and the inconsistencies in energetics of the other cyclic compounds investigated in our work, an investigation of the excess energies of the ion fragments of the ring systems of cyclopropanone, cyclopropene, and cyclobutanone should lead to a better understanding of these systems. This appendix is devoted to the development of the experimental methods and of the results from this excess energy investigation.

Introduction

The literature abounds with examples of fragmentations that contain excess energy. In general, the parent molecular ion contains no excess translational energy and little excess vibrational energy (< 0.2 eV). For fragment ions, however, the probability of excess energies increases with the number of bonds broken. Also, if the decomposition of the parent molecular ion involves an activation energy, the fragments will possess excess energies. From a study of paraffin hydrocarbons, Stevenson[112] observed that, for a molecule R_1R_2 in which $I(R_1) < I(R_2)$,

the process $R_1R_2 \longrightarrow R_1^+ + R_2$ will occur in such a way that $R_1^+ + R_2$ are in their ground states. On the other hand, the process involving R_2^+ will usually occur with the appearance of excess energy in any possible form. This excitation can also lead to the further fragmentation of the neutral fragment and, in the end, the excitation energy is found as the bond strength of this further fragmentation. This observation, "Stevenson's Rule,[112]" suggests that at least half of the total possible fragmentation processes will involve excitation problems. In a study of small hydrocarbon molecules (i.e., methane, ethane, propane, ethylene, propene, etc.), Taubert[94] found that at 70 eV all fragments possessed some excess translational energy. He found that: ions formed by breaking a single C-C bond have low initial energy while ions which can be formed by splitting two C-C bonds have high initial energy; the amount of energy increases with the number of bonds broken; and normally a more abundant fragment ion has less kinetic energy and vice versa. These findings indicate a high probability of excess energy in the fragmentation of cyclic compounds which (a) must involve the breaking of two C-C bonds and (b) usually produces ions of low abundance.

Two types of methods are used to detect and measure kinetic energy of the fragment ions: those involving the use of retarding potentials in the ion source and those based on the focusing properties of ions formed with translational energy. These methods were developed for either conventional magnetic mass spectrometers or for specially designed instruments. Recently, Franklin[28] has developed a technique by which these measurements can be made with a time-of-flight mass spectrometer. More significantly, he has correlated the total excess energy E^* with

the experimentally measured excess translational energy of the fragmentation, $\bar{e}_t$, as[1]:

$$\bar{e}_t = \frac{E^*}{\alpha N} \tag{8}$$

This correlation considers the fragmentation process as basically a kinetic problem and thereby relates the energetic quantities using this empirical equation whose form is suggested by previous correlations of kinetic data. The energetic quantities are related by the arbitrary parameter α which is shown (see following section) to be approximately the same for a large number of fragmentation processes involving a varied array of molecules with a variable number of classical oscillators, N.

We wanted to apply this correlation to rectify inconsistent thermochemical data derived from experimental ms measurements. Assuming that the inconsistencies were attributable to excess energies (electronic or E^*), we proposed to use the correlation to predict E^* from measurements of $\bar{e}_t$. To do this, we had to assume that the empirical parameter was constant at the average value of 0.44 and applicable to the ring molecules to be studied. Because of the possible occurrence of excess electronic energy, this correlation should not be used blindly. In this appendix we have attempted to put the E^* problem on a sounder basis by calculating E^* from the thermodynamic properties of the gaseous molecules, ions, and fragments at an elevated, hypothetical temperature (T_p) associated with the $\bar{e}_t$ measurements. We proposed to determine whether the fragmentation process was basically a thermodynamic rather than a kinetic problem and hence allow a more fundamental, more precise, thermodynamic treatment. These exploratory calculations were also done to evaluate the thermodynamic reasonableness of the assigned E^* quanti-

ties which, once ascertained for a given fragmentation, would allow a discussion of the possibility of excess electronic energies and provide a basis for a critical analysis of the experimental data. For example, from the experimental E^* data on a particular molecule, one could calculate and study the variance of $\overline{C}_v$ with temperature and therefrom ascertain the precision and reliability of the experimental measurements. Approximate thermodynamic calculations were also made to point out the nature of the approximations that would necessarily have to be used for molecules for which no thermodynamic property measurements were available.

Correlation of Excess Energies

Theory

For the process, $R_1R_2 + e^- \longrightarrow R_1^+ + R_2 + 2e^-$, the difference between the measured experimental appearance potential of a fragment ion and the ground state heat of reaction at 25°C, $A(R_1^+) - \Delta H_r^o$ is defined by Franklin[1] to be the excess energy, E^*, of the decomposition as:

$$E^* = A(R_1^+) - \Delta H_r^o \ . \tag{9}$$

For a diatomic molecule, this excess energy is equal to the sum of the translational energies of the fragments and is explained by noting that the Frank-Condon region is entirely above the decomposition asymtope. For polyatomic molecules, part of the excess energy may now survive in the internal vibrational modes of the products. The fraction depends on the potential energy surface of the activated complex, which is completely unknown. This lack of knowledge of potential-energy surfaces

has been circumvented by treating complex molecules as a collection of simple harmonic oscillators. To apply this theory to the calculation of excess energies, Franklin[1] neglects rotational energy and sets the excess energy equal to the vibrational $\bar{e}_v$ and translational energies $\bar{e}_t$ of the reaction coordinate, $E^* = \bar{e}_v + \bar{e}_t$. Assuming the activated complex and the products to have the same ground state energies and neglecting any activation energy in the reverse direction, the translational energy $\bar{e}_t$ in the reaction coordinate in the activated complex becomes the translational energy observed in the dissociation products. The calculation of $\bar{e}_t$ becomes the problem of calculating the distribution of vibrational energy among a collection of N oscillators in the parent molecular ion whose total excess energy is E^*. The classical result is $\bar{e}_t = E^*/N$. Because rate constants for unimolecular dissociations calculated using the classical enumeration of states will fit experimental data only when the number of oscillators used is on the order of N/2, Franklin suggests that $\bar{e}_t$ be approximated by

$$\bar{e}_t = \frac{E^*}{\alpha N} \tag{8}$$

where α is an arbitrary parameter.

Method

The translational energy of the fragment ion, $\bar{e}_i$, is measured by the technique discussed later in this appendix. From this measured value of $\bar{e}_i$, the total excess translational energy of the dissociation products is obtained by subtracting the thermal motion of the parent ion, 3/2kT, and using the conservation of linear momentum to get the

translational energy of the products in the stationary center-of-mass frame of reference. This relation may be deduced by starting with the linear velocities in the X direction, V_x. By conservation of linear momentum

$$M_p V_{px} = M_i V_{ix} + M_n V_{nx}$$

where M_i, M_n, and M_p are the masses of the ion, neutral, and parent molecular ion activated complex, respectively. Assuming the center of mass at rest

$$M_p V_{px} = 0 = M_i V_{ix} + M_n V_{nx}$$

$$- M_i V_{ix} = M_n V_{nx}$$

$$\frac{M_i^2 V_{ix}^2}{2} = \frac{M_n^2 V_{nx}^2}{2}$$

$$M_i e_{ix} = M_n e_{nx}$$

Assuming this to hold on the average and in three dimensions

$$M_i \bar{e}_i = M_n \bar{e}_n$$

$$\bar{e}_n = \frac{M_i}{M_n} \bar{e}_i$$

so that

$$\bar{e}_t = \bar{e}_i + \bar{e}_n$$

$$\bar{e}_t = \bar{e}_i + \frac{M_i}{M_n} \bar{e}_i$$

$$\bar{e}_i \Big|_{\text{stationary}} = \left(\frac{M_n}{M_n + M_i}\right) \bar{e}_t$$

is the result for a stationary center-of-mass system. Note that the parent molecule may itself have a thermal motion which would impart an energy to the ion fragment. Distributing the thermal motion of the parent molecule into the neutral and ion groups to be gives:

$$e_{px} = \frac{M_p V_{px}^2}{2} = \frac{(M_i + M_n)\ V_{px}^2}{2}$$

$$e_{px} = \frac{M_i V_{ix}^2}{2} + \frac{M_n V_{nx}^2}{2}$$

$$e_{px} = e_{ix} + e_{nx}$$

so that

$$\frac{e_{ix}}{e_{px}} = \left[\frac{M_i V_{ix}^2}{2} \Big/ \frac{(M_i + M_n)}{2}\ V_{px}^2\right] = \frac{M_i}{M_i + M_n}$$

$$e_{ix} = \left(\frac{M_i}{M_i + M_n}\right) e_{px}$$

$$\bar{e}_i \Big|_{\text{thermal}} = \left(\frac{M_i}{M_i + M_n}\right) \bar{e}_p = \left(\frac{M_i}{M_i + M_n}\right) (3/2\ kT)$$

is the contribution from the thermal motion of the parent. The observed translational energy of the fragment ion is then the sum of these two contributions and thus

$$\bar{e}_i = \bar{e}_i \Big|_{\text{thermal}} + \bar{e}_i \Big|_{\text{stationary}}$$

$$\bar{e}_i = \left(\frac{M_i}{M_i + M_n}\right) (3/2\ kT) + \left(\frac{M_n}{M_i + M_n}\right) \bar{e}_t$$

or

$$\bar{e}_t = \left(\frac{M_i + M_n}{M_n}\right) \bar{e}_i - \left(\frac{M_i}{M_n}\right) (3/2\ kT) \qquad (10)$$

where $\bar{e}_i$ is the experimentally measured translational energy of the fragment ion and $\bar{e}_t$ is the excess translational energy of the ion plus neutral (or molecular ion) as produced only from the collision of the parent molecule and the electron. From appearance potential and $\bar{e}_i$ measurements and ΔH_r^o calculated from the heats of formation of the ions, Franklin[1] calculated E^*, $\bar{e}_t$, and α from equations 9, 10, and 8, respectively, and his results are listed in Table 21.

Discussion

The reactions studied by Franklin[1] represented a broad spectrum of structure, oscillators, and excess energies. Only α from reaction 11 departs radically from the others and this was brought into better agreement by using the first excited state of CH_2^+. The average value of α is 0.44 which is in good agreement with the results from calculating rate constants using the classical counting of states.

Franklin[1] also tried to use a better approximation of the number of oscillators, that given by Rabinovitch and Diesen,[111] but he obtained poorer correlations with the excess experimental energies.

Table 21. Calculations with Literature[1] Excess Energy Data

No.	Process	Literature[1] Data					Temp.-°K		$\Delta H\Big\vert_{T_{rt}}^{T_p}$ (lit.[73,104])			
		ΔH_r^o	AP	E^*	$\bar{e}_t$	α	T_p-T_{rt}	T_p	R_1^+	R_2	$R_1^+ + R_2$	$R_1 - R_2^+$
1	$CH_3CH{=}CH_2 \rightarrow C_2H_2^+ + CH_4$	294	325	31	3.1	0.48	1030	1330	15.5	15.2	30.7	30.4
2	$\rightarrow CH_3^+ + C_2H_3$	319	344	25	2.4	0.42	795	1095	9.7			22.0
3	$cy\text{-}C_3H_6 \rightarrow C_2H_2^+ + CH_4$	287	302	15	1.6	0.45	532	832	7.2	6.4	13.6	13.2
4	$\rightarrow CH_2^+ + C_2H_4$	333	446	113	12.1	0.45	4030	4330	47.7	108.4	156.	
5	$\rightarrow C_2H_3^+ + CH_3$	283	310	21	2.8	0.41	930	1230		11.8		
6	$CH_3NH_2 \rightarrow CH_3^+ + NH_2$	305	338	33	5.7	0.39	1900	2200	28.5	20.0	48.5	
7	$\rightarrow NH_2^+ + CH_3$	342	361	19	2.8	0.45	925	1225	8.6	11.7	20.3	
8	$CH_3NO_2 \rightarrow CH_3^+ + NO_2$	285	314	29	4.2	0.46	1400	1700	19.6	16.8	36.4	
9	$CH_3NCO \rightarrow CH_3^+ + NCO$	287	336	49	7.6	0.43	2530	2830	40.2			
10	$CH_3CN \rightarrow CH_2^+ + HCN$	344	361	17	2.8	0.50	930	1230	9.2	10.4	19.6	
11	$CH_3OH \rightarrow CH_2^+ + H_2O$	323	352	29	3.0	0.11	1000	1300	9.3	9.3	18.6	
	$\rightarrow$(triplet)	(339)		(13)	3.0	(0.36)	1000	1300	9.3	9.3	18.6	
12	$CH_2Cl_2 \rightarrow CH_2^+ + Cl_2$	355	391	36	8.3	0.48	2770	3070	33.6	25.1	59.	61.7
13	$C_2N_2 \rightarrow CN^+ + CN$	452	471	19	4.8	0.56	1660	1960	13.5	13.5	27.0	29.0
14	$C_2H_2 \rightarrow CH^+ + CH$	487	506	19	6.4	0.42	2140	2440	17.1	17.1	34.2	36.8
1	table column	2	3	4	5	6	7	8	9	10	11	12
	text equation	11		9	10	8	13	14			15	

Table 21. Calculations with Literature[1] Excess Energy Data (Concluded)

No.	ΔE T_p (lit.[73,104]) T_{rt}				$\bar{C}_v^*(T_p)$	Literature[73,104]				Approximations			
						$\bar{C}_v(T_p) \simeq \bar{C}_v$		$C_v(T_{rt})$	$C_v(T_p)$	$C_v(T_{rt})$	$C_v^{max}(T_p)$	$\bar{C}_v^{max}$	
	R_1^+	R_2	$R_1^+ + R_2$	$R_1 - R_2^+$	$R_1 - R_2^+$	$R_1 - R_2$	$R_1 - R_2$	$R_1 - R_2$	$R_1 - R_2$	$R_1 - R_2^+$	$R_1 - R_2^+$	$R_1 - R_2^+$	ΔE^{max}
1	13.5	13.2	26.7	28.4	30.3	27.5	25.1	13.3	36.8	6	96	51	53
2	8.1			20.4	31.3	25.5	23.6	13.3	34.0	6	96	51	40
3	6.2	5.4	11.6	12.2	28.2	21.1	22.7	13.4	32.0	6	96	51	27
4	39.7	100.4	141.		28.2					6	96	51	210
5		9.8			22.6					6	96	51	47
6	24.5	16.0	40.5		17.3					6	72	39	74
7	6.6	9.7	16.3		20.5					6	72	39	36
8	16.6	13.8	30.4		20.6					6	72	39	54
9	35.2				19.3					6	72	39	98
10	7.2	8.4	15.6		18.2					6	60	33	31
11	7.3	7.3	14.6		29.0					6	60	33	33
	7.3	7.3	14.6		13.0					6	60	33	33
12	28.1	19.6	47.7	56.2	13.0	20.3	16.6	10.2	23.0	6	48	27	74
13	10.3	10.3	20.6	25.8	11.4	15.5	14.5	11.5	17.6	6	38	22	36
14	13.0	13.0	26.0	32.7	8.9	15.2	13.3	8.5	18.1	6	38	22	47
1	13	14	15	16	17	18	19	20	21	22	23	24	25
			16	15	17	18	19			20	21	19	22

Note: All energetic values are in kcal/mole except C_v which is in cal/mole.

Thermodynamic Calculations

We have attempted to correlate the data reported by Franklin on the basis of internal energy changes at the temperature of the fragmentation assuming that the molecular ion activated complex or fragment ion oscillators reach equilibrium before molecular ion decomposition or fragment ion analysis. Franklin has assumed that the heat of reaction calculated at 298°K should be equal to the AP of the fragmentation with no excess energy. A more exact statement would be to calculate the AP as the change in internal energy of the reaction at 298°K because this would seem to beter describe the actual ionization taking place in the source of the mass spectrometer. However, when the reaction takes place at room temperature, the effect of replacing E for an ideal gas with H is to introduce an error less than a kcal* and the equations are:

$$R_1\text{-}R_2\Big|_{T_{rt}} + e^- \longrightarrow R_1^+\Big|_{T_{rt}} + R_2\Big|_{T_{rt}} + 2e^-$$

$$A(R_1^+) = \Delta E^o_{T_{rt}} \simeq \Delta H^o_{T_{rt}} = \Delta H^o_f(R_1^+) + \Delta H^o_f(R_2) - \Delta H^o_f(R_1\text{-}R_2)$$

---

*Note that:

$$H = E + PV = E + RT$$

$$E = H - Rt$$

$$A(R_1^+) = \Delta E^o_{T_{rt}} = E^o(R_1^+) + E^o(R_2) - E^o(R_1\text{-}R_2)$$

$$= H^o(R_1^+) + H^o(R_2) - H^o(R_1\text{-}R_2) + [(-RT)+(-RT)-(-RT)]$$

$$= \Delta H^o_{T_{rt}} - RT$$

or $$\Delta E^o_{T_{rt}} - \Delta H^o_{T_{rt}} = -RT_{rt} \simeq -0.60 \text{ kcal/mole}$$

where

$$\Delta H^{o}_{T_{rt}} = \Delta H_r \equiv \Delta H^{o}_f(R_1^+) + \Delta H^{o}_f(R_2) - \Delta H^{o}_f(R_1\text{-}R_2) \qquad (11)$$

The presence of excess energy can be handled by assuming an increase in internal energy in either the fragment products or, as Franklin suggests, in the activated complex before fragmentation. This internal energy is calculated at the elevated temperature of the excess energy fragmentation, T_p, where T_p is calculated from the measurement of the ion translational energy, $\bar{e}_i$. We could calculate T_p from knowing $\bar{e}_p$, the total translational energy of the parent molecular ion activated complex before fragmentation as:

$$\bar{e}_p = 3/2\ RT_p \qquad (12)$$

but since this translational $\bar{e}_p$ is equal to the translational energy the parent had at 298°K before collision plus the excess translational energy resulting from the electron collision, we have

$$\bar{e}_p = 3/2\ RT_p = 3/2\ RT_{rt} + 3/2\ R(T_p\text{-}T_{rt})$$

where

$$\bar{e}_t = 3/2\ R(T_p\text{-}T_{rt}) \qquad (13)$$

therefore, $(T_p\text{-}T_{rt})$ was calculated from $\bar{e}_t$, and T_p was calculated as

$$T_p = (T_p\text{-}T_{rt}) + T_{rt} \qquad (14)$$

$(T_p\text{-}T_{rt})$ and T_p are listed in columns 7 and 8 of Table 21. The equations then become:

$$R_1\text{-}R_2 + e^- \longrightarrow (R_1\text{-}R_2^+)^{\ddagger}\Big|_{T_p} + 2e^- \longrightarrow R_1^+\Big|_{T_p} + R_2\Big|_{T_p} + 2e^-$$

$$A(R_1^+) = \Delta H_r^o + E^*$$

where

$$E^* \simeq \Delta E\Big|_{T_{rt}}^{T_p} \begin{cases} \simeq E(R_1^+)\Big|_{T_{rt}}^{T_p} + E(R_2)\Big|_{T_{rt}}^{T_p} \\ \simeq E(R_1\text{-}R_2^+)\Big|_{T_{rt}}^{T_p} \end{cases} \tag{15}$$

so

$$A(R_1^+) \begin{cases} \simeq \Delta H_r^o + \Delta E(R_1^+)\Big|_{T_{rt}}^{T_p} + \Delta E(R_2)\Big|_{T_{rt}}^{T_p} \\ \simeq \Delta H_r^o + \Delta E(R_1\text{-}R_2^+)\Big|_{T_{rt}}^{T_p} \end{cases}$$

and

$$\Delta E\Big|_{T_{rt}}^{T_p} = E\Big|_{T_p} - E\Big|_{T_{rt}} = \int_{T_{rt}}^{T_p} C_v \, dT = \overline{C}_v(T_p - T_{rt})$$

where $\overline{C}_v \equiv$ average C_v.

ΔE for the species involved can be calculated if one knows the internal energy (E) or the heat capacity as a function of temperature over the range of temperatures in question. ΔE was calculated from the available literature[104,73] values for ΔH by the following reasoning:

$^{\ddagger}(R_1\text{-}R_2^+) \equiv$ molecular ion activated complex.

since $H = E + PV$

for an ideal gas $H = E + RT$

$E = H - RT$

and
$$\Delta E\Big|_{T_{rt}}^{T_p} = \Delta(H-RT)\Big|_{T_{rt}}^{T_p} = \Delta H\Big|_{T_{rt}}^{T_p} - R(T_p - T_{rt}) \qquad (16)$$

Note that an assumed approximate equivalence of H and E in this case would introduce a significant error at higher temperatures. ΔH^{**} and ΔE^{**} values for the ion**, neutral, sum of ion** and neutral and the molecular ion** appear in columns 9 and 13, 10 and 14, 11 and 15, and 12 and 16, respectively. Columns 11 and 12 and 15 and 16 are to be compared to E^* in column 4. Although neither $\Delta H\Big|_{T_{rt}}^{T_p}$ nor $\Delta E\Big|_{T_{rt}}^{T_p}$ consistently compare well with the experimentally derived E^*, the comparisons are sufficiently accurate in many cases such that the difference may well be within the precision of the E^* values. Assuming that the precision of these E^* values is good, these calculations show that the correlation with the kinetic base appears to perform more satisfactorily than the thermodynamic calculations. However, we are not going to conclude whether or not the thermodynamic approach is fundamentally incorrect. Furthermore, these calculations reveal that the magnitudes of the assigned excess vibrational energies are thermodynamically reasonable and support the proposal that the excess energy is found to be in the internal modes and not in excited electronic state.

**The enthalpy change for the ion was taken to be the same as the unionized species.

Knowing E^*, T_p, and T_{rt}, one can calculate $\overline{C}_v^*$ as

$$E^* = \Delta E\Big|_{T_{rt}}^{T_p} = \overline{C}_v^*(T_p - T_{rt}) \tag{17}$$

These values are listed in column 17. Also shown is the actual $\overline{C}_v$ calculated from literature ΔE values as

$$\Delta E\Big|_{T_{rt}}^{T_p} = \overline{C}_v(T_p - T_{rt}) \tag{18}$$

and a rough average of $\overline{C}_v$ calculated as

$$\overline{C}_v = [C_v(T_p) + C_v(T_{rt})]/2 \tag{19}$$

Assuming C_v is a steadily increasing function of temperature, one would expect $\overline{C}_v$ also to be a steadily increasing function of temperature as

$$\overline{C}_v = \left[\int_{T_{rt}}^{T_p} C_v \, dt\right]/(T_p - T_{rt}) = \overline{C}_v(T_p)$$

and, since T_{rt} is fixed in these fragmentations, $\overline{C}_v$ should be a function of T_p. Although data were available for only reactions 1 and 2 to verify this trend in $\overline{C}_v(T_p)$, we think it is reasonable to assume it should hold for reactions 3, 4, and 5 and 6 and 7. Assuming the data of Franklin precise enough for analysis, the $\overline{C}_v^*(T_p)$ values calculated (equation 17) from the experimental E^* and shown in column 17 reveal that the expected

trend is almost never verified. From this calculation, we would have to conclude that these data were either thermodynamically inconsistent or that the data of Franklin were too imprecise to be analyzed this way. If we assumed an imprecision in the data of Franklin as high as ± 25 percent, then reactions 1 and 2 and 6 and 7 are within experimental error leaving only reaction 4, itself at an extremely high and questionable temperature (4330°K), on which to base our conclusions. In any event, it appears that the precision and reliability of the experimental data from Franklin's work or from this thesis cannot be judged by this $\overline{C}_v^*(T_p)$ calculation.

For molecules for which neither H nor C_v data nor vibrational frequencies from which one could calculate the enthalpy data were available, one would have to make some gross approximations to determine the thermodynamic reasonableness of the experimental data. Since E^* cannot be calculated precisely, perhaps an upper limit on E^* would be of some value and we calculated an upper limit, designated as ΔE^{max}. At room temperature and above the heat capacity will normally consist of translational and rotational contributions at their classical values and a vibrational contribution whose magnitude varies with temperature as:

$$C_v = \underset{(trans)}{C_v} + \underset{(rot)}{C_v} + \underset{(vib)}{C_v} \tag{20}$$

$$C_v = \underset{(trans)}{3/2R} + \underset{(rot)}{3/2R} + \underset{(vib)}{C_v} \quad \text{(nonlinear)} \tag{21}$$

If we assume that no vibrational modes are active at T_{rt} but that all

are active at T_p, we would calculate ΔE^{max} as:

$$C_v(T_{rt}) = 3/2R + 3/2R + 0 = 6/2R = 3R$$

$$C_v^{max}(T_p) = 3/2R + 3/2R + (3n-6)R$$

assuming $$\overline{C}_v^{max} = [C_v(T_p) + C_v(T_{rt})]/2 \qquad (19')$$

then $$\Delta E^{max} = \overline{C}_v^{max}(T_p - T_{rt}) \qquad (22)$$

If we wanted to calculate $\overline{C}_v^{*}(T_p)$ for an analysis of $\overline{C}_v^{*}(T_p)$ variance with temperature, we would calculate $\overline{C}_v^{*}(T_p)$ from knowing E^* as

$$E^* = \Delta E = \overline{C}_v^{*}(T_p - T_{rt}) \qquad (17)$$

This is the same calculation as equation 17 and we have shown that the variance of $\overline{C}_v^{*}$ with T_p does follow the expected trend. The reliability of $\overline{C}_v^{max}$ (equation 19′) as an average $\overline{C}_v$ can be judged by comparing this type of average calculated from available thermodynamic C_v values in column 19 with the exact $\overline{C}_v$ values in column 18. The approximate average appears reliable enough to use with the gross approximation that C_v is at its classical limit at T_p. The calculations of ΔE^{max} are shown in column 25 and are two to three times greater than the experimentally derived E^*. If it were the case that the inconsistency in energetic calculations involved an energy amount that was less than a ΔE^{max} as calculated here, then we would recommend assuming this energy lay in the vibrational modes and applying the kinetic correlation to calculate an E^*. However, if the amount of energy were greater than a ΔE^{max}, we would

propose that the energetic discrepancy was of an electronic or some other nature.

If the assumption of obtaining equilibrium holds, then this problem is a thermodynamic one and the excess energies should be exactly calculable from the thermodynamic properties. However, the data of Franklin do not seem precise enough to treat the matter precisely. Also, the data reported in this thesis were judged to be even less precise than the data of Franklin. Even if it were shown that E^* could be calculated from T_p for compounds with available C_v data, this calculation would be virtually impossible for unknown cryogenic molecules. For these reasons: the lack of precision; the lack of available C_v data; the difficulty in interpreting the meaning of temperature of the systems particles; the tenuous assumption of attaining equilibrium; and the equating of properties of the ion plus neutral to the parent, it was decided not to pursue the matter any further and, theoretically unsatisfying and fortuitous as it may seem, use the correlation of $\bar{e}_t = E^*/0.44\ N$ given by Franklin.[1]

Measurement of $\bar{e}_i$

Instrumental

Data were obtained on a Bendix time-of-flight mass spectrometer, model 12, with a S14-107 source and 110 cm drift tube. Using an analog scanning speed of one and a Honeywell Visicorder running at 25 in./min, enabled 10^{-8} ‡ seconds of real time to be displayed on 1.28 inches of recorder paper. The highly responsive magnetic galvanometers and mirrored

‡See section in this appendix "Discussion of Procedure."

light deflecting recording mechanism of the Visicorder responded satisfactorily to all but the most erratic signals. The mechanical-electrical response of a Hewlett-Packard model 7001 X-Y recorder did not record the ion peak shapes as well as the Visicorder did.

Flight Times and Ionization

The TOF mass spectrometer has three principal regions: an ionization region, bounded normally by the grounded backing plate and the ion focus grid; an acceleration region, bounded by the ion focus and the ion energy grids; and the drift tube, a field free region extending to the ion collector. A pulsed, collimated, electron beam is directed through the ionization region parallel to the ion grid and, upon collision with the sample gas, produces positive ions. After the electron pulse, a voltage pulse adjustable from 0-280 volts is applied to the ion focus grid creating an electric field, E_S, to draw the ions into the acceleration region where a -3000 volts applied continuously to the ion energy grid accelerates the ions for their flight down the drift tube. If all the ions were formed with no velocity along the axis of the drift tube (X direction) and were all located in a plane parallel to the ion focus grid at distance S_o from it, then all ions of same mass to charge ratio (m/q) would arrive at the collector at the same time. Different m/q would separate during the flight and the mass spectrum would consist of a series of lines corresponding to each m/q. As by the equation

$$\text{work} = qES = \tfrac{1}{2}MV^2_t \qquad (23)$$

Each mass of the same charge accelerated through the same distance, S, by the same field strength, E, receives the same amount of kinetic energy

and thus the arrival time (time = [length of flight tube]/V_t) at the collector is directly proportional to the square root of the mass. Actually the ions are formed over the finite thickness of the electron beam and with an initial velocity in the X direction which leads to variations in flight times and causes each mass peak to broaden. The problems due to this initial position and initial velocity are referred to as space and energy resolution, respectively.

Space Resolution

As shown by equation 23, ions further away from the ion focus grid will be accelerated through a larger distance and hence will leave the acceleration region (i.e. enter the drift tube) after the other ions, but with a larger velocity. At some distance down the drift tube, those faster moving ions overtake and pass the other slower ions. The basic principle of T-O-F mass spectrometry is to adjust the voltage of the ion focus pulse so that this merging occurs at the ion collector. A too high ion focus pulse causes premature passing; too low leads to no passing by the time the ions reach the collector; and both produce a distribution of flight times and a consequential peak broadening. By careful adjustment of the ion focus voltage, i.e. "focusing" the ion beam, one can effectively reduce peak broadening due to initial position.

Energy Resolution

Consider the case of an ion formed with an initial velocity V_x in a direction opposite to the collector. It is first decelerated by the electric field to rest then accelerated back to original position and possesses a velocity equal in magnitude but directionally opposite to its original velocity. Compared with the ion whose original velocity

was equal but opposite it would therefore arrive at the collector at a time later by the deceleration and acceleration time; compared to the ion initially at rest, it would arrive later by half this amount. The acceleration and deceleration time are the same and this time lag with reference to the ion initially at rest, Δt, can be derived as follows: Letting S and S_i represent the total distance traveled and the instantaneous position anywhere along the path, respectively; Assuming the ion has been decelerated to rest and begins to return to its original position; Starting from this point of rest, we have:

$$\text{work} = qES_i = \tfrac{1}{2} MV^2_{xi}$$

$$V_{xi} = K\, S_i^{\frac{1}{2}}$$

where

$$K^2 = \frac{2qE}{m}$$

now

$$\Delta t = \int_o^t dt = \int_o^s \frac{dS_i}{V_{xi}} = \int_o^s \frac{dS_i}{kS_i^{\frac{1}{2}}} = \frac{2S^{\frac{1}{2}}}{K}$$

but

$$V_x = K\, S^{\frac{1}{2}}$$

so

$$\Delta t = \frac{2V_x}{K^2} = \frac{mV_x}{qE} \qquad (24)$$

Note that the flight times are independent of any velocities in the Y or Z direction. If one knows the probability distribution for the component of initial velocity along the direction of the flight tube $f(V_x)$, then the probability distribution for Δt and, hence, peak shape can be deduced. For example, consider ions with a thermal energy dis-

tribution. Each of the three components of velocity has a Gaussian distribution, e.g.,

$$f(V_x) = (A\pi^{\frac{1}{2}})^{-1} \exp\ (-V_x^2/A^2)$$

$$A^2 = 2kT/M$$

substituting: $$\Delta t = \frac{mV_x}{qE} = CV_x$$

$$C = M/qE \ ; \quad V_x = \Delta t/C \ ; \quad V_x^2 = \Delta t^2/C^2$$

one gets: $$f(\Delta t/C) = (A\pi)^{\frac{1}{2}} \exp\ (-\Delta t^2/B^2) \ ; \quad B^2 = C^2A^2$$

The function $f(\Delta t)$ would represent the probability that an ion of a given m/q will have a total flight time differing by a small amount Δt from the flight time of an identical ion formed with zero translational energy or no V_x component of velocity. The ion peak corresponding to a thermal ion should then reflect the shape of $f(\Delta t)$ versus Δt which, in turn, is the Gaussian shape of $f(V_x)$ versus V_x. An experimental thermal ion peak is compared to Gaussian $f(V_x)$ versus V_x in the bottom right hand corner of Figure 29. Note the excellent agreement except for a small instrumental deviation on one side of the experimental curve. Also shown is $W_{\frac{1}{2}}$ which is the peak width when the ion intensity has fallen to half of its maximum value which can be shown to be:

$$W_{\frac{1}{2}} = 2(\ln 2)^{\frac{1}{2}}\ B = 1.66(2kMT)^{\frac{1}{2}}/qE_s \qquad (25)$$

Knowing M, q, and E_s, one could calculate T from a measurement of $W_{\frac{1}{2}}$.

The initial translational energy of mass M is then

$$\bar{e}_i = (3/2)\ RT = (N_o^2/3.69)(qE_s)^2\ [(W_{\frac{1}{2}})^2/M] \qquad (26)$$

Excess Energy Ions

The distribution of initial velocities of an ion produced by electron impact can vary from a narrow range to a wide range, depending on the potential energy curves.

If the excess energy ion produced has a Gaussian distribution of velocities one would observe the same shaped, but with increased half width, peak as a room temperature thermal ion peak of the same mass. Figure 30 is an example of this as it compares the peak widths of CH_2^+ from cyclopropane and cyclopropene. The excess energy peak would coincide with a room temperature thermal peak of a higher mass. This type of excess energy is easily interpreted as being produced by an apparent increase in temperature of the ion, and its temperature and $\bar{e}_i$ are forthrightly calculated from equations 25 and 26.

If the fragment ions are produced with an initial translational energy over a very narrow range of velocities, then the resulting ion peak approaches a rectangular shape.

The interpretation of any peak shape different from the above two is difficult to discuss in terms of the initial velocity distribution. For these peaks, as for the rectangular peaks, a measurement of the peak width at the base W_b gives the maximum initial translational energy for the group of ions and not the average.

$$W_b = 2\left(\frac{mV^{max}}{qE_s}\right)$$

$$\bar{e}_i^{\,max} = \frac{m(V^{max})^2}{2} = (1/8)\ N_o\ (qE_s)^2\ [W_b^2/M] \qquad (27)$$

All of the ions possessing excess energy in this work were Gaussian in shape and hence equation 26 was used exclusively.

Instrumental Adjustments Affecting Peak Shape

Intensity Adjustments

The instrumental adjustments that affect the intensity of the peak in a multiplicative manner did not significantly affect the peak shape. These include: the pressure of the gas in the source; the multiplier voltage; the analog sensitivity; and the Visicorder sensitivity.

Focusing Adjustments

All focusing adjustments affect the experimentally measured peak shape and must be adjusted properly if one is to obtain the correct peak shape. Both the horizontal and vertical deflection plates should be adjusted to give maximum peak heights. Adjustment to positions other than this causes the peaks to become highly unsymmetrical near the bases. This is perhaps due to some discrimination toward the ions with large translational energies. During the measurements, the ion lens was not used. As discussed earlier, the ion focus voltage is adjusted to eliminate peak broadening due to variations in initial ion position by arranging for these ions to reach the collector simultaneously. Figure 31 shows the effect of the ion focus voltage on peak width (by measuring $W_{\frac{1}{2}}$) for masses 4 and 266. As can be seen, small changes in ion focus voltage

produce little change in the peak width of mass 4 but larger changes in mass 266. The accuracy at high masses becomes important when one needs to fix the position of the calibrating curve relative to the theoretical curve as discussed in the next section. The adjustment of the ion focus voltage can be accomplished in either of two ways: (1) by measuring the voltage applied to the ion focus grid or (2) visually, by observing the peaks on the oscilloscope as one adjusts the ion focus voltage to obtain the tallest, thinest peaks.

Detecting Adjustments

When an ion packet for a particular mass strikes the collector cathode, electrons are ejected from its surface and directed onto and down the multiplier glass and subsequently onto the oscilloscope anode. This ion current is measured by deflecting these electrons onto a recording anode. This deflecting or "gating" is achieved by timed pulses. Because the pulses last a finite length of time, the instantaneous ion intensity is actually the sum of all the ions that have arrived during that time interval. This can be more clearly understood by visualizing a gate of finite time width moving slowly across an ion peak and recording the sum of all intensities between its time borders. Figure 29 shows the effect of the gate width on peak shape. A very wide gate distorts the Gaussian peak into a nearly symmetrical, very wide, flat peak. As the gate width decreases, the ion peak retains its symmetry and approaches the Gaussian shape. At very small gates, an unexplainable peak was produced (see dashed peak of Figure 29). One would expect the effect of gate width to become increasingly insignificant at higher masses and this is, in fact, the case as shown by Figure 32.

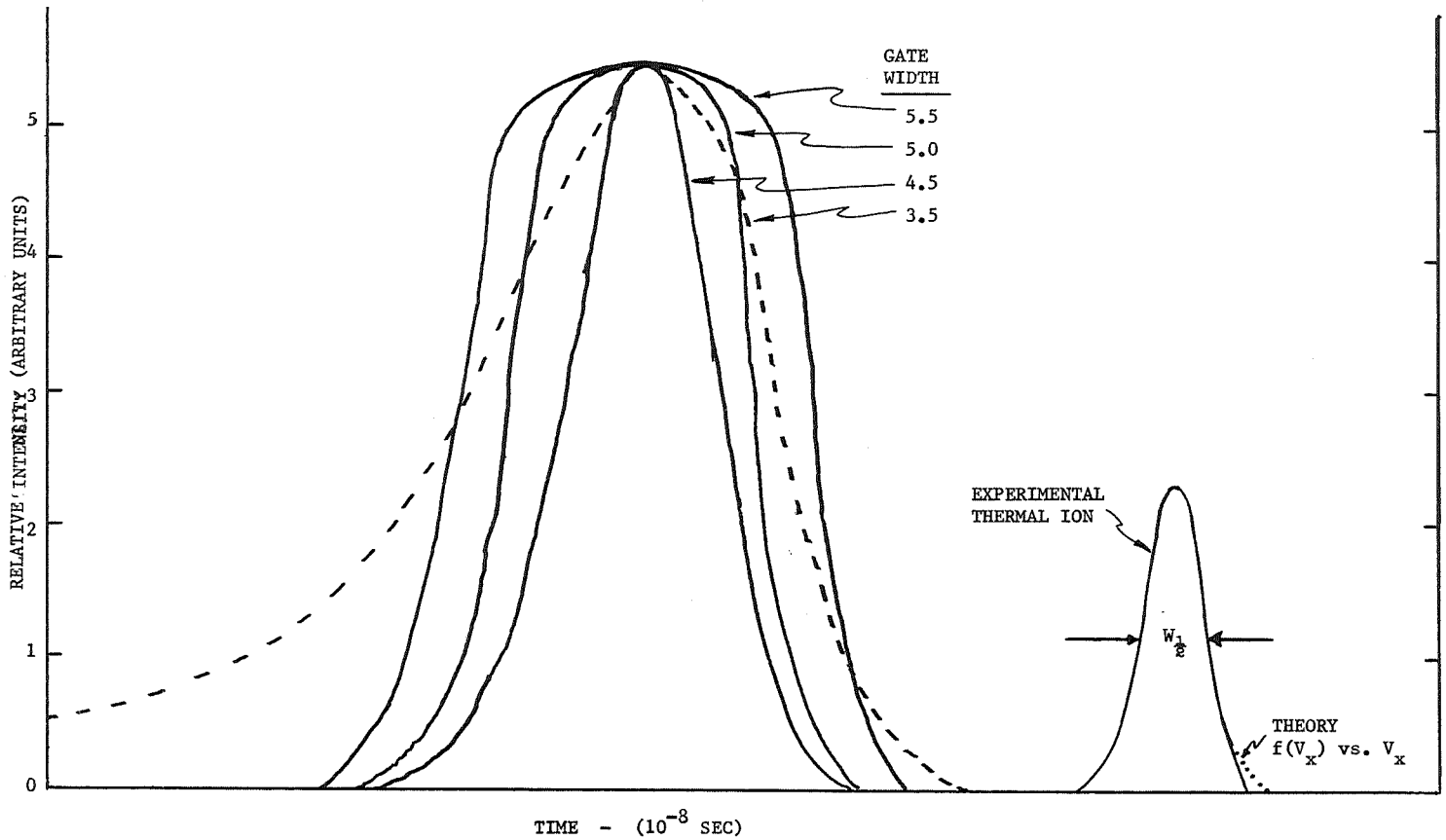

Figure 29. Peak Shapes of He Ion at Various Gate Widths

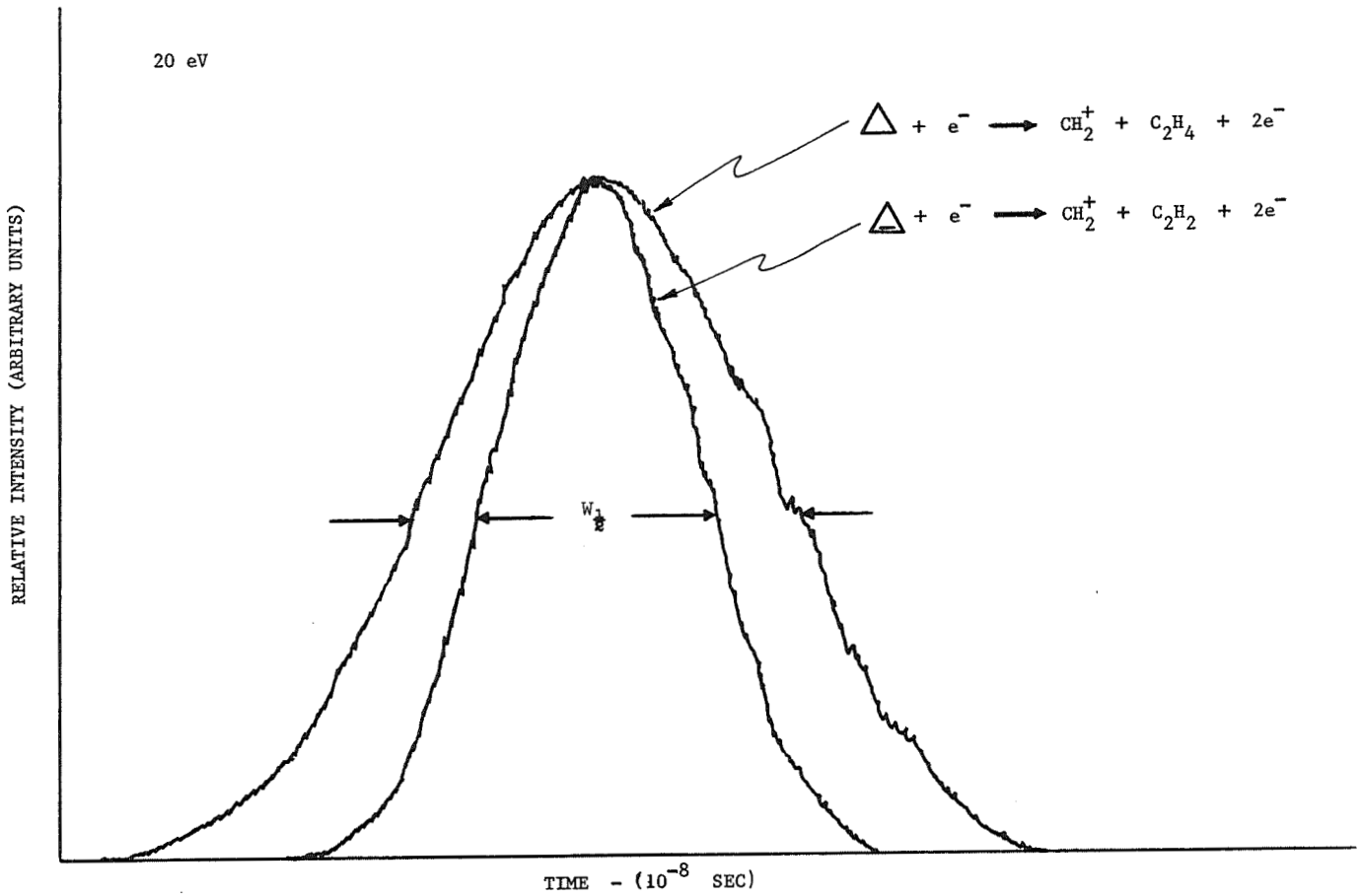

Figure 30. Comparison of Peak Widths of CH_2^+ from cy-C_3H_4 and cy-C_3H_6

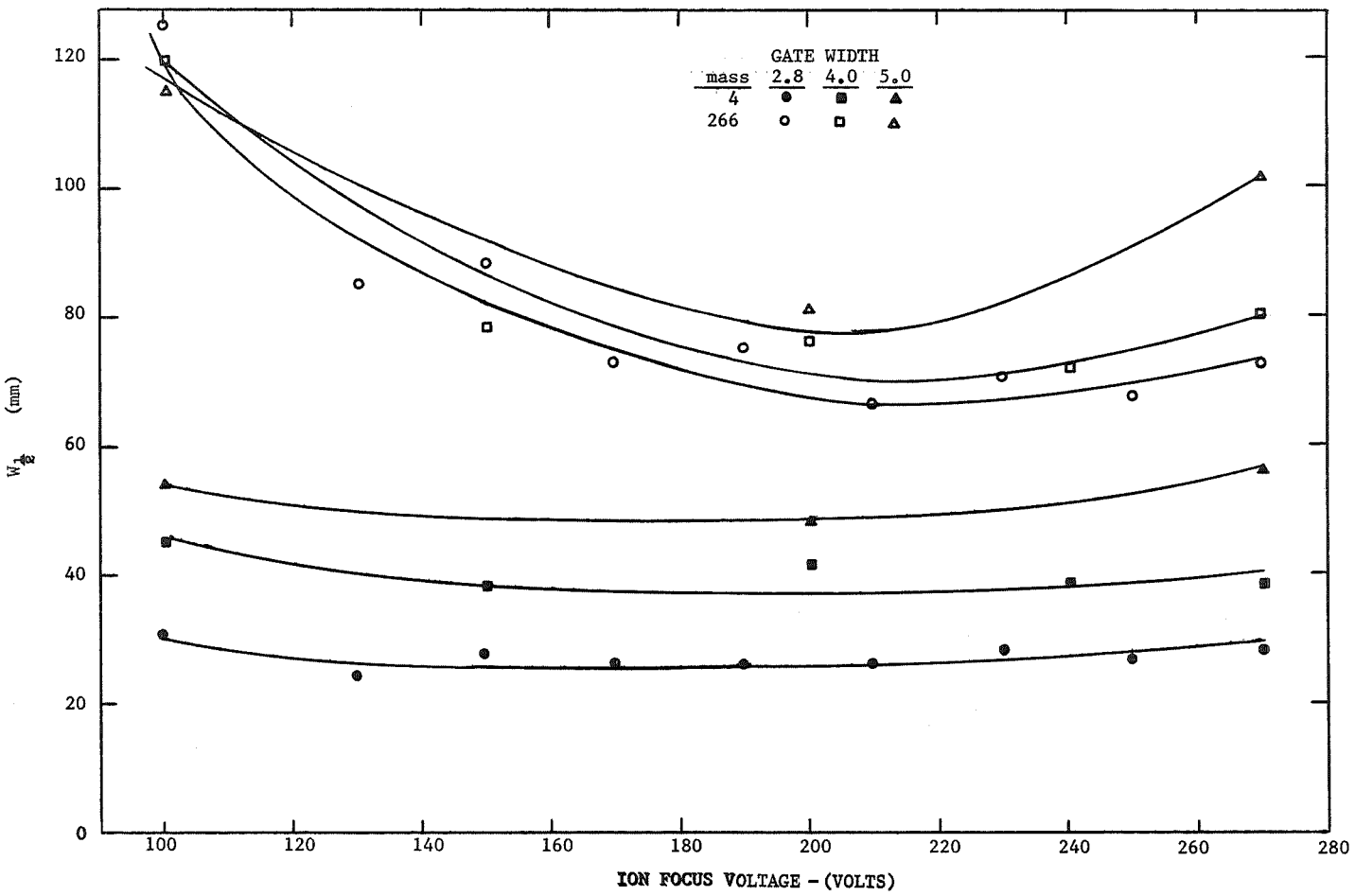

Figure 31. Peak Width Versus Ion Focus Voltage

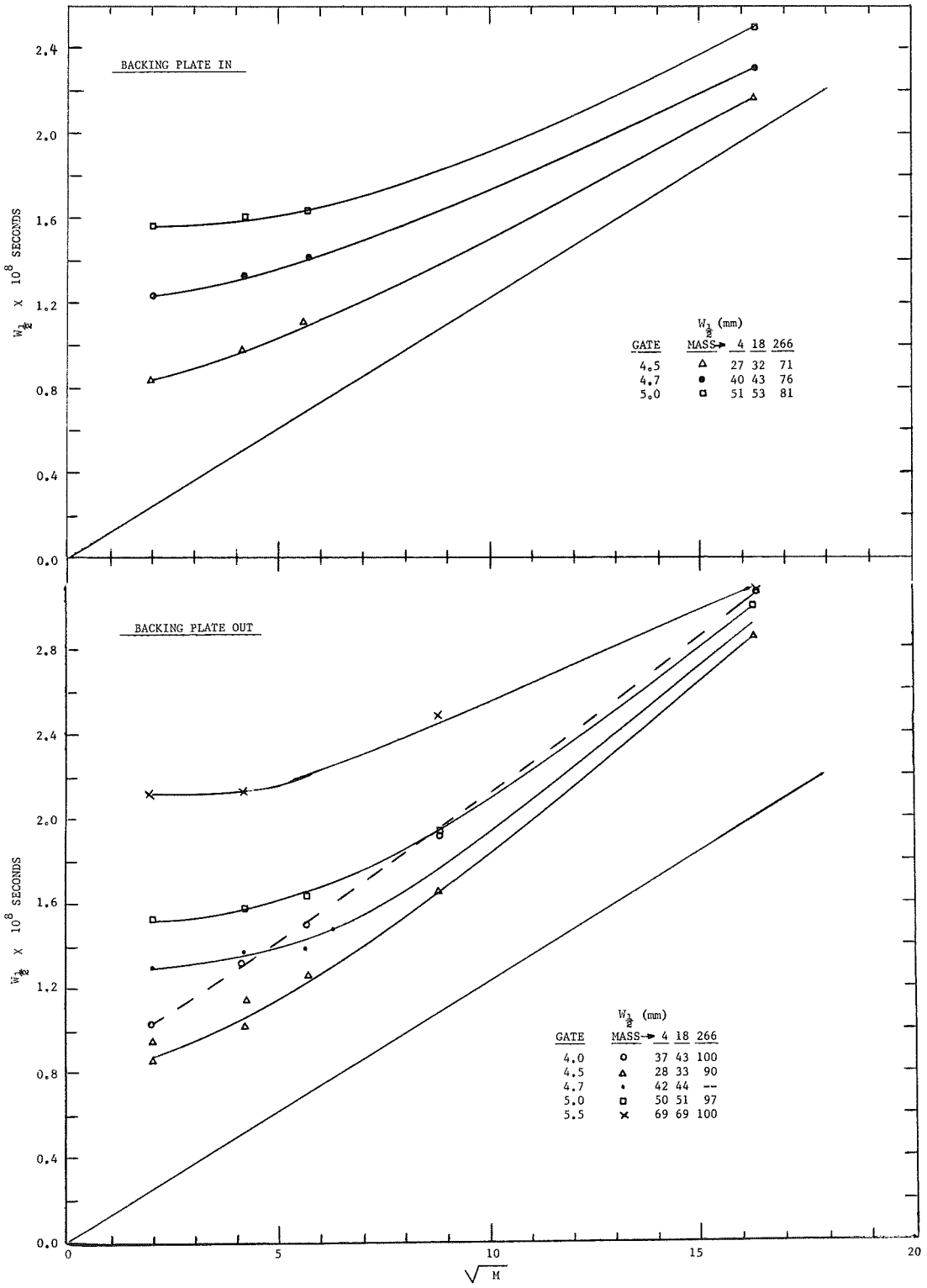

Figure 32. $W_{1/2}$ Versus $\sqrt{M}$

Recording Adjustments

The performance of the analog unit was judged to be poor because of the difficulty in obtaining reproducible data. For one thing, the gate width as indicated by markings on the front panel cannot be moved and reset to the same mark and produce the same gate width. This means that a gate producing thin ion peak shapes at one setting, being reset, may produce a wider peak. Resetting the gating speed did not seem entirely satisfactory. What is even worse, successive measurements on the same ion without moving any settings produced slightly different $W_{\frac{1}{2}}$ which would lead to significant errors in calculated $\bar{e}_i$ of ions with little excess energy. The gating rate or "scan rate" is known to drift as the mass scale needs to be periodically recalibrated. It was concluded that drift in the gate width and/or scan rate caused the variations. The paper speed mechanism of the Visicorder performed satisfactorily. The only problems resulted from improper paper feedout and were immediately obvious. The peak intensity recording mechanism (the magnetic galvanometers) was most satisfactory if the peak heights were generally kept in the same region, i.e. very small peaks and very large peaks varied somewhat in shape due to the sensitivity-inertia of the Visicorder system.

Experimental Work

Procedure

The procedure for obtaining the excess energies of fragment ions and fragmentation processes was:

1. obtain a calibration curve relating $W_{\frac{1}{2}}$, $\sqrt{M}$ and gate width for room temperature thermal ions;

2. obtain $W_{\frac{1}{2}}$ versus electron energy for each fragment ion;

3. obtain $\bar{e}_i$ at the AP by extrapolating a plot of $\bar{e}_i$ (calculated from $W_{\frac{1}{2}}$) versus electron energy;

4. Calculate $\bar{e}_t$ at the AP from $\bar{e}_i$ by equation 10;

5. calculate E^* at the AP from $\bar{e}_t$ by equation 8 ($\alpha = 0.44$).

Discussion of Procedure

1. Calibration Curve. Because of the effect of gate width and other factors on the peak shape, for each set of data it was necessary to obtain a calibration curve relating $W_{\frac{1}{2}}$, $\sqrt{M}$, and gate width. This was done by using a number of parent molecular ions ranging in mass from 4 to 266. The result was curves of the types in Figure 32. The lower graph refers to data taken with the backing plate removed from the source. Under these conditions, the ion focus voltage could not be adjusted to focus the ions at the collector. As a result, the higher masses showed considerable peak broadening due to the variation in initial position (in addition to energy broadening). With the backing plate inserted, the ions could be focused and curves like those in the upper plot were obtained. At higher masses, the curves approached the theoretical curve, a plot of equation 25 shown on Figure 32 as starting from the origin. One has to decide what gate width to use. The basic difference in a large or small gate width is that at any instant the large gate is integrating much more data and, consequently, produces much smoother ion peaks. Besides more consistent data, the large gate can record lower intensity peaks and, hence, as the intensity of a peak drops sharply at its appearance potential, a large gate allows one to record peak shapes at electron energies much closer to the AP. The major

disadvantage in a large gate is that for small masses the calibration curve is almost horizontal and thus the presence of a significant amount of excess translational energy in these masses might not be detected. For example, if a parent of mass 40 produces an ion of mass 14 with $E^* = 15$ kcal/mole, $\bar{e}_t = 2.4$ kcal/mole, and $\bar{e}_i = 0.08$ eV, this would produce a change in $W_{\frac{1}{2}}$ of two to three percent for a gate of 5.0. Considering the fact that $\bar{e}_i$ is gotten from an extrapolation to the appearance potential, this much energy could easily go undetected with the large gate. The major advantage of a thin gate is that the calibration curve has enough slope at small masses so that small excess energies (hence small variations of $W_{\frac{1}{2}}$ will be observed. The major difficulty with thin gates is that the low ion intensities near the AP produce erratic peak shapes, and $W_{\frac{1}{2}}$ and $\bar{e}_i$ data near the AP become scattered and involve a more subjective extrapolation. For low mass ions with low ion intensities and little excess energy, we used a three-step procedure to detect the presence of excess translational energy. First, a large gate was used to give an upper limit on the excess energy. Then a small gate was used to also detect any excess energy. Thirdly, the two $\bar{e}_i$ versus electron energy curves were compared and both used to determine how the curves and extrapolation should be drawn.

For neighboring ion peaks both with large translational energies, it was found that a wide gate would record the latter section of one peak with the initial portion of its neighbor. This problem is immediately obvious by the failure of the ion peak to return to the baseline of the Visicorder record. In this case, it is necessary to use a thin gate. It was a very rare occurrence for neighboring ions to possess enough

excess translational energy such that the real peaks overlapped.

In general, then, the optimum gate width was the smallest gate that would give the correctly shaped ion peaks and still produce easily extrapolatable $\bar{e}_i$ versus electron energy data.

2. $W_{\frac{1}{2}}$ Versus Electron Energy. After obtaining the calibration curve, fragment ion peak widths were obtained at a number of electron energies down to the AP of the ion. The procedure was to start at 70 eV, proceed down to the AP, and return making a check at each previously measured electron energy. Before, during, and after the measurements, spot checks on one of the parent ions of the calibrating curves were made (usually He or H_2O). This was the manner in which the consistency and credibility of the data were ascertained. During some measurements, particularly those with small gates, the variations in half widths of the spot checked calibrating ions were quite large. For these situations, a second procedure was used which involved recording half widths of a series of calibrating ions at each electron energy along with the fragment ions desired. By this method, it could be observed whether the variations in half width represented random fluctuations or an actual change in calibration. In a test run on the calibrating molecular ions, the peak half widths of calibrating masses 4, 18, and 266 were measured at electron energies down to the IP using a thin gate. Also, similar data on mass 4 with a large gate were obtained. With a thin gate, $W_{\frac{1}{2}}$ were obtained to within 1.5, 3.0, and 0.5 eV of the AP for masses 4, 18, and 266, respectively; for the wide gate, mass 4 to within 0.5 eV. Although the data became scattered near the AP, the choice of extrapolation was not difficult. The half width of all three compounds remained constant

with electron energy (as expected). These results indicated that, for ions of sufficient intensity, the extrapolation to the AP would not be difficult.

3. $\bar{e}_i$ Versus Electron Energy. $W_{\frac{1}{2}}$ data were obtained in millimeters. Multiplication by 0.0308 (10^{-8}) sec/mm* gives an uncorrected $W_{\frac{1}{2}}$ in time. Use of the applicable gate width curve from Figure 32 corrects $W_{\frac{1}{2}}$ to give the $W_{\frac{1}{2}}$ needed to calculate T from equation 18 and $\bar{e}_i$ from equation 19. An alternative procedure to calculating $\bar{e}_i$ is to note what the half width should be for this mass as a room temperature, thermal ion ($W_{\frac{1}{2}}\Big|_{T_{rt}}$). From equation 26 we see that:

$$\frac{e_i\Big|_T}{e_i\Big|_{T_{rt}}} = \left(\frac{W_{\frac{1}{2}}\Big|_T}{W_{\frac{1}{2}}\Big|_{T_{rt}}}\right)^2 \tag{28}$$

where

$$\bar{e}_i\Big|_{T_{rt}} = 3/2RT_{rt} = \frac{(3/2)\ (1.987)\ (298)\ (10^{-3})}{23.06} = 0.039 \text{ eV}$$

$W_{\frac{1}{2}}\Big|_T$ is the corrected peak half width for the excess energy ion

so $$\bar{e}_i\Big|_T = (0.039 \text{ eV})\ (W_{\frac{1}{2}} \text{ ratio})^2$$

$\bar{e}_i$ is then plotted versus electron energy and extrapolated to the AP of the ion.

---

*This conversion was determined by comparing the T-O-F mass spectrometer of this work with reference 1 and adjusting the position of the calibration curve to reproduce the published results.

Results

The raw experimental $W_{\frac{1}{2}}$ (mm) versus electron energy data are given in Tables 22-26. Also shown are the calculated quantities: uncorrected $W_{\frac{1}{2}}$ (sec), corrected $W_{\frac{1}{2}}$ (sec), and $\overline{e}_i$. Some sample plots of $\overline{e}_i$ versus electron energy are given in Figures 33-35. Table 27 summarizes the $\overline{e}_i$ and E^* data for all processes studied in this thesis and lists the available literature data for comparison.

Discussion of Results

Four compounds that were reported by Franklin,[1] CH_2Cl_2, C_2H_2, CH_3NO_2, and cy-C_3H_6, were investigated in this work to provide a verification of the method for obtaining excess energies. The original $W_{\frac{1}{2}}$ versus electron energy data were obtained with the backing plate out (Figure 32) and by the first technique discussed in the section of $W_{\frac{1}{2}}$ versus electron energy. A summary of the $W_{\frac{1}{2}}$ and calculated results is shown in Table 23. The extrapolated curves of $\overline{e}_i$ versus electron energy are shown in Figures 33-35. Figure 33 for CH_3NO_2 compares the data from this work with those from Franklin.[1] The curves are in general agreement in shape and in the extrapolated result but the data developed here include much more scatter. Of course, the data published by Franklin must be the average of his original data. For the rest of the $\overline{e}_i$ curves of this work, the data were averaged to produce a single point at each electron energy unless there was a reason that the scatter in data was to be shown and discussed. In Figure 33, CH_2Cl_2 and C_2H_2 show a very rapid decrease in $\overline{e}_i$ near the AP. For these types of curves an error in the $\overline{e}_i$ extrapolation could be large and result in a large error in E^*. Figure 34 for the production of $C_2H_2^+$ from cy-C_3H_6 indicates a very gently sloped curve.

Table 22. Peak Widths and Ion Translational Energies for Verification of Experimental Technique

Parent	Ion Mass	electron energy eV	$W_{\frac{1}{2}}$ uncor.[a] mm	$W_{\frac{1}{2}}$ uncor.[a] 10^{-8}secs.	$W_{\frac{1}{2}}$ cor.[a] 10^{-8}secs.	$\bar{e}_i$ (eV)
H_2O	18	70	48	1.48		
CH_2Cl_2	14	70	75	2.31	1.52	0.42
		25	70	2.16	1.40	0.37
		20	65	2.00	1.28	0.31
		18	63	1.94	1.22	0.28
He	4	70	44	1.36		
C_2H_2	13	70	61	1.89		
		40	67	2.06	1.34	0.37
		35	67	2.06	1.34	0.37
		30	66	2.04	1.31	0.35
		28	64	1.98	1.26	0.33
		26	61	1.88	1.18	0.29
		24	58	1.79	1.11	0.25
		22	58	1.79	1.11	0.25
He	4	70	42	1.30		
CH_3NO_2	15	30	57	1.76	1.09	0.21
		25	57	1.76	1.09	0.21
		20	56	1.73	1.05	0.197
		18	55	1.70	1.03	0.184
		16	57	1.76	1.09	0.21
		16	55	1.70	1.03	0.184
		14	54	1.67	1.00	0.17
		13	55	1.70	1.03	0.184
		13	54	1.67	1.00	0.170
		13	52	1.60	.92	0.15
He	4	70	41	1.26		
cy-C_3H_6	14	70	92	2.86	1.96	0.72
		40	75	2.32	1.52	0.43
		30	74	2.28	1.48	0.41
		20	74	2.28	1.48	0.41
		18	67	2.08	1.34	0.34
		17	60	1.85	1.16	0.25

a. Uncorrected or corrected for effect of gate width on peak width

Table 23. Cyclopropane Peak Widths and Ion Translational Energies

Parent	Ion Mass	eV	Run 1 $W_{\frac{1}{2}}$(mm)[a]	Run 1 $\bar{e}_i$(eV)[b]	Run 2 $W_{\frac{1}{2}}$(mm)[a]	Run 2 $\bar{e}_i$(eV)[b]	Run 3 $W_{\frac{1}{2}}$(mm)[a]	Run 3 $\bar{e}_i$(eV)[b]
He	4	70	28	.04	28	.04		
H_2O	18	70	33	.04	34	.04		
cy-C_3H_6	42	70	42	.04	42	.04		
	28	70	48	.118	46	.082		
		40	48	.121	45	.077		
		30	46	.111	44	.074		
		25			40	.053		
		20	45	.104	46	.082		
		18	46	.098	44	.073		
		17	46	.111				
		16	51	.148	45	.079		
		15	55	.168				
		14	55	.168	60	.153		
He	4	70	28		28		54	.04
H_2O	18	70	34		33		56	.04
cy-C_3H_6	42	70	37		42			
	27	70	38	.064	41	.061	58	.044
		40	40	.077	42	.066	59	.061
		30	41	.083	39	.051	59	.061
		25			43	.069		
		20	40	.061	41	.077	59	.061
		19					59	.061
		18	40	.077	40	.055	59	.061
		16	40	.077	38	.047	59	.061
		14	42	.090	42	.067	59	.061
		13	44	.10	45	.080	58	.044
He	4	70	26		28		54	
H_2O	18	70	32		34		56	
cy-C_3H_6	42	70	42		42			
	26	70	46	.090	45	.080	59	.063
		40	43	.071	44	.077	59	.063
		30	42	.065	42	.065	59	.063
		25			38	.049		
		20	41	.061	41	.061	59	.063
		18	44	.077	42	.065	58	.045
		16	42	.065	40	.055	59	.063
		15	43	.071				
		14	40	.055	41	.061	59	.061
		13	42	.065			59	.044

a. Uncorrected
b. Corrected

Table 24. Cyclopropene Peak Widths

		$W_{\frac{1}{2}}$ (mm)[a]									
Gate		(He)				(H_2O)				(O_2)	(cy-C_3H_4)
Width	eV	4	13[b]	14[b]	15[b]	18	26[b]	27[b]	28[b]	32	40
3.6	70	39	47	49	45	43	53	50	45	46	49
	40	40	45	44	45	43	49	48	45	46	49
	30	40	44	45	45	43	48	47	47	46	49
	25	40	45	47	44	43	49	48	44	46	49
	22		44			43					
	20			45	45	43	48	46	45	45	48
	18			42		43	46	46	45	46	49
	16							45		46	
	⋮										
	$W_{\frac{1}{2}}$(mm)[a]	40	44	44	45	43	47	45	45	46	49
	DP(eV)		20	15	16		15	14			
3.0	70	27	49	38	36	33	49	43	34	36	43
	40	27	37	35	33	32	46	41	35	37	43
	30	27	33	33	33	32	39	40	34	35	45
	25		33	33	32	32	40	38	35	37	43
	22		34			32					
	20	27		35	35	33	35	38	34	36	46
	18			31	31	31	40	36	33		42
	16										
	⋮										
	$W_{\frac{1}{2}}$(mm)[a]	27	33	33	32	32	40	36	34	36	43
	DP(eV)		20	15	17		15	14			
4.3	70	49	55	56	52	49	58	55	51	51	55
	40	48	53	54	50	52	56	55	53	53	56
	30	48	53	54	53	53	57	54	52	54	56
	25		53	52	53	52	55	54	53	55	56
	23		55			53					56
	21		53			52					
	20	48		53	53	53	55	54	53	53	56
	19	52		52	52	52	53	54	51	53	56
	18	48		53	54	52	54	55	54	53	57
	17				54	52	54	53	52	52	57
	16				53	52	53	53	53	53	56
	15									54	57
	14										56
	⋮										
	$W_{\frac{1}{2}}$(mm)[a]	51	53	53	53	52	53	53	53	53	56
	DP(eV)		19	14	15		14	13	13		

a. Uncorrected; b. Ion Mass

Table 25. Cyclopropene Excess Energies

Gate Width	Quantity	Ion Mass 13	14	15	26	27	28
4.3	$\bar{e}_i$ (eV)	<0.10	<0.10	<0.10	<0.055	<0.055	<0.055
3.6	$\bar{e}_i$	<0.09	<0.09	<0.09	.05-.065	<0.05	<0.05
3.0	$\bar{e}_i$	.065	.04-.065	.04-.065	.04-.05	.04-.05	.04
4.3	E^* (kcal)	<20	<20	<20	<13	<13	<13
3.6	E^*	<18	<18	<18	12-17	<12	<12
3.0	E^*	12	0-12	0-12	0-12	0-12	0
Summary	E^*	12	0	0	12	12	0

Table 26. Cyclopropanone and Cyclobutanone Peak Widths and Excess Energies

		$W_{\frac{1}{2}}$ (mm)[a]						
		(H_2O)			(O_2)			($cy-C_4H_6O$)
Parent	eV	14[c]	18	27[c]	28[c]	32	42[c]	70
$cy-C_4H_6O$	70	48	43	56	49	44	53	52
	40	46	41	53	50	44	53	50
	30	45	44	56	49	46	53	54
	25	44	44	53	47	44	53	52
	20	47	46	52	47	43	52	52
	18	46	46	52	47			
	16	45	44	52	47	46	53	53
	13		44	52	47		52	53
	11						53	53
	DP(eV)	14	10	11	11		8	
	$W_{\frac{1}{2}}$(mm)[a]	45	44	52	47	45	53	53
	$W_{\frac{1}{2}}(10^{-8}sec)$[a]	1.38	1.35	1.60	1.45	1.38	1.63	1.63
	$W_{\frac{1}{2}}(10^{-8}sec)$[b]	0.69		1.00	0.76		1.03	
	$\bar{e}_i$(eV)	0.09		.098	.055		.067	
$cy-C_3H_4O$	70		42		43	43	48	
	40		39		46	40	43	
	30		42		45	43	49	
	20		42		45	46	49	
	16		41		46	42	48	
	DP(eV)		10		9	10	9	
	$W_{\frac{1}{2}}$(mm)[a]		41		46	43	48	
	$W_{\frac{1}{2}}(10^{-8}sec)$[a]		1.26		1.41	1.32	1.48	
	$W_{\frac{1}{2}}(10^{-8}sec)$[b]				0.84		0.92	
	$\bar{e}_i$(eV)				0.067		0.053	

a. Uncorrected
b. Corrected
c. Ion Mass

Table 27. Summary of Excess Energies at AP for All Compounds (kcal/mole)

Parent	i	M_i	N[a]	M_N	$\bar{e}_i$[b]	$\bar{e}_i$	$\bar{e}_t$	E^*	Literature[1] $\bar{e}_t$	Literature[1] E^*
CH_2Cl_2	CH_2	14	Cl_2	70	.24	5.5	6.5	28	8.3	36
C_2H_2	CH	13	CH	13	.16	3.7	7.0	21	6.4	19
CH_3NO_2	CH_3	15	NO_2	46	.15	3.5	4.2	29	4.2	29
cy-C_3H_6	C_2H_3	27	CH_3	15	.06	1.4	2.1	19		21
	C_2H_2	26	CH_4	16	.06	1.4	1.8	16		15
	CH_2	14	C_2H_4	28	.35	8.0	11.5	103		113
					.08	1.6		18		
	C_2H_4	28	CH_2	14	--			--		
	CH_3	15	C_2H_3	27	.04			0		
cy-C_3H_4O	C_2H_4	28	CO	28	.067	1.54	2.2	17		
	C_2H_2O	42	CH_2	14	.053	1.22	2.2	17		
cy-C_4H_6O	C_2H_2O	42	C_2H_4	28	.067	1.53	2.5	26		
	C_2H_4	28	C_2H_2O	42	.055	1.27	1.7	18		
	C_2H_3	27	C_2H_3O	43	.098	2.25	3.1	33		
	CH_2	14	C_3H_4O	56	.09	2.08	2.3	24		
cy-C_3H_4	CH	13	C_2H_3	27	.65	1.5	1.8	12		
	C_2H_2	26	CH_2	12	.055	1.25	2.0	13		

a. most likely neutral fragments
b. electron volts

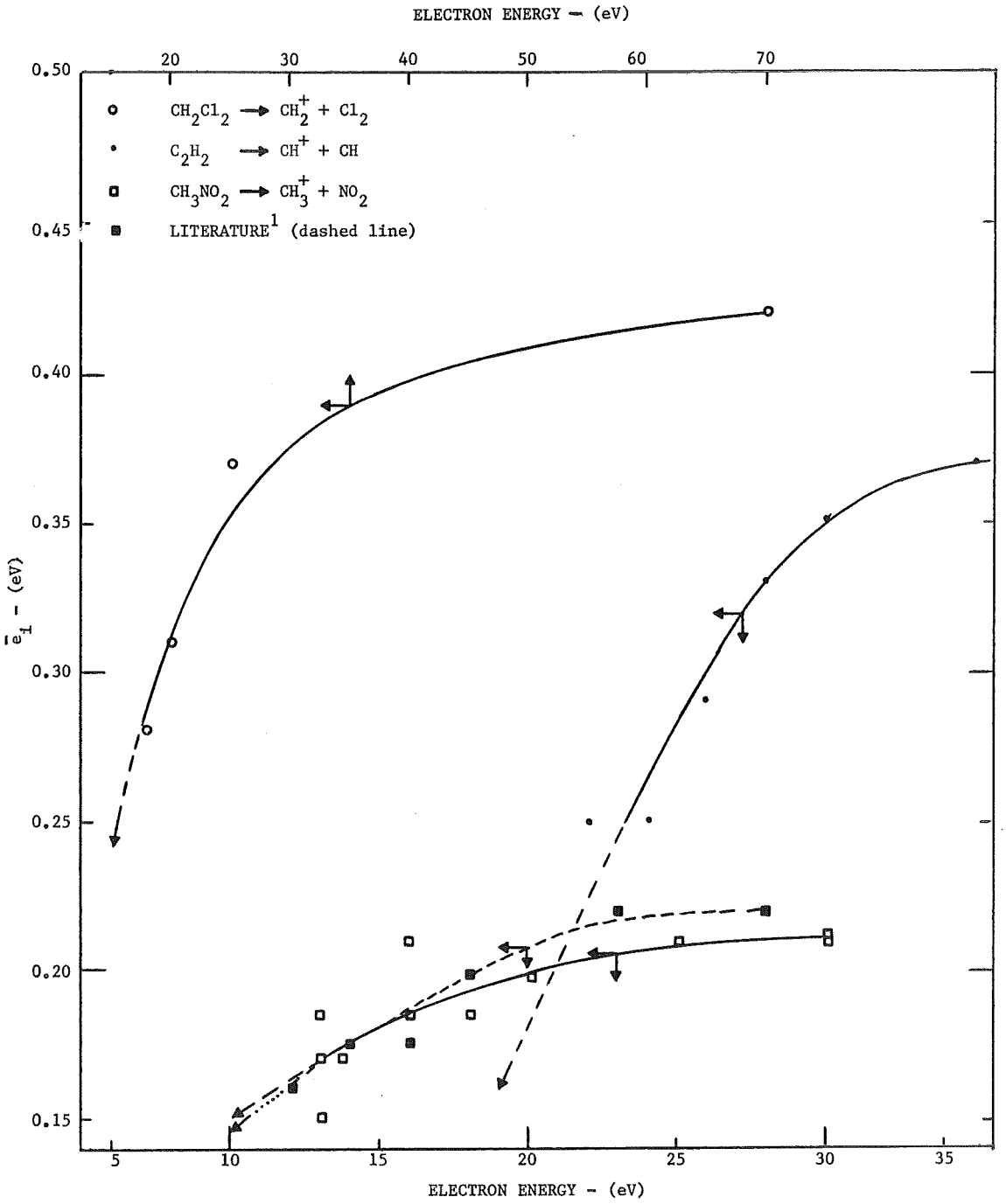

Figure 33. $\bar{e}_i$ Versus Electron Energy for Verification of Experimental Technique

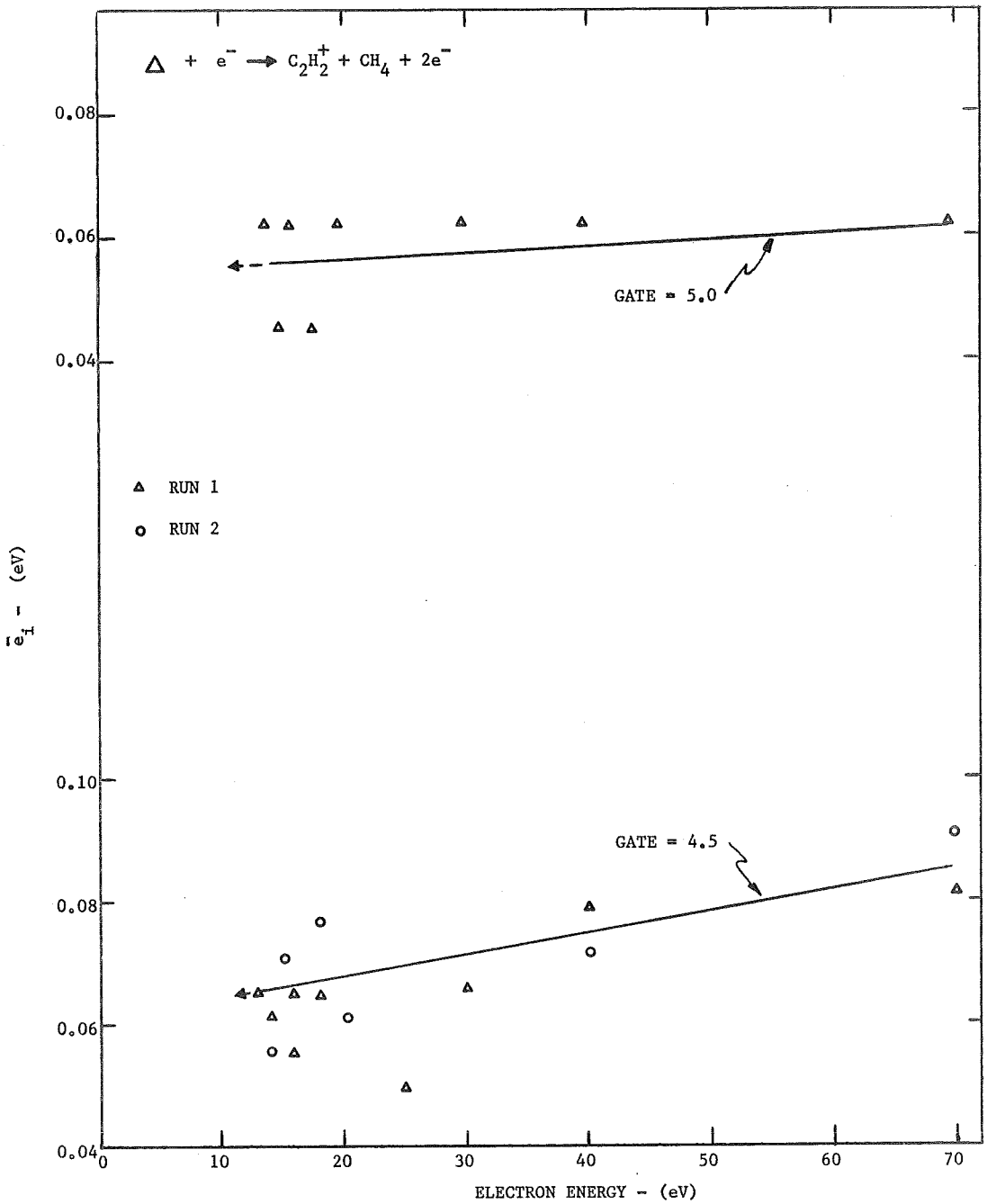

Figure 34. $\bar{e}_i$ Versus Electron Energy for cy-$C_3H_6 \longrightarrow C_2H_2^+$

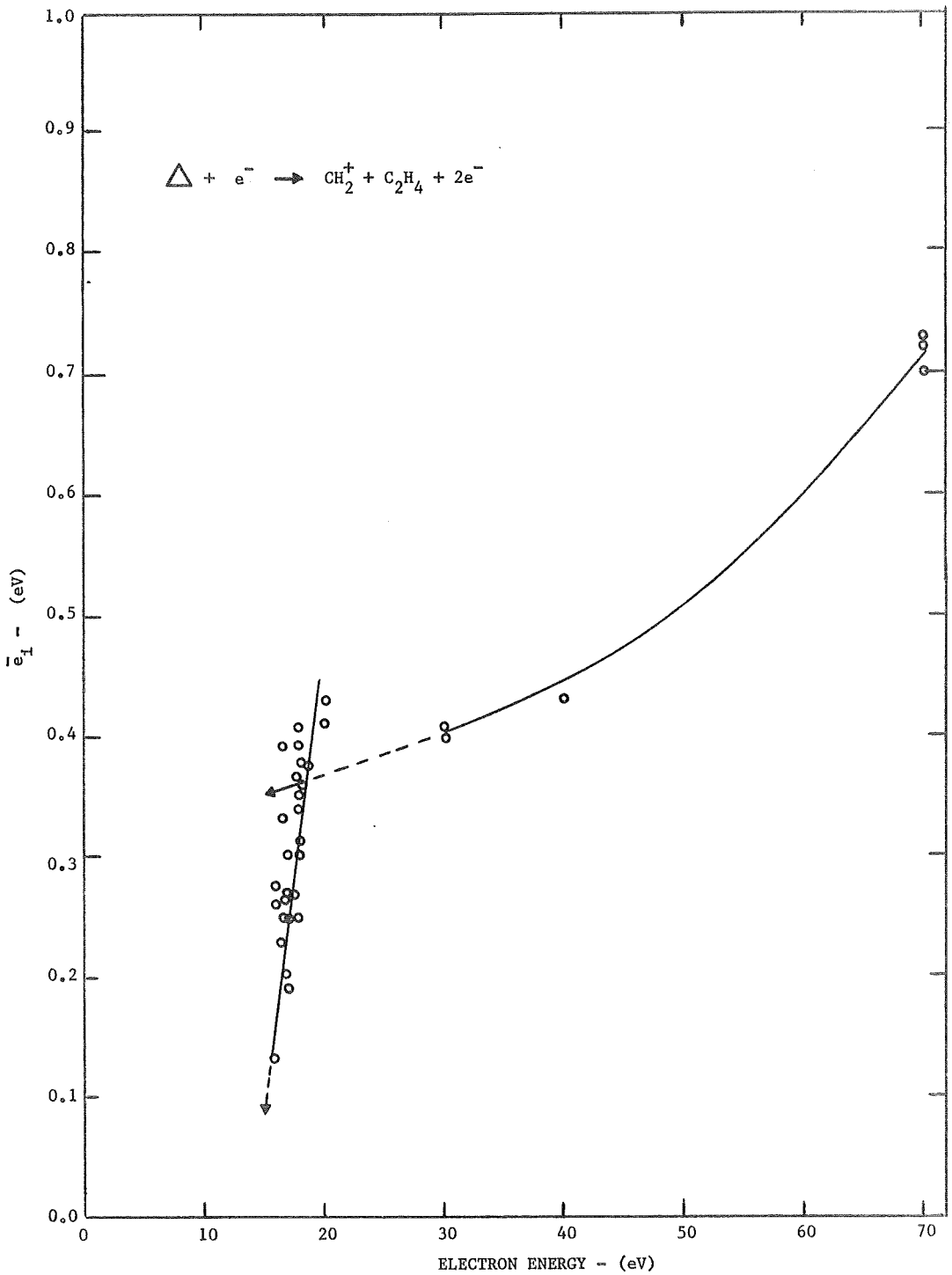

Figure 35. $\bar{e}_i$ Versus Electron Energy for cy-$C_3H_6 \longrightarrow CH_2^+$

Extrapolation of this type of curve was less subjective and, hence, should involve less error. Data from both a large and a small gate are plotted and comparison shows that, although there is more scatter for the smaller gate width, the two curves are consistent. In general, it was found that ions involving a large amount of excess translational energy (> 0.4 eV) at 70 eV had $\bar{e}_i$ curves that decreased rapidly near the AP; those involving a moderate amount (~ 0.2 eV) decreased at a moderate rate; and those of small amount (< 0.10 eV) decreased very slowly. Comparison of the results from this work with Franklin's published data (Table 27) shows fair agreement. From these results, it was concluded that the experimental technique was well understood and the method was then extended to the cyclic compounds of interest, each of which is discussed individually.

<u>cy-C_3H_6</u>. The $W_{\frac{1}{2}}$ versus electron energy data were taken with the backing plate out and by the first technique discussed in the $W_{\frac{1}{2}}$ versus electron energy section of the procedure. The data and calculated results appear in Tables 22, 23, and 27. Figure 34 for the $C_2H_2^+$ ion has been discussed in the last paragraph. Figure 35 for the CH_2^+ ion fragment reveals some peculiar results. From 70 eV there is a rapid decrease in $\bar{e}_i$ which begins to level off and is then followed by an extremely steep decrease near the AP. Since the steep curve near the AP was subject to a possible large extrapolation error, the measurements were repeated and these resulted in a large volume of badly scattered data near the AP. The ion currents are very small near the AP and, as detected, oscillate over a large range which produces peaks that one must analyze by drawing a best curve for the peak shape through the data. If one concluded that all the data near the AP are so poor that they should be neglected, then

the extrapolated result at the AP would yield $\bar{e}_i$ = 0.35 eV and E^* = 103 kcal/mole which is approximately what Franklin[1] reported and which allows the energetics of the CH_2^+ fragmentation to be interpreted in terms of the ground electronic states with an excess energy of 103 kcal/mole. However, all the data near the AP, even though scattered, are not both above and below $\bar{e}_i$ = 0.35 eV and they seem to indicate a sharp downward trend. Furthermore, this type of scatter was not observed for any calibration molecular ions--only occasionally for these ring systems. If one accepts the sharp drop, then the energetics can be interpreted by assuming that C_2H_4 and CH_2^+ are produced in excited triplet states (see section on energetics). Figure 35 could be rationalized by observing that, at the appearance potential, the ionization produces CH_2^+ and C_2H_4 fragments in electronically excited triplet states. As the electron energy is increased some ions are produced as excited triplets with little excess energy while others degenerate to the ground electrnoic singlet states; this electronic energy difference of the ion is converted into a large amount of excess vibrational and translational energy in the ion. This combination of singlet and triplet product ions produces scattered data. At some higher electron energy, almost all of the fragments are in the ground electronic states with excess vibrational energy and the upper curve is produced.

<u>cy-C_3H_4</u>. The $W_{\frac{1}{2}}$ versus electron energy data were taken with the backing plate in place. cy-C_3H_4 produces very low intensity fragment ions and, consequently, more scattered data; hence, the second technique discussed under the $W_{\frac{1}{2}}$ versus electron energy section of the procedure was used. The $W_{\frac{1}{2}}$ results are shown in Table 24. Not only were the data

scattered, but all ions appeared to have little or no excess energy which resulted in imprecise $W_{\frac{1}{2}}$ measurements. For these reasons, an estimate $\bar{e}_i$ at the AP was obtained simply by extrapolating the uncorrected $W_{\frac{1}{2}}$ data to the AP and then correcting this one $W_{\frac{1}{2}}$ value to calculate $\bar{e}_i$ at the AP. These results are listed as $W_{\frac{1}{2}}$ (mm) at the disappearance potential (DP). Data were obtained with large, medium, and thin gate widths. The data from the large gate were used to put an upper limit on E^* and were compared with the results from the smaller gates. The results are shown in Table 25. As can be seen, the data are consistent and none of the ion fragmentations appears to have an excess energy, E^*, greater than 12 kcal/mole.

<u>cy-C_4H_6O and cy-C_3H_4O.</u> $W_{\frac{1}{2}}$ versus electron energy data were taken with the backing plate in place and using method 2. The $W_{\frac{1}{2}}$ data and calculated quantities at the AP are listed in Table 26. The data for cy-C_4H_6O were obtained using an authentic sample and, therefore, no ions are present from cy-C_3H_4O. However, as discussed more fully in Chapter III, it was never possible to completely separate cy-C_3H_4O and cy-C_4H_6O. During the experiments for obtaining data for cy-C_3H_4O, 95 percent of mass 28 but only 50 percent of mass 42 were from cy-C_3H_4O. Consequently, since $W_{\frac{1}{2}}$ (corrected) for $C_2H_4^+$ from cy-C_3H_4O and cy-C_4H_6O were 0.84 and 0.76, respectively, the effect of having five percent of the ion peak 28 from cy-C_4H_6O would be to lower the measured $W_{\frac{1}{2}}$ slightly. For this reason, $\bar{e}_i$ and E^* calculated for $C_2H_4^+$ are believed to be only slightly lower than the result one would measure if only cy-C_3H_4O were present. On the other hand, for $C_2H_2O^+$, 50 percent from cy-C_4H_6O ($W_{\frac{1}{2}}$ = 1.03 (10^{-8}) sec) plus 50 percent from cy-C_3H_4O ($W_{\frac{1}{2}}$ = ?) produced an experimental value of

$W_{\frac{1}{2}} = 0.92\ (10^{-8})$ seconds. Reasoning that the peak resulting from the mixture of ions is produced by simply adding the respective contributions of $C_2H_2O^+$ yields a $W_{\frac{1}{2}}$ from cy-C_3H_4O of 0.81 (10^{-8}) seconds and calculated values of $\bar{e}_i \sim 0.035$ eV and $E^* \sim 0$ kcal/mole.

Precision, Accuracy, and Limitations

The precision of the data varied greatly from one ion to the next, as it depends entirely on how well the $\bar{e}_i$ data can be extrapolated to the AP which, in turn, depends on: 1) the steepness of the $\bar{e}_i$ curve; 2) the scatter of the data; and 3) how near to the AP $W_{\frac{1}{2}}$ data can be obtained. The accuracy is believed to be limited only by the precision as the $\bar{e}_i$ results agree well with other measurements of excess translational energies and the correlated excess energies, E^*, have explained the energetic inconsistencies in fragmentation processes in this thesis.

APPENDIX D

MOLECULAR ORBITAL CALCULATIONS

The purpose of this appendix is to present the results of MO calculations of quantities related to the mass spectrometric analysis of low temperature, strained ring molecules. Since a large portion of potential cryogenic molecules is strained ring molecules, it is believed that these results can also be extended to other ring molecules of future interest.

Introduction

Although MO calculations have been performed for some time, it has not been until the past few years that new notions as well as efficient computer programs have been developed which seem to permit the calculation of quantities of chemical interest with useful accuracy. The four computer programs used in this work were written by G. Klopman[11] and N. C. Baird,[99] both working with M. J. S. Dewar, J. A. Pople,[97] and R. Hoffmann.[98] These programs are, in turn, referred to as the Klopman, MINDO, Pople, and Hoffmann programs and, in this thesis, are designated K, M, P, and H, respectively. The H program performs extended Huckel theory calculations on molecules composed of first and second row atoms. This program determines molecular orbital wave functions, energy levels, bond orders, charge densities, and atomic charges. The P program performs calculations on the first row atoms but was not extensively used because of the approximate IP results. The K program is applicable only

to hydrocarbons and gives more accurate results for the molecular parameters mentioned above. The M program is basically an extension of the K program to other first row atoms. The K and M programs are semi-empirical in that they require the use of "standard" geometries and must be calibrated on a class of known compounds with known experimental IP and ΔH_f^o by fitting parameters such that good results are achieved on the average for the entire class.

Program Procedure

Input Data

The programs need information on the atomic number and coordinates of each atom of the molecule, the multiplicity, and the charge. The geometry is supplied either as X, Y, Z coordinates or bond angles and lengths. The multiplicity is calculated in the usual way from the number of unpaired electrons as singlet, doublet, and triplet have multiplicity, 1, 2, and 3, respectively. Charge refers to positive ion (+1), neutral molecule (o), or negative ion (-1).

Computation

For a given molecular geometry, the computer program attempts to calculate a total energy (TE) for the molecule for an assumed linear combination of atomic orbitals (LCAO). By changing the LCAO, other TE can be calculated. The changes are determined in a systematic way based on the differences between successive TE. In this manner, the computer searches for a minimum TE for the given geometry. This minimum is detected when this difference is less than a predetermined number. At this point, the program is said to have "converged." "No convergence"

means that the necessary requirement for the minimum was not met within a prescribed number of iterations. Thus, for each geometry, the program searches for the best LCAO to obtain a minimum TE.

Output

The output chemical parameters of most interest to this work were the TE, MO energy levels, ΔH_a, and IP for both singlet and triplet states. For each molecular geometry, the total energy of the molecule is the sum of the total electronic energy, electron-nuclear core energy, and nuclear core-core energy. The ΔH_a is calculated as the TE of the molecule minus the sum of the energies of the isolated constituent atoms. The IP is taken as the energy of the highest occupied molecular orbital. This assumes the particular MO from which the electron is removed, and it also assumes that the structure of this molecule minus one electron is the same as the structure of the molecule. This may or may not be a good assumption. However, any errors in this assumption seem to be adequately overcome in the programs using adjusted parameters. Only with the K program is the IP calculable by the difference of the TE of the molecule and molecular ion. The programs that use all the valence electrons calculate the molecular orbital energy levels and begin by filling up these orbitals by pairing the valence electrons. Only the P and the K programs handle electronically excited molecules and of these two, only K produces usable numbers. In the Klopman program, triplet states are formed by simply promoting an electron from the highest occupied molecular orbital of the singlet ground state molecule to the next highest orbital and TE, ΔH_a, and IP are calculated from this structure. (Note that this promoted electron now becomes the highest occupied energy level.)

Goals and Outline of Calculations

The following areas were deemed of most interest in applying these programs to the mass spectrometric investigation of strained ring molecules:

1. predicting whether a molecule will exist
2. predicting molecular structure
3. predicting ΔH_a and IP sensitivities to geometry changes
4. confirmation of ms analysis and identification by measuring IP for:
   a) distinguishing between isomers
   b) distinguishing between singlets and triplets
5. supporting ms derived energetics
   a) ΔH_a and ring strain
   b) singlet versus triplet fragments
   c) energy of triplet fragments for bond energy estimations
6. prediction of most stable products.

(1) The achievement of this goal would provide a guide in selecting potential cryogenic molecules for future study. No work was done in this area.

(2) For a given molecule, the TE for various geometries may be calculated and compared. The most negative TE should be the most stable structure. In this work, the structure of many of the compounds was known. By systematically varying the geometry about this known structure, one could tell whether the program predicted the trends needed for structure prediction. In this way, one can observe whether the predicted most stable structure corresponds to the known structure.

(3) Ideally, one would like the predicted most stable structure to correspond to the known structure and for the ΔH_a and IP calculated from this structure to correspond to the experimental values. If this cannot be realized, then one would like the ΔH_a and IP calculated from either the predicted most stable or known structure to correspond to the experimental ΔH_a and IP. If neither of these two is possible, then a third possibility is that ΔH_a and IP for some "standard" structure will correspond to the experimental for some broad, general class of compounds. As we shall see, only the third approach was successful.

Also, by varying the geometry, the sensitivity of ΔH_a and IP to geometry changes could be determined.

(4) Because ms analysis cannot distinguish between isomers or determine whether the parent molecule is in an excited electronic state, this distinction and identification might be made by comparing the MO calculated IP for isomers and excited states with the experimental IP.

(5) The ΔH_a calculated from ms data depend on the assumption of the state of the fragment ion and neutral for which the ΔH_a must be known. Also, the interpretation of the bond dissociation energies of the ring compounds in this thesis depends on estimating the relative energies of various structures. We reasoned that MO energetic results, even in a relative sense, would be useful in these decisions and calculations.

(6) As discussed in the text of this work, a possible reason for the failure to isolate cyclopropenone was that it had either reacted with or was hydrogen bonded by water. The MO programs were used in an attempt to calculate the TE of these various systems and predict the

most stable system. This is, in a sense, a thermodynamic argument as to the most stable system and would suggest that, if kinetically feasible, the more stable system should exist.

Data for Calculations

Figure 36 presents the schematic structure of five ring molecules investigated, possible isomers of these ring molecules, other possible cyclopropenone products, and the fragments encountered in the electron bombardment of these rings. The standard geometries[99] used for the M and K programs are reported in Table 28. The X-Y-Z coordinates for the calculations are presented in Table 29.

Results

Table 30 gives the geometry variations for the four ring molecules that were studied. Note that, if the bond angles or lengths were not changed from one case to the next, the dimension is not repeated. In this way, the dimensions were systematically varied about a known value such that the changes were easily analyzed. Similar geometry variations (such as C-H lengths) were not repeated for each molecule if it had been varied before in another molecule and, thus, the geometry variations of the four ring molecules will be discussed together. Also, the C=O length was varied for a number of molecules in an attempt to get better IP correlations with experimental data, and these variations are also listed in Table 30. The MO results of these geometry changes are recorded in Table 31 in exactly the same manner for easy comparison to Table 30. Table 32 collects the standard and known geometries for the molecules. In Table 33 the MO results for Table 32 are presented

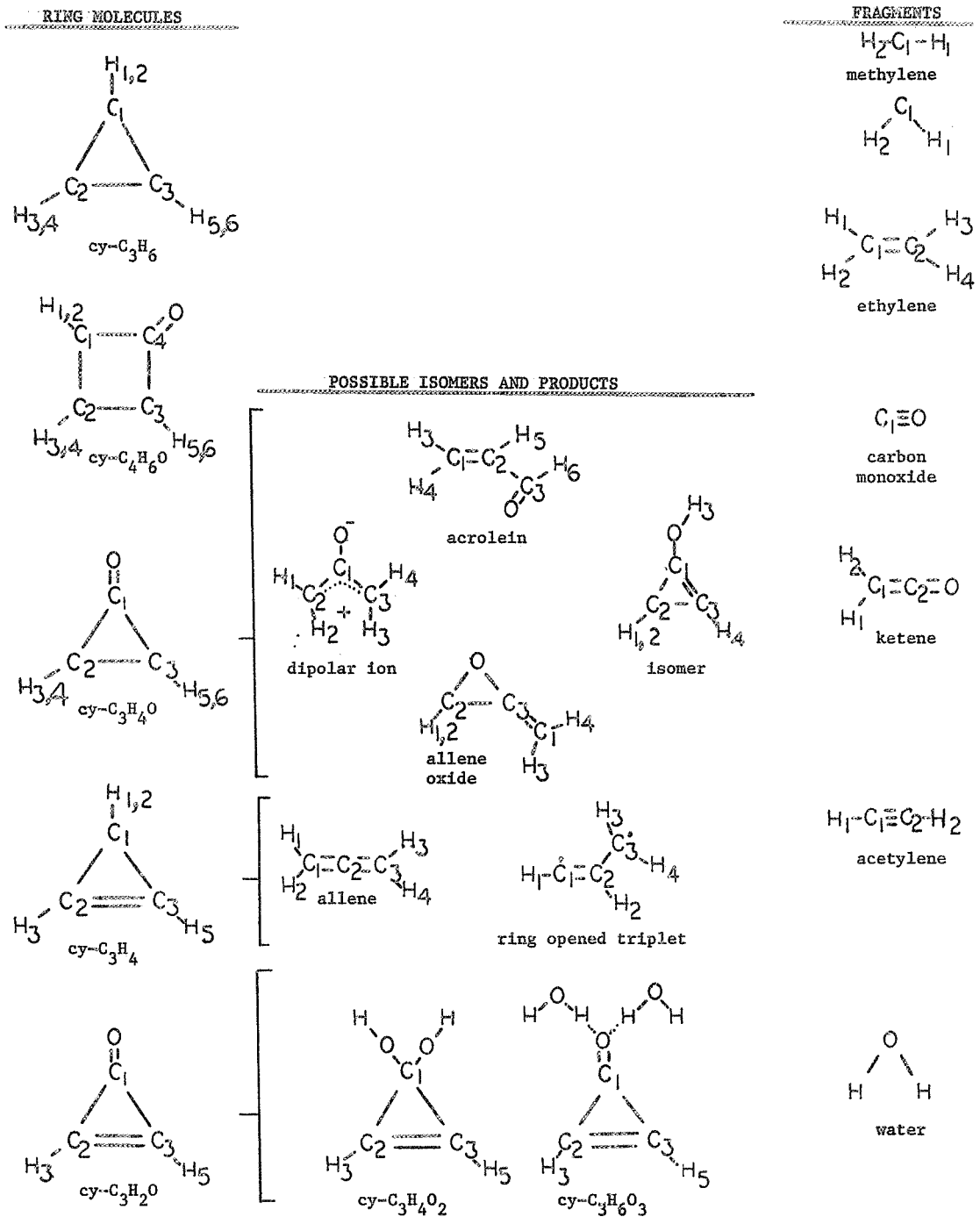

Figure 36. Schematic Structure of Molecules Used in MO Calculations

Table 28. Standard Bond Lengths[f] for MO Calculations

Atoms in Molecule	Bond	Hybrid	Standard Bond Length (Å) Normal[a]	3C-ring[b,e]	4C-ring[c,d,e]
H	H-H	s-s	0.7417		
C,H	C-H	sp^3-H	1.093	1.093	1.093
	C-H	sp^2-H	1.083	1.083	1.083
(Aromatic)	C-H	sp^2-H	1.084		
	C-H	sp-H	1.059		
	C-C	sp^3-sp^3	1.534	1.514	1.555
	C-C	sp^3-sp^2	1.520	1.520	1.520
	C-C	sp^2-sp^2	1.483	1.480	
	C-C	sp^3-sp	1.459		
(Aromatic)	C=C		1.397		
	C=C	sp^2-sp^2	1.337	1.337	1.37
C,H,O	C-C	>C-C<=O	1.506		
	C-O	>C-O-	1.426		
	C-O	>C-O-	1.380		
	C=O	>C=O	1.215		
	C=O	-C<=O, -O	1.24		
	C=O	O=C=O	1.16		
	C≡O	C≡O	1.129		
	O-H		0.970		

a. Open chain molecules
b. For three membered rings, the exocyclic bond angle at saturated carbon is taken as 120°
c. For four membered rings, the exocyclic bond angle at saturated carbon is taken as 114°
d. The four carbon atoms in ring are coplanar
e. All exocyclic groups are taken to bisect CCC angle in the ring
f. Suggested in MINDO reference 99

Table 29. X, Y, Z Coordinates Used in MO Calculations

Molecule	Case	Charge	Multiplicity	Coordinate	Geometry	X, Y, Z Coordinates of Atoms (Å)											
						C_1	C_2	C_3	H_1	H_2	H_3	H_4	H_5	H_6	O_1	O_2	O_3
$cy\text{-}C_3H_6$	1	0	1	X	*	0	- .755	.755	0	0	-1.259	-1.259	1.259	1.259			
				Y		0	1.308	1.308	- .583	- .583	1.600	1.600	1.600	1.600			
				Z		0	0	0	.918	- .918	.918	- .918	.918	- .918			
	2			X		0	- .755	.755	0	0	-1.257	-1.257	1.257	1.257			
				Y		0	1.308	1.308	- .579	- .579	1.597	1.597	1.597	1.597			
				Z		0	0	0	.913	- .913	.913	- .913	.913	- .913			
	3			X		0	.755	.755	0	0	-1.268	-1.268	1.268	1.268			
				Y		0	1.308	1.308	- .592	- .592	1.615	1.615	1.615	1.615			
				Z		0	0	0	.928	- .928	.928	- .928	.928	- .928			
	4			X		0	- .755	.755	0	0	1.268	-1.268	1.268	1.268			
				Y		0	1.308	1.308	- .610	- .610	1.615	1.615	1.615	1.615			
				Z		0	0	0	.905	- .905	.905	- .905	.905	- .905			
	5			X		0	- .755	.755	0	0	-1.227	-1.227	1.227	1.227			
				Y		0	1.308	1.308	- .545	- .545	1.580	1.580	1.580	1.580			
				Z		0	0	0	.944	- .944	.944	- .944	.944	- .944			
	6			X		0	- .725	.725	0	0	-1.229	-1.229	1.229	1.229			
				Y		0	1.25	1.25	- .583	- .583	1.542	1.542	1.542	1.542			
				Z		0	0	0	.918	- .918	.918	- .918	.918	- .918			
	7			X		0	- .795	.795	0	0	-1.299	-1.299	1.299	1.299			
				Y		0	1.38	1.38	- .583	- .583	1.672	1.672	1.672	1.672			
				Z		0	0	0	.918	- .918	.918	- .918	.918	- .918			
	8		3			same as case 1, but triplet											
	9			X	**	0	- .757	.757	0	0	-1.230	-1.230	1.230	1.230			
				Y		0	1.312	1.312	- .547	- .547	1.585	1.585	1.585	1.585			
				Z		0	0	0	0.947	- .947	.947	- .947	.947	- .947			
	10		3			same as case 9, but triplet											
$cy\text{-}C_3H_4$	1	0	1	X	*	0	- .650	.650	0	0	-1.576		1.576				
				Y		0	1.368	1.368	- .586	- .586	1.905		1.905				
				Z		0	0	0	.915	- .915	0		0				
	2			X		0	- .650	.650	0	0	-1.572		1.572				
				Y		0	1.368	1.368	- .586	- .586	1.901		1.901				
				Z		0	0	0	.915	- .915	0		0				
	3			X		0	- .650	.650	0	0	-1.582		1.582				
				Y		0	1.368	1.368	- .586	- .586	1.910		1.910				
				Z		0	0	0	.915	- .915	0		0				

Table 29. X, Y, Z Coordinates Used in MO Calculations (Continued)

Molecule	Case	Charge	Multiplicity	Coordinate	Geometry	X, Y, Z Coordinates of Atoms (Å)											
						C_1	C_2	C_3	H_1	H_2	H_3	H_4	H_5	H_6	O_1	O_2	O_3
$cy\text{-}C_3H_4$	4			X		0	- .675	.675	0	0	1.602		1.602				
				Y		0	1.360	1.360	- .586	- .586	1.895		1.895				
				Z		0	0	0	.915	- .915	0		0				
	5			X		0	- .625	.625	0	0	-1.552		1.552				
				Y		0	1.384	1.384	- .586	- .586	1.919		1.919				
				Z		0	0	0	.915	- .915	0		0				
	6			X		0	- .650	.650	0	0	-1.577		1.577				
				Y		0	1.395	1.395	- .586	- .586	1.930		1.930				
				Z		0	0	0	.915	- .915	0		0				
	7			X		0	- .650	.650	0	0	-1.577		1.577				
				Y		0	1.342	1.342	- .586	- .586	1.877		1.877				
				Z		0	0	0	.915	- .915	0		0				
	8			X	**	0	- .669	.669	0	0	-1.645		1.645				
				Y		0	1.37	1.37	- .547	- .547	1.845		1.845				
				Z		0	0	0	.947	- .947	0		0				
	9		3			same as case 8, but triplet											
	1[a]		1	X	**	0	1.34	2.68	- .563	- .563	3.24		3.24				
				Y		0	0	0	- .929	.929	- .929		.929				
	2[b]		3	X	**	0	1.34	2.08	- 1.06	1.903	1.54		3.16				
				Y		0	0	-1.28	0	.929	-2.21		-1.28				
$cy\text{-}C_3H_4O$	1	0	1	X	*	0	- .790	.790			-1.285	-1.285	1.285	1.285	0		
				Y		0	1.260	1.260			1.534	1.534	1.534	1.534	-1.18		
				Z		0	0	0			.927	- .927	.927	- .927	0		
	2			X		0	- .812	.812			1.306	-1.306	1.306	1.306	0		
				Y		0	1.202	1.202			1.467	1.467	1.467	1.467	-1.18		
				Z		0	0	0			.927	- .927	.927	- .927	0		
	3			X		0	- .768	.768			-1.263	-1.263	1.263	1.263	0		
				Y		0	1.23	1.23			1.504	1.504	1.504	1.504	-1.18		
				Z		0	0	0			.927	- .927	.927	- .927	0		
	4			X		0	- .811	.811			-1.306	-1.306	1.306	1.306	0		
				Y		0	1.30	1.30			1.574	1.574	1.574	1.574	-1.18		
				Z		0	0	0			.927	- .927	.927	- .927	0		
	5			X		0	- .857	.857			-1.351	-1.351	1.351	1.351	0		
				Y		0	1.27	1.27			1.535	1.535	1.535	1.535	-1.18		
				Z		0	0	0			.927	- .927	.927	- .927	0		

Table 29. X, Y, Z Coordinates Used in MO Calculations (Continued)

Molecule	Case	Charge	Multiplicity	Coordinate	Geometry	X, Y, Z Coordinates of Atoms (Å)											
						C_1	C_2	C_3	H_1	H_2	H_3	H_4	H_5	H_6	O_1	O_2	O_3
	6			X		0	- .725	.725			-1.217	-1.217	1.217	1.217	0		
				Y		0	1.26	1.26			1.525	1.525	1.525	1.525	-1.18		
				Z		0	0	0			.927	- .927	.927	- .927	0		
	7			X		0	- .765	.765			-1.257	-1.257	1.257	1.257	0		
				Y		0	1.325	1.325			1.590	1.590	1.590	1.590	-1.18		
				Z		0	0	0			.927	- .927	.927	- .927	0		
	8		3			same as case 1, but triplet											
	9		3			same as case 1, but changed oxygen position to -1.40											
	10[c]		1	X	**	0	-1.213	1.213			-2.25	-1.213	1.213	2.250	0		
				Y		0	0.70	0.70			0.16	1.783	1.783	0.16	-1.38		
	11[d]			X	**	1.895	- .735	.735			-1.208	-1.208	1.895	2.842	0		
				Y		1.887	1.217	1.217			1.490	1.490	2.967	1.341	0		
				Z		0	0	0			.947	-0.947	0	0	0		
$cy\text{-}C_3H_4O$	12[e]			X	**	0	- .760	.760			-1.233	-1.233	.918	1.698	0		
				Y		0	1.106	1.106			1.379	1.379	-1.696	1.646	-1.38		
				Z		0	0	0			.947	- .947	0	0	0		
	13			X	**	0	- .757	.757			-1.230	-1.230	1.230	1.230	0		
				Y		0	1.312	1.312			1.585	1.585	1.585	1.585	-1.215		
				Z		0	0	0			0.947	-0.947	.947	- .947	0		
	14[f]			X	**	0	1.337	2.11			-0.567	-0.567	1.90	3.19	1.50		
				Y		0	0	1.16			-0.85	0.85	-0.85	1.16	2.22		
	15					same as case 13, changed O position to									-1.15		
	16														-1.18		
	17														-1.25		
	18														-1.30		
	19														-1.40		
	20														-1.16		
	21														-1.15		
	22														-1.12		
	23														-1.10		
	24														-1.05		
	25					same as case 1, but changed oxygen position to									-1.16		
	26														-1.15		
	27														-1.12		
	28														-1.10		
	29														-1.05		

Table 29. X, Y, Z Coordinates Used in MO Calculations (Continued)

Molecule	Case	Charge	Multiplicity	Coordinate	Geometry	X, Y, Z Coordinates of Atoms (Å)											
						C_1	C_2	C_3	H_1	H_2	H_3	H_4	H_5	H_6	O_1	O_2	O_3
$cy\text{-}C_3H_4O$	30					same as case 6, but changed oxygen position to									-1.16		
	31														-1.15		
	32														-1.12		
	33														-1.10		
	34														-1.05		
$cy\text{-}C_3H_2O$	1	0	1	X		0	- .675	.675			-1.602		1.602		0		
				Y		0	1.33	1.33			1.865		1.865		-1.18		
	2			X		0	- .70	.70			-1.627		1.627		0		
				Y		0	1.315	1.315			1.850		1.850		-1.18		
	3			X		0	- .65	.65			-1.577		1.577		0		
				Y		0	1.344	1.344			1.879		1.879		-1.18		
	4			X		0	- .675	.675			-1.602		1.602		0		
				Y		0	1.352	1.352			1.887		1.887		-1.18		
	5			X		0	- .675	.675			-1.602		1.602		0		
				Y		0	1.310	1.310			1.845		1.845		-1.18		
	6			X		0	- .675	.675			-1.602		1.602		0		
				Y		0	1.288	1.288			1.823		1.823		-1.18		
	7			X		0	- .675	.675			-1.602		1.602		0		
				Y		0	1.262	1.262			1.797		1.797		-1.18		
	8					same as case 1, but changed oxygen position to									-1.10		
	9														-1.25		
	10														-1.30		
	13			X	**	0	- .669	0.669			-1.645		1.645		0		
				Y		0	1.37	1.37			1.845		1.845		-1.215		
CH_2O	1	0	1	X	**	0	-0.938	0.541							0		
				Y		0	0.938	0.541							-1.215		
	2					same as case 1, but changed oxygen position to									-1.25		
	3														-1.18		
	4														-1.16		
	5														-1.12		
CH_2CO	1	0	1	X	**	0	1.34		-0.563	-0.563					2.55		
				Y		0	0		-0.929	0.929					0		

Table 29. X, Y, Z Coordinates Used in MO Calculations (Continued)

Molecule	Case	Charge	Multiplicity	Coordinate	Geometry	X, Y, Z Coordinates of Atoms (Å)											
						C_1	C_2	C_3	H_1	H_2	H_3	H_4	H_5	H_6	O_1	O_2	O_3
CH_2CO	3					same as case 1, but changed oxygen position to									1.25		
	4														1.18		
	5														1.16		
	6														1.12		
	7	0	1	X		0	1.49		- .563	- .563					2.70		
				Y		0	0		- .929	.929					0		
$cy\text{-}C_4H_6O$	1	0	1	X		0	0	1.52	- .392	- .392	- .392	- .392	1.940	1.940	2.36		1.52 (C_4)
				Y		0	1.555	1.555	- .392	- .392	1.940	1.940	1.940	1.940	-0.845		0
				Z		0	0	0	.927	- .927	.927	- .927	.927	- .927	0		0
	2					same as case 1, but changed oxygen position to									1.25		
	3														1.18		
	4														1.16		
	5														1.12		
	6			X		0	0	1.555	-0.420	-0.420	-0.420	-0.420	1.975	1.975	2.39		1.555 (C_4)
				Y		0	1.555	1.555	-0.420	-0.420	1.975	1.975	1.975	1.975	-0.835		0
				Z		0	0	0	0.92	-0.92	0.92	-0.92	0.92	-0.92	0		0
	7			X		0	0	1.555	-0.420	-0.420	-0.420	-0.420	1.975	1.975	2.415		1.55 (C_4)
				Y		0	1.55	1.55	-0.420	-0.420	1.975	1.975	1.975	1.975	-0.860		0
				Z		0	0	0	0.92	-0.92	0.92	-0.92	0.92	-0.92	0		0
	8			X	**	0	0	1.555	-0.420	-0.420	-0.420	-0.420	1.975	1.975	2.38		1.518 (C_4)
				Y		0	1.555	1.555	-0.420	-0.420	1.975	1.975	1.975	1.975	-0.823		0.037
				Z		0	0	0	-.920	-0.920	0.920	-0.920	0.920	-0.920	0		0
$cy\text{-}C_4H_8$	1	0	1	X	**	0	0	1.555	-0.420	-0.420	-0.420	- .420	1.975	1.975	1.975 (H_7)	1.975 (H_8)	1.555 (C_4)
				Y		0	1.555	1.555	-0.420	-0.420	1.975	1.975	1.975	1.975	- .420	- .42	0
				Z		0	0	0	0.92	-0.92	0.92	-0.92	0.92	-0.92	0.92	-0.92	0
	2			X													
				Y													
				Z													
CO	1	0	1	X	**	0									1.129		
	2			X		0									1.16		
	3			X		0									1.18		
	4			X		0									1.215		
	5			X		0									1.24		
	6		3	X		0									1.129		
	7		3	X		0									1.16		

Table 29. X, Y, Z Coordinates Used in MO Calculations (Continued)

Molecule	Case	Charge	Multiplicity	Coordinate	Geometry	X, Y, Z Coordinates of Atoms (Å)											
						C_1	C_2	C_3	H_1	H_2	H_3	H_4	H_5	H_6	O_1	O_2	O_3
CO	8		3	X		0									1.18		
	9		3	X		0									1.215		
	10		3	X		0									1.24		
cy-$C_3H_4O_2$	1	0	3	X		0	-0.675	0.675	-1.602	1.602	-2.06	2.06			-1.23	1.23	
				Y		0	1.288	1.288	1.823	1.823	-1.19	-1.19			-0.71	-0.71	
			4	X		0	-0.675	0.675	-1.602	1.602	-2.06	2.06			-1.23	1.23	
				Y		0	1.33	1.33	1.865	1.865	-1.19	-1.19			-0.71	-0.71	
cy-$C_3H_6O_3$	1	0	1	X		0	-0.675	0.675	-1.602	1.602	-2.35	-0.86	2.35	0.86	0.0	-1.69	1.69
				Y		0	1.288	1.288	1.823	1.823	-1.68	-1.47	-1.68	-1.47	-1.18	-2.16	-2.16
			2	X		0	-0.675	0.675	-1.602	1.602	-2.35	-0.86	2.35	0.86	0.0	-1.69	1.69
				Y		0	1.33	1.33	1.865	1.865	-1.60	-1.39	-1.60	-1.39	-1.10	-2.08	-2.08
CH_2	1	0	3	X	*	0			-1.03	1.03							
	2		1	X	*	0			- .875	.875							
				Y		0			.697	.697							
	3		3	X	**	0			-1.07	1.07							
	4		1	X	**	0			- .852	.852							
				Y		0			.692	.692							
	5		1	X		0			- .876	0.876							
				Y		0			0.699	0.699							
	6		1	X		0			-0.922	0.922							
				Y		0			0.584	0.584							
	7		1	X		0			-0.945	0.945							
				Y		0			0.544	0.544							
	8		1	X		0			-0.926	0.926							
				Y		0			0.567	0.567							
	9		3	X		0			-0.876	0.876							
				Y		0			0.699	0.699							
	10		3	X		0			-0.922	0.922							
				Y		0			0.584	0.584							
	11		3	X		0			-0.945	0.945							
				Y		0			0.544	0.544							

Table 29. X, Y, Z Coordinates Used in MO Calculations (Continued)

Molecule	Case	Charge	Multiplicity	Coordinate	Geometry	X, Y, Z Coordinates of Atoms (Å)											
						C_1	C_2	C_3	H_1	H_2	H_3	H_4	H_5	H_6	O_1	O_2	O_3
CH_2	12		3	X		0			-0.926	0.926							
				Y		0			0.567	0.567							
C_2H_2	1	0	3	X		0	1.54		-1.10		2.64						
				Y		0	0		0		0						
	2		3	X		0	1.20		-1.06		2.26						
				Y		0	0		0		0						
	3		3	X		0	1.34		- .929		2.27						
				Y		0	0		- .563		- .563						
	4		3	X		0	1.34		-1.09		2.43						
				Y		0	0		0		0						
	5		3	X		0	1.20		-1.057		2.26						
	6		1	X	**	0	1.20		-1.057		2.26						
C_2H_3	1	0	2	X		0	1.34			- .563	1.903	1.903					
				Y		0	0			.929	- .929	.929					
	2	0	2	X		0	1.30			-1.06	1.863	1.863					
				Y		0	0			0	- .929	.929					
C_2H_4	1	0	3	X		0	1.534		0	0	1.534	1.534					
				Y		0	0		-1.093	1.093	-1.093	1.093					
	3		3	X		0	1.34		0	0	1.34	1.34					
				Y		0	0		-1.093	1.093	-1.093	1.093					
	2		3	X		0	1.483		- .541	- .541	2.024	2.024					
				Y		0	0		- .938	.938	- .938	.938					
	4		3	X		0	1.34		- .541	- .541	1.881	1.881					
				Y		0	0		- .938	.938	- .938	.938					
	6		3	X		0	1.34		-0.563	- .563	1.903	1.903					
				Y		0	0		-0.929	+ .929	- .929	.929					
	7		3	X		0	1.51		- .563	- .563	2.073	2.073					
				Y		0	0		- .929	.929	- .929	.929					
	8		3	X		0	1.58		- .563	- .563	2.143	2.143					
				Y		0	0		- .929	.929	- .929	.929					

Table 29. X, Y, Z Coordinates Used in MO Calculations (Concluded)

Molecule	Case	Charge	Multiplicity	Coordinate	Geometry	X, Y, Z Coordinates of Atoms (Å)											
						C_1	C_2	C_3	H_1	H_2	H_3	H_4	H_5	H_6	O_1	O_2	O_3
C_2H_4	5		1		**	same as case 6, but singlet											
	9		1			same as case 7, but singlet											
	10		1			same as case 8, but singlet											

*known molecular geometry

**standard molecular geometry

C_4 fourth carbon atom in 4C-membered ring

H_7,H_8 hydrogen atoms on C4

a. allene
b. ring opened triplet
c. ring opened dipolar ion
d. allene oxide
e. isomer of cy-C_3H_4O
f. acrolein

Table 30. Geometry Variations

Molecule	Case	Bond Length (Å)					Bond Angle (Degrees)				
		C_1-C_2^a	C_2-C_3	C_1-H_1	C_2-H_3	C_1=O	$C_2C_1C_3$	$C_1C_2C_3^a$	$H_1C_1H_2$	$H_3C_2H_4$	$C_3C_2H_3$
cy-C_3H_6	2			1.080							
	1*	1.510	1.510	1.089	1.089		60	60	115.1	115.1	150
	3			1.100							
	4								112.		
	1*								115.1		
	5								120.		
	6	1.45									
	1*	1.51									
	7	1.59									
cy-C_3H_4O	3	1.45	1.54				64	58			
	1*	1.45	1.58		1.085	1.18	64	58		117.3	151
	4	1.53	1.62				64	58			
	2	1.45	1.62				68	56			
	5	1.53	1.70				68	56			
	6	1.45	1.45				60	60			
	7	1.53	1.53				60	60			
	6	1.45	1.45				60	60			
	3	1.45	1.54				64	58			
	2	1.45	1.62				68	56			
	7	1.53	1.53				60	60			
	4	1.53	1.62				64	58			
	5	1.53	1.70				68	56			
	19					1.40					
	18					1.30					
	17					1.25					
	13**	1.514	1.514		1.093	1.215	60	60		120	150
	16					1.18					
	20					1.16					
	21					1.15					
	22					1.12					
	23					1.10					
	24					1.05					
	1*	1.49	1.58		1.085	1.18	64	58		117.3	151
	25					1.16					
	26					1.15					
	27					1.12					
	28					1.10					
	29					1.05					
cy-C_3H_4	2				1.065						
	1*	1.515	1.30	1.087	1.070		50.	65		114.7	150
	3				1.075						
	4	1.515	1.35				53	63.5			
	1*	1.515	1.30				50	65			
	5	1.515	1.25				48	66			
	6	1.54	1.30				50.8	64.6			
	1*	1.515	1.30				50	65			
	7	1.49	1.30				52	64			

Table 30. Geometry Variations (Concluded)

Molecule	Case	Bond Length (Å)					Bond Angle (Degrees)				
		C_1-C_2[a]	C_2-C_3	C_1-H_1	C_2-H_3	C_1=O	$C_2C_1C_3$	$C_1C_2C_3$	$H_1C_1H_2$	$H_3C_2H_4$	$C_3C_2H_3$
cy-C_3H_2O	2	1.49	1.40				56	62			
	1	1.49	1.35		1.070	1.18	54	63			150
	3	1.49	1.30				52	64			
	4	1.51	1.35				53.2	63.4			
	1	1.49	1.35				54	63			
	5	1.47	1.35				54.8	62.6			
	6	1.45	1.35				55.4	62.3			
	7	1.43	1.35				57.4	61.8			
	8					1.10					
	1	1.49	1.35			1.18	54	63			
	9					1.25					
	10					1.30					
C_2H_2O	3					1.25					
	1**	1.34		1.083		1.21				120	
	4					1.18					
	5					1.16					
	6					1.12					
	7	1.49				1.21					
cy-C_4H_6O	2					1.25					
	1	1.555	1.52[C_4]	1.093		1.215	88.0[C_4]	90.9	114		135
	3					1.18					
	4					1.16					
	5					1.12					
	6	1.555		1.093		1.18			114		
	7					1.215					
cy-C_4H_8	1	1.555		1.093					114		
CH_2O	2					1.25					
	1**			1.083		1.215					
	3					1.18					
	4					1.16					
	5					1.12					
	6					1.10					
CO	1**					1.129					
	2					1.16					
	3					1.18					
	4					1.215					
	5					1.24					

*known molecular geometry

**standard molecular geometry

a. $d(C_1\text{-}C_2) = d(C_1\text{-}C_3)$ and $\angle(C_1C_2C_3) = \angle(C_1C_3C_2)$ for these symmetrical 3 C-membered rings.

C_4 $d(C_1\text{-}C_4)$; $\angle(C_2C_1C_4)$

Table 31. Geometry Variations – MO Results

Molecule	Case	-TE (eV) P	-TE (eV) H	$-\Delta H_a$ (kcal/mole) lit. exp[b]	$-\Delta H_a$ (kcal/mole) M	$-\Delta H_a$ (kcal/mole) K	IP (eV) lit. exp[b]	IP (eV) M[d]	IP (eV) K[c]	IP (eV) K[d]	IP (eV) P[d]	IP (eV) H[d]
cy-C_3H_6	2		314.390		822	835		10.20	10.31	11.19		13.07
	1*	25.9409	314.353	813 813	817	830	10.2 10.2	10.21	10.25	10.20	15.3	13.07
	3	25.9462	314.246			725			9.23	10.36		13.07
	4	25.9419	314.323		501			7.81				13.09
	1*	25.9409	314.353		817	830		10.21	10.25	10.20	15.3	13.07
	5	25.9360	314.314		814	828		10.14	10.26	11.15		13.03
	6	25.9402	313.704		860	873		10.35	10.43	11.37	13.3	13.04
	1*	25.9409	314.353		817	830		10.21	10.25	10.20	15.3	13.07
	7	25.8878	314.931		766	766		10.01	10.07			13.07
cy-C_3H_4O	3		428.756		822			10.06				13.49
	1*		428.907	753	797		9.1	10.0				13.46
	4		428.983		769			9.92				13.44
	2		429.118		808			10.12				13.34
	5		429.257		755			9.98				13.27
	6		428.266		840			9.96				13.63
	7		428.607									13.60
	6		428.266		840			9.96				13.63
	3		428.756		822			10.06				13.49
	2		429.118		808			10.12				13.34
	7		428.607									13.60
	4		428.983		769			9.92				13.44
	5		427.257		755			9.98				13.27
	19				N.C.			N.C.				
	18				731			10.10				
	17				755			10.02				
	13**				773			9.94				
	16				792			9.85				
	20				804			9.81				
	21				810			9.76				
	22				828			9.71				
	23				841			9.66				
	24				875			9.53				
	1*				797			10.0				
	25				808			9.95				
	26				814			9.93				
	27				832			9.85				
	28				845			9.80				
	29				879			9.67				
cy-C_3H_4	2	24.146	280.265			685			9.73			12.28
	1*	24.147	280.3675	656	679	684	9.9 9.7	9.8	9.73		11.0	12.33
	3	24.148	280.2118		676	681		9.85	9.73			12.28
	4	24.143	280.065		655	660		9.74	9.51			12.17
	1*	24.147	280.3675		679	684		9.8	9.73			12.33
	5	24.135	280.426		602	705		8.16	9.88			12.42
	6	32.928	280.366		669	673		9.74	9.73			12.36
	1*	24.147	280.367		679	684		9.8	9.73			12.33
	7					694			9.73			

Table 31. Geometry Variations —MO Results (Concluded)

		-TE (eV)		$-\Delta H_a$ (kcal/mole)			IP (eV)					
Molecule	Case	P	H	lit. exp[b]	M	K	lit. exp[b]	M[d]	K[c]	K[d]	P[d]	H[d]
cy-C_3H_2O	2		395.114		646			9.99			13.70	
	1		N.C.		N.C.			N.C.			N.C.	
	3		395.073		681			9.82			13.86	
	4		395.008		653			9.87			12.25	
	1		N.C.		N.C.			N.C.				
	5		395.196		N.C.			N.C.			12.32	
	6				681			9.98				
	7		395.388		693			10.03			13.87	
	8				711			9.74				
	1				N.C.			N.C.				
	9				626			10.05				
	10				N.C.			N.C.				
C_2H_2O	3				475			10.30				
	1**			520	494		9.6	10.21				
	4				513			10.11				
	5				525			10.06				
	6				550			9.95				
	7				427			9.77				
cy-C_4H_6O	2				1070			10.22				
	1			1042	1098		9.4	10.12				
	3				1108			10.08				
	4				1116			10.04				
	5				1142			9.95				
	6				1073			10.13				
CH_2O	2				346			11.64				
	1**			363	365		10.9	11.58				
	3				385			11.53				
	4				397			11.49				
	5				422			11.41				
	6				435			11.37				
CO	1**			256	242		14.1	11.8				
	2				221			12.14				
	3				208			12.15				
	4				187			12.15				
	5				172			12.14				

*known molecular geometry

**standard molecular geometry

b. mass spectrometric measured number from experiments in this thesis

c. IP calculated as difference in TE of the molecule and molecular ion

d. IP taken as the energy of the highest occupied molecular orbital

Table 32. Standard and Known Geometries for ΔH_a and IP

Molecule	Case	Geom.	Bond Length (Å)					Bond Angle (Degrees)				
			C_1-C_2^a	C_2-C_3	C_1-H_1	C_2-H_3	C = O	$C_2C_1C_3$	$C_1C_2C_3^a$	$H_1C_1H_2$	$H_3C_2H_4$	$C_3C_2H_3$
cy-C_3H_6	1	*[108]	1.510	1.510	1.089	1.089		60.0	60.0	115.1	115.1	150.
cy-C_3H_4O	1	*[58]	1.49	1.58		1.085	1.18	64.0	58.0		117.3	151.
cy-C_3H_4	1	*[67]	1.515	1.30	1.087	1.070		50.8	64.6	114.7		150
cy-C_3H_2O	1	est.	1.49	1.35		1.070	1.18	54	63			150.
cy-C_4H_8	1	*[109]	1.548		1.092							
cy-C_4H_6O	1	*[106]	1.556	1.527[C_4]	1.110	1.089	1.20	88.0[C_4]	90.9	112.5		
cy-C_3H_6	9	**	1.514	1.514	1.093	1.093		60.0	60.0	120	120	150
cy-C_3H_4O	13	**	1.514	1.514		1.093	1.215	60	60	120	120	150
cy-C_3H_4	8	**	1.52	1.337	1.093	1.083		52	64	120		148
cy-C_3H_2O	13	**	1.52	1.337		1.083	1.215	52	64			148
cy-C_3H_2O	11	**	1.50	1.40		1.083	1.215	56	62			149
cy-C_4H_8	1	**	1.555		1.093			90	90	114		135
cy-C_4H_6O	8	**	1.555	1.52[C_4]	1.093		1.215	89[C_4]	90	114		135
C_2H_2O	1	**	1.34		1.083		1.215					135
CH_2O	1	**			1.083		1.215			120		
CO	1	**					1.129					
		(O-H)								(O-C_1-O)		
cy-$C_3H_4O_2$	1	0.96	1.45	1.35		1.070	1.22	55.4	62.3	120		150
	2						1.426					
	3	0.96	1.49	1.35		1.070	1.22	54	63			150
	4						1.426					
		(O...H)								(H..O..H)		
cy-$C_3H_6O_3$	1	1.0	1.45	1.35		1.070	1.18	55.4	62.3	120		150
	2	1.0	1.49	1.35		1.070	1.10	54	63	120		150
	3	1.5										
	4	2.0										
	5	3.0										

*known molecular geometry

**standard molecular geometry

a. $d(C_1\text{-}C_2) = d(C_1\text{-}C_3)$ and $\angle(C_1C_2C_3) = \angle(C_1C_3C_2)$

C_4. $d(C_1\text{-}C_4)$; $\angle(C_2C_1C_4)$

Table 33. Standard and Known Geometries for ΔH_a and IP – MO Results

Molecule	Case	Geometry	$-\Delta H_a$ (kcal/mole) lit.	exp[b]	M	K	IP (eV) lit.	exp[b]	M[d]	K[d]	K[c]
cy-C_3H_6	1	*	813	813	817	830	10.2	10.2	10.21	11.20	10.25
cy-C_3H_4O	1	*		753	797			9.1	10.0		
cy-C_3H_4	1	*	656		679	684	9.9	9.7	9.8	10.51	9.7
cy-C_3H_6	9	**	813	813	808	822	10.2	10.2	10.13	11.14	10.24
cy-C_3H_4O	13	**		753	773			9.1	9.9		
cy-C_3H_4	8	**	656		651	657	9.95	9.7	9.8	10.35	9.56
cy-C_4H_8	1	**	1094		1086				10.3		
cy-C_4H_6O	8	**		1042	1069			9.4	10.3		
C_2H_2O	1	**	520		494		9.6		10.21		
CH_2O	1	**	28		28		10.9				
CO	1	**	256		242		14.1		11.8		
		Singlet versus Triplet									
cy-C_3H_6	1	* sing.	813	813	817	830			10.21	11.20	10.25
	8	* trip.				779				9.0	
	9	** sing.			808	822			10.13	11.14	10.24
	10	** trip.				772				8.98	
cy-C_3H_4	8	** sing.	656			657	9.95			10.35	9.56
	9	** trip.				620				8.72	
		Isomers or Other Possible Products[e]									
cyclopropene	8		656			657	9.95	9.7		10.35	9.56
allene	1		676			636	10.2			8.80	7.8
ring open trip.	2					638				10.68	
ring open dipolar ion	10				N.C.				N.C.		
allene oxide	11				694				9.0		
isomer	12				803				9.74		
cyclopropanone	13			753	773			9.1	9.9		
acrolein	14		803[3]		845		10.3[3] 10.25[102]		10.65		

*, **, b, c, and d Refer to Table 31.

e. obtained no convergence for cy-$C_3H_4O_2$ and cy-$C_3H_6O_3$ molecular geometries.

Table 34. Geometry Variations and MO Results — Fragments Containing H and C

Molecule	Case	Geometry	Bond Length C_1-C_2	Bond Length C_1-H_1	Bond Angle $H_1C_1H_2$	Bond Angle $H_1C_1C_2$	$-\Delta H_a$ (kcal/mole) lit	$-\Delta H_a$ (kcal/mole) M	$-\Delta H_a$ (kcal/mole) K	IP (eV) lit	IP (eV) M[d]	IP (eV) K[d]	IP (eV) K[c]
CH_2	1	* trip		1.03	180		200		206			11.1	
	2	* sing		1.12	103		182	171	188	12.0,10.3	10.79	11.8	11.6
	3	** trip		1.07	180				194			11.1	
	4	** sing		1.093	103			177	194		10.78	11.88	11.68
	5	sing		1.12	103				188			11.88	11.66
	6	sing		1.089	115				194			11.58	11.35
	7	sing		1.089	120				194			11.46	11.20
	8	sing		1.085	117				196			11.53	11.28
	9	trip		1.12	103				172			11.40	
	10	trip		1.089	115								
	11	trip		1.089	120								
	12	trip		1.085	117								
C_2H_2	1	trip	1.54	1.10		180			330			10.31	
	2	trip	1.20	1.057		180			363			8.68	
	3	trip	1.34	1.086		120			311			10.28	
	4	trip	1.34	1.086		180			293			9.23	
	5	trip	1.20	1.057		180			363			8.68	
	6	** sing	1.20	1.057		180	392		417	11.4		11.1	10.6
C_2H_4	1	trip	1.534	1.093	180	90			392			8.4	
	3	trip	1.34	1.093	180	90			433			8.97	
	2	trip	1.48	1.083	120	120			480			10.09	
	4	trip	1.34	1.083	120	120			N.C.			N.C.	
	6	trip	1.34	1.083	117	121			501[a]			9.5[a]	
	7	trip	1.51	1.083	120	120			471			10.1	
	8	trip	1.58	1.083	120	120			455			10.3	
	5	** sing	1.34	1.083	117	121	538		538	10.6		10.85	10.16
	9	sing	1.51	1.083	120	120			470			10.1	9.47
	10	sing	1.58	1.083	120	120			405			9.97	9.15

*, **, c, and d Refer to Table 31.

a. No convergence (N.C.)

Table 35. MO Results[a] for Oxygen Containing Molecules

Molecule	$-\Delta H_a$ or $-\Delta H_f$ (kcal/mole) lit.	MINDO	exp.[b]	IP (eV) lit.	MINDO	exp.[b]	lit.-MINDO exp.-MINDO
methanol	48	52		10.9	11.7		+0.8
ethanol	56	56		10.6	11.2		+0.6
1-propanol	61	60		10.4	10.9		+0.5
2-propanol	62	65		10.4	10.7		+0.3
(avg.)∿							+0.6
formaldehyde	28	28		10.9	11.6		+0.7
acetaldehyde	39	37		10.3	11.0		+0.7
propionaldehyde				9.7	10.1		+0.4
(avg.)∿							+0.6
acetone	51	50		9.9	10.5		+0.6
methylethylketone	58	55					
acrolein	803	845[c]		10.1	10.7[c]		+0.6
cyclopropanone		773[c]	753		9.9[c]	9.1	+0.8
cyclobutanone		1069[c]	1042		10.3[c]	9.4	+0.9
ketene	520	494[c]		9.6	10.2[c]		+0.6
2-butanone				9.7	10.3		+0.6
(avg.)∿							+0.7
dimethylether	44	51		10.1	11.4		+1.3
diethylether	60	59		9.7	10.7		+1.0
methylethylether	52	55					--
(avg.)∿							+1.1
(grand avg.)∿							+0.8

a. Majority of data was taken from MINDO reference 99 and 101
b. Numbers measured by ms experiment in this work
c. MINDO-this work

along with comparisons of singlets versus triplets, comparisons of isomers and comparisons of other products. Table 34 presents the geometry variations and MO results for the H and C fragments. Table 35 compares the MO results from the MINDO program with experimental values for many oxygen containing molecules.

Discussion

Analysis of the MO results for cyclopropane, cyclopropanone, cyclopropene, and cyclopropenone in Table 31 reveals that, for all the geometry variations with the four programs, the most stable molecule predicted from the minimum TE did not correspond to the known experimentally measured geometry for any molecule. Furthermore, there was no agreement among programs as to the most stable structure. Systematic variations about known geometries for K, M, and H programs almost never predicted the known geometries as the most stable. For the many M cases involving lengthening the carbon-oxygen bond, it can be seen that only a consistent increase in ΔH_a (not a minimum) was produced. From all of these results, it appeared that only the P program gave any promise of predicting structure correctly. Analysis of Tables 31 and 33 for both M and K programs shows that, invariably, the ΔH_a calculated from the standard geometry was more accurate than that from the known geometry which, in turn, was more accurate than that from the program predicted most stable geometry. This result, although not as consistent, was also true for the IP. The P and H programs calculated IP much too high and were not used for further calculations. For both the ΔH_a and IP, all programs showed much greater sensitivity towards C-C than C-H geometry

changes. In particular, the K and M programs showed a very large ΔH_a sensitivity (100 kcal/mole for geometry variations of Table 30) toward C-C and C=O changes and much smaller C-H dependence. Except for some erratic MINDO cyclopropene IP data, the IP's calculated by the M and K programs were fairly insensitive (0.3 eV) to the geometry variations.

Comparing the K standard geometry data for C and H containing molecules to experiment in Tables 33 and 34, one finds that the average deviations of ΔH_a and IP are around 15 kcal/mole and 0.4 eV, respectively. Similarly, from Tables 33 and 35 one finds for M data on C, H, and O containing molecules that this deviation is about five kcal/mole and 0.8 eV. All the errors are random, except the IP from MINDO, which is systematically high for oxygen containing molecules. The accuracy of the calculated numbers seems to depend on how well the actual experimental molecular geometry (in each particular case) corresponds to the standard geometry used for the class of compounds upon which the program was calibrated. Herein lies the real problem in applying these MO programs to strained ring molecules. It is because these rings have unusual bonding that they are cryogenic molecules. But the more unusual the bonding, the poorer the molecules fit neatly into any class with standard geometries. Thus, the goal of synthesizing these types of cryogenic molecules and calculating MO numbers seems to be mutually exclusive. The great majority of the molecules from which the set of standard geometries was extracted and used to calibrate the MINDO program were, of course, open chain, aliphatic compounds. When the work was extended to cyclic systems,[100] a new set of standard geometries was used for 3-carbon membered ring systems, another set for 4-carbon membered ring systems, and so on.

The standard geometries chosen for 3-carbon membered ring molecules corresponded closely to the known geometry for cyclopropane and the ΔH_a and IP calculated by M and K programs from known and standard geometries of cyclopropane differed by only 10 kcal/mole and 0.1 eV, respectively. However, the standard geometry for cyclopropene assumes a C=C bond length of 1.337 Å as compared to the measured value of 1.28-1.30 Å and produces a difference in known and standard geometry calculated ΔH_a and IP of about 30 kcal/mole and 0.15 eV, respectively. Dewar justifies this C=C bond length by stating he sees no reason for departing from the open-chain 1.337 Å value although he had already departed for the C-C value. His assumption produced a very good agreement with the experimental ΔH_a value. Using these standard geometries for 3-carbon membered ring compounds, he obtains[100] good agreement also for cyclopropane and cyclopropene derivatives. This is not surprising since the actual ring geometry for the parent molecule and the system of derivatives is probably similar and once the molecular parameters were adjusted to correlate with experimental data, all of the molecules fit rather well into these new standard geometries. Consider the case of cyclopropanone which has considerably different geometry than the standard (d(C-C) = 1.58 Å versus 1.514 Å; d(C=O) = 1.18 Å versus 1.215 Å) and whose C-C bonds are described chemically as intermediate between sp^3 and sp^2. In this case, it seems unreasonable to expect the standard geometry to calculate an accurate ΔH_a. The approach suggested by this author is to define a standard geometry for cyclopropanone and its substituted derivatives such that, again, good results are obtained on the average. Lacking experimental ΔH_a and IP data on these derivatives precludes the possibility of this

approach and leaves one still guessing what geometry to use. Only a person well acquainted with the detailed nature of these MO programs could make an honest, accurate guess.

Table 33 shows that the K program makes the very reasonable estimate that the ΔH_a should be raised and the IP lowered by about 40 kcal/-mole (~ 2 eV) for the triplet versus the singlet cyclopropane and cyclopropene (from the program calculation method, these changes in ΔH_a and IP should be equal). Presently, none of the programs can ably handle the cyclopropanone triplet but, assuming it is similar to the other ring molecules, a 20 percent conversion to the triplet state would lower the IP by 0.4 eV, an amount that would begin to be detectable in the experiments of cyclopropene and cyclopropanone specifically looking for this. The ΔH_a and IP calculated for the open chain isomers of cyclopropene and cyclopropanone show such a significant difference (up to 50 kcal/mole and 0.8 eV, respectively) that the comparisons of ΔH_a and IP offer a very strong potential as a means to identify an unknown mass parent from amongst its isomers.

The data in Table 34 were calculated to determine whether or not the program calculations on the triplet versus ground states for various geometries on the small ring fragments would be of use in the ms assumptions and derived energetics. The data for CH_2 are inconsistent for the various geometries; the poorer quality of these data may be due to their non-classifiable structure. The results for C_2H_2 are improved over CH_2 and the results for C_2H_4 show a marked improvement. The ΔH_a for C_2H_4 is the same as the experimental value. Also, for C_2H_4, the lowering of stability and IP for triplets seems to progress in a reasonable

fashion. The ΔH_a difference between structures 7 and 5 is -67 kcal/mole which compares fairly well to the estimate -47 to -57 kcal/mole from thermochemical data. As in the other calculations, once again it seems that the accuracy depends on how well the actual geometry is adaptable to the standard. Since the Pople triplets were found to be inaccurate, no work was done on C, H, and O triplets.

In attempting to decide which of the possible products in the cyclopropenone system were most stable, it was decided to compare the TE of the cyclopropenone plus a water molecule with the TE of the reaction product of cyclopropenone and water (the gem diol) and also to compare the TE of the hydrogen bonded product (refer to Figure 36) as:

$$TE(cy\text{-}C_3H_2O) + TE(H_2O) \text{ vs. } TE(cy\text{-}C_3H_4O_2)$$

and

$$TE(cy\text{-}C_3H_2O) + 2TE(H_2O) \text{ vs. } TE(cy\text{-}C_3H_6O_3)$$

Since M and K do not print out TE, it is shown as follows that comparing ΔH_a is equivalent to comparing TE

since,

$$\Delta H_a(\text{molecule}) = TE(\text{molecule}) - \sum TE(\text{separate atoms})$$

and

$$A + B \longrightarrow A - B$$

then

$$\Delta TE = TE(A\text{-}B) - [TE(A) + TE(B)]$$

$$+ [\Delta H_a(A\text{-}B) + \sum^{A-B} TE(\text{separate atoms})]$$

$$\left\{ \begin{array}{l} = - [\Delta H_a(A) + \sum^{A} TE(\text{separate atoms})] \\ \quad - [\Delta H_a(B) + \sum^{B} TE(\text{separate atoms})] \end{array} \right.$$

$$= \Delta H_a(A\text{-}B) - [\Delta H_a(A) + \Delta H_a(B)]$$

The ΔH_a for water was calculated from its known geometry (bond length 0.958 Å and angle 104°). The cy-$C_3H_4O_2$ structure was calculated extending the cy-C_3H_2O cases 6 and 8 structures by assuming both 1.22 Å and 1.42 Å for the C-O distance, by assuming normal O-H distance of 0.958 Å, and by using a O-C-O angle of 120°. The hydrogen bonded cy-$C_3H_6O_3$ cases were calculated by placing two water molecules about the carbonyl carbon such that hydrogen bonded H···O···H angle was 120° and the C=O···H hydrogen bond length was varied at 1.0, 1.5, 2.0, and 3.0 Å. However, none of these structures would converge. The value of this calculation remains to be determined.

Since the M program calculates the cy-$C_3H_6O_3$ structure as normal bonds at the hydrogen bond, it may be a situation that the program was not designed to handle. Perhaps the P program could better be used for this calculation. However, there is no reason that the cy-$C_3H_4O_2$ gem diol should not converge except the usual rationalization that the structure is unstable.

It is of much interest to correct the M program oxygen molecules systematic high IP errors (~ 0.7 eV). As can be seen in Table 35, Dewar adjusted the molecular parameters to give good ΔH_a agreement at the expense of IP accuracy. Some aspects of this problem were investigated. One possible explanation was that Dewar made a poor choice in C-O

standard bond lengths and Tables 30 and 31 present the results of varying the C=O bond distances. The IP can be corrected somewhat by this means, but only about 0.3 eV and at the expense of ΔH_a accuracy. Dewar[101] suggests that he used the poor data for atomic oxygen. Another possible explanation is that the program, even though it considers the four P level oxygen electrons as valence electrons included in the molecular orbitals, does not account well for the removal of one of these non-bonding electrons by ionization.

BIBLIOGRAPHY*

1. M. A. Haney and J. L. Franklin, J. Chem. Phys. 48 (9), 4093 (1968).

2. F. H. Field and J. L. Franklin, "Electron Impact Phenomena and the Properties of Gaseous Ions," Academic Press, New York, 1957.

3. R. R. Bernecker and F. A. Long, J. Phys. Chem. 65, 1565 (1961).

4. S. W. Benson, J. Chem. Educ. 42, 502 (1965).

5. J. A. Kerr, Chem. Rev. 66, 465 (1966).

6. B. E. Knox and H. B. Palmer, Chem. Rev. 61, 247 (1961).

7. M. J. S. Dewar and G. J. Gleicher, J. Chem. Phys. 44, 759 (1966).

8. C. T. Mortimer, "Reaction Heats and Bond Strengths," Pergamon Press, New York, 1961.

9. "Selected Values of Chemical Thermodynamic Properties," NBS Circular 500, U. S. Gov. Printing Office, Washington 25, D. C., 1952.

10. "Tables of Interatomic Distances and Configurations in Molecules and Ions," (Ed. L. E. Sutton), Special Publications 11 and 18, The Chemical Society (London), 1958.

11. M. J. S. Dewar and G. Klopman, J. Am. Chem. Soc. 89, 3089 (1967).

12. T. L. Cottrell, "The Strength of Chemical Bonds," 2nd ed., Butterworths Scientific Publ., London, 1958.

13. J. Hine, "Divalent Carbon," The Ronald Press Co., New York, 1963.

14. H. Prophet, J. Chem. Phys. 38, 2345 (1963).

15. V. I. Vedeneyev, L. V. Gurich, V. N. Kondratey, V. A. Medvedev, and Ye. L. Frankevich, "Bond Energies, Ionization Potentials, and Electron Affinities," St. Martin's Press, New York, 1966.

16. R. Hoffmann, G. D. Zeiss, and G. W. Van Dine, J. Am. Chem. Soc. 90, 1484 (1968).

* Abbreviations follow the form described in Chemical Abstracts, Supplement (1967).

BIBLIOGRAPHY (Continued)

17. S. Tsuda and W. H. Hamill, J. Chem. Phys. 41, 2713 (1964).

18. L. Pauling, "The Chemical Bond," Cornell University Press, Ithaca, New York, 1967.

19. J. H. S. Green, Quart. Rev. 15, 125 (1961).

20. M. J. S. Dewar and H. N. Schmeising, Tetrahedron 5, 166 (1959).

21. G. S. Paulett and R. Ettinger, J. Chem. Phys. 39, 825 (1963).

22. A. Langer, J. A. Hipple, and D. P. Stevenson, J. Chem. Phys. 22, 1836 (1954).

23. H. M. Frey, Trans. Farraday Soc. 56, 1201 (1960).

24. H. M. Frey and G. B. Kistiakowsky, J. Am. Chem. Soc. 79, 6373 (1957).

25. H. M. Frey, Proc. Roy. Soc. (London) A250, 409 (1959).

26. R. F. Pottie, A. J. Lorquet, and W. H. Hamill, J. Am. Chem. Soc. 84 (1), 529 (1962).

27. F. H. Field, J. Chem. Phys. 20 (11), 1734 (1952).

28. J. L. Franklin, P. M. Hierl, and D. A. Whan, J. Chem. Phys. 47 (9), 3148 (1967).

29. R. F. Pottie, A. G. Harrison, and F. P. Lossing, J. Am. Chem. Soc. 83 (3), 3024 (1961).

30. F. H. Field and E. A. Hinkle, J. Chem. Phys. 18, 1122 (1950).

31. D. P. Stevenson, J. Am. Chem. Soc. 80, 1571 (1958).

32. R. D. Brown and V. G. Krishna, J. Chem. Phys. 45 (5), 1482 (1966).

33. W. A. Bernett, J. Chem. Educ. 44 (1), 17 (1967).

34. K. Watanabe, J. Chem. Phys. 26 (3), 542 (1957).

35. G. Z. Whitten and B. S. Rabinovitch, J. Chem. Phys. 38 (10), 2466 (1963).

36. R. A. Ogg and W. J. Priest, J. Chem. Phys. 7, 736 (1939).

BIBLIOGRAPHY (Continued)

37. E. S. Corner and R. N. Pease, J. Am. Chem. Soc. 67, 2067 (1945).

38. H. O. Pritchard, R. G. Sowden, and A. F. Trotman-Dickenson, Proc. Roy. Soc. A 217, 563 (1953).

39. R. A. Ogg, private communication.

40. N. J. Turro, W. B. Hammond, and P. A. Leermakers, J. Am. Chem. Soc. 87, 2774 (1965).

41. J. F. Paros and F. O. Greene, J. Am. Chem. Soc. 89, 1030 (1967).

42. W. B. Hammond and N. J. Turro, J. Am. Chem. Soc. 88, 2880 (1966).

43. N. J. Turro and W. B. Hammond, J. Am. Chem. Soc. 87, 3258 (1965).

44. P. Lipp and R. Koster, Ber. 64, 2823 (1931).

45. D. A. Semenow, E. F. Cox, and J. D. Roberts, J. Am. Chem. Soc. 78, 3221 (1956).

46. G. B. Kistiakowsky and K. Sauer, J. Am. Chem. Soc. 78, 5669 (1956).

47. G. B. Kistiakowsky and P. H. Kidd, J. Am. Chem. Soc. 79, 4825 (1957).

48. W. B. Demore, H. O. Pritchard, and N. Davidson, J. Am. Chem. Soc. 81, 5874 (1959).

49. W. L. Mock, Diss. Abst. 26 (11), 6374 (1965).

50. I. Haller and R. Srinivasan, J. Am. Chem. Soc. 87, 1144 (1965).

51. N. J. Turro and W. B. Hammond, J. Am. Chem. Soc. 88, 3672 (1966).

52. S. E. Schaafsma, H. Steinberg, and Th. J. De Boer, Rec. Trav. Chim. 85, 1170 (1966).

53. N. J. Turro and W. B. Hammond, J. Am. Chem. Soc. 89, 1028 (1967).

54. H. H. Wasserman and D. C. Clagett, J. Am. Chem. Soc. 89, 5368 (1967).

55. S. E. Schaafsma, H. Steinberg, and Th. J. De Boer, Rec. Trav. Chim. 85, 73 (1966).

56. W. J. M. Van Tilborg, S. E. Schaafsma, H. Steinberg, and Th. J. De Boer, Rec. Trav. Chim. 86, 417 and 419 (1967).

BIBLIOGRAPHY (Continued)

57. N. J. Turro and W. B. Hammond, Tetrahedron 24, 6017 and 6029 (1968).

58. J. M. Pochan, J. E. Baldwin, and W. H. Flygare, J. Am. Chem. Soc. 90, 1072 (1968).

59. A. Ohno, D. J. Grosse, and R. E. Davis, Tetrahedron Letters 8, 963 (1968).

60. N. J. Turro, Acc. Chem. Res. 1 (2), 33-41 (1969).

61. H. J. Hoffman, Tetrahedron Letters 34, 2329 (1964).

62. F. L. Carter and V. L. Frampton, Chem. Rev. 64 (5), 497 (1964).

63. K. B. Wiberg and W. J. Bartley, J. Am. Chem. Soc. 82, 6375 (1960).

64. G. L. Closs and K. D. Krantz, J. Org. Chem. 31, 638 (1965).

65. K. B. Wiberg and W. J. Bartley, J. Am. Chem. Soc. 84, 3980 (1960).

66. R. W. Mitchell, E. A. Doeka, and J. A. Merritt, J. Mol. Spectr. 26, 197 (1968).

67. P. H. Kasai, R. L. Meyers, D. F. Eggers, and K. B. Wiberg, J. Chem. Phys. 30, 512 (1959).

68. D. F. Eggers, J. W. Schultz, K. B. Wiberg, E. L. Wagner, L. M. Jackman, and R. L. Erskine, J. Chem. Phys. 47, 946 (1967).

69. J. Collin and F. P. Lossing, J. Am. Chem. Soc. 80, 1568 (1958).

70. J. Collin and F. P. Lossing, J. Am. Chem. Soc. 81, 2064 (1958).

71. P. Dowd and A. Gold, Tetrahedron Letters 2, 85 (1969).

72. M. A. Bell, Synthesis and Mass Spectra of Cyclopropene and Cyclopropenone, M. S. Thesis, Georgia Institute of Technology (1968).

73. "Selected Values of Physical and Thermodynamic Properties," API Research Project 44, Carnegie Press, Pittsburg, Pa., 1953.

74. R. Breslow, T. Eicher, A. Krebs, R. Peterson, and J. Posner, J. Am. Chem. Soc. 87, 1320 (1965).

75. R. Breslow and L. J. Altman, J. Am. Chem. Soc. 88, 504 (1966).

BIBLIOGRAPHY (Continued)

76. R. Breslow and G. Ryan, J. Am. Chem. Soc. 89, 3073 (1967).

77. S. W. Tobey and R. West, Tetrahedron Letters 18, 1179 (1963).

78. H. G. Kuivila and O. F. Beumel, Jr., J. Am. Chem. Soc. 83, 1248 (1969).

79. Private communication with G. Ryan at Columbia University.

80. R. West, J. Chickos, and E. Osawa, J. Am. Chem. Soc. 90 (14), 3885 (1968).

81. R. E. Honig, J. Chem. Soc. 16, 105 (1948).

82. W. M. Hickam, R. E. Fox, and R. Kjeldaas, Phys. Rev. 96, 63 (1954).

83. W. M. Hickam, R. E. Fox, and T. Kjeldaas, Phys. Rev. 90, 386 (1953).

84. P. T. Smith, Phys. Rev. 36, 1293 (1930).

85. H. D. Smyth, Proc. Roy. Soc. (London) A102, 283 (1922).

86. J. W. Warren, Nature 165, 810 (1950).

87. J. W. Warren and C. A. McDowell, Discussions of Farraday Society 10, 53 (1951).

88. R. E. Honig, J. Chem. Phys. 16 (2), 105 (1948).

89. F. P. Lossing, A. W. Tichner, and W. A. Bryce, J. Chem. Phys. 19 (10), 1254 (1951).

90. S. N. Foner and R. L. Hudson, J. Chem. Phys. 25, 602 (1956).

91. R. E. Fox, W. M. Hickam, T. Kjeldaas, and D. J. Grove, Phys. Rev. 84, 859 (1951).

92. J. D. Morrison, J. Chem. Phys. 21, 1767 (1953).

93. J. D. Morrison, J. Chem. Phys. 22, 1219 (1954).

94. R. Taubert, Adv. Mass. Spect., 489 (1963).

95. J. Bracher, H. Ehrhardt, L. Fuchs, O. Osberghaus, and R. Taubert, Adv. Mass. Spect., 385 (1963).

BIBLIOGRAPHY (Concluded)

96. E. Klots, J. Chem. Phys. 41 (1), 117 (1964).

97. J. A. Pople and G. A. Segal, J. Chem. Phys. 44, 3289 (1966).

98. R. Hoffman, J. Chem. Phys. 39, 1397 (1963).

99. N. C. Baird and M. J. S. Dewar, J. Chem. Phys. 50, 1262 and 1275 (1969).

100. N. C. Baird and M. J. S. Dewar, J. Am. Chem. Soc. 89, 3966 (1967).

101. M. J. S. Dewar and S. D. Worley, J. Chem. Phys. 50 (2), 654 (1969).

102. R. I. Reed, "Ion Production by Electron Impact," Academic Press, New York, 1962.

103. T. J. Malone, Mass Spectrometric Studies of the Synthesis, Reactivity, and Energetics of the Oxygen Difluorides at Cryogenic Temperatures, Ph. D. Thesis, Georgia Institute of Technology, (1966).

104. Joint Army-Navy-Air Force JANAF "Interim Thermochemical Tables," (D. R. Stull, Project Director), The Dow Chemical Company, Midland, Michigan, 1960.

105. A. T. Blades, Can. J. Chem. 47, 615 (1969).

106. L. H. Scharpen, V. W. Laurie, and W. Victor, J. Chem. Phys. 49, 221 (1968).

107. A. Bauder, F. Tank, and H. Guenthard, Helv. Chim. Acta. 46, 1453 (1963).

108. O. Bastiansen, F. Fritsch, and K. Hedberg, Acta. Cryst. 17, 538 (1964).

109. A. Almenningen, O. Bastiansen, and P. Skancke, Acta. Chem. Scand. 15, 711 (1961).

110. C. T. Genaux and W. D. Walters, J. Am. Chem. Soc. 73, 4497 (1951).

111. B. S. Rabinovitch and R. W. Diesen, J. Chem. Phys. 30, 735 (1959).

112. D. P. Stevenson, Disc. Faraday Soc. 10, 35 (1951).

113. J. D. Roberts and M. C. Caserio, "Basic Principles of Organic Chemistry," W. A. Benjamin, Inc., New York, 1965.

VITA

Richard was born on September 4, 1942, in Blue Island, Illinois, the first child of three to Mr. and Mrs. R. J. Holt. He attended grammar school in Temple City, California, and then East Jefferson High School in Metairie, Louisiana, from which he graduated in 1960 as valedictorian of his class. He entered the Georgia Institute of Technology in the Fall of 1960 under the Cooperative Plan under which he worked the equivalent of two years for Mississippi Gulf Refining Company in Purivs, Mississippi, and received the degree of Bachelor of Chemical Engineering with highest honors in June, 1965. During his undergraduate years, he received a Universal Oil Products scholarship and entered into the Tau Beta Pi, Phi Kappa Phi, and the Briaerean societies.

During the summer of 1965, he worked for Universal Oil Products in Riverside, Illinois. He chose to remain at Georgia Tech for graduate studies and proceeded to pursue a Ph.D. degree in Chemical Engineering. His graduate studies were supported by an NSF traineeship and a Universal Oil Products scholarship.

In June 1968, he married Patricia Westmoreland, a young nursing graduate. They plan to begin their careers in Houston, Texas, where he will work for the Esso Research and Engineering Company.